Impact du R-2HG sur l'environement immunitaire des gliomes IDH1 mutés

Quentin Richard

université PARIS-SACLAY

Impact du R-2HG sur l'environnement immunitaire des gliomes IDH1 mutés

Impact of R-2HG on the immune microenvironment of IDH1-mutant gliomas

Thèse de doctorat de l'université Paris-Saclay

École doctorale n°582 : cancérologie : biologie - médecine - santé (CBMS)
Spécialité de doctorat : Aspects moléculaires et cellulaires de la biologie
Graduate School : Life Sciences and Health. Référent : Faculté de médecine

Thèse préparée à l'Institut du Cerveau (CNRS, Inserm),
sous la direction de **Marc Sanson**, Professeur.

Thèse soutenue à Paris-Saclay, le 29 novembre 2022, par

Quentin RICHARD

Composition du Jury

François GHIRINGHELLI Professeur des universités - Praticien hospitalier, Université de Bourgogne Franche-Comté	Rapporteur & Examinateur
Lukas BUNSE Principal inverstigator, University of Heidelberg	Rapporteur & Examinateur
Virginie PENARD-LACRONIQUE Directrice de recherche, Université Paris-Saclay	Examinatrice
Cécile ALANIO Directrice de recherche, Université PSL	Examinatrice
Luc DE CHAISEMARTIN Maître de conférences, Université Paris-Saclay	Examinateur

THESE DE DOCTORAT

NNT : 2022UPASL074

« Science sans conscience n'est que ruine de l'âme »

Pantagruel, François Rabelais, 1532

ACKNOWLEDGMENTS

Tout d'abord, je souhaite remercier les membres du jury d'avoir accepté d'évaluer ce travail de thèse. Je remercie particulièrement le Dr. Lukas Bunse et le Pr. François Ghiringhelli d'avoir accepté d'être mes rapporteurs. Je remercie également le Dr. Virginie Penard-Lacronique, le Dr. Cécile Alanio, et le Pr. Luc de Chaisemartin d'avoir accepté d'être mes examinateurs. J'espère que ce travail vous plaira et sera à la hauteur de vos attentes.

Plus particulièrement, je souhaite remercier le Dr. Virginie Penard-Lacronique pour ses conseils scientifiques lors des comités de suivi individuel et d'avoir motivé le choix de ne plus utiliser de lignées immortalisées pour étudier les modifications épigénétiques. Je souhaite aussi vous remercier de votre aide, de votre bienveillance et de votre disponibilité lors de la fin de cette thèse.

J'adresse évidemment mes plus sincères remerciements au Pr. Luc de Chaisemartin pour toute l'aide apportée lors de cette thèse. Tes réponses à mes questions, à toute heure de la journée, ont toujours été d'une grande aide et surtout d'un grand réconfort. Merci de m'avoir guidé pendant mes années d'études, pendant mon stage américain, pendant ma thèse d'exercice et, maintenant, pendant ma thèse de science. Tu es un modèle de pédagogie et j'espère être digne de la formation que tu m'as dispensée. Tu as été un superviseur non officiel de ce travail et je voudrais t'en remercier car il n'aurait jamais pu être ce qu'il est sans toi. Merci d'être praticien hospitalier, enseignant universitaire, et chercheur et de démontrer qu'il est possible d'exceller dans ces trois fonctions. J'ai hâte de collaborer avec toi de manière officielle et je te souhaite toute la réussite professionnelle et personnelle que tu mérites.

J'aimerais maintenant remercier le Pr. Marc Sanson de m'avoir fait confiance pour porter ce projet de thèse et de l'autonomie dont j'ai pu bénéficier. Merci également au Dr. Michel Mallat d'avoir participé à nos discussions scientifiques et pour ses conseils. Merci au Dr. Luis J. Castro-Vega pour son investissement dans la vie de l'équipe, que ce soit à travers les recherches de financement ou les invitations de nombreux chercheurs extérieurs garantissant des échanges de qualité lors des réunions d'équipes et d'avoir corrigé ce manuscrit de thèse.

Je tiens à remercier l'intégralité du laboratoire Sanson/Huillard et particulièrement le Dr. Emmanuelle Huillard pour ses précieux conseils en fin de thèse.

Un très grand merci à Julie Lerond et au Dr. Isabelle Leroux pour leur grande aide scientifique et technique et leur disponibilité qui m'ont permis d'avancer plus vite et plus sereinement. Un très grand merci, également, à Lisa Salhi pour son immense aide en bioinformatique. Merci de ta patience et de ta grande curiosité scientifique. Nos débats m'ont beaucoup apporté et ont rendu cette thèse indéniablement meilleure. Merci au Dr. Alice Laurenge-Leprince pour nos échanges et ton expertise médicale.

J'aimerais également remercier Annick Prigent, Célia Sayetta, et Bineta Faye de la plateforme d'histologie, pour leur grande aide et sympathie. C'était un véritable plaisir de travailler avec vous et d'utiliser votre plateforme. Merci aussi à Florence Deknuydt, Aurélie Gestin, et Jérôme Van Wassenhove de la plateforme de cytométrie, pour leur aide. Enfin, j'adresse tous mes remerciements à Justine Guegan et Corentin Raoux de la plateforme de bioinformatique pour leur grande aide et rapidité.

Merci à Coralie Gimmonet et Pietro Pugliese pour leur contribution bioinformatique à ce travail de thèse sans qui ce projet n'aurait pas pu avancer.

***

Dr. Mohammed Ahmed (King Ahmed Ahmed), Dr. Yanis Khenniche (Professeur tout court), Dr. Isaias Hernandez (Gato mexicano), future Dr. Irma Segoviano (Ricolina), future Dr. Alexa Saliou (Queen of chisme), future Dr. Noémie Barillot (comment se fait-il de ne pas avoir de surnom pour toi ?), et enfin, Non Dr. et heureuse ainsi Eva Kirasic (Madame Serpentard), je manque de mots pour vous remercier de toute l'aide et de tout le soutien que vous m'avez apportés pendant cette thèse. Sans vous, ces trois ans auraient été peut-être plus courts.

Mohammed, thank you so much for welcoming me into this lab with open arms. I wish you all the best with Sarah and hope to see you soon.

Yanis, que dire que je n'ai pas déjà écrit dans ton livre de départ ? Encore une fois, merci de ton accueil, merci de ton aide scientifique, merci pour nos échanges, et surtout merci de ton soutien sans faille d'un point de vue professionnel comme personnel. Merci aussi de nous avoir accompagnés dans des bars où le prix du jus de tomate est scandaleux. Je suis ravi que tu ais trouvé un métier qui te convienne, tu le mérites amplement. La science est incertaine, mais une chose est sûre, notre labo aurait été une incroyable aventure.

Isaias, merci d'avoir été un ami fidèle pendant cette thèse. Merci d'avoir pris le temps de m'enseigner la bioinformatique, sans quoi je n'aurais pas pu mener ce travail. Je ne te remercie pas, cependant, de m'avoir empoisonné un soir dans un bar de Montparnasse. Tu es un scientifique incroyable et je te souhaite le meilleur dans le public comme dans le privé.

Irma, merci pour tes cours de danse, pour nos fous rires, et pour nous avoir accueillis chez toi quand le déclic café devenait trop populaire. Je chéris les moments passés en Dordogne et au cours de cette thèse avec toi. C'est maintenant à toi d'être la prochaine à passer sa thèse. Je te souhaite d'ores et déjà bon courage pour cette épreuve mais surtout, j'espère que tu trouveras un métier qui te plaira par la suite.

Alexa, dire que tu as bien failli ne pas faire de thèse dans ce laboratoire. Quelle tristesse cela aurait été pour nous ! Je te remercie infiniment de ta joie de vivre, de tes sourires en toutes circonstances et de la cohésion d'équipe que tu as réussie à entretenir, sans parler des nombreux gâteaux, tous aussi bons les uns que les autres. Je n'arrive pas à imaginer ce que cette thèse aurait été sans toi et ton soutien. Je te souhaite le meilleur pour la suite et je serai là pour toi comme tu l'as été pour moi. A très bientôt à Bordeaux.

Noémie, tu as été la dernière arrivée, mais la touche finale à ce bouquet de doctorants. Merci beaucoup de ton soutien scientifique mais aussi sportif et de tes encouragements pour ma carrière débutante de marathonien. J'espère un jour arriver à ton niveau et que tu retiendras, de ton côté, de bons moments de ta thèse. N'hésite pas à me tenir au courant.

Eva, notre collaboration est la preuve qu'une Serpentard et un Gryffondor peuvent être une équipe de choc. Avec nous, Voldemort n'aurait pas fait long feu. Je ne pourrais jamais te remercier assez de toute l'aide que tu m'as apportée pendant cette dernière année de thèse, qu'elle soit technique ou morale. Tu m'as redonné l'envie de poursuivre mon projet et de transmettre ma passion de l'immuno-oncologie. Je ne serais jamais arrivé à produire le travail décrit plus bas sans toi. Encore une fois, merci.

***

Mina, Vitto, Gab votre aide dépasse largement le contenu de cette thèse. Merci de me supporter, de me soutenir, d'être tout simplement les meilleurs amis dont je pourrais rêver.

Originals, merci de votre soutien et du refuge que je trouve avec vous. Marion, Denis, merci des moments passés avec vous et de votre aide. Merci, sister, d'être toujours là pour moi. A&F. Gabin, ton arrivé dans ce monde a été le plus heureux évènement de cette thèse. J'espère améliorer, à ma petite échelle, le monde que nous te laissons en espérant que, quand tu seras grand, le cancer ne soit plus le fléau qu'il est aujourd'hui.

TABLE OF CONTENT

LIST OF FIGURES

LIST OF TABLES

LIST OF SUPPLMENTAL FIGURES

LIST OF SUPPLEMENTARY TABLES

ABBREVIATIONS

5caC: 5-carboxylCytosine
5fC: 5-formylCytosine
5hmC: 5-hydroxymethylCytosin
5mC: 5-methylCytosin
AC-like: AstroCyte-like
APC: Antigen Presenting Cell
ATRX: Alpha Thalassemia/mental Retardation syndrome X-linked
BBB: Blood-Brain Barrier
CAR: Chimeric Antigen Receptor

CBTRUS: Central Brain Tumor Registry of the United States
CGI: CpG Island
ChIP-seq: Chromatin ImmunoPrecipitation sequencing
CIITA: Class II TransActivator
CITE-seq: Cellular Indexing of Transcriptomes and Epitopes by sequencing
CNS: Central Nervous System
CpG: CG dinucleotide
CSC: Cancer Stem Cell
CSF: CerebroSpinal Fluid
CT: Computed Tomography
CTLA-4: Cytotoxic T Lymphocyte Antigen 4
CyTOF: Cytometry by Time-Of-Flight
DC: Dendritic Cell
DNMT: DNA MethylTransferase
DP T cell: Double Positive T cell
ECM: Extra-Cellular Matrix
EFS*: Etablissement Français du Sang*
FACS: Fluorescence Activated Cell Sorting
GBM: GlioBlastoMas
G-CIMP: Glioma-CpG Island Methylator Phenotype
GSC: Glioblastoma Stem Cell
H3K27me3: histone H3 lysine 27 trimethylation
H3K4me3: histone H3 lysine 4 trimethylation
HIF-1α: Hypoxia-Inducible Factor 1-alpha
ICB: Immune Checkpoint Blockade
IDH: Isocitrate DeHydrogenase
IDH-A: Astrocytomas
IDHi: IDHm Inhibitor
IDHm: Isocitrate DeHydrogenase mutated
IDH-O: Oligodendrogliomas
IDHwt: Isocitrate DeHydrogenase wild-type
ISF: cerebral InterStitial Fluid
ITAMs: Immunoreceptor Tyrosine-based Activation Motifs
iTreg: induced regulatory T cell
KPS: Karnofsky Performance Status
L-2HG: S-2-HydroxyGlutarate
LAG3: Lymphocyte Activation Gene 3 protein
LC-MS: Liquid Chromatography coupled to Mass Spectrometry
m6A: N6-MethylAdenosine
MDMs: Monocyte-Derived Macrophages
MDSC: Myeloid-Derived Suppressor Cell
MES-like: MESenchymal-like
MG: MicroGlia cell
MGMT: O-6-MethylGuanine-DNA MethylTransferase
MHC: Major Histocompatibility Complex
M-MDSC: Monocytic MDSC
MRI: Magnetic Resonance Imaging
NET: Neutrophil Extracellular Trap
NF1: NeuroFibromin 1
NFAT: Nuclear Factor of Activated T cells
NK: Natural Killer
NKT: Natural Killer T
NPC-like: Neural-Precursor-Cell-like
OPC-like: Oligodendrocyte-Precursor-Cell-like
OSM: OncoStatin M

PBMC: Peripheral Blood Mononuclear Cell
PCV: Lomustine, procarbazine, vincristine
PD-1: Programmed cell Death 1
PMN-MDSC: PolyMorphoNuclear MDSC
PRC2: Polycomb Repressive Complex
R-2HG: R-2-HydroxyGlutarate
T_{RM}: non-circulating tissue-Resident Memory
RNA-Seq: RNA-Sequencing
ROS: Reactive Oxygen Species
RT: Radiation Therapy
scRNA-seq: single-cell RNA sequencing
scTHI: single-cell Tumor Host Interaction
SP T cell: Single Positive T cell
TAM: Tumor-Associated Macrophage and Microglia cell
TCA: TriCarboxylic Acid
TCGA: The Cancer Genome Atlas
T_{CM}: Central Memory
TCR: T Cell Receptor
TDG: Thymine-DNA Glycosylase
T_{EM}: Effector Memory
T_{EMRA}: Terminally differentiated Effector Memory
TERT: Telomerase Reverse Transcriptase
TET: Ten Eleven Translocation
Th: T helper
TIL: Tumor-Infiltrating Lymphocyte
TME: Tumor MicroEnvironment
TMZ: Temozolomide
TMZ: TeMoZolomide
Treg: CD4 REGulatory T cell
T_{SCM}: Stem Cell Memory
WHO: World Health Organization
α-KG: α-KetoGlutarate
α-KGDDs: 2-Oxoglutarate-Dependent Dioxygenases
γδ T cell: gamma-delta T cell

ABSTRACT

Adult-type diffuse gliomas are the most frequent primary brain tumors, which, despite extensive fundamental and clinical research, remain incurable. A deeper understanding of gliomas' highly immunosuppressive immune tumor microenvironment (TME) may shed light on novel therapeutic strategies. The goal of my PhD was to compare the TMEs of isocitrate dehydrogenase wild-type (IDHwt) and mutant (IDHm) tumors and to investigate the potential effects of R-2 hydroxyglutarate (R-2HG).

In a first study, we performed a bulk transcriptome/methylome profiling of CD11b+ cells isolated from human gliomas. In line with previous studies, we found that these cells display different transcriptional landscapes according to the IDH status, suggestive of different cell types. In addition, we revealed methylation differences at both promoter and distal regulatory regions, with a marked bias towards global hypermethylation in CD11b+ cells from IDHm tumors. Our integrative analysis indicates that methylation and expression differences are connected and may underlie the distinctive hyporesponsive and mesenchymal-like phenotypes of microglia cells and tumor-associated macrophages in IDHm and IDHwt gliomas, respectively. Moreover, we hypothesized that the downregulation of both major histocompatibility complexes I and II (MHC I/II) expressions may be mediated by methylation in the promoter of CIITA in CD11b+ cells of IDHm gliomas.

In this context of lack of antigen presentation in IDHm gliomas, we sought to investigate T cell phenotypes and functions by single-cell RNA-seq profiling. We found that T cells from IDHm tumors have a more naïve and central memory phenotype, and discovered a significant cluster expressing the inhibitory receptor NKG2A/CD94. This NKG2A+ CD8+ T cells may react to advanced MHC-deficient tumors through acquired TCR-independent cytotoxicity mechanisms and could be potentially used for immune modulation in IDHm patients.

Taken together, our findings point to critical differences in the myeloid and lymphoid compartments of IDHwt and IDHm gliomas while revealing potential signaling mechanisms underlying the phenotypes of these immune cell populations. Determining these differences could be relevant for the design of more precise targeted immune therapies for glioma patients.

RESUME

Les gliomes diffus de type adulte sont les tumeurs cérébrales primaires les plus fréquentes qui, malgré des recherches fondamentales et cliniques approfondies, restent incurables. Une compréhension plus approfondie du microenvironnement tumoral (TME) hautement immunosuppressif des gliomes pourrait conduire à de nouvelles stratégies thérapeutiques. L'objectif de ma thèse était de comparer les TME des tumeurs sauvages et mutantes pour le gène de l'isocitrate déshydrogénase (IDHwt et IDHm, respectivement). et d'étudier les effets potentiels du R-2 hydroxyglutarate (R-2HG).

Dans une première étude, nous avons réalisé un profilage transcriptomique/méthylomique en masse de cellules CD11b+ isolées de gliomes humains. En accord avec les études précédentes, nous avons constaté que ces cellules présentent des paysages transcriptomiques différents selon le statut IDH, ce qui suggère des types cellulaires différents. En outre, nous avons révélé des différences de méthylation à la fois au niveau des promoteurs et des régions régulatrices distales, avec une tendance marquée vers l'hyperméthylation des cellules CD11b+ provenant de tumeurs IDHm. Notre analyse intégrative indique que les différences de méthylation et d'expression sont liées et peuvent sous-tendre les phénotypes distincts d'hyposensibilité et de type mésenchymateux des cellules de la microglie et des macrophages associés aux gliomes IDHm et IDHwt, respectivement. De plus, nous avons émis l'hypothèse que la régulation négative de l'expressions des complexes majeurs d'histocompatibilité I et II (MHC I/II) pouvait être médiée par la méthylation du promoteur de CIITA dans les cellules CD11b+ des gliomes IDHm.

Dans ce contexte d'absence de présentation d'antigène dans les gliomes IDHm, nous avons cherché à étudier les phénotypes et les fonctions des lymphocytes T par séquençage ARN à l'échelle de la cellule unique. Nous avons constaté que les lymphocytes T des tumeurs IDHm ont un phénotype naïf et central mémoire, et avons découvert un groupe important de cellules exprimant le récepteur inhibiteur NKG2A/CD94. Ces cellules T CD8+ NKG2A+ pourraient réagir aux tumeurs déficientes en MHC par des mécanismes de cytotoxicité acquis indépendants du TCR et pourraient potentiellement être modulées chez les patients IDHm.

En conclusion, nos résultats indiquent des différences critiques dans les compartiments myéloïdes et lymphoïdes des gliomes IDHwt et IDHm, tout en révélant des mécanismes de signalisation potentiels qui sous-tendent les phénotypes de ces

populations de cellules immunitaires. La détermination de ces différences pourrait être pertinente pour la conception de thérapies immunitaires ciblées plus précises pour les patients atteints de gliomes.

SYNTHESE

Les gliomes diffus de type adulte sont les tumeurs primaires malignes les plus fréquentes des tumeurs du cerveau et du système nerveux. Le diagnostic moléculaire différencie les gliomes sauvages des gliomes mutants pour le gène de l'isocitrate déshydrogénase (IDHwt et IDHm, respectivement). En plus de la mutation IDH, la perte des chromosomes 1p et 19q sépare les oligodendrogliomes (IDH-O) des astrocytomes (IDH-A). L'hétérogénéité intra-tumorale, définie par des techniques de séquençage ARN en *bulk* ou à l'échelle de la cellule unique, est une des raisons pour laquelle les gliomes diffus résistent aux thérapies actuelles. Ainsi, malgré des recherches fondamentales et cliniques approfondies, ces tumeurs restent incurables.

L'hétérogénéité intra-tumorale ne touche pas que les cellules tumorales mais aussi le microenvironnement dans lequel elles évoluent. Le microenvironnement immunitaire (TME) des gliomes est composé de cellules immunitaires infiltrantes la tumeur mais également de cellules immunitaires résidentes dans le cerveau, appelées cellules microgliales. Les gliomes IDHm et IDHwt présentent un TME radicalement différent. Le TME des gliomes IDHm est majoritairement composé de cellules microgliales, avec peu de cellules infiltrantes ; alors que le TME des gliomes IDHwt est majoritairement composé de macrophages dérivés de monocytes. L'infiltration lymphocytaire est faible avec un peu moins de lymphocytes T dans les gliomes IDHm comparés aux gliomes IDHwt.

La mutation, dans les cellules tumorales IDH-mutantes, favorise la conversion presque totale de l'alpha-cétoglutarate (αKG) en R-2hydroxyglutarate (R-2HG). Ce déséquilibre permet une inhibition compétitive fonctionnelle des enzymes-dépendantes de l'αKG, ce qui entraîne l'initiation et le maintient de la gliomagénèse. Parmi les enzymes-dépendantes de l'αKG, les enzymes TET1/2 sont responsables de la déméthylation de l'ADN. A très forte concentration (environ 5 mM), le R-2HG inhibe ces enzymes, ce qui produit une hyper-méthylation globale de l'ADN dans les cellules tumorales IDH-mutantes. Le R-2HG est exporté hors des cellules tumorales et inonde le microenvironnement à des concentrations estimées de l'ordre de 3 mM à un rayon de 2 cm du centre de la tumeur. La question posée par cette thèse est : « quel est l'impact du R-2HG sur les cellules immunitaires du microenvironnement des gliomes IDHm ? ».

Le système immunitaire adaptatif présente une plasticité phénotypique et fonctionnelle remarquable au cours des réponses immunitaires. L'activation des cellules T naïves, par exemple, déclenche des modifications étendues du cycle cellulaire, du métabolisme et de l'expression de protéines, qui entraînent la génération de cellules aux phénotypes distincts. Bien que cette flexibilité soit codée dans l'ADN, les cellules elles-mêmes sont génotypiquement identiques. La capacité des cellules à utiliser des génomes sous-jacents identiques pour générer divers phénotypes est en partie expliquée par l'épigénétique. La réponse des cellules immunitaires est régie par un large éventail de mécanismes épigénétiques. Nous nous sommes concentrés, dans ce manuscrit, à l'étude de la déméthylation de l'ADN, médiée par les enzymes TET, chez les lymphocytes T. Il est pour le moment admis que l'activation de lymphocytes T naïfs conduit à une diminution progressive du 5hmC et, à moindre mesure, du 5mC. Cela établit une identité de la lignée qui sera conservée lors de la différentiation en lymphocytes T mémoires et effecteurs.

Dans une première étude, nous avons réalisé un profilage transcriptomique/méthylomique en masse de cellules CD11b+ isolées de gliomes humains. En accord avec les études précédentes, nous avons constaté que ces cellules présentent des paysages transcriptomiques différents selon le statut IDH, ce qui suggère des types cellulaires différents. En outre, nous avons révélé des différences de méthylation à la fois au niveau des promoteurs et des régions régulatrices distales, avec une tendance plus marquée vers l'hyper-méthylation des cellules CD11b+ provenant de tumeurs IDHm. Notre analyse intégrative indique que les différences de méthylation et d'expression sont liées et peuvent sous-tendre les phénotypes distincts d'hyposensibilité et de type mésenchymateux des cellules de la microglie et des macrophages associés aux gliomes IDHm et IDHwt, respectivement. De plus, nous avons émis l'hypothèse que la régulation négative de l'expressions des complexes majeurs d'histocompatibilité I et II (MHC I/II) pouvait être médiée par la méthylation du promoteur de CIITA dans les cellules CD11b+ des gliomes IDHm. Nous n'avons pas démontré que le R-2HG était capable de diminuer l'expression de CIITA directement, ce qui suggère que l'expression de CIITA est différente selon les types cellulaires, avec une probable hypo-méthylation associée à une expression dans les cellules tumorales IDHwt et macrophages et une hyper-méthylation associée à une perte d'expression dans les cellules tumorales IDHm et microglie. La sous-expression des MHC-I/II dans les cellules CD11b+, ainsi que celle démontrée par la littérature dans les cellules tumorales IDHm, participe au fait que les gliomes IDHm sont des tumeurs froides.

Dans ce contexte d'absence de présentation d'antigène dans les gliomes IDHm, nous avons cherché à étudier les phénotypes et les fonctions des lymphocytes T par séquençage ARN à l'échelle de la cellule unique. Nous avons observé plus de lymphocytes T naïfs et plus de lymphocytes associés à un phénotype mixte central mémoire/effecteur mémoire dans les gliomes IDHm comparé aux IDHwt. Inversement, nous avons observé plus de lymphocytes effecteurs mémoires dans les gliomes IDHwt comparé aux IDHm. Cette différence phénotypique ne s'explique pas une inhibition directe de la différentiation par le R-2HG, comme démontrée *in vitro*. De plus, nous avons découvert, pour la première fois à notre connaissance, un groupe important de cellules exprimant le récepteur inhibiteur NKG2A/CD94. Ces lymphocytes T CD8+ NKG2A+ sont caractérisés par des marqueurs de lymphocytes résidents mémoires (CD69, ITAGE, ITGA1), l'expression de récepteurs activateurs (CD226, KLRK1), un marqueur antiprolifératif (TOB1) et la sous expression du CD28. NKG2A est acquis après un programme d'exhaustion, suite à des stimulation chroniques du TCR. Ces lymphocytes T CD8+ NKG2A+ conservent une forte expression de molécules cytotoxiques (GZMB, PRF1). En conclusion, ce cluster de lymphocytes pourrait réagir aux tumeurs déficientes en MHC par des mécanismes de cytotoxicité acquis indépendants du TCR et pourraient potentiellement être modulées par l'anticorps bloquant NKG2A (monalizumab) chez les patients IDHm.

En conclusion, nos résultats indiquent des différences critiques dans les compartiments myéloïdes et lymphoïdes des gliomes IDHwt et IDHm, tout en révélant des mécanismes de signalisation potentiels qui sous-tendent les phénotypes de ces populations de cellules immunitaires. Les cellules tumorales et autres cellules présentatrices d'antigène dans les gliomes IDHm sont caractérisées par une faible expression de molécules du MHC, en regard desquelles, les lymphocytes T ont développé un programme de cytotoxicité indépendant du TCR. Nous proposons le blocage du NKG2A chez les patients IDHm comme nouvelle stratégie thérapeutique.

INTRODUCTION

Today, cancer is the second leading cause of death worldwide. It accounted for 8.8 million deaths in 2015, or nearly one in six deaths, and its incidence continues to rise yearly. The disease burden is immense, not only for patients but for families as well. The search for an effective treatment is as old as the disease itself. First, therapeutics were developed to target tumor cells and their rapid rate of expansion. If chemotherapy mainly remains the first-line treatment option, its clinical outcomes, as well as the numerous side effects are not satisfactory and fuel the idea of one day finding a more effective and better-tolerated remedy.

During the last twenty years, discoveries in molecular immunology and investigations on the immune microenvironment surrounding tumor cells enabled the development of new therapeutics that demonstrated unprecedented efficacy in multiple cancers. It appears that what is now known as "immunotherapy" has the potential to improve not only clinical response but also the overall survival of patients in a sustainable manner. Unfortunately, only a subset of patients responds to this therapy. It is therefore necessary to understand the underlying mechanisms of immune activation and inhibition and find new targets to improve anti-tumor immunity.

In the introduction of this research work, we will first introduce critical concepts of cancer immunology and emphasize some of the epigenetic mechanisms underlying the functional states of immune cells. Then, we will detail adult diffuse gliomas and their molecular defining features. This will lead us to the depiction of the isocitrate dehydrogenase mutation and the effects of the metabolite it produces on tumor cells and on the immune cells of their microenvironment.

I) CANCER IMMUNOLOGY

In this first section, we will describe the universal hallmarks of cancer, among which interaction with the immune system and nonmutational epigenetic reprogramming will be of the essence in this manuscript. To understand these two characteristics, we will first describe cancer immunology and then explore how epigenetics shapes immune cell fates.

A. Essential features of cancers

1) Universal hallmarks of cancers

Cancer is one of the oldest described diseases in the world. Its first observation was made on fossil bones and human mommies from ancient Egypt when it was considered incurable [1]. Since then, considerable efforts have been made to understand cancer development. The best illustration of these efforts is President Nixon's signature of the National Cancer Act of 1971, which facilitated research funding for understanding the origins of this disease to propose effective and sustainable treatments. Until the 2000s, cancer research generated rich and complex knowledge defining cancer as a multifactorial disease involving dynamic changes in the genome. Dominant gain-of-function mutations that induce oncogenes and recessive loss-of-function mutations that inhibit tumor suppressor genes were discovered. Consequently, cancer development - or tumorigenesis - was defined as a sequence of steps governing the progressive transformation of a normal cell into a malignant cancer cell. The general concept was that the development of a tumor follows the Darwinian evolution, during which a succession of genetic alterations occurs, each leading to the transformation into a cancerous cell.

Douglas Hanahan *et al.* studied several molecular, biochemical, and cellular capacities acquired and shared by most or all human cancers and postulated that the vast genotypic repertoire of cancers is only a manifestation of eight essential alterations in cell physiology that collectively dictate the malignant growth of cancer cells. This simplification derives from the fact that all mammalian cells possess similar molecular machinery regulating their proliferation, differentiation, and death. These common alterations provide a framework for rationalizing the complexity of neoplasms and therefore offer a conceptual scaffold that makes possible the rationalization of the complex phenotypes of diverse human tumors in terms of a standardized set of underlying cellular parameters. It is now accepted that a normal cell progressively evolves toward a neoplastic stage by acquiring one or more of these alterations. Each of these physiological changes and new abilities acquired during tumor development represents the ability of tumor cells to hijack host defense mechanisms. These distinct and complementary abilities thus enable tumor growth and metastasis. Initially listed in 2000, these capabilities were revised in 2011 and 2022. They include both non-

immunological and immunological features. The eight hallmarks, described in 2000, comprised:

- the acquired capabilities for sustaining proliferative signaling,
- evading growth suppressors,
- resisting cell death,
- enabling replicative immortality,
- inducing/accessing vasculature,
- activating invasion and metastasis [2].

In 2011, two "emerging hallmarks" were added:

- deregulating cellular metabolism and
- avoiding immune destruction [3].

Today, eleven years later, it is evident that they can be considered core hallmarks of cancer, much like the original six. Still, in 2011, the authors added the concept of "enabling characteristics," which provide means by which cancer cells and tumors can adopt these functional traits. These two enabling processes were:

- genome instability and
- tumor-promoting inflammation [3].

In 2022, D. Hanahan presented new prospective hallmarks and enabling capabilities:

- unlocking phenotypic plasticity
- senescent cells
- polymorphic microbiomes and
- nonmutational epigenetic reprogramming (Figure 1) [4].

Notably, the eight-core and these novel capabilities are each, by definition, distinguishable from each other. Still, aspects of their regulation are partially interconnected in some and probably many cancers.

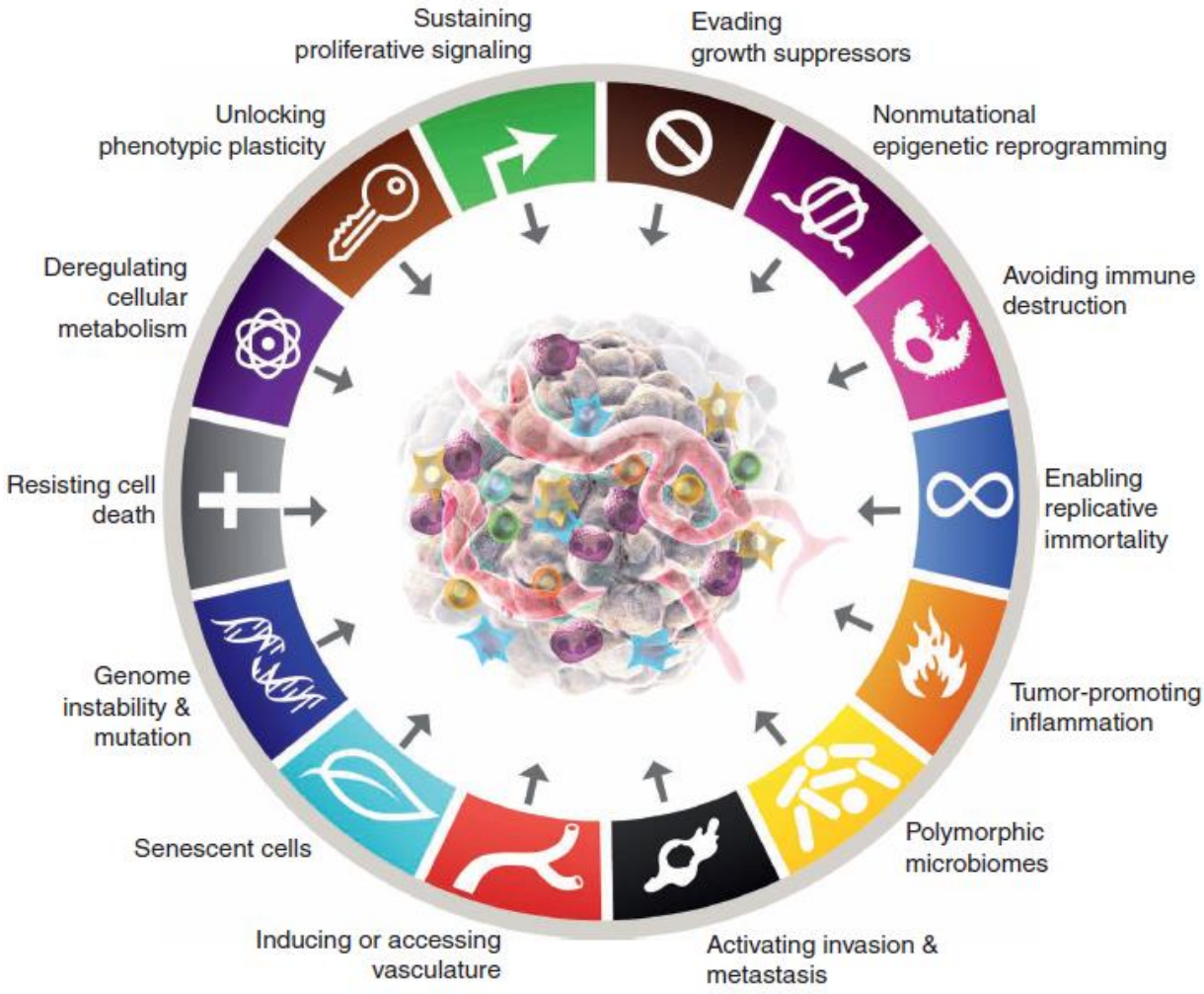

Figure 1| Hallmarks of Cancer.

In addition to the six acquired capabilities proposed in 2000 [2], the two provisional "emerging hallmarks" introduced in 2011 [3] - cellular energetics (now described more broadly as "reprogramming cellular metabolism") and "avoiding immune destruction" have been sufficiently validated to be considered part of the core set. "Tumor-promoting inflammation" and "genome instability and mutation," which activate the eight hallmark capabilities necessary for tumor growth and progression, were described as enabling characteristics. The 2022 new revision proposes "unlocking phenotypic plasticity," "nonmutational epigenetic reprogramming," "polymorphic microbiomes," and "senescent cells" as new emerging hallmarks [4].

Avoiding immune destruction and nonmutational epigenetic reprogramming are critical features that we will now focus on.

2) Heterogeneity of cancers

Acquired resistance to therapy is a direct consequence of pre-existing intratumor heterogeneity and ongoing diversification during the course of therapy, which enables some tumor cells to survive treatment while facilitating the development of new therapy-resistant clones. Cellular phenotypic heterogeneity of cancers is a

complex, multifactorial phenomenon which integrates genetic, epigenetic, and environmental cues.

a. Genetic heterogeneity of cancers

In 2004, B. Vogelstein and K. W. Kinzler wrote, "the revolution in cancer research can be summed up in a single sentence: cancer is, in essence, a genetic disease" [5]. Since then, the evolution of DNA sequencing technologies has enabled the documentation of intratumor genetic heterogeneity. Mutational errors, in the form of nucleotide substitutions and small deletions, can affect genes with known cancer relevance, leading to the activation of oncogenes and the inactivation of tumor suppressors. One example of these errors is the mutations in the genes encoding the cytoplasmic and mitochondrial forms of isocitrate dehydrogenase (IDH1 and IDH2, respectively; collectively referred to as IDH). Large-scale genomic events, related to chromosomal instability, involve loss, gains, and translocations of large fragments of genomic DNA. One example of these events is the 1p19q codeletion. These two molecular events are found in specific types of brain tumors called diffuse gliomas (*cf* II) Malignant primary adult diffuse gliomas).

b. Epigenetic heterogeneity of cancers

The term "epigenetics" was introduced in 1942 by Waddington to describe phenotypical alterations that were not associated with genetic changes. Epigenetics regulate gene expression programs' inheritance while keeping DNA sequences intact. It requires one of the following criteria: cell division results in signal propagation; daughter cells inherit the signal; or the signal impacts gene expression.

Despite the critical importance of genetic heterogeneity on clinically relevant phenotypic features, such as responses to growth signaling, proliferation, and death, epigenetic mechanisms have been demonstrated to play a more significant role in tumor cell phenotypes. For example, in a type of diffuse gliomas called glioblastomas, it was described that progenitor-like cancer cells show closer resemblance to the profiles of normal neural cells than to that of more differentiated cancer cells from the same tumor [6]. These data suggest that differentiation state-related epigenetic programs have a dominant impact in shaping phenotypes compared with cancer-related genetic aberrations.

Determining the role of epigenetic heterogeneity in tumor resistance to therapies is very challenging since, in contrast to genetic heterogeneity, the phenotypes of tumor cells are highly plastic. Epigenetically defined phenotypic traits range from silencing key tumor suppressor genes, mediated by DNA hypermethylation, to noise-driven cell-to-cell differences that dissipate within a few cell divisions [7]. Studies assessing epigenetic heterogeneity within tumors have mainly focused on DNA methylation since this is technically less challenging to measure than chromatin modification. Because of the reversible nature of epigenetic modifications, it was unclear if they could be used to define subclones, track tumor evolution, and assess intratumoral heterogeneity. However, studies in diffuse gliomas and other cancers have demonstrated that inferring tumor evolution based on genetic and DNA methylation patterns largely overlaps [8]. Intra-tumoral heterogeneity for DNA methylation has consistently been observed in regulatory regions that affect the transcription of genes relevant to the initiation and evolution of the disease.

3) Microenvironmental heterogeneity of cancers

The existence of different spatial and temporal microenvironmental components also leads to intratumoral phenotypic heterogeneity, reflective of cellular responses to these contextual signals, rather than specific well-defined phenotypes.

Microenvironmental heterogeneity also involves heterogeneity in immune cell infiltration. Leukocytes are frequently one of the most abundant cell types within tumors, and their highly mobile nature can lead to rapidly changing spatial heterogeneity that can create immunologically active or silent niches. For example, T cells can directly eliminate specific cancer cells. Therefore, the frequency and location of T cells have directly been related to subclonal heterogeneity in cancer. Furthermore, since T cells are activated by specific tumor neoantigens, many of which are generated by tumor-specific mutations, the location of T cells with specific T cell receptors also varies within tumors and correlates with the number and types of mutations [9].

The tumor microenvironment (TME) is composed of a heterogeneous mixture of tissue-resident immune cells, such as microglia cells or macrophages, fibroblasts, endothelial cells, and neurons that predate tumor formation, together with blood-derived cells that are recruited to the tumor bed. Each of these cell types can be co-opted by the tumor and contribute to tumor heterogeneity and resistance to therapies. However, there are significant differences in the composition and spatial organization of the TME across cancer types, including differences in tissue vascularization,

innervation, and tissue-resident immune and stromal cells that may impact anti-tumor immunity (Figure 2).

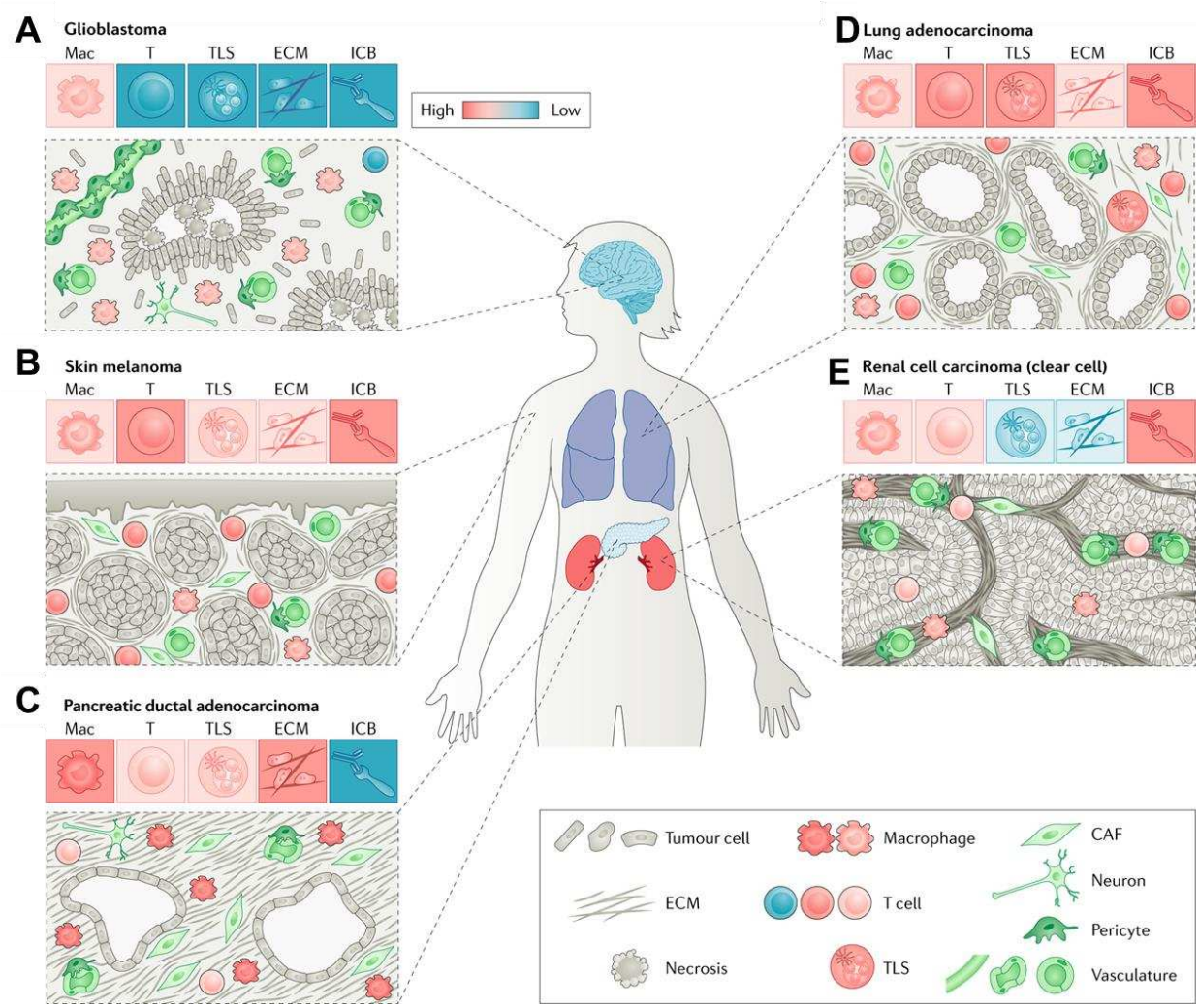

Figure 2| Cellular and architectural heterogeneity of the tumor microenvironment for different cancers.

Representation of histological patterns of glioblastoma (A), skin melanoma (B), pancreatic ductal adenocarcinoma (C), lung adenocarcinoma (D) and clear-cell renal cell carcinoma (E). In addition to tumor cells, each microenvironment contains cells derived from both circulating cells and local cells that may differentially impact antitumor immune responses across cancer sites. For each tumor type, a color-coded heatmap (red: high; blue: low) shows the level of dominance of macrophage or lymphocyte infiltrate, presence of tertiary lymphoid structures (TLSs), matrix deposition and response to immune checkpoint blockade (ICB). CAF: cancer-associated fibroblast; ECM: extracellular matrix; Mac: macrophage; T: T cell. Adapted from [10]

In this manuscript, we will focus on the immune TME, which form a major cellular compartment of tumor lesions. The current classification of tumor immune microenvironment phenotypes mainly focuses on T cell abundance. The immune inflamed phenotype is characterized by the presence in the tumor parenchyma of both CD4 and CD8 T cells, often accompanied by myeloid cells and monocytic cells. Immune

cells are positioned close to the tumor cells. A dependence on tumor progression and invasion was first demonstrated in colorectal tumors. T cell infiltrates, and IFNγ signatures showed predictive value superior to TNM with respect to the natural history of primary cancers [11]. The second profile is the immune excluded phenotype, which is also characterized by the presence of abundant immune cells. However, they do not penetrate the tumor parenchyma but are instead retained in the stroma. The last profile is the immune-desert phenotype. It is characterized by a paucity of T cells in either the parenchyma or the stroma of the tumor, although myeloid cells may be present (Figure 3).

Transcriptional analysis of 10,000 tumor samples comprising 33 different cancer types performed by The Cancer Genome Atlas (TCGA) consortium identified several immune expression signatures that interestingly spanned anatomical location yet substantially varied in their proportion across cancers. Diffuse gliomas have the lowest immune cell infiltration, dominated by macrophages over lymphocytes and natural killer (NK) cells, which likely contributes to their limited response to immune checkpoint blockade. Conversely, tumors containing the highest immune cell fraction include cancers most responsive to immunotherapy, such as lung carcinoma and skin melanoma [12].

The strong variations in lymphocytic infiltration across cancers may be driven by the distinct molecular compositions and states of antigen-presenting cells (APCs) found between tissues. Non-lymphoid tissue APCs present in sterile tissues such as the brain, filtering sites such as the kidney and liver, and environmental interfaces such as the skin, lung and gut differ from each other. This diversity likely shapes tumor T cell infiltrates in tumor lesions (Figure 3).

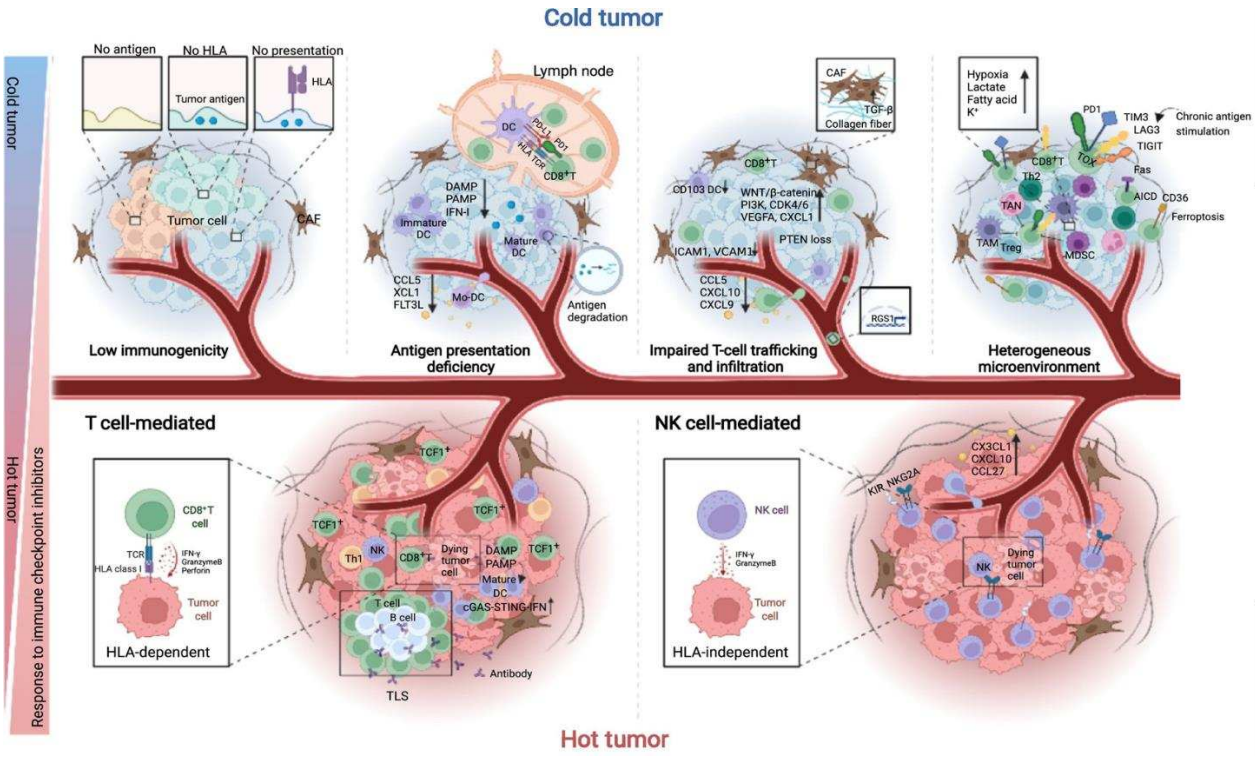

Figure 3| Hot and cold tumors are defined by distinct microenvironments.

Representation of tumor mechanisms exploited to evade immunosurveillance, leading to an immune-cold phenotype. From [13].

4) Immunotherapy

Despite our increasing knowledge about cancer, the more we learn, the more we are confronted with the reality that we are still far from a universal cure. Its ability to resist and evade the therapies mentioned above remains a difficult challenge to overcome. Unraveling the resistance mechanisms to active ingredients and thus developing new therapeutic solutions to target the relevant pathways has become the logical next step in the global cancer treatment strategy. However, given the genetic and epigenetic instability of neoplastic cells, it is likely that the new generation of targeted therapies will encounter even more complex resistance mechanisms, undoubtedly leading to disease progression. Consequently, it is possible to assume that the vast repertoire of immune cells provides sufficient diversity, adaptability, and cytotoxicity to compete with the complexity of neoplasms.

The body's response to cancer is not a unique mechanism but shares many similarities with inflammation and wound healing. The relationship between immune function and cancer management was first considered by Rudolf Virchow 150 years ago when he observed the presence of leukocytes within tumor tissue. He suggested that the leukocyte infiltration reflected that cancer developed in sites of chronic

inflammation. Over the past two decades, discoveries in molecular immunology have led to developing novel therapeutics that have recently demonstrated unprecedented efficacy for multiple cancers. These therapeutics can potentially improve not only a clinical response but also the overall survival of patients in a sustainable manner. This new pillar of cancer treatment is so promising that it was named "Breakthrough of the Year" by Science magazine in 2013. The discovery of the surface molecules Cytotoxic T Lymphocyte Antigen 4 (CTLA-4) and Programmed cell Death 1 (PD-1) won James Allison and Tasuku Honjo the Nobel Prize in October 2018. Many immunotherapy approaches have already demonstrated efficacy in patients, while others remain in development. One of the most attractive features of immunotherapy is its ability to target cancer cells and, thus, spare healthy tissue. This feature differentiates immunotherapy from other "classical" therapies, whose significant side effects contribute to patient morbidity and mortality. The primary role of immunotherapy is to reactivate the host's deficient immune system so that it is once again capable of initiating and sustaining attacks against tumor cells. A non-exhaustive summary of TME-directed therapies is available in Supplementary Table 1.

To understand these new therapeutics, it is essential to comprehend the complex dialog between cancer cells and immune cells, a notion called “cancer immunology”.

B. Cancer immunology

1) The concept of immunosurveillance: anti-tumoral immunity

The concept that the immune system can effectively recognize and eliminate developing primary tumors without therapeutic intervention has been around for over 100 years. However, the validity of this concept has been very challenging. When it was proposed in 1909, this hypothesis could not be experimentally tested because little was known about the molecular and cellular basis of immunity. Later, when the field of immunology developed and the concept acquired its name - cancer immunosurveillance - animal experiments became possible but failed to provide evidence. Experimental mice had spontaneous mutations that made them immunocompromised but not completely immunodeficient. The development of genetics, transgenic mouse models, and monoclonal antibodies capable of specifically blocking immune components have made it possible to test the hypothesis in

immunodeficient mouse models. Analysis of individuals with congenital or acquired immunodeficiency syndromes or treated with immunosuppressive therapies revealed three pieces of evidence highlighting that cancer immunosurveillance does exist in humans: (a) immunocompromised transplant recipients have a higher incidence of non-viral cancer than the age-matched immunocompetent control population, (b) cancer patients can develop both innate and adaptive immune responses, and (c) the presence of T cells within a tumor is a favorable prognostic factor of patient survival [14].

In parallel with the evolution of knowledge about the genetics and biology of cancers, understanding the fundamental cellular and molecular mechanisms that orchestrate the innate and adaptive components of the immune system has improved. In summary, the innate system consists of cytokines, the complement system, phagocytes such as macrophages, neutrophils, dendritic cells (DCs), and innate lymphoid cells such as NK cells. Cells of the innate system have receptors that allow them to detect foreign microorganisms and dying cells. Macrophages and neutrophils provide early defense against microorganisms, while DCs provide a key interface with the adaptive component of the immune system. The latter consists of B and T cells and their antigen receptor repertoires [15]. Immunological rejection of a developing tumor as a defense against infection, requires an integrated response involving not only the innate but also the adaptive component of immunity [14]. The immune system represents an extrinsic mechanism of tumor suppression and manifests its effect only after transformed cells have bypassed their own intrinsic mechanisms of tumor suppression. According to our current understanding of immune responses, several distinct steps must be completed, either endogenously or therapeutically, to produce an effective anti-tumor response. The order of these steps varies according to the authors, as it is, in fact, a cycle that must first be initiated and then progress and grow iteratively (Figure 4).

2) Cancer-Immunity cycle

The anti-tumor response initiates when innate immune cells are alerted to the presence of a growing tumor. This is partly due to local tissue disruption resulting from stromal remodeling processes. The latter may result from two of the standard features of cancer: angiogenesis and invasive growth (cf on page 26 Universal hallmarks of cancer). It produces pro-inflammatory molecules that, with the help of chemokines released by the tumor cells themselves, recruit innate immune cells to this local source

of "danger". Once they arrive at the tumor site, Natural Killer T (NKT)[1] cells, gamma-delta T cells (γδ T cells)[2], NK cells, and macrophages recognize molecules on the surface of tumor cells (such as NKG2D ligands, HLA-E, etc..) that have been induced either by the incipient inflammation or by the cellular transformation processes themselves. In addition, γδ T cells and NKT cells also recognize developing cancer cells through interaction with their T Cell Receptor (TCR) and NKGD2 ligands or CD1 glycolipid complexes, respectively. Irrespective of the precise mechanism of recognition, these events lead to a common outcome critical for the continuation of the anti-tumor response: the production of IFNγ [14]].

Second, the effects of tumor recognition by the innate immune system are amplified. Indeed, the initial amount of IFNγ released at the tumor bed induces local production of chemokines that recruit more and more innate immune cells. The products generated by ECM remodeling also induce tumor-infiltrating macrophages to produce low amounts of IL-2, which stimulates tumor-infiltrating NKs to produce low amounts of IFNγ, which in turn activates IL-12 production by macrophages present in the tumor, leading to increased IFNγ production by NK cells. In addition to this up-regulation system, the binding of NK activating receptors to their cognate ligands on tumor cells further stimulates IFNγ production by NKs. This activates numerous IFNγ-dependent processes, including antiproliferative, pro-apoptotic, and angiostatic effects that lead to a reduction of tumor burden. In addition, IFNγ-activated macrophages that release tumoricidal products such as reactive oxygen species (ROS) and NK cells activated either by IFNγ or via stimulation of their activating receptors can kill tumor cells via mechanisms involving TRAIL or perforin, respectively. As a result of these processes, tumor antigens from dead tumor cells are released into the microenvironment, and the adaptive immune system comes into play [14].

Third, tumor antigens released by the effects of innate immunity on the tumor lead to the recruitment of acquired immunity and its specific responses directed against the tumor. Immature DCs recruited to the tumor site become activated by exposure to immunogenic signals. These include the pro-inflammatory cytokine environment generated by the ongoing innate immune attacks, interaction with tumor-

[1] NKT cells are T lineage cells that share morphological and functional characteristics with both T cells and NK cells. recognize antigen presented by the nonpolymorphic MHC class I-like CD1d molecules and are characterized by a restricted TCR repertoire due to the presence of an invariant TCR alpha chain paired with a limited number of TCR beta chains.

[2] γδ T cells are defined by expression of heterodimeric TCRs composed of γ and δ chains, which sets them apart from the classical CD4 and CD8 T cells that express αβ TCRs.

infiltrating NK cells, factors released by dying cancer cells, or the gut microbiota. This maturation allows them to differentiate considerably and promote immunity instead of tolerance. Activated DCs can then acquire tumor antigens by ingesting cancer cell debris [14]. These antigens may reflect one or more of the various mutated proteins of tumor cells; products of non-mutated genes preferentially expressed by these cells; differentiation antigens associated with the tissue of origin where cancer has developed but against which thymic or peripheral tolerance has not been fully established. Tumor antigens are then presented by the major histocompatibility complex (MHC) class I or II [16]. Mature, activated, antigen-presenting DCs then migrate to the lymph node, where they induce the activation of tumor-specific Naïve CD4+ Th1 cells. These Th1 T cells facilitate the development of tumor-specific CD8+ CTLs, which are in turn induced by the prior cross-presentation of tumor antigenic peptides presented by MHC-I on the surface of DCs [14]. DCs are key players in this step as they are able to induce priming and activation of effector T cells directed against tumor-specific antigens. However, they can also promote a state of tolerance when not stimulated by an immunogenic maturation signal. This state of tolerance is characterized by the production of regulatory T cells (Tregs) that oppose the anti-tumor action. The nature of the immune response is determined at this stage by the critical balance of effector to regulatory T cells ratio [17].

Finally, the deployment of tumor-specific adaptive immunity allows the host to eliminate the developing tumor completely. CD4+ and CD8+ T cells arrive at the tumor site, where they efficiently and specifically recognize tumor targets. Recognition of cancer cells is achieved by the interaction of the TCR with the associated MHC-related antigen. CD4+ T cells produce IL-2, which, in addition to IL-15 produced by the body, helps to maintain the viability and cytotoxic functions of CD8+ T cells [14]. The latter induces tumor cell death by direct and indirect mechanisms. In this way, the destroyed cancer cells release antigens again, increasing the response's extent and magnitude in successive cycles (Figure 4) [17].

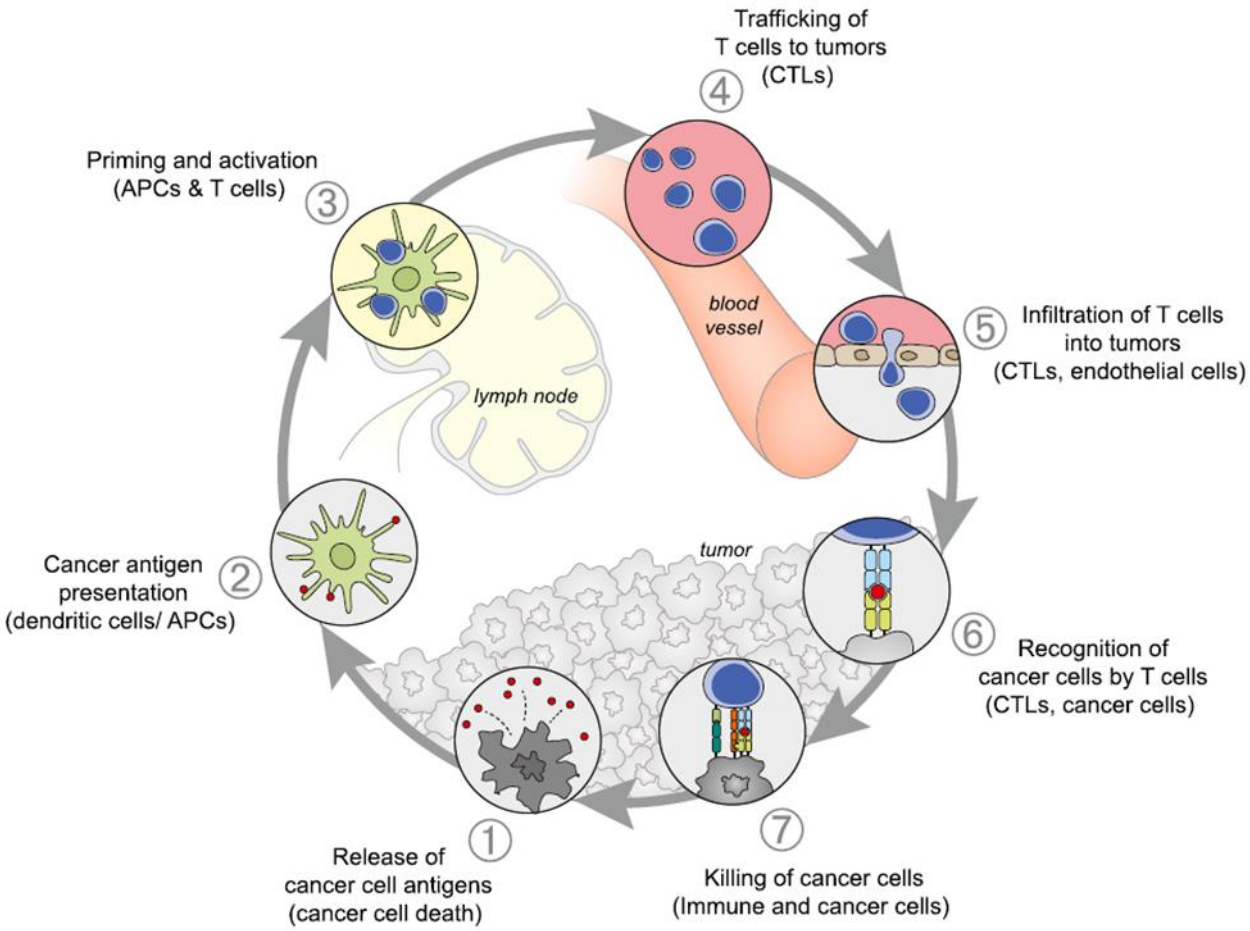

Figure 4| The cancer-immunity cycle.

APCs: Antigen Presenting Cells; CTLs: Cytotoxic T Lymphocytes. From [17].

3) Concept of immunoediting: the three Es

The term "cancer immunosurveillance" was discredited in 2003. As described above, this process was initially thought to be a host protective function by the immune system at the onset of malignant cell transformation. However, it has been recognized that both the adaptive and innate compartments of the immune system serve not only to protect the host from tumor development but also to sculpt and edit the immunogenicity of the tumors that may eventually form. Thus, the term "cancer immunoediting" has been proposed to more appropriately emphasize the dual role of the immune system in not only preventing but also shaping neoplastic diseases. This process is composed of three phases, named the "three Es": elimination, equilibrium, and escape [14].

a. Elimination

Elimination represents the original concept of cancer immunosurveillance. The cancer elimination phase is a continuous process that must be repeated each time antigenically distinct neoplastic cells are born. For this reason, cancer is more frequent in elderly people in whom the immune function, and thus the immunosurveillance of cancer, declines [14].

b. Equilibrium

During the equilibrium phase, the host immune system and the tumor cells that survived the elimination phase enter a state of dynamic equilibrium. T cells and IFNγ exert relentless selective pressure on the tumor cells, sufficient to contain but not completely eradicate a tumor bed containing many genetically unstable cells. This phase should be viewed as a Darwinian selection process. Thus, although many original tumor cells are destroyed, new variants arise. These variants carry different mutations that give them an advantage and increase immune attack resistance—this equilibrium phase results in the survival of a new population of tumor clones with reduced immunogenicity. Equilibrium is probably the longest of the three phases and can last for several years in humans. Indeed, for some solid cancers, it is estimated that 20 years may separate the initial exposure to the carcinogen and the clinical detection of the tumor. During this period, the heterogeneity and genetic instability of the cancer cells that survive the elimination phase are probably the main factors that allow cancer to resist the host immunological siege.

A clinical illustration of this phase may come from the transmission of cancer following organ transplantation from a donor to a recipient. Thus, metastatic melanoma has been reported to occur one to two years after transplantation of two kidney allografts from the same donor. Analysis of these cases showed that the donor had been treated for a primary melanoma 16 years before her kidney donation but was reported as healthy at the time of her death. Three other cases of melanoma were reported following kidney and liver transplantation less than a year after these organs were transplanted from a donor with no history of cancer. These observations, along with others in the literature, suggest that pharmacological suppression of recipient immune systems facilitated the rapid and progressive growth of tumors previously maintained in equilibrium by the competent donor immune system [14].

c. Escape

Escape from the immune system is now one of the common characteristics of cancer cells described above (cf on page 26 Universal hallmarks of cancer). During this phase, tumor cells selected during the equilibrium phase can grow. This breach of host immune defenses probably occurs when genetic and epigenetic changes within the tumor cells confer resistance to detection and/or elimination by the immune system allowing the tumor to become clinically detectable. Tumor cells must employ multiple evasion strategies to thwart the immune system's innate and adaptive anti-tumor responses. Thus, it is likely that several tumor-sculpting immunological events occur before the immunogenic phenotype of a malignant cell is finally established. Much work has focused on defining tumor escape's molecular and cellular mechanisms. They operate at many levels and involve the tumor, the tumor microenvironment, and the innate and adaptive components of immunity. In general, two categories can be identified: induction of immune tolerance by the tumor and resistance to destruction by activated effector immune cells [18]. These mechanisms include:

- Downmodulating tumor antigen presentation
- Inducing Tregs
- Disabling antigen presentation cells such as DC but also macrophages and microglia
- Promoting tolerogenic CD4+ T cells
- Causing dysfunctioning CD8+ T cells
- Coinhibiting cytotoxic T cells

Although cancer immunology is a growing field of research, immune activation and differentiation mechanisms of immune cells are still poorly described. However, the study of epigenetics of immune cells, particularly T cells, has greatly increased over the past decades. Below we will highlight epigenetic aspects underlying immune cell functions, emphasizing DNA methylation modifications occurring in T cells.

C. Epigenetics of adaptative immune cells

As described earlier, the adaptive immune system exhibits remarkable phenotypic and functional plasticity during immune responses. Activation of Naïve T cells triggers widespread alterations in cell cycle, metabolism, and protein expression, resulting in the generation of cells with distinct cellular phenotypes. While this flexibility is encoded in the DNA, cells themselves are genotypically identical. The ability of cells

to use identical underlying genomes to generate diverse phenotypes is partly accounted for by epigenetics.

Immune cells response is governed by a wide range of epigenetic mechanisms. In this manuscript, we will focus on the description of DNA methylation in T cells.

1) Overview of DNA methylation

In somatic cells, 5-methylcytosine (5mC) is predominantly found on CG dinucleotide (CpG)-dense regions, termed CpG islands (CGIs), which are located primarily at transcriptional start sites. Genome-wide studies employing whole genome bisulfite sequencing assessed cytosine methylation and have demonstrated that highly transcribed genes have largely unmethylated CpG promoters. In contrast, non-transcribed genes exhibit high levels of cytosine methylation in the CpG context of their promoters [19], [20]. That is why DNA methylation is considered a gene repressive mark. Although high DNA methylation levels lead to gene silencing, in cancer cells DNA hypermethylation also correlates with overexpression of a fraction of genes. The correlation between DNA methylation and transcriptome in cancer cells is, therefore, not straightforward and rather reflects a broader reprogramming of the epigenome. For instance, redistribution of the polycomb repressive complex (PRC2) leads to ectopic activation of developmental genes harboring bivalent chromatin modifications [21]. The role of methylation in neighboring CGI shores and shelves, intergenic non-coding regions, and gene bodies remains poorly understood. However, increasing evidence also implicates DNA methylation and chromatin modifications as mechanisms governing the functionality of enhancers to keep genes expressed at low levels but poised for rapid activation.

Cytosine DNA methylation is achieved by the family of DNA methyltransferases (DNMTs). DNMT3A and DNMT3B establish *de novo* methylation patterns, whereas DNMT1 is responsible for methylation maintenance during DNA replication.

Until a decade ago, it was believed that 5mC was exclusively diluted during cell division. The discovery that Ten Eleven Translocation (TET) proteins regulate active DNA demethylation revolutionized our understanding of the DNA demethylation process [22]. TET demethylases comprise three members (TET1, 2, and 3). and are DNA hydroxylases that convert 5mC to 5hmC [23], [24]. TET enzymes can further oxidize 5hmC to generate 5-formylcytosine (5fC) and 5-carboxylcytosine (5caC) [24], [25]. During active DNA demethylation (replication-independent), the 5-caC is eventually

decarboxylated by thymine-DNA glycosylase (TDG) and converted to cytosine through base excision repair [26], [27]. During passive demethylation, 5hmC is diluted via replication [28], [29]. 5hmC is found at both genic and intergenic regions of the genome, where it correlates with transcriptional activation [30]. Besides promoting DNA demethylation, 5hmC and the less abundant 5fC and 5caC are stable epigenetic marks that can recruit specific readers to impact genomic stability, DNA repair, and transcriptional elongation.

TET proteins exhibit cell type-specific binding patterns and affect chromatin accessibility. Significantly, enrichment of 5hmC correlates with open chromatin conformation and increased chromatin accessibility. Recent studies reveal that different genomic loci exhibit varying sequences of epigenetic reorganization to govern gene expression. Moreover, some genomic loci first show changes in chromatin and then show altered methylation, some loci exhibit simultaneous alterations of chromatin and DNA methylation, and some undergo methylation changes before chromatin rearrangements, although less frequently [31]. In all these cases, TET proteins interact with pioneer transcription factors and subsequently influence the binding of transcription factors to regulatory elements such as enhancers [32]. Other studies in murine immune cells established that a lack of TET proteins does not result in global DNA hypermethylation. Instead, TET proteins exert a focal impact on the DNA methylation status at specific genomic loci during development to establish cell lineage identity.

2) Lineage specification

Underlying all immune responses are the developmental programs that give immune cells their identities. These cells are derived from hematopoietic stem cells, which differentiate into lymphoid progenitors that further branch out to either CD8 or CD4 T cells. Naïve CD8 and CD4 T cells encounter an antigen presented by an APC, which activates differentiation programs toward memory and effector functions. Once activated, CD4 T cells initiate distinct gene expression programs that produce multiple functionally specialized T helper (Th) subsets such as Th1, Tregs, etc...

a. 5hmC remodeling precedes T cell lineage specifications

TET proteins in T and B-cells ensure proper maturation and cell fate establishment [33]. However, 5hmC is infrequent in immune populations, where it is reported to account for only 1% of the total level of 5mC. Studying the distribution of

5hmC in the genome, which is cell type-specific, is challenging and requires sensitive techniques at nucleotide resolution.

Tsagaratou *et al*. looked at 5hmC across sequential, well-defined, steps of T cell development. This system has the advantages of i) having a well-established precursor-progeny relationship, ii) describing transcriptional networks that govern the distinct decisions of lineage choice versus alternate lineage rejection, and iii) enabling the isolation of highly pure populations at distinct stages. Thus, the authors isolated *ex vivo* T cells subsets during thymic development, starting with double positive (DP) thymocytes, CD4 single positive (SP) cells, CD8 SP cells, naïve CD4 and CD8 T cells from the periphery, and CD4 T cells that were polarized and subsequently expanded *in vitro* towards Th1 and Th2 lineages. CD4 and CD8 SP cells exhibit the highest levels of 5hmC, while differentiated Th1 and Th2 cells have the lowest levels. Time course experiments until five days reveal that 5hmC is abundant in Th1 and Th2 subsets up to 48 hours of culture but is passively diluted across cell division. Gene-body 5hmC positively correlates with Pol II, H3K4me3, and H3K36me3 (markers of active transcription) and negatively correlates with H3K27me3 (a marker of negative transcription). Intragenic 5hmC levels are very high in Zbtb7b (encodes ThPOK), which is essential in CD lineage fate, and RUNX3, which determines CD8 lineage differentiation. Substantial intragenic gain of 5hmC is also observed in other important genes of the T cell lineage, such as Bcl11b, Satb1, and Gata3 [28]. This elegant experiment reveals that TET proteins turn on the expression of lineage specifying transcription factors that govern cell differentiation. Then, 5hmC levels are gradually diminished as the cell identity is established. *In vitro* polarization of human naïve CD4 T cells towards helper lineages demonstrate that 5hmC remodeling across the genome occurs early after activation and before any differentiation [34], [35]. Thus, 5hmC seems critical for the initial step of the specification to helper lineages but is not required during the expansion phase.

Interestingly, the analysis of simultaneous Tet2/3 KO mice did not reveal compromised CD4 and CD8 SP differentiation, nor differential expression of Runx3, but a dysregulated development and proliferation of NKT cells. More precisely, NKT cells display pronounced skewing toward the NKT17 lineage, which was attributed to increased DNA methylation and impaired expression of genes encoding the key lineage-specifying factors T-bet and ThPOK, which then repress the expression of RORγt [36].

b. TET enzymes stably maintain T cell fates

TET proteins and 5hmC are instrumental in maintaining the cell's identity. In Tregs, they prevent the methylation of regulatory elements, which in turn prevent the silencing of Foxp3. Tet2-deficient mice exhibit reduced numbers of Tregs [37]. In human cells, simultaneous deletion of TET1 and TET2 significantly reduces the abundance of Tregs due to defective demethylation of the CNS2 locus of FOXP3, and notably, TET1 and TET2 directly associate with CNS2 [38]. Moreover, concomitant deletion of TET2 and TET3 at the DP cell stage using CD4-cre mice exerts a more severe impact on the stability of Foxp3 expression due to aberrant methylation of the CNS2 locus [39]. Deleting TET2 and TET3 specifically in Tregs using Foxp3-cre mice not only compromises the stability of the Treg lineage but also results in a gain of effector fate function and aberrant hyperactivation [40], [41]. These articles demonstrate that stable expression of FOXP3 requires the cytosine demethylation of the CNS2 intronic enhancer, which is actively regulated by all three TET proteins. Locus-specific recruitment of TET proteins might be facilitated through direct interaction with transcription factors. In Tregs, members of the STAT family recruit TET proteins at enhancers [42].

It has also been shown that TET1 and TET3 can act together during thymic development to control the methylation status of enhancers that later regulate Cd4 gene expression in the periphery of mice [43]. This observation suggests that 5hmC deposition enables enhancers to be in an open conformation to control gene expression at subsequent developmental stages. A hypothesis that needs to be validated would be that the dynamic distribution of 5hmC in highly expressed genes during T cell lineage specification could potentially be involved in priming enhancers that will become fully activated and induce gene expression later in development.

In conclusion, despite the increasing discoveries related to TET proteins, the precise mechanisms of TET functions in immune cells remain elusive. This is attributed in part to the complexity of emerging phenotypes upon TET loss in mice model and the technical challenges that hinder the detailed investigation of the individual role played by each TET protein. As we move forward, it is critical to take advantage of novel techniques to decipher the TET interactome.

c. Regulation of memory differentiation

The functional and phenotypic changes during the differentiation process are well characterized, but the epigenetic states that underlie these changes are

incompletely understood. Different T cell lineage relationship models have been proposed over time to account for the predominance of effector T cells during the acute phase of immune responses and memory T cells at later stages after an antigenic challenge. According to the circular model (Figure 5 A), Naïve T cells differentiate into effector T cells. After pathogen clearance, effector T cells either undergo apoptosis or differentiate into memory T cells, where they await secondary antigen encounter before beginning the cycle again [44], [45]. The circular nature of this model suggests cycles of dedifferentiation and redifferentiation, a process not known to occur in adult somatic tissues [46]. Alternatively, according to the developmental or linear differentiation model (Figure 5 B), the strength and duration of antigenic and inflammatory signals are critical determinants of T cell differentiation. Strong or repetitive signals progressively drive the acquisition of effector and terminal effector characteristics. In contrast, weak signals fail to drive complete effector differentiation and, instead, result in the differentiation of memory cells. Thus, although effector cells are predominant during the early stages of immune responses, these cells represent the final stage of T cell differentiation and die upon antigen withdrawal. Left behind is the comparatively smaller population of memory T cells that failed to fully differentiate into effector T cells but persist as long-lived memory T cells [47]–[49].

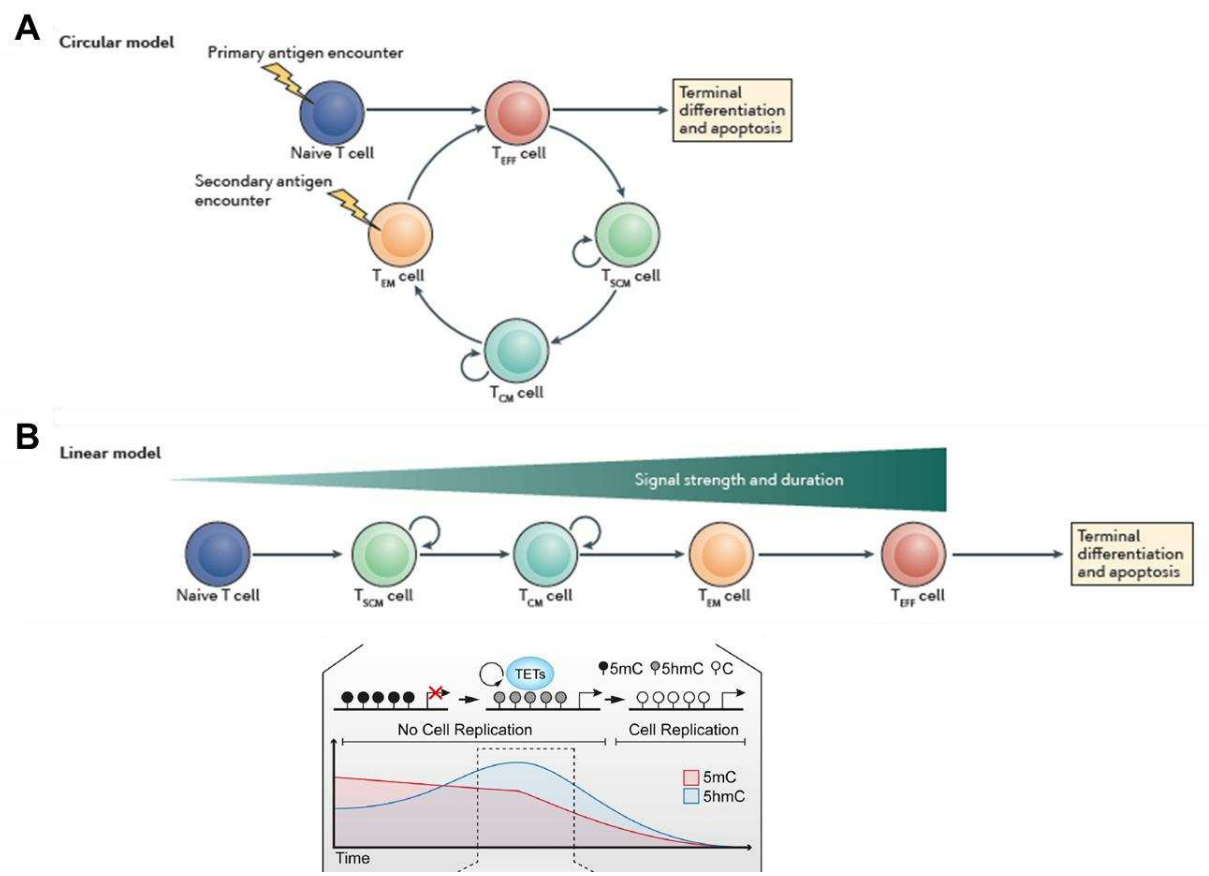

Figure 5| CD8 T cell differentiation models.

A| In the circular model of CD8+ T cell differentiation, effector T cells represent biological intermediaries that either undergo apoptosis or differentiate into memory T cell subsets following antigen withdrawal. **B|** In the developmental, or linear, differentiation model, the progressive acquisition of effector function during CD8+ T cell differentiation depends on the strength and duration of antigenic signaling. It results in the gradual loss of memory-associated gene expression and the gain of effector-associated gene expression. These transcriptional changes are accompanied by early 5hmC gains, which then predict the loss of DNA methylation in differentiated cells. TCM: central memory T; TEM: effector memory T; TSCM: stem cell memory T. Adapted from [34], [50]

This is illustrated in the work of Abdelsamed et *al.*, who observed the changes in DNA methylation as cells differentiate from Naïve cells into memory subsets: stem cell memory T (T_{SCM}) cells, central memory T (T_{CM}) cells, and effector memory T (T_{EM}) cells. They showed that cytokine-driven proliferation of T_{CM} and T_{SCM} cells resulted in phenotypic conversion into T_{EM} cells and was coupled to increased methylation of the CCR7 and TCF7 loci. Interestingly, the epigenome of T_{CM} and T_{SCM} cells is similar to both naïve and effector T cells, which places memory T cells as an intermediate step within T cell differentiation [51]. Overall, multiple studies in mice and humans found that histones activation-associated modifications, such as H3K4me3 and H3K9ac, are lost during T cell differentiation and that repressive DNA methylation and H3K27me3 modifications are gained at gene loci whose expression is reduced in effector cells. This includes memory-cell-associated transcription factors such as FOXO1, KLF2, LEF1, and TCF7, and genes highly expressed in memory cell subsets, including IL2RA, CD27, TNF, CCR7, and SELL. Alternatively, effector-cell-associated transcription factors (EOMES, TBX21, and PRDM1) and functional effector genes (GZMA, GZMB, PRF1, IFNG, and KLRG1) demonstrate decreased repressive and increased activating epigenetic modifications in effector cells [50]. All these results prompted researchers to establish an epigenetic atlas of both murine and human CD8+ T cells in which they describe ~250 CpG sites that are predictive of the cell's developmental potential and can therefore be used to delineate the differentiation status of CD8 T cells [45], [52].

In conclusion, transient exposure to antigen induces effector and memory-associated functions coupled to epigenetic programs, which are preserved during T cell homeostasis, ultimately maintaining cell fate decisions.

3) Therapeutic modulation of T cell differentiation

In addition to terminal differentiation, strong or chronic antigen exposure, such as in the context of cancer, induce extrinsic and intrinsic immunosuppressive mechanisms that can become imprinted to stably reduce T cells' effector functions. Immunotherapeutic options to increase cancer-specific T cell responses include, but

are not limited to, immune checkpoint blockade (ICB) and cellular therapies such as chimeric antigen receptor (CAR)-T cell transfer[3]. Several research groups have begun to identify further the specific subsets that contribute to the clinical response and define the cell fate-determining mechanisms that reinforce anti-tumor functions.

a. Immune checkpoint blockade

Recent studies have shown that the expression of TCF7 by CD8+ T cells can predict the response to ICB in melanoma patients. Downregulation of the TCF1 protein (encoded by TCF7) in the memory–precursor-like T cell subset was coupled to a failure to respond to immunotherapy, while the less terminally differentiated TCF1+ memory–precursor-like T cell subset correlated with a more robust response to ICB [53]. Moreover, transcriptome analysis of early-emerging exhausted cells shows an increased expression of multiple repressive DNA and histone-modifying enzymes, including DNMT1, DNMT3B, and EZH2 [54], suggesting epigenetic regulation of exhaustion. Although the conditional loss of DNMT3A in CD8 effector T cells did not abolish the development of exhaustion, it did alter the phenotypic composition of exhausted cells. Specifically, an increase in the frequency of less-differentiated exhausted T cell subsets was observed in conditional knockout mice, characterized by high levels of T-bet and TCF1 expression and decreased TIM3 and EOMES expression. The loss of DNMT3A acts synergistically with checkpoint inhibition during a chronic LCMV infection mice model [55]. Moreover, scRNA-Seq analyses suggest that metallothionein 1 and GATA3 function as specific contributors to T cell dysfunction [56], and ATAC–seq analysis identifies multiple exhaustion-specific chromatin accessibility loci [57]. This includes *PDCD1* and lymphocyte activation gene 3 protein (LAG3), which display both exhaustion-specific and activation-specific enhancers. Motif analysis at the potential exhaustion-specific enhancers identifies an enrichment of nuclear receptor subfamily 4 group A and nuclear factor of activated T cells (NFAT) binding sites, suggesting that these transcription factors specifically regulate the described exhausted state [57], [58].

In a tumor-driven model of exhaustion, drug-mediated reduction of NFAT activity results in decreased expression of PD1 and LAG3 and increased expression of TCF1 in adoptively transferred cells, in addition to increasing polyfunctionality after *ex vivo* culture with IL-15 [58].

[3] Immunotherapeutic approach whereby T cells are engineered to express an antibody-derived surface receptor specific for a tumor antigen, and subsequently transferred into patients.

b. CAR T cells

During CAR T cell production, allogenic bulk T cells from a patient's blood are isolated and then activated with CD3/CD28 ligation antibodies, genetically modified to express tumor-targeting TCRs or CARs, and expanded with IL-2 for 7–14 days. While this allows for the reliable generation of clinical CAR T cell products, T cells are skewed toward terminal differentiation during the amplification process.

Investigators have shown that preselecting naïve T cells and T_{CM} subsets prior to T cell activation improves CAR T cells' effector functions. However, peripheral T cells of cancer patients, who are heavily pretreated, have a predominant T_{EM} phenotype [59]. Thus, current approaches to preserve CAR T cell function include modulating the signaling domains of CARs and additional genetic modifications. For example, human CD19.41BBz CARs induce a central memory phenotype poststimulation compared to CD19.CD28z CAR T cells, resulting in improved persistence during *ex vivo* culture [60]. Additionally, mutating immunoreceptor tyrosine-based activation motifs (ITAMs) in the CD3z signaling domain preserves effector function while maintaining memory programs, which resulted in the persistence of functional long-lived CAR T cells in mice [61].

Purposefully modifying the epigenetic profile of human T cells might allow for engineered resistance to T cell exhaustion and yield a long-lived pool of CAR T cells that can maintain anti-tumor responses during chronic tumor antigen exposure. Interestingly, *ex vivo* culture with the bromodomain inhibitor JQ1 results in increased memory formation, greater T cell persistence, and anti-tumor activity upon adoptive transfer. Mechanistically, the BET protein BRD4 directly regulated the expression of the transcription factor BATF in CD8+ T cells, which was associated with differentiating T cells into an effector memory phenotype. JQ1 directly inhibits the histone acetylation reader BRD4 and indirectly inhibits the histone deacetylase SIRT1 [62].

Very importantly, a paper published in 2016 demonstrates that the metabolic by-product L-2-hydroxyglutarate (L-2HG) accumulates in mouse CD8+ T cells in response to TCR triggering and accumulates to millimolar levels in physiological oxygen conditions through a hypoxia-inducible factor 1-alpha (HIF-1a)-dependent mechanism. *Ex vivo* culture of naïve CD8 T cells with L-2HG decreases phenotypic effector markers, and L-2HG treatment promotes *in vivo* homeostatic renewal, persistence, and anti-tumor capacity of transferred cells in mice. These effects were attributed to L-2HG-mediated alteration of H3K27me3, 5hmC, and 5mC [63]. These

results encouraged the authors to study the generation of CAR T cells in the presence of L-2HG. After eight days of culture, they showed that L-2HG drives human pan-T cells toward a TCM phenotype. Treatment during twelve days with L-2HG results in significantly higher numbers of T_{CM} and T_{EM} cells and lower T_{EMRA} cells compared to vehicle. This was reproduced during CAR T cell *ex vivo* generation and resulted in enhanced anti-tumor activity compared to CAR T cells generated without L-2HG. Intriguing, they observed that tumor progression is significantly lower when naïve populations were used for CAR-T generation compared to the generation of these cells from total CD8 T cells [64]. This suggests that the epigenetic program of differentiated cells has already been established and that L-2HG alone is not capable of epigenetically rewriting cells to a memory state. Moreover, a recent case report on the vector integration-mediated disruption of TET2 in CAR T cells resulted in the clonal expansion of a single CAR T cell that induced leukemia remission [65].

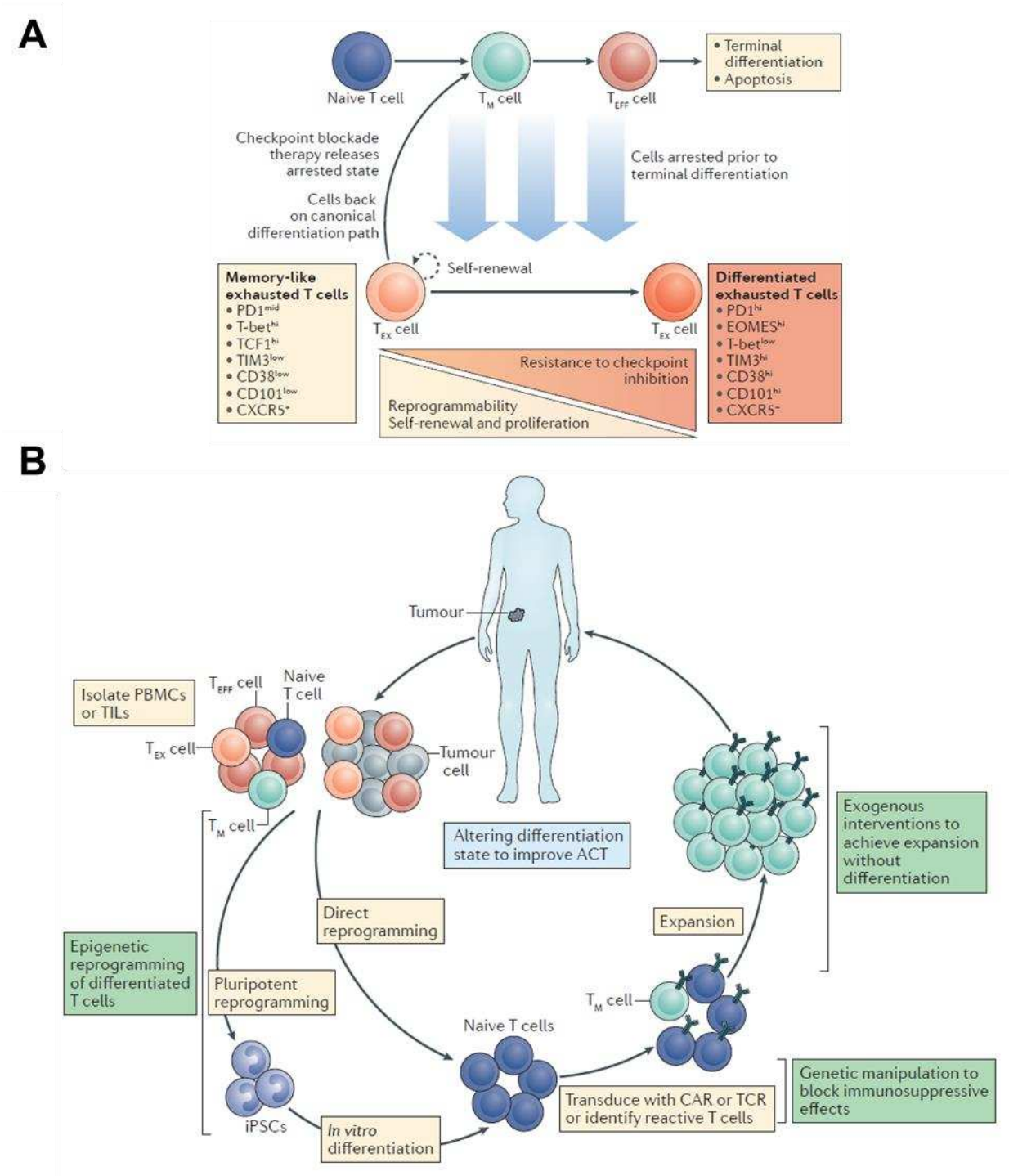

Figure 6| Epigenetics modulation to improve immunotherapy.

A| The arrested model of CD8+ T cell exhaustion. This model represents a branchpoint of the linear differentiation model, at which strong and/or repetitive antigenic stimulation, often accompanied by a lack of co-stimulatory signals, arrests canonical differentiation. Increasingly, it has been shown that the exhausted state is heterogeneous, with a subset of exhausted T (T_{EX}) cells exhibiting memory-like phenotypes and characterized by specific cell surface markers (left side, light orange box). Conversely, more differentiated T_{EX} cells exhibit their own unique cell surface marker expression (right side, dark orange box). The stage along the linear T cell differentiation at which cells become arrested may determine their T_{EX} cell phenotype (light blue arrows); however, continued differentiation within the exhausted state may also occur. **B|** Epigenetic interventions for improving immunotherapy. Currently, T cells used for adoptive cell therapy are either obtained directly from the tumor (TIL) or the peripheral

blood (PBMC) of the patient. These cells are then activated and transduced with a tumor-reactive chimeric antigen receptor (CAR) or T cell receptor (TCR), followed by an extensive ex vivo expansion step before reinfusion into the patient. One limiting factor of this therapeutic is that, in both the starting T cell population and the population obtained following expansion, cells exhibit a more differentiated and/or exhausted phenotype, which may hinder in vivo effectiveness. Cellular reprogramming of PBMCs or TILs would obtain a less differentiated starting population, and pharmacological interventions to target relevant signaling pathways and/or epigenetic modifying proteins could allow for T cell expansion without differentiation. CXCR5: CXC-chemokine receptor 5; EOMES: eomesodermin hhomolog PD1: programmed cell death protein 1; TCF1: transcription factor 1; TIM3: T cell immunoglobulin mucin receptor 3; T_M: memory T; T_{EFF}: effector T, iPSCs: induced pluripotent stem cells; T_{EX}: exhausted T. Adapted from [50]

Altogether, these data demonstrate that pharmacological manipulation of epigenetic mechanisms can alter T cell differentiation in a clinically relevant manner. Of note, L-2HG is the enantiomer of R-2HG, an oncometabolite produced by IDH mutant glioma tumor cells and various tumor types. In the next section, we will describe these very special tumors to understand the implication of cell-intrinsic and cell-extrinsic roles of R-2HG on gliomagenesis.

II) MALIGNANT PRIMARY ADULT DIFFUSE GLIOMAS

In this section, we describe adult-type diffuse gliomas clinically and genetically and focus on the comparison of glioblastomas (GBM) with both oligodendrogliomas (IDH-O) and astrocytomas (IDH-A).

A. Definition and classification of central nervous system tumors

In 2012, the World Health Organization (WHO) defined cancer as a large group of diseases that can start in almost any organ or tissue of the body when abnormal cells grow uncontrollably, go beyond their usual boundaries to invade adjoining parts of the body, and/or spread to other organs. Nowadays, cancer is the second cause of death worldwide after cardiovascular diseases and accounted for an estimated 9.6 million deaths, or one in six deaths, in 2018. According to the WHO, cancer incidence will have doubled in 2040. The cancer burden continues to grow, exerting tremendous physical, emotional, and financial strain on patients, families, and health systems. Many health systems of developing countries are least prepared to manage this burden, where large numbers of patients do not have access to timely quality diagnosis and treatment. In developed countries, the survival rates of many cancers are improving

thanks to accessible early detection, quality treatment, and survivorship care. Lung, prostate, colorectal, stomach, and liver cancer are the most common types of cancer in men, while breast, colorectal, lung, cervical, and thyroid cancers are the most common among women. Cancers represent a very heterogeneous group of diseases with diverse prognoses. Their distribution depends on the patient's age and sex [66].

Regarding the tumors of the Central Nervous System (CNS), the fifth edition of the WHO Classification was published in 2021 and introduced new molecular diagnostic technologies such as DNA methylome profiling to complete other established approaches like histology and immunohistochemistry to offer a more integrated approach with hopes that oncology clinicians can more accurately diagnose, predict the efficacy of treatments, and enhance individualized therapeutic plans for patients. As the use of molecular biomarkers has been further elucidated, challenges have grown in how to properly organize the classification of CNS tumors. Indeed, some tumors are consistently characterized by defining molecular features; others have molecular parameters that are not required but may support their classification. Others are rarely or never diagnosed using molecular approaches. The new WHO taxonomy has grouped tumors according to the genetic changes that enable a complete diagnosis (e.g., IDH and H3 status); by looser oncogenic associations, such as MAPK pathway alterations; by histological and histogenetic similarities even though molecular signatures vary (e.g., neoplasms listed under Other Gliomas, Glioneuronal Tumors, and Neuronal Tumors); or by using molecular features to define new types and subtypes (e.g., medulloblastoma). This hybrid classification represents the field's current state but is likely only an intermediate stage to an even more precise future classification.

From 2014 to 2018, in the USA, brain and other CNS tumors (both malignant and non-malignant) were the most common cancer in children aged 0–14 years. They were the second most frequent for people aged 15-39 years after breast cancer (women only). Finally, they were the eighth most common cancer among persons aged 40+ years (Figure 7).

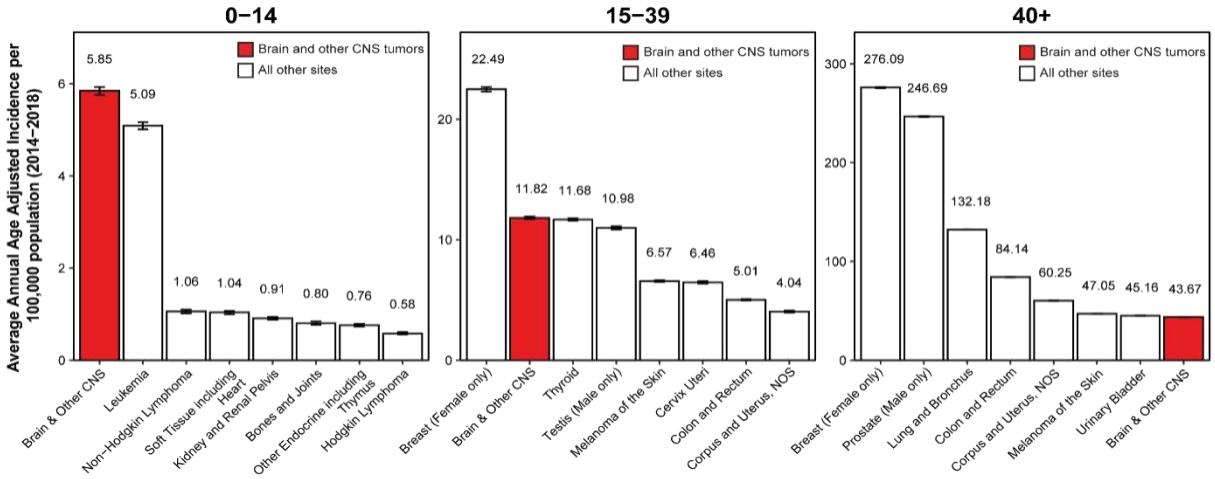

Figure 7| Average Annual Age-Adjusted Incidence Rates of cancers in the USA from 2014 to 2018.

95% Confidence Intervals of All Primary Brain and Other CNS Tumors in Comparison to Top Eight Highest Incidence Cancers for Children aged 0–14 Years, Adolescents and Young Adults aged 15–39 Years, and Older Adults aged 40+ Years [67].

More than 150 different brain tumors have been documented and display various histological features, localization, and aggressiveness. The two main groups of brain tumors are termed primary and metastatic. Primary brain tumors originate from the brain's tissues or the brain's immediate surroundings. Primary tumors are categorized as glial (composed of glial cells) or non-glial (developed on or in the brain's structures, including nerves, blood vessels, and glands) and benign or malignant. However, metastatic brain tumors include tumors that arise elsewhere in the body (such as the breast or lungs) and migrate to the brain, usually through the bloodstream. Metastatic tumors are always considered malignant. The distribution of malignant and non-malignant primary CNS tumors is shown in Figure 8. According to the Central Brain Tumor Registry of the United States (CBTRUS), the worldwide incidence rate of primary malignant brain and other CNS tumors in 2020, age-adjusted using the world standard population, was 3.5 per 100,000. Therefore, these tumors are relatively rare in humans and are only at the eighth place of most prevalent cancers for people over 40 years. Incidence rates by sex were 3.9 per 100,000 males and 3.0 per 100,000 females. This represented an estimated 168,346 males and 139,756 females diagnosed worldwide with a primary malignant brain tumor in 2020, 308,102 individuals. Incidence rates were higher in high-income countries (7.4 per 100,000) than in low-income countries (1.8 per 100,000). The average annual mortality rate in the US between 2014 and 2018 was 4.43 per 100,000 population, with 83,029 total deaths. This represents an average of 16,666 deaths per year. It was estimated that there would be 18,020 deaths in the US in 2020.

The frontal (24.4%), temporal (17.5%), parietal (10.4%), and occipital (2.6%) lobes accounted for 54.9% of tumors. The most frequently reported histology was glioblastoma (GBM, 49.1%), followed by IDH-A (11.9%), which are both parts of the broad group of diffuse gliomas (Figure 8) [68].

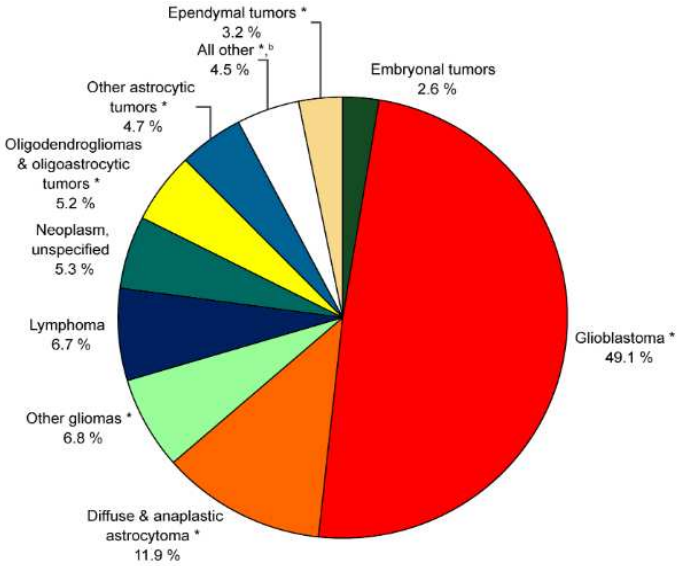

Figure 8| Distribution of All Primary Brain and Other CNS Tumors by histology.
From [67]

B. Description of primary malignant adult diffuse gliomas

1) Epidemiology

Gliomas arise from the supporting cells of the brain, called the glia. These cells are subdivided into astrocytes, the most abundant CNS cells that regulate neuronal activity and homeostasis; ependymal cells, a component of the Blood-Brain Barrier (BBB); and oligodendroglial cells, which produce myelin wrapping axons. Gliomas are divided into four grades. According to the 2021 WHO classification, diffuse gliomas comprise GBM (grade 4), IDH-A (grade 2-4), and IDH-O (grade 2-3). They are defined as diffuse because they progress and invade the brain parenchyma in an uncircumscribed way.

Risk factors for gliomas and, particularly for GBM, are largely unknown. Genetic risk factors currently identified are the hereditary genetic predisposition syndromes to cancers involved in neurofibromatosis type 1, tuberous sclerosis of Bourneville, Li-Fraumeni syndrome, and Turcot syndrome. However, these factors only explain a small

proportion of gliomas. Similarly, familial glioma cases are reported in the literature, but they account for less than 5% of patients [69]. Several common genetic polymorphisms of single base have been associated with a moderate increased relative risk [70], [71]. Among other risk factors, exposure to ionizing radiation is the most documented. Several pathophysiological factors, such as the influence of non-ionizing radiation (e.g., cell phones) or electromagnetic fields, have been discussed with currently inconclusive results. Allergic conditions (asthma, eczema, specific food allergies, etc.) are associated with a significant decrease in developing gliomas. The contribution of other environmental factors has also been studied. Contradictory results have been demonstrated for pesticides or chlorinated solvents, requiring further research [70], [71].

2) Prognosis

The median age at diagnosis for GBM is 65 years for 38 and 45 for IDH-A and IDH-O, respectively. The overall survival for GBM tumors is meager with 15 months and is longer for IDH-A and IDH-O with 6 years and 15 years, respectively (Figure 9). Age at diagnosis significantly impacts survival time. For instance, 40+ years old patients have poorer survival compared to children, and women have better outcomes than men [67].

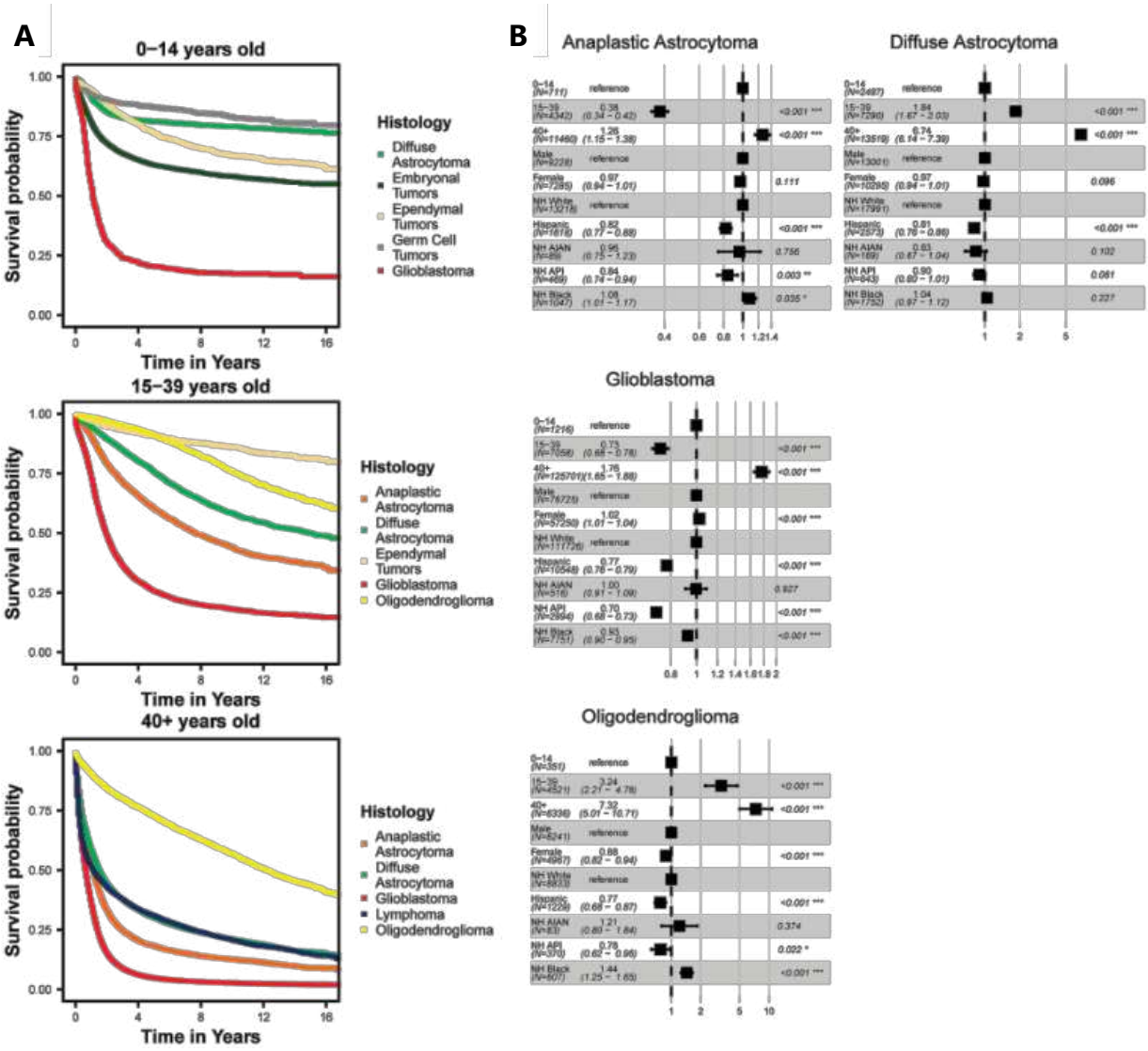

Figure 9| Survival analysis of the five most common histologies of malignant gliomas.

A| Kaplan-Meier survival curves for the five most common histologies of malignant gliomas within the age group at diagnosis (0–14, 15–39, and 40+ years). **B|** Hazard Ratios and 95% confidence intervals for sex, age at diagnosis, race, and ethnicity [67].

3) Symptoms

The evolution of neurological symptoms enables the estimation of the growth dynamics of gliomas. Tumors that cause symptoms only weeks before diagnosis are usually fast-growing, whereas those that cause symptoms for years before diagnosis are typically slow-growing. A discussion of the patient's history might reveal familial risk or rare exogenous risk factors (such as exposure to radiation) associated with developing brain tumors. When proliferating, glioma cells exert pressure on the brain or spinal cord, which causes symptoms. The diagnosis of a diffuse glioma is most often suspected when neurological signs worsen progressively. They are diverse, insidious,

and non-specific, such as progressively worsening headaches, new-onset epilepsy, focal deficit, neurocognitive impairment, etc.

The physical examination of patients focuses on the neurological deficits and general examination. Brain scans, including Magnetic Resonance Imaging (MRI), are the reference tool that confirms the mass syndrome and assesses the lesion's extent, vascularization, metabolism, and anatomical localization. It can also refine the differential diagnosis (brain abscess, metastasis, or lymphoma). A thoracic-abdominal-pelvic computed tomography (CT) scan may be performed in case of doubt with the metastatic lesion.

4) Diagnosis

Intraoperative assessment of cytological specimens or frozen sections ensures that sufficient tumor tissue is obtained to establish a diagnosis. Tumor tissue is formalin-fixed and embedded in paraffin for histological and immunohistochemical staining as well as for molecular genetic and cytogenetic biomarkers studies. Some tumor tissues are also cryopreserved for molecular assessments that require high-quality DNA and RNA samples.

a. Histology

Despite the efforts of harmonization and the different technologies available to improve glioma diagnosis, the latter remains complex due to the significant heterogeneity of these tumors. The desirable criteria of the 2021 classification is a flagrant example of this diversity. Nevertheless, the diagnosis of glioma is validated based on neuropathologist observations of hematoxylin and eosin and immunohistochemistry staining of tumor resection or biopsy samples. Adult gliomas are also distinguished on the histological level. They present proliferative characteristics measured by mitosis indexes and necrosis, vascular alterations, and cytomorphological changes.

Histologically, IDH-O presents a unique feature by the presence of a white halo at the perinuclear level, as shown in Figure 10. Cells are very rounded, and density increases with the grade of the tumor as well as the presence of necrosis. IDH-A have a lower cell density with a typical fibrillary aspect. Mitotic abnormalities and, sometimes, giant cells can also be observed. GBMs show necrosis and

pseudopalisading, with hypercellularity, and mitotic abnormalities of hypertrophied cells.

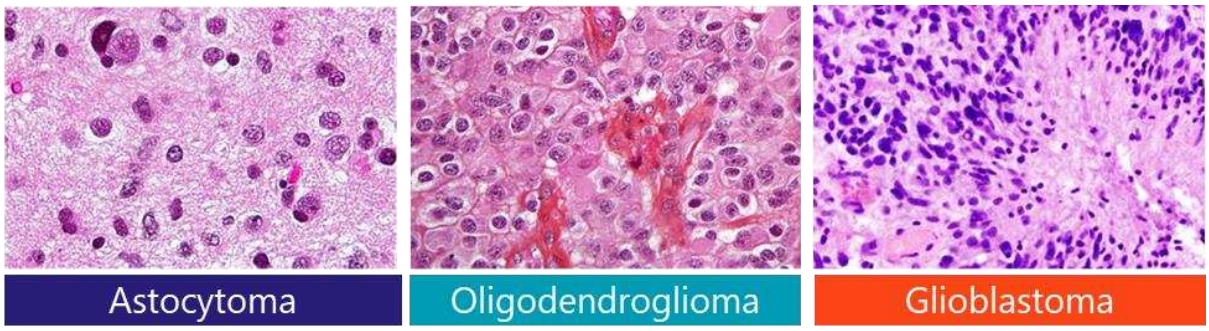

Figure 10| Histological characteristics of diffuse gliomas.

Images from K. Mokhtari.

The heterogeneity of the histological characteristics of these tumors and their similarities from one type to another made the diagnosis difficult. This was notably the case of a kind of adult glioma, called "oligoastrocytoma", which disappeared in the 2016 classification, which resulted from mixed features between IDH-A and IDH-O. That is why the development of technologies for characterizing DNA, RNA, and DNA methylation led to the inclusion of genetic biomarkers in the 2016 WHO Classification.

b. Genetic biomarkers

The following molecular biomarkers are now central to categorizing diffuse gliomas in adults: IDH mutation, 1p/19q co-deletion, histone H3 K27M mutation, histone H3.3 G34R/V mutation, TERT promoter mutation, EGFR gene amplification, chromosome 7 gain combined with chromosome 10 loss, and homozygous deletions on 9p21 involving the CDKN2A and CDKN2B gene loci (CDKN2A/B homozygous deletion). One of the earliest discoveries in glioma biomarkers was that IDH-O has the specificity to harbor complete deletions of the short arm of chromosome 1 (1p) and the long arm of chromosome 19 (19q), associated to an improved response to chemotherapy, radiation, and increased survival [72]–[74]. Moreover, a mutation in IDH 1/2 is common in IDH-O and IDH-A and has also been associated with improved prognosis [75]–[77]. Both of these alterations are thought to occur relatively early in gliomas' development, as discussed later.

IDH-A usually also has a loss of nuclear expression of alpha thalassemia/mental retardation syndrome X-linked (ATRX) and mutations in TP53. Indeed, detecting nuclear ATRX loss in an IDHm glioma is even sufficient for diagnosing an astrocytic

lineage tumor without needing 1p/19q codeletion analysis. By contrast, retained nuclear ATRX positivity in an IDHm glioma should prompt investigation for 1p/19q codeletion to distinguish IDH-A from IDH-O [78]. This genetic feature is also related to an increased survival time [77], [79], [80]. IDH-A is now stratified into three WHO grades from 2 to 4. In addition to the established histological features, such as the presence of necrosis and/or microvascular proliferation, homozygous CDKN2A/B deletion is a marker of WHO grade 4 IDH-A and is indicative of a poor prognosis [81].

IDH-O are defined as IDHm gliomas that also harbor 1p/19q codeletion1 and are stratified into WHO grade 2 or 3 tumors based on the absence or presence of histological features of anaplasia. The role of molecular alterations in the grading of these tumors has not been defined. However, similar to IDH-A, the homozygous deletion of CDKN2A at 9p21 has been associated with shorter survival durations [82].

The absence of IDH mutation defines GBMs. They can display methylation of the promoter of O-6-methylguanine-DNA methyltransferase (MGMT). This gene is located on chromosome 10q26 and encodes a DNA repair enzyme that can limit the effects of alkylating chemotherapy. This class of medicine is administered to damage tumor DNA and lead to cell death. If the MGMT gene is active, DNA damage can be repaired, thus rendering the chemotherapy less effective. DNA methylation is a process by which methyl groups are added to DNA, and methylation of the MGMT gene makes the repair mechanisms inactive. Methylation of MGMT promoter is found in 35% to 45% of high-grade gliomas and about 80% of low-grade. In GBMs, methylation of MGMT is a favorable marker and can predict response to chemotherapy. They can also have a glioma-CpG island methylator phenotype (G-CIMP) or genome-wide DNA methylation that has significantly increased survival. However, the amplification of epidermal growth factor receptor (EGFR) activates the RTK/RAS/PI3K pathway, leading to increased proliferation and is associated with poorer survival in lower grade gliomas [77], [83], [84].

Some alterations are not mutually exclusive to either IDHm or IDHwt gliomas. For instance, the majority of IDH-O and GBM have a mutation of the promotor of Telomerase reverse transcriptase (TERT), another telomere maintenance-related gene with ATRX, which facilitates increased telomere lengthening and has been shown to decrease survival only in IDHwt glioma [85], [86]. An overview of the molecular features of diffuse gliomas is presented in Figure 11.

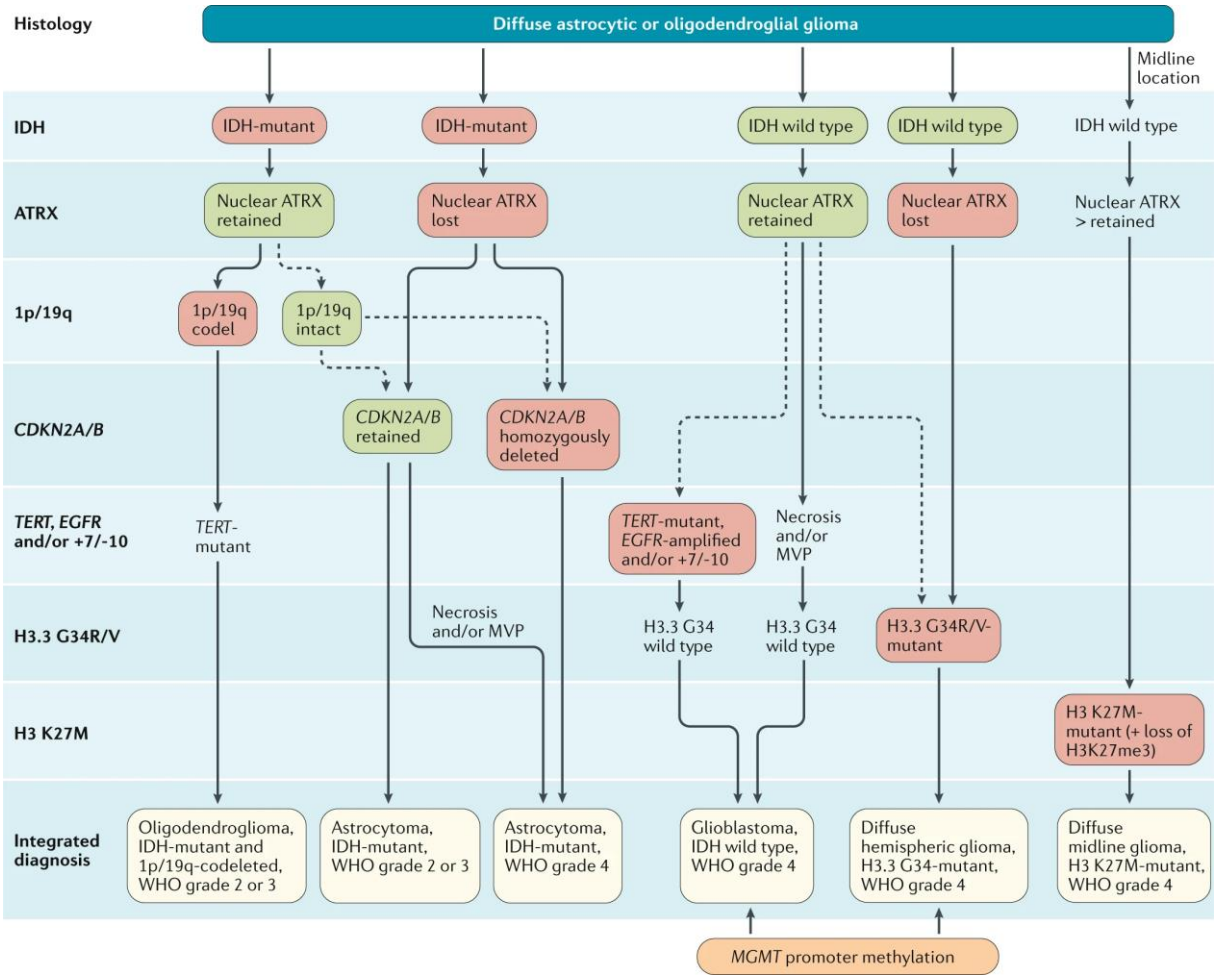

Figure 11| Diagnostic pathway for the major diffuse gliomas in adults.

Tissue specimens obtained through biopsy sampling in patients with diffuse gliomas are routinely assessed by immunohistochemistry for the presence of R132H-mutant IDH1 and loss of nuclear ATRX. In patients aged >55 years with a histologically typical glioblastoma, without a pre-existing lower grade glioma, with a non-midline tumor location, and with retained nuclear ATRX expression, immunohistochemical negativity for IDH1 R132H suffices for the classification as GBM. In all other instances of diffuse gliomas, a lack of IDH1 R132H immunopositivity should be followed by IDH1 and IDH2 DNA sequencing to detect or exclude the presence of non-canonical mutations. IDHwt diffuse astrocytic gliomas without microvascular proliferation or necrosis should be tested for EGFR amplification, TERT promoter mutation, and a +7/–10 cytogenetic signature as molecular characteristics of GBM. In addition, histone H3.3 G34R/V mutations should be assessed by immunohistochemistry or DNA sequencing to identify H3.3 G34-mutant diffuse hemispheric gliomas, particularly in young patients with IDHwt gliomas (such as those <50 years of age with nuclear ATRX loss in tumor cells). Diffuse gliomas of the thalamus, brainstem, or spinal cord should be evaluated for histone H3 K27M mutations and loss of nuclear K27-trimethylated histone H3 (H3K27me3) to identify H3 K27M-mutant diffuse midline gliomas. The presence and absence of the diagnostically most relevant molecular alterations for each tumor type are highlighted with red and green boxes. MVP, microvascular proliferation. From [78].

5) Standards of care

Glioma treatment is carried out by an interdisciplinary team as soon as the diagnosis is suspected and depends on their types and grades. The standard of care

for an individual patient considers the tumor location, potential symptoms, and benefit/risk ratio of the different treatment modalities.

a. Surgery

Treatment decisions are made based on tissue diagnosis, including the assessment of molecular markers relevant for diagnosis; therefore, upfront surgery is commonly performed with both diagnostic and therapeutic intent.

Surgery, also called "open surgery" (because it requires an opening in the skull), is usually the initial therapeutic approach to reduce tumor volume and relieve pressure in the brain. In addition to its diagnostic role, it contributes to the quality and duration of survival, depending on the localization of the tumor. In certain cases, excision surgery is not feasible for topographical or functional reasons or due to the patient's general condition or refusal. Once removed, the tumor is sent to the laboratory for analysis.

b. Radiation therapy and chemotherapy

Radiation therapy (RT) and chemotherapy usually follow surgery within six weeks once the diagnosis is established. The goal of radiotherapy is to improve local control without inducing neurotoxicity.

RT may be exclusive or combined with chemotherapy in a concomitant or sequential manner. Chemotherapy is most often administered systemically (oral or IV) and sometimes locally (intracavitary implant). An essential piece of information is that chemotherapy regimens are not internationally standardized, and most of the time, they are different in hospitals in the same country. Most patients with glioma receive Temozolomide (TMZ), an oral DNA alkylating agent that penetrates the BBB. This agent has a favorable safety profile, with myelosuppression, notably thrombocytopenia, as its main dose-limiting toxicity. Alkylating agents from the nitrosourea class, such as lomustine, are often combined with procarbazine and vincristine in a regimen called PCV.

i) GBM

The standard of care for GBM is currently defined by radiotherapy with or without TMZ. This standard is based on the trial (EORTC - NCIC trial) [87], [88] and has been supported by population studies in different countries [89]–[98]. Across studies,

there was a significant increase in median overall survival and the rate of long-surviving patients [88], [99]. TMZ is taken on an empty stomach (or at least 2 hours after the previous meal or 2 hours before the next meal), one hour before radiation therapy, at 75mg/m^2/day, for the duration of radiation therapy (total duration 42 days, maximum 49 days), including weekends. Even though small, the risk of severe and prolonged aplasia and thrombocytopenia on TMZ warrants weekly monitoring of blood counts during chemoradiotherapy. TMZ is discontinued if platelets are 100,000/mm^3, and a platelet transfusion pool is indicated if platelets are less than platelets below 20,000/mm^3 or if there are signs of bleeding. Hepatic toxicity may occur. Therefore, liver enzymes are checked before each treatment and during the concomitant phase. Antiepileptic treatment may also induce liver toxicity.

Adjuvant chemotherapy is started four weeks after the end of the radiochemotherapy. TMZ is taken at a dose of 150 mg/m^2/day for five days for the first course. The dose is increased to 200 mg/m^2/day for five days, starting with the second course if there is good hematological tolerance. Cures are repeated every 28 days for a duration of 6 cycles. They are given every 28 days after verification of the blood count and liver function. A phase III study has not evaluated the continuation of TMZ every month beyond six months.

Bevacizumab, an anti-VEGF antibody, is approved to treat recurrent GBM in the USA, Canada, Switzerland, and several other countries outside the European Union. Still, no overall survival benefit has been demonstrated from its use.

Standard-of-care treatments for patients with recurrent GBM are not well defined; treatment is selected based on prior therapy, age, Karnofsky Performance Status (KPS), MGMT promoter methylation status, and patterns of disease progression (Figure 12). Second surgery is an option for ~20–30% of patients with accessible circumscribed relapses diagnosed not earlier than six months after the initial surgery. Second surgery earlier than six months after initial surgery increases the risk of unnecessary intervention based on pseudoprogression and is unlikely to provide durable benefit if the initial surgery followed by RT did not provide tumor control for more than a few months [78].

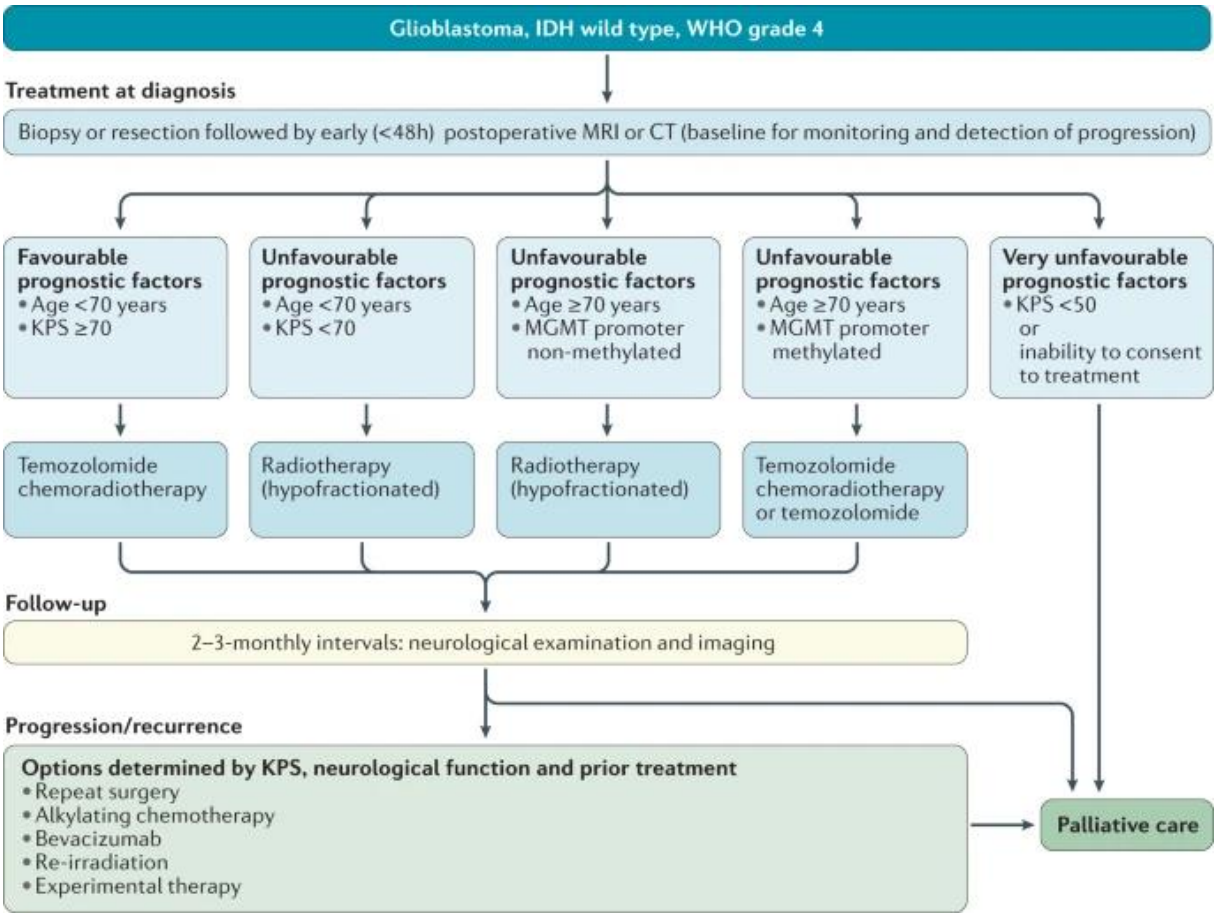

Figure 12| Clinical pathway for GBM.

MRI: magnetic resonance imaging; CT: computed tomography; KPS: Karnofsky performance status. From [78].

ii) Grade 3 IDHm gliomas

Compared to GBM, the standard of care for grade 3 IDH-O and IDH-A is much less standardized and often left to the clinician's appreciation.

Grade 3 IDH-O treatment consists of radiotherapy followed by PCV. This choice relies on the results of two phase III studies (EORTC 26951 [100] and RTOG 9402 [101]) which span from 1994 to 2002 and compared RT versus RT plus PCV (Supplementary Figure 1).

There are two options for the treatment of grade 3 IDH-A. The first is a combination of RT and PCV (evaluated in the previous trial, which also enrolled patients with non 1p 19q codeletions), and the second is a combination of RT and adjuvant TMZ. The second option was studied in the CATNON trial (EORTC study 26053-22054) (Supplementary Figure 2).

The response to first-line therapy influences the choice of treatment at progression. A second surgery may be considered. If neither RT nor alkylating agents are options owing to ineffectiveness or intolerance in the first-line setting, bevacizumab can be used to control symptoms. However, the anti-tumor efficacy of bevacizumab is unknown, and no evidence supports its combination with cytotoxic agents in this setting [78].

iii) Grade 2 IDHm gliomas

Chemotherapy for grade 2 gliomas is only reserved for patients with negative risk factors such as age superior to 40, diameter superior to 40 mm, crossing the median line, and neurological signs of deficit. When chemotherapy is needed, TMZ used to be given, but the results of clinical trials were very heterogeneous, and responses were observed in about 10 to 30% of patients. A phase 3 clinical trial (EORTC 22033-26033) studied the use of TMZ chemotherapy vs. RT. Results are not yet available [102]. More precisely, the effect of TMZ was inferior to RT in IDH-A patients and similar to RT in IDH-O patients.

A clinical trial published in 2016 shows that adding PCV to RT increased median survival from 7,8 to 13,3 years [103]. It is now the standard of care for patients with grade 2 IDHm gliomas with pejorative prognostic factors (Supplementary Figure 3).

Treatment at progression depends on neurological status, progression patterns, and first-line therapy. Second surgery is always considered, usually followed by RT in patients who had not previously received irradiation or alkylating agent-based chemotherapy (Figure 13) [78].

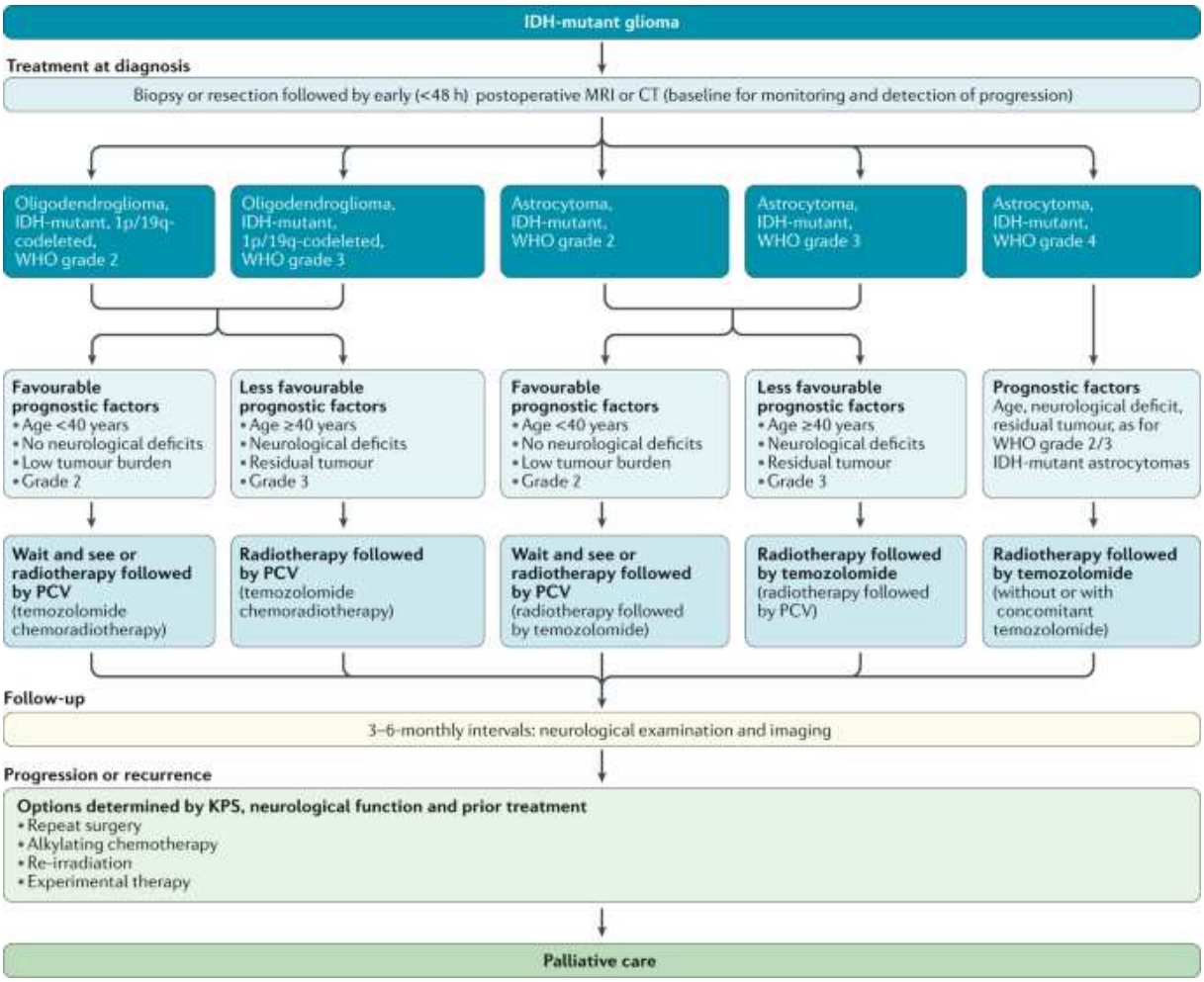

Figure 13| Clinical pathway for IDHm gliomas.

KPS, Karnofsky performance status; PCV, procarbazine, lomustine and vincristine. From [78].

6) Experimental therapies

a. Immune checkpoint blockade

The success of immunotherapies involving ICB targeting PD1 and/or CTLA-4 or CAR-T cells transfer in other types of cancer has led to their evaluation in brain malignancies. However, recent phase 3 clinical trials all failed to demonstrate the benefit of ICB in newly diagnosed [104] and recurrent IDHwt tumors [105], [106]. A phase 2 clinical trial in IDHm gliomas showed no clear benefit [107]. Investigations on subsets of patients which may respond to ICB are currently being conducted [108]. Although promising, immunotherapy did not yet show significant improvement in patient survival in both IDHm and IDHwt gliomas. Aside from tumor-intrinsic mechanisms, limitations to immunotherapy efficacy include abundant immunosuppressive myeloid cells and the paucity of tumor-infiltrating lymphocytes, expressing low levels of classical immune checkpoint receptors [109]–[111].

b. CAR-T cells

Currently, 26 clinical trials using CAR-T cells have been registered. Most of these CAR-T cells target EGFR, HER2, or IL13Rα2, but some novel targets, such as GD2, EphA2, MUC1, and CD147, are also included. The use of CAR-T cells enables precise targeting of tumor cells, thus not only increasing the efficacy but also reducing concurrent toxicity. However, the efficacy of CAR-T cell therapy remains moderate because of heterogeneous antigen expression and limited T cell function in the tumor site [112].

c. Dendritic cells vaccines

Relative safety and promising efficacy have been seen using dendritic cells vaccines for the treatment of gliomas. Currently, two phase II trials are enrolling patients. One study uses a dendritic cells vaccine primed with tumor samples, allogeneic hematopoietic stem cells, and cytotoxic lymphocytes as first-line therapy in patients with GBM (NCT01759810). The other study is employing an mRNA-transfected dendritic cells vaccine and compares whether treatment with adjuvant TMZ is advantageous in patients with GBM (NCT03548571) [112]. Evaluation in large phase III clinical trials will give more insight into the efficacy of these therapeutics.

d. Oncolytic viruses

Various studies have confirmed the safety and efficacy of oncolytic viruses alone or with TMZ, IFNγ, or pembrolizumab[4] for the treatment of gliomas. However, large-scale studies are required to determine whether oncolytic viruses can be used as standard therapy in glioma [112].

e. Cytokines

Although studies of IL-2 and IL-4 did not reach conclusions regarding their efficacy, these two treatment strategies are thought to be safe and have acceptable toxicity profiles. Further studies are needed to establish proof of IL-2 and IL-4 efficacy in cases of gliomas. IL-13-based targeted toxins also require further clinical studies. The combination of IFN-α or IFN-β with TMZ exhibits promising efficacy in patients with gliomas, whereas the roles of IFN-γ and IFN-λ in the clinical treatment of glioma require further evaluation [112].

[4] Pembrolizumab is a monoclonal antibody targeting the anti–programmed death-1 (anti-PD1) protein found on Tcells.

f. Tumor associated macrophages/microglia cells therapy

Emerging evidence has shown that tumor-associated macrophages and microglia cells contribute significantly to the formation and maintenance of immunosuppression and tumor cell migration. To date, inhibition of these cells has not demonstrated efficacy in humans [112].

g. IDHm targeted therapy

So far, a total of 66 patients with advanced IDH1m gliomas (including oligoastrocytoma and IDHm glioblastoma) received ivosidenib, an IDHm inhibitor, in a phase I trial (NCT02073994). Outcomes varied based on the presence or absence of contrast enhancement in the tumor on cross-sectional imaging. For patients with non-enhancing gliomas, 85.7% of patients achieved stable disease with a median PFS of 13.6 months. Historically, PFS is around 7 months for similar patients who received chemotherapy. Patients with enhancing gliomas fared worse, with only 45.2% of patients achieving stable disease, and the median PFS was just 1.4 months [113].

A phase I trial, carried out in 33 patients, studied the safety and tolerability of a peptide vaccine targeting the IDH1R132H mutation (NCT02454634). Vaccine-induced immune responses were observed in 93.3% of patients across multiple MHC alleles. Patients with immune responses showed a two-year progression-free rate of 0.82. Two patients without an immune response showed tumor progression within two years of first diagnosis.

C. Heterogeneity of adult diffuse gliomas

As mentionned earlier, diffuse gliomas are very heterogeneous in terms of histology and genetic alterations. Below, we decipher how they differ at the inter- and intra-tumoral levels.

1) Bulk analysis inferred the inter tumoral heterogeneity

Deciphering diffuse glioma heterogeneity and complexity is the key to understanding its progression and offering effective therapies. Some essential and aberrant molecular events drive malignant transformation, highlighting the importance of molecular classification.

a. Expression profiling reveals different molecular classifications

TCGA Research Network has been established to generate a comprehensive catalog of genomic abnormalities driving tumorigenesis. It revealed significant mutations in GBM, including TP53 (34.4%), EGFR (32.6%), PTEN (32%), NF1 (Neurofibromin 1, 13.7%) etc. In 2009, *Verhaak et al.* used bulk expression profiling (RNA-Sequencing or RNA-Seq) to provide a detailed view of the genomic changes in a large GBM cohort containing 206 patient samples and highlighted four molecular subgroups.

- The Proneural subgroup is characterized by the amplification of PDGFRA and IDH mutation, a reduced CDKN1A expression (encoding p21CIP1), and frequent TP53 mutations.
- The Neural subgroup is defined by the expression of NEFL, GABRA1, SYT1, and SLC12A5.
- The Classical subgroup is distinguished by the amplification of EGFR, the amplification of chromosome 7, a loss of chromosome 10, and a focal loss of 9p21.3 locus targeting CDKN2A but lacks TP53 mutations.
- The Mesenchymal subgroup is identified by the deletion of NF1 and mutation of PTEN. It expresses CHI3L1 and MET. In addition, this subgroup presents an increased expression of genes related to the NF-κB and TNF signaling pathways.

This analysis also illustrated that a survival advantage in heavily treated patients varied by subtype, with Classical or Mesenchymal subtypes having significantly delayed mortality that was not observed in the Proneural subtype (Figure 14) [114].

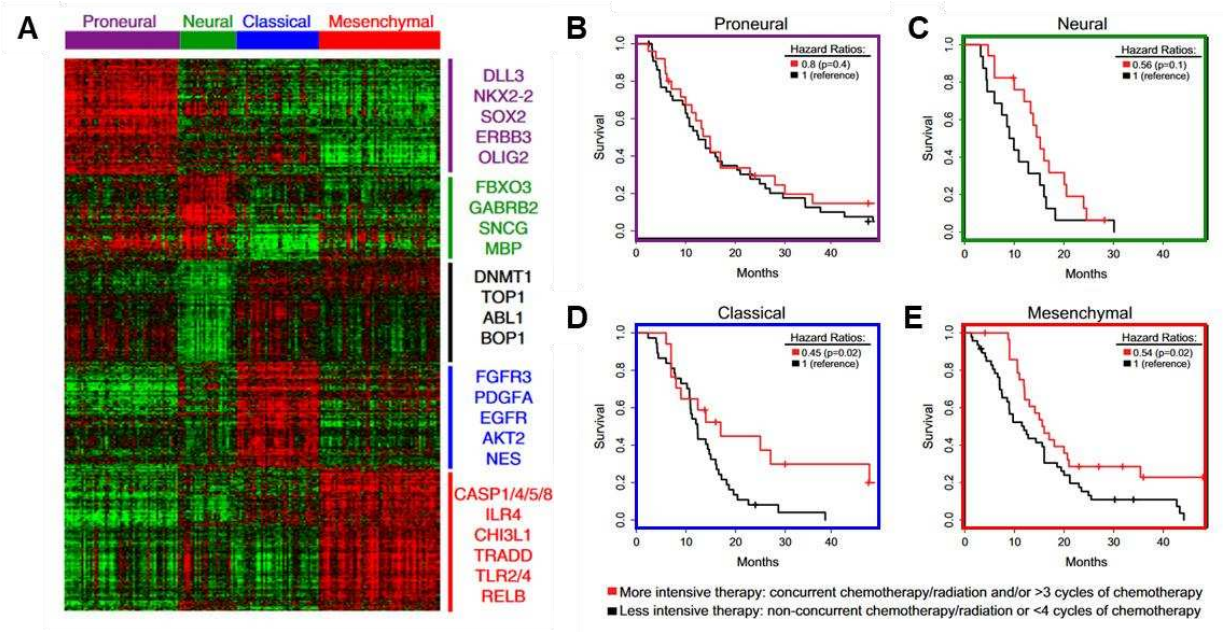

Figure 14| Gene expression data of the four GBM subtypes and corresponding Kaplan-Meier estimates of overall survival by treatment type.

A| Using the predictive 840 gene list, samples were ordered based on subtype predictions, and genes were clustered using the core set of 173 TCGA GBM samples. **B, C, D, and E|** Patients from TCGA and *Murat et al* [115] were classified by therapy regimen. Red denotes more intensive therapy, w including concurrent chemotherapy and radiation or more than four cycles of chemotherapy. Black indicates less intensive therapy, which includes nonconcurrent chemotherapy and radiation or less than four cycles of chemotherapy [114].

They also found that these subtypes were reminiscent of distinct neural cell types from mouse databases. The Proneural class was highly enriched with the oligodendrocytic signature such as PDGFRA, OLIG2, NKX2-2, DCX, ASCL1, TCF4, and SOX genes but not the astrocytic signature. In contrast, the Classical group was strongly associated with the murine astrocytic signature as well as Notch and Sonic hedgehog signaling pathways. The Neural class showed an association with oligodendrocytic and astrocytic differentiation and had a strong enrichment for genes differentially expressed by neurons. The Mesenchymal subtype was strongly associated with the cultured astroglial signature. These findings suggested a link to alternative cells of origin (cf. page 75 Heterogeneity of gliomas' cells of origin).

This classification rapidly became the gold standard for characterizing GBM's heterogeneity. However, it has limitations. The first is that, at the time of the study, some IDHm tumors could be defined as "secondary GBM" (now called grade 4 IDH-A). A second study was published a few years later in which they included only GBM without IDH mutations and eliminated the "neural" subtype that they described as non-tumoral contamination of the margins of the samples [116]. A second limitation is due to the cellular plasticity of GBMs. Indeed, one patient's tumor can be composed of a

mixture of glioma cells from different subtypes. Although subtypes of GBM are associated with a specific clinical prognosis, these predictions are not used in the clinic as 63% of GBMs show a shift in subtype at recurrence after treatment. In particular, proneural prone to evolve to a mesenchymal subtype which is less favorable in terms of survival [117]. Therefore, the major limitation of GBMs is the lack of molecular biomarkers that could lead to precise stratification of patients for therapeutic interventions.

With this in mind, *Park et al.* used different datasets to identify 80 genes most associated with GBM prognosis. Functional annotation revealed that invasion and cell cycle-related gene sets were enriched in the poor and favorable groups, respectively. Therefore, the three GBM subtypes were named invasive (poor), mitotic (favorable), and intermediate. Interestingly, the invasive subtype showed increased invasiveness, and MGMT methylation was enriched in the mitotic subtype, indicating the need for different therapeutic strategies according to prognostic subtypes. In this study, immunohistochemical staining showed higher expression of PDPN in the invasive subtype and TMEM100 in the mitotic subtype.

Like GBM, IDH-O tumors are also a heterogeneous group of gliomas. Our team participated in the integrated analysis of the transcriptome, genome, and methylome of 156 IDH-O tumor samples. They revealed three subgroups associated with specific expression patterns of nervous system cell types: oligodendrocyte (O3), oligodendrocyte precursor cell (O1), and neuronal lineage (O2). Importantly, they found that the OPC-like group was associated with more aggressive molecular patterns, including MYC activation. This activation was shown to occur through various alterations, including MYC genomic gain, MAX genomic loss, MYC hypomethylation, and microRNA-34b/c down-regulation. This OPC-like group is associated with a poorer outcome independently of histological grade (Figure 15) [118].

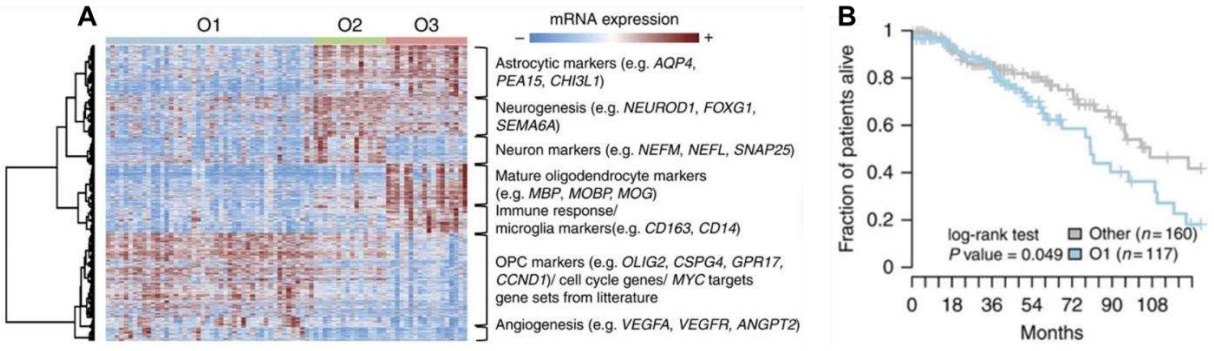

Figure 15| Gene expression data of the three IDH-O subtypes and corresponding Kaplan-Meier estimates of overall survival by subtype.

A| Selection of the most differential probe sets in each subtype compared to the others. The authors performed gene-set enrichment analysis for each of the eight clusters of probe sets highlighted on the heatmap and annotated the clusters on the right with the most relevant significantly enriched gene sets and corresponding relevant gene markers. **B|** Overall survival of all 278 patients with 1p/19q co-deleted tumors after pooling patients with available clinical data from TCGA (n=118 patients), POLA (n=80 patients), Gravendeel (n=42 patients) and REMBRANDT (n=37 patients) cohorts [118].

b. Methylation profiling

As said earlier, DNA methylation has become a key factor when measuring heterogeneity and stratification of glioma patients.

Epigenetic modifications of GBM are related to biological characteristics, correlate with survival, and are therefore considered therapeutic targets. GBM genome-wide methylation data show biologically distinct subtypes. For example, DNA methylation of the MGMT gene promoter occurs in 48.5% of GBM patients (174/359). Additionally, GBM patient data show other methylated genes, including GATA6 (68.4%), CASP8 (56.8%), and others. However, different methylation profiles are also different in IDHm tumors.

That is why, in 2016, Ceccarelli *et al*. assembled a dataset comprising all TCGA newly diagnosed diffuse glioma consisting of 1,122 patients and identified new diffuse glioma subgroups with distinct molecular and clinical features. Interestingly, unsupervised clustering identifies six methylation groups and four RNA expression groups associated with IDH status. The LGm1/LGm2/LGm3 DNA methylation macro-group carried IDH1 or IDH2 mutations, while LGm4/LGm5/LGm6 were IDHwt. LGm1–3 showed genome-wide hypermethylation compared to LGm4–6 clusters, documenting the association between IDH mutation and increased DNA methylation. The gene expression clusters LGr1–3 harbored *IDH1* or *IDH2* mutations, while the LGr4 was exclusively IDHwt. More precisely, the three IDHm epigenetic subtypes separated samples carrying the IDH-O samples into a single cluster and IDH-A samples into two clusters (G-CIMP-low with low methylation levels and G-CIMP-high with higher levels of methylation). Conversely, IDH-A samples clustered nearly exclusively into a single expression cluster, and IDH-O samples were split into two separate expression clusters. G-CIMP-low group was associated with significantly worse survival than the G-CIMP-high and IDH-O groups. They observed a mechanistic relationship between methylation and increased transcript levels. The enrichment in cell cycle gene expression in G-CIMP-low provided additional support to the notion that the development of this subtype may be mediated by a loss of CpG methylation and binding of SOX factors to candidate genomic enhancer elements. A simplified graphical

summary of the identified groups and their main clinical and biological characteristics is reported in (Figure 16)Figure 16 [119].

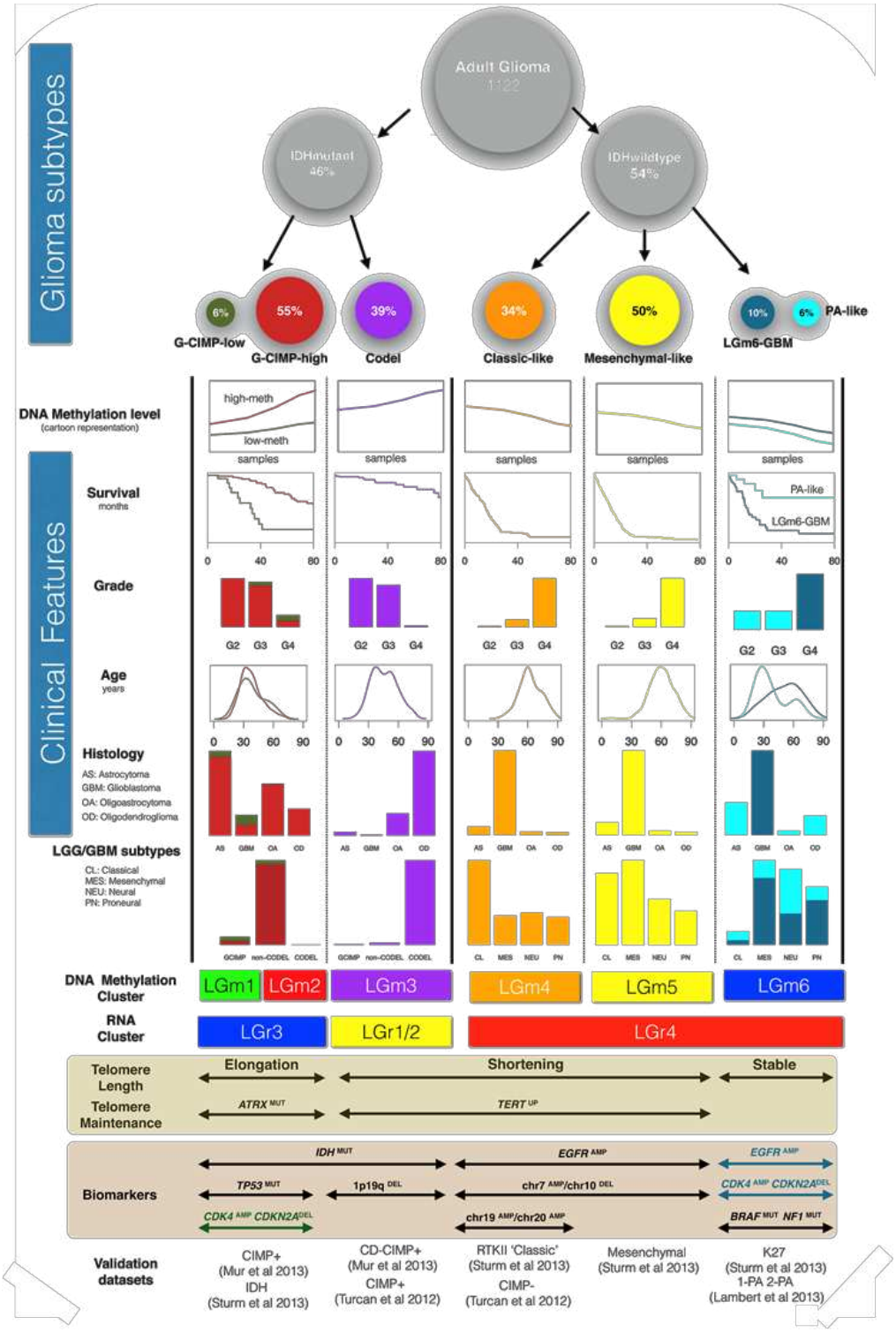

Figure 16| Overview of major subtypes of adult diffuse glioma.

Integrative analysis of 1,122 adult gliomas resulted in 7 different subtypes with distinct biological and clinical characteristics. The groups extend across six DNA methylation subtypes, of which the LGm6 cluster was further separated by tumor grade into PA-like and LGm6-GBM. The size of the circles is proportional to the percentages of samples within each group. DNA methylation plot is a cartoon

representation of the overall genome-wide epigenetic pattern within glioma subtypes. Survival information is represented as a set of Kaplan-Meier curves, counts of grade, histology, and LGG/GBM subtypes within the groups are represented as bar plots, whereas age is represented as density. Labeling of telomere length and maintenance status is based on the enrichment of samples within each column, similarly to the biomarkers and the validation datasets. From [119].

2) Single-cell analysis enables in-depth characterization of the intra-tumoral heterogeneity

The advent of powerful single-cell RNA sequencing technologies (scRNA-seq) largely contributed to deciphering the transcriptional and cellular heterogeneities among the malignant cells of a tumor.

a. IDHm

In 2016, Tirosh *et al*. profiled six grade 2 IDH-O tumor samples and reconstructed their developmental programs from genome-wide expression signatures. They found that most cancer cells are differentiated along two specialized glial programs: oligodendrocyte-like (OPC-like) and astrocytoma-like (AC-like). In contrast, a rare subpopulation of cells is undifferentiated and associated with a neural stem cell expression program (NPC-like). This rare subpopulation possesses stem cell expression signatures and enriched proliferative potential., consistent with a model in which CSCs are primarily responsible for fuelling the growth of IDH-O in humans [120].

The following year, they published an additional sequencing of ten grade 2, 3, and 4 IDH-A. Interestingly, they found that differences in bulk expression profiles between IDH-A and IDH-O were primarily explained by the impact of signature genetic events and TME composition but not by distinct expression programs of glial lineages in the malignant cells. Indeed, both IDH-A and IDH-O share the same developmental hierarchy, consisting of three subpopulations of malignant cells, which are nonproliferating cells differentiated along the astrocytic and oligodendrocytic lineages proliferative undifferentiated cells that resemble neural stem/ progenitor cells. Analyzing tumors of different clinical grades showed that higher-grade tumors present enhanced proliferation, larger pools of undifferentiated glioma cells, and increased macrophage over microglia programs in the TME [121]. Altogether, these data suggest a common origin of IDH-A and IDH-O gliomas (Figure 19).

b. GBM

In 2019, Neftel *et al*. used an integrative approach spanning scRNA-Seq of 28 tumors and bulk genetic and expression analysis of 401 specimens from the TCGA to show that each tumor is unique and a combination of factors drives the diversity within a tumor: genetic, epigenetic, and microenvironmental. Yet, they found that the variety of malignant cells in GBM converged to few recurrent expression signatures and highlighted a limited set of four central cellular plastic states. Although each GBM sample contains cells in multiple states, the relative frequency of each state is associated with genetic alterations:

- The oligodendrocyte-precursor-cell-like (OPC-like) is characterized by the amplification of PDGFRA.
- The Neural-precursor-cell-like (NPC-like) is defined by the expression of NEFL, GABRA1, SYT1, and SLC12A5 is defined by the expression of CDK4.
- The Astrocyte-like (AC-like) is distinguished by the amplification of EGFR.
- The Mesenchymal-like (MES-like) state, identified by the deletion of NF1.

One given cellular state is defined by the relative score of a meta-module defined as a network of genes enriched in a recurrent expression program (Figure 17) and bears different proliferative potentials. The OPC-like and NPC-like states are the most proliferative ones. Malignant cells can display intermediate hybrid states, and the proportion of these cellular states within the tumor defines the tumor transcriptional subtype. Thus, Proneuronal GBM is enriched in OPC-like and NPC-like states, whereas Classical and Mesenchymal are enriched in AC-like and MES-like states, respectively [6].

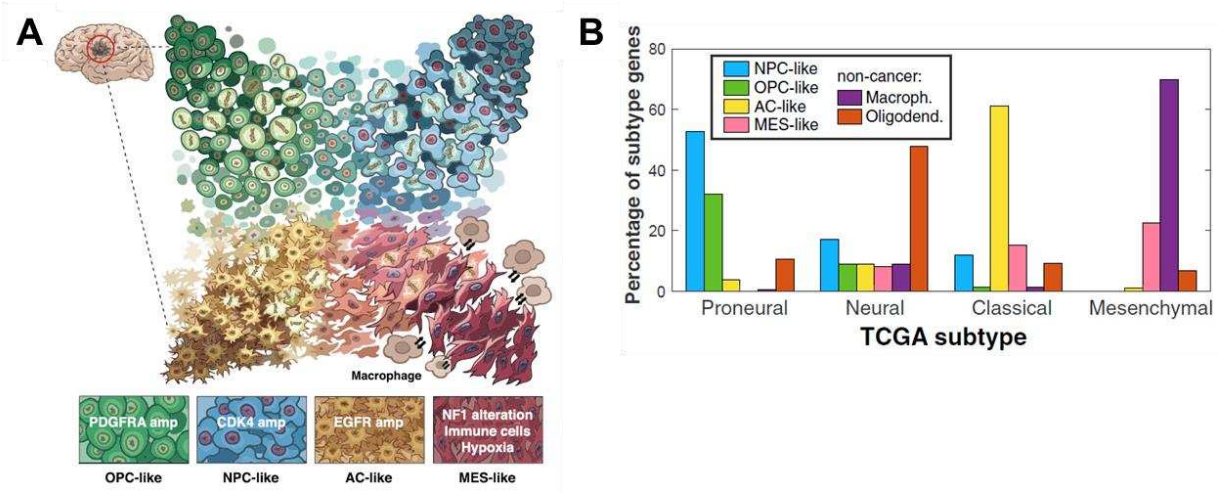

Figure 17| Two-dimensional representation of cellular states of GBM malignant cells.

A| Model for the cellular states and their genetic and micro-environmental determinants. Mitotic spindles indicate cycling cells. Lighter or darker tones indicate the strength of each program. Intermediate states are shown between the four states and indicate transitions [6]. **B|** Marker genes for

each of the GBM subtypes [114] were classified into one of six cellular programs corresponding to the four malignant states (as defined by the meta-modules) and two non-malignant cell types: macrophages and oligodendrocytes [6].

The dynamic interconversion between these states was demonstrated in lineage-tracing experiments using a genetic mouse model and patient-derived xenografts, in which one single cell gives rise to the four archetypal subtypes. Moreover, spatiotemporal heterogeneity was highlighted as the proportion of the four cell states varies between different regions of the same tumor, changes over time, and is influenced by therapy [122].

3) Heterogeneity of gliomas' cells of origin

The switching model, which argues for a dynamic plasticity of four different cell states, contrasts with two other scRNA-seq studies supporting the cancer stem cell (CSC) hypothesis, in which a cellular hierarchy prevails [123]–[125]. Nevertheless, it should be noted that Neftel *et al.* highlighted that malignant cells express the proliferation marker Ki67+. In contrast, a signature of quiescent (non-proliferative) CSCs was identified in genetically defined mouse models of GBM and human tumors [123]. Notably, such a signature remains stable and independent of the transcriptional signatures representing the four archetypal cellular states.

Tumors develop from cells of origin. In these cells, genetic and epigenetic events occur, leading to mutations. They must occur in cell types that provide a favorable context for oncogenic development. The brain parenchyma is a space of great cellular diversity ranging from neurons, the effector cells of the CNS, to glial cells, which have a trophic, conductive, and homeostatic supportive role. These glial cells include macroglia, composed of oligodendrocytes (cells responsible for the formation of the myelin sheath) and their progenitors, astrocytes (trophic support and regulation of neurotransmitters), and ependymocytes (cells constituting a barrier between the cerebral parenchyma and the cerebrospinal fluid) as well as microglial cells (immune cells with phagocytic functions). Glial cells are the only cells capable of proliferation in the adult brain (Figure 18). However, only OPCs and NSCs can proliferate in physiological conditions, whereas microglia and astrocytes can proliferate when they sense a stimulus (astrocytic reaction or microglial activation). Thus, OPCs and NSCs constitute privileged cellular actors in the development of tumors. More precisely, OPCs constitute the largest population of proliferative cells in the adult brain, accounting for ~5% of neural cells.

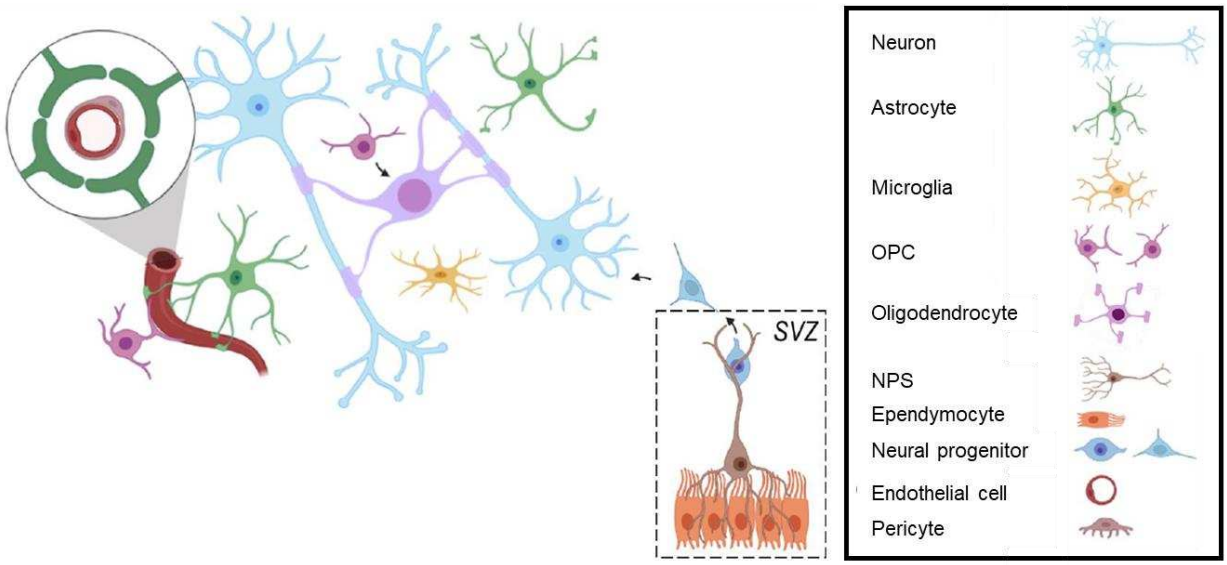

Figure 18| Diversity of adult brain parenchyma cell types.

Black arrows represent differentiation from one cell type to another. SVZ: subventricular zone; OPC: oligodendrocyte progenitor cell; NPS: neural progenitor cell. Illustration by Y. Khenniche.

It is essential to distinguish between cells that cause mutations (initial cells) from cells that drive tumor amplification (amplifying cells). The first is where the initial mutational events occur without necessary transformation and proliferation. The latter corresponds to the cell population responsible for the production of the tumor mass. Cells responsible for the tumor amplification are necessarily carriers of the initial mutations, while the initiating cells may or may not be cells of origin of the amplification.

GBM hijacks mechanisms of neural development and contains subsets of glioblastoma stem cells (GSCs) that are thought to represent its driving force, possess tumor-propagating potential, and exhibit preferential resistance to radiotherapy and chemotherapies. No universal marker of GSCs has been discovered; rather a combination of markers is required (e.g., CD133, CD44, A2B5, SSEA1). Castellan *et al.* identified a glioma stem cell signature reflecting the stemness property and is differentially expressed in GSCs compared with differentiated GBM cells [126]. Recent single-cell transcriptomics studies combined with TCGA bulk analysis further described a transcriptional gradient spanning two cellular states reminiscent of normal neural development and inflammatory wound response. Orthogonal to this GSC gradient, they identified an astrocyte maturation gradient in patient tumor cells, highlighting the transcriptional programs implicated in differentiating GSCs into mature tumor cells that comprise the bulk of the tumor. Thus, they hypothesized that GBM forms as a response to neural tissue wounding in the context of a mutated genomic background. The output of this process is the dual generation of a brain growth and repair response

derived from genetically abnormal brain precursor cells. This tissue regeneration-oriented interpretation contrasts with the traditional cancer stem cell discourse that solely emphasizes cancer stem cell roots in a developmental stem cell paradigm [127] [128]. Overall, GSCs are now considered a gradient of different states, including stemness, metabolism, and cellular specialization, and it is now considered that the amplifying cells that constitute the glioma tumor mass are diverse.

In IDHm gliomas, cells resembling OPCs, astrocytes, and neural progenitors are found, whereas, in GBM, MES-like cells associated with hypoxia, glycolysis, microglia, and macrophages are found (Figure 19). The presence of GSCs in GBM may explain the aggressiveness and recurrence observed in these tumors, particularly in mesenchymal subtypes. Overall, OPC-like and NPC-like cells represent the most proliferative cell clusters constituting amplifying cells.

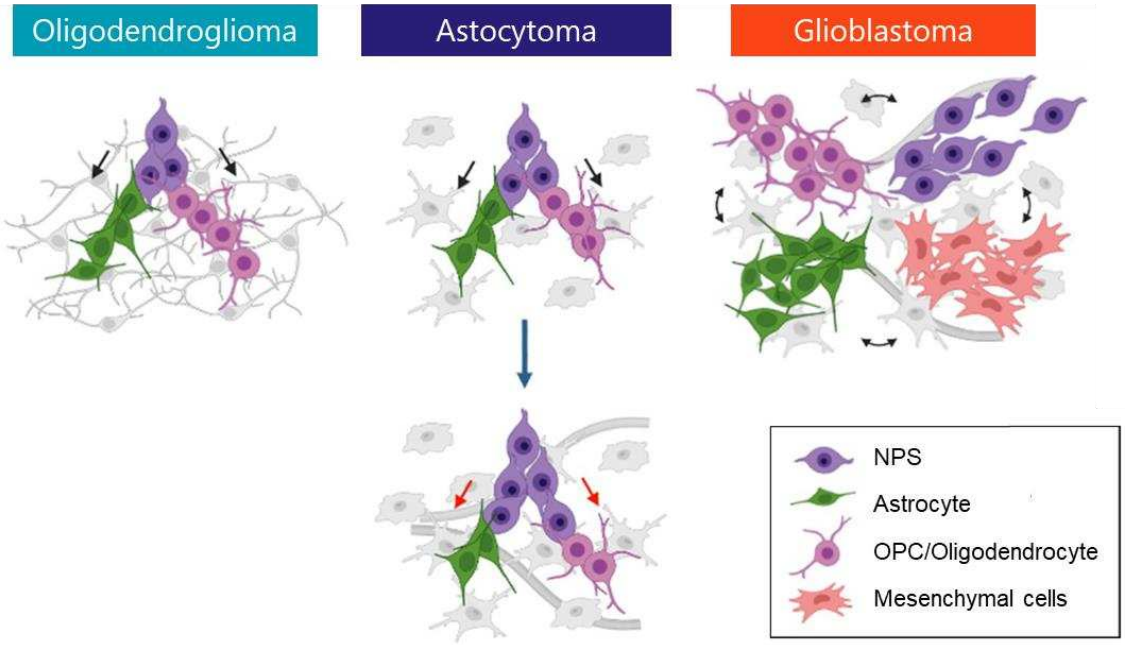

Figure 19| Cellular and phenotypic heterogeneity of diffuse gliomas.
From [6], [120], [121]. OPC: oligodendrocyte progenitor cell; NPS: neural progenitor cell. Illustration by Y. Khenniche.

In conclusion, it is critical to better understand the various sources of genetic, epigenetic, and microenvironmental intratumoral heterogeneity of gliomas to propose more relevant therapeutics. In the next section, we will describe how the IDH mutation is a driver of IDH-A and IDH-O and its functional consequences on the induction of gliomagenesis.

III) IDHM GLIOMAS PRODUCE R-2HG, AN IMMUNO-ONCOMETABOLITE

A. IDH mutations lead to the neomorphic overproduction of R-2HG

1) Identification of IDH mutation

The IDH1 enzyme is localized in the cytoplasm and peroxisomes, whereas the IDH2 enzyme is found in the mitochondrial matrix. These homodimeric enzymes both catalyze a redox reaction that converts isocitrate to α-ketoglutarate (α-KG) while reducing NADP to NADPH and liberating CO_2. IDH1 and IDH2 (collectively referred to as IDH) are highly homologous to each other. Still, they are structurally, functionally, and evolutionarily distinct from the NAD-dependent, heterotrimeric IDH3 enzyme that functions in the tricarboxylic acid cycle (TCA) to produce the NADH required for oxidative phosphorylation. Interestingly, the reaction catalyzed by IDH1 and IDH2 is thought to be one of only three significant mechanisms of NADPH production in mammalian cells [129]. In 2008 and 2009, two independent whole-exome sequencing studies identified recurrent mutations in IDH1 in diffuse glioma and acute myeloid leukemia. Subsequent investigations revealed that IDH mutations are prevalent in various types of cancer, including diffuse gliomas (80%), acute myeloid leukemia (AML; 20%), cholangiocarcinoma (20%), chondrosarcoma (80%), sinonasal undifferentiated carcinoma (49–82%) and angioimmunoblastic T cell lymphoma (32%), among others ([130]), thereby solidifying a critical pathogenetic role for such mutations.

Approximately 90% of IDH1/2 mutations are arginine-to-histidine heterozygous substitutions in codon 132 of the IDH1 gene (IDH1 R132H). A small fraction consists of different amino acid substitutions at the R132 position of IDH1 or substitutions of the structurally analogous R172 residue of the homolog IDH2. Crystallographic analyses revealed that IDHwt proteins form homodimers that can transition between an inactive open state, an inactive semi-open state, and a catalytically active closed conformation. The presence of a mutant IDH subunit in the enzymatic complex favors the closed conformation and confers a high affinity for NADPH. The key breakthrough in understanding the effects of IDH1/2 mutations was a discovery made by scientists at Agios Pharmaceuticals in 2009. Using a metabolite profiling strategy, they discovered that the mutant IDH enzymes acquire a neomorphic activity in which the standard product α-KG is converted to R-2-hydroxyglutarate (R-2HG) in a reaction that consumes, rather than produces, NADPH. They found that the quaternary structure of

the homodimeric R132H mutant enzyme adopts the same closed catalytically competent conformation as the wild-type enzyme (Figure 20 A). However, the mutation modifies two essential features: the effect on conformation equilibrium and the reorganization of the active site, which results in this neomorphic activity. More precisely, R132 acts as a gatekeeper residue and orchestrates the hinge movement between the open and closed conformations. Substitution of histidine for arginine likely changes the equilibrium in favor of the closed conformation that forms the catalytic cleft for cofactor and substrate to bind efficiently, which partly explains the high affinity for NADPH shown by the mutant enzyme. This feature may be advantageous for the NADPH-dependent reduction of α-KG to R-2HG in an environment with low NADPH concentrations. Moreover, in addition to the mutation at residue 132, the significant changes are the positions of the catalytic residues Tyr 139 and Lys 212' (Figure 20 B) [131].

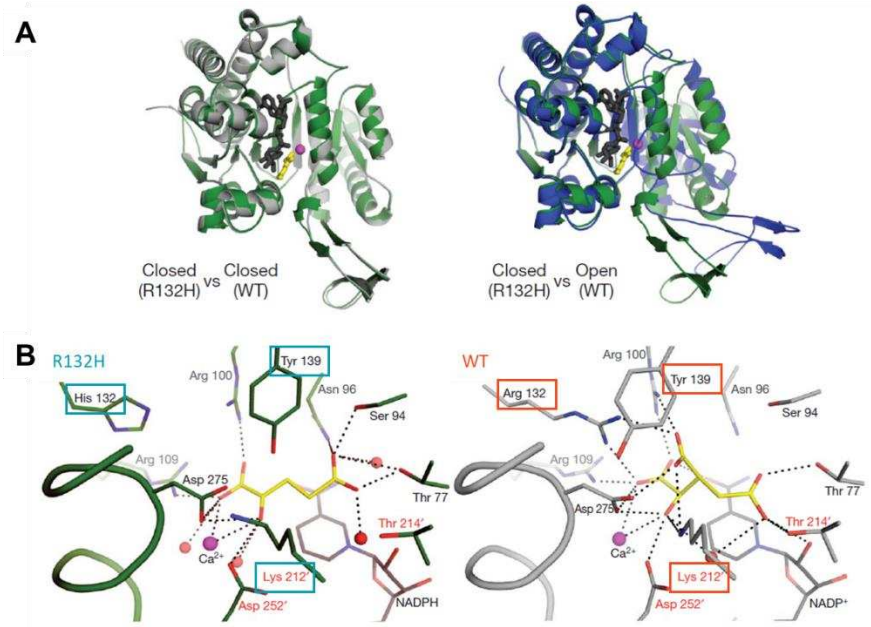

Figure 20| Structural analysis of R132H mutant IDH1.

A| Overlay of R132H mutant IDH1 (green) and wild-type IDH1 (grey) structures in the 'closed' conformation (on the left). Overlay of R132H mutant IDH1 (green) and wild-type IDH1 (blue) structure in the 'open' conformation (on the right). **B|** Close-up comparison of the R132H IDH1 active site (left) with a-ketoglutarate (yellow) and NADPH (grey) and the wild-type IDH1 active site (right) with isocitrate (yellow) and NADP (grey). Residues coming from the other monomer are denoted with a prime symbol. Adapted from [131]

2) Accumulation of R-2HG in IDHm tumor cells

Metabolites refer to the intermediate or end products of the metabolic pathways involved in cell growth, development, and survival. Dysregulation of cell metabolism is one of the hallmarks of cancer (cf page 26 Universal hallmarks of cancer). It leads to

the abnormal production and accumulation of oncometabolites involved in various critical aspects throughout cancer progression. In contrast to adaptive metabolic reprogramming, the production of oncometabolites commonly results from genetic abnormalities in the genes encoding essential metabolic products such as IDH.

As a result of the structural changes induced by the mutation described above, the affinity of the mutant enzymes for isocitrate is reduced, and their affinity for α-KG and NADPH is increased. Moreover, the mutations enable the near-complete elimination of the normal oxidation and decarboxylation of isocitrate to α-KG and the neomorphic overproduction of R-2HG. In contrast, several wild-type metabolic enzymes produce both R-2HG and L-2HG enantiomers as low-efficiency by-products. Both are maintained at low concentrations in normal cells by 2-HG dehydrogenase housekeeping enzymes that recycle these compounds back to α-KG. *In vitro* and *in vivo* experiments have shown that the mutant IDH enzymes exclusively produce the R form of 2-HG.

In IDHm patients, R-2HG production outstrips its elimination such that it builds up to concentrations that are orders of magnitude higher than normal, in some cases to millimolar levels [129]. As seen in Figure 23, R-2HG functions as a weak antagonist of α -KG. For a clear inhibition of α -KG-dependent enzymes, a 100-fold molar excess of R-2-HG over α -KG is required. Under physiological conditions, the level of R-2HG is too low to inhibit these enzymes significantly. Liquid chromatography coupled to mass spectrometry (LC-MS) dosages and mathematical models of R-2HG release and diffusion based on fluid dynamics in the brain enabled the approximation of the rate of R-2HG release by one patient's IDHm glioma at 3.2–83.0 × 10−12 mol/mL/sec. Overall, in even the most conservative of these models, the extracellular concentration of R-2HG exceeds 3 mM within a 2 cm radius from the center of the tumor (Figure 21). In the cerebrospinal fluid (CSF), it was measured at levels up to 100 μM [132].

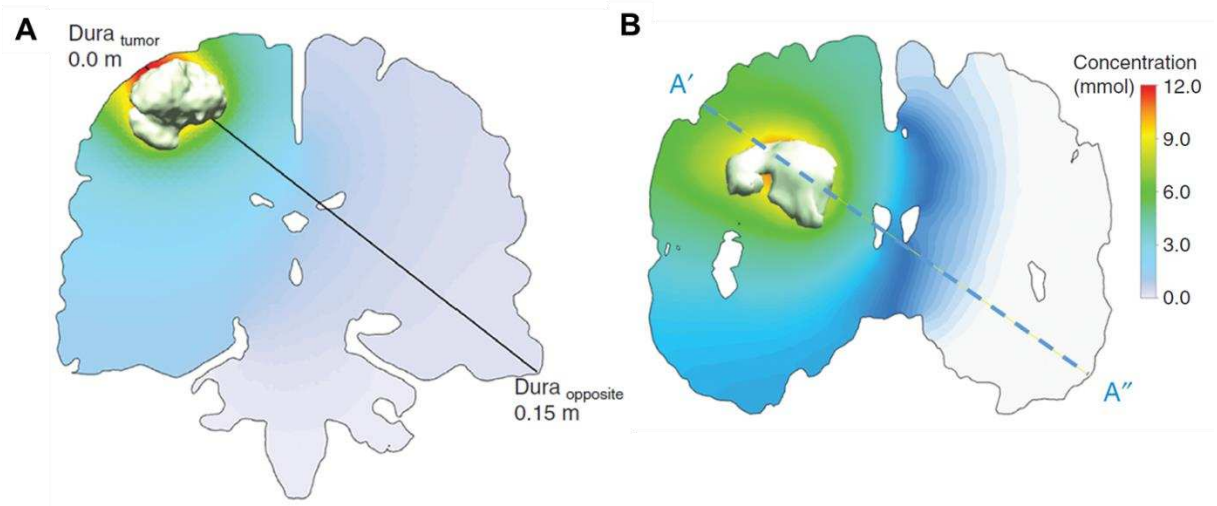

Figure 21| Predicted R-2HG concentration profiles around the IDH1mut glioma.
A| Patient 1 and **B|** Patient 2. Adapted from [132].

Overall, in IDHm tumor cells, the imbalance of R-2HG over α-KG concentrations enables the competitive inhibition α-KG-dependent enzymes and, thus, the induction of gliomagenesis.

3) 2-Oxoglutarate-dependent dioxygenases

2-Oxoglutarate-dependent dioxygenases (α-KGDDs) are a superfamily of more than 80 enzymes that play diverse roles in many biological processes, including regulation of hypoxia-inducible factor-mediated adaptation to hypoxia, extracellular matrix formation, epigenetic regulation of gene transcription and the reprogramming of cellular metabolism. These enzymes generally require oxygen, ascorbate, and iron as cofactors (Figure 22) and convert α-KG to succinate and CO_2 while carrying out their specific enzymatic activities. α-KGDDs all share the same reaction mechanism but act on different substrates, including proteins, DNA, RNA, fatty acids, and other small molecules. The affinity of specific α-KGDDs for oxygen, iron, and ascorbate varies, providing a mechanism of regulation at the level of co-substrate availability. In addition, several endogenous α-KG analogs, including pyruvate, citrate, isocitrate, succinate, fumarate, malate, oxaloacetate, R-2HG, and its enantiomer S2-HG, can act as competitive inhibitors of α-KGDDs, modulating their activity in both physiologic and pathophysiologic states (Figure 23).

These enzymes include EGLN prolyl 4-hydroxylases (also known as PHDs) and the FIH1 asparaginyl hydroxylase, which regulate the hypoxia-inducible transcription factors HIF1a and HIF2a. In turn, HIF transcriptionally regulates hundreds of genes, including genes that contribute to the Warburg effect and genes linked to DNA and

histone methylation. Other α-KGDDs play direct roles in the control of DNA (TET and ABH enzymes) and histone (KDM enzymes) methylation, as well as mRNA processing (FTO) and protein translation (OGFOD1, MINA53, and NO66) [133].

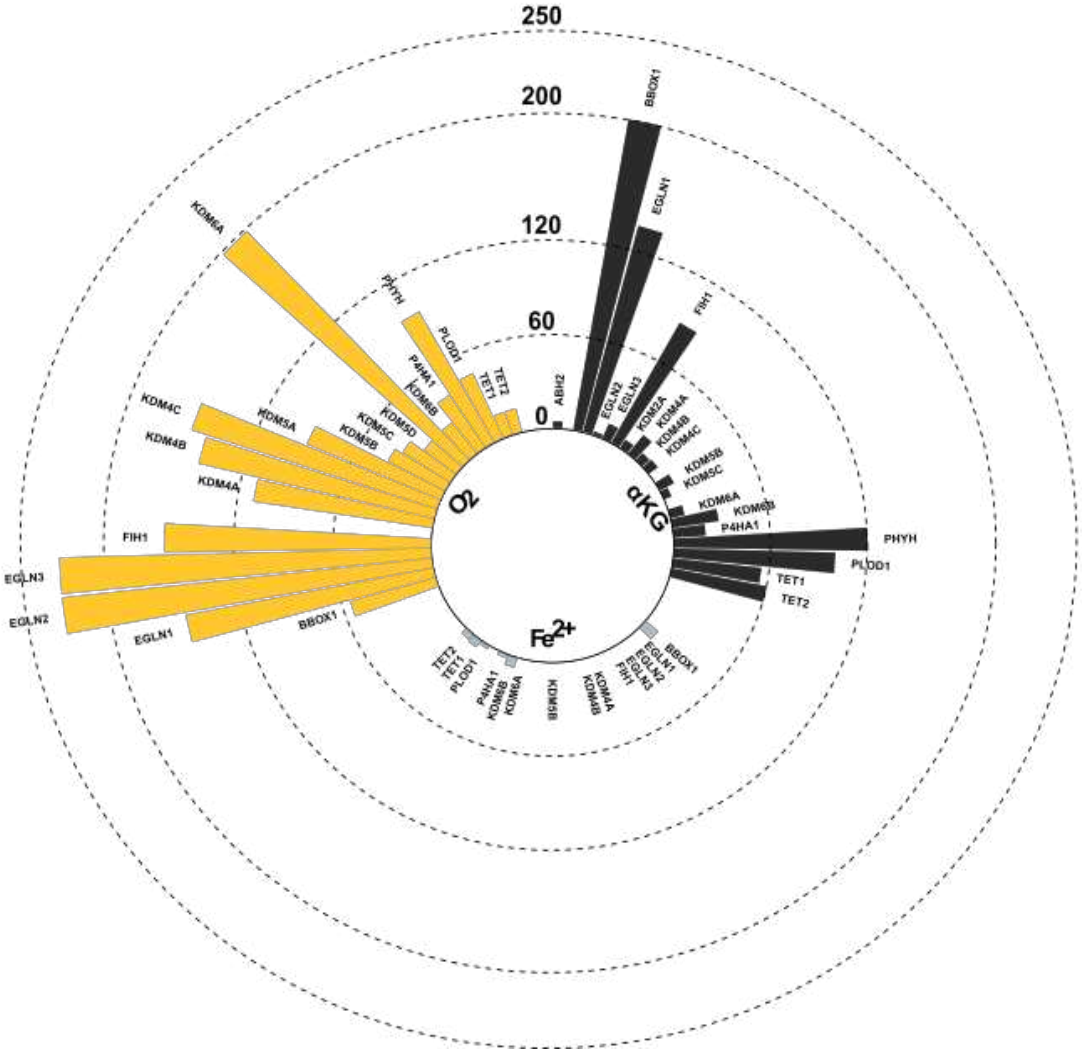

Figure 22| Kinetic values of α-KGDD for co-substrates.

Km (μM) values. In the case of divergent reported Km/IC50 values, the values presented are those determined by Losman et al. or are an average of all reported values. See Supplementary Table 3 for full values. Adapted from [133]

a. O2

The extent to which α-KGDDs can act as direct oxygen sensors is an area of active investigation. Until recently, it was unclear whether hypoxia-associated histone hypermethylation was a direct consequence of inhibition of oxygen-sensitive JmjC domain-containing histone lysine demethylases (KDM), which are α-KGDDs, or an indirect effect of hypoxia on chromatin structure. The group from William G. Kaelin Jr. showed that KDM6A, but not its paralogue KDM6B, is highly oxygen-sensitive

(Supplementary Table 3) and that KDM6A regulates cellular differentiation in an oxygen-dependent but HIF-independent manner. Mechanistically, they identified structural differences in the JmjC catalytic domains of KDM6A and KDM6B that likely explain their differential oxygen-sensing capacities [134]. Another study found that acute inactivation of KDM5A rapidly induces H3K4 methylation that resembles the effects of acute hypoxia, which is consistent with its high O2 Km value (Supplementary Table 3) [135].

Regarding the TET family of DNA hydroxylases, two studies determined that the O2 Km values of TET1 and TET2 are very low, suggesting that these α-KGDDs do not act as oxygen sensors [136], [137].

EGLN enzymes are the major cellular oxygen sensors, having O2 Km values above atmospheric oxygen concentrations. On the opposite end of the spectrum are the collagen prolyl 4-hydroxylases (P4HA1–3), which have high affinities for oxygen and are, therefore, catalytically active even in profound hypoxia. The asparaginyl hydroxylase FIH1 has an intermediate affinity for oxygen. It remains active under moderately hypoxic conditions sufficient to affect EGLN activity but becomes inactive under more severe hypoxia.

b. Iron

Functional iron deficiency may inhibit α-KGDDs that require high iron concentrations for catalysis, such as peroxisomal phytanoyl-CoA dioxygenase (PHAX), γ-butyrobetaine dioxygenase (BODG), KDM6B, TET1 and TET2 (Supplementary Table 3) [138]. Moreover, it is interesting to note that several highly iron-dependent α-KGDDs, including KDM6B, TET1, and TET2, suppress tumor growth in specific cellular contexts [139], [140].

c. Ascorbate

It was shown that ascorbate deprivation in Gulo–/– mice impairs TET function and expands the hematopoietic stem cell compartment. In contrast, ascorbate supplementation suppresses mutant Tet2-mediated leukemogenesis, possibly by augmenting residual TET2 function and/or activating other TET paralogues [141], [142]. Ascorbate supplementation also restores TET function and decreases renal cell cancer cell growth *in vitro* and *in vivo* [143], [144]. Interestingly, the anti-tumor effects of ascorbate supplementation have been observed even in mice expressing wild-type

GULO [156], suggesting that ascorbate is limiting even in tumor cells that can synthesize ascorbate. Since this molecule s very sensitive to degradation, it is possible that the increased requirement for ascorbate under 21% oxygen in tumors *in vivo* is due to an increased rate of ascorbate oxidation in these settings.

d. α-KG

The concentration of α-KG in cells is estimated to be in the high micromolar to low millimolar range under physiological conditions. Given that the measured α-KG Km values for α-KGDDs are in the low micromolar range, it is generally assumed that α-KG is not limiting for α-KGDD activity in cells. However, accurate measurement of metabolite concentrations in living cells is complicated. Cellular volumes fluctuate dramatically and vary significantly from cell to cell, even in clonal cell populations, and metabolites turn over very rapidly and exist at different concentrations in different subcellular compartments. Researchers recently reported that acute inhibition of EGLN activity, either by genetic deletion of Egln1 or by small-molecule EGLN inhibition, increases total levels of intracellular α-KG in cell lines, mouse liver, and muscle [145]. Interestingly, another study found that physiologic changes in the levels of intracellular α-KG can indeed modulate the activity of specific α-KGDDs [146]. Whether dysregulation of α-KG homeostasis directly contributes to tumorigenesis is unknown. However, one recent study found that the p53 tumor suppressor promotes the activities of specific α-KGDD tumor suppressors, including TET enzymes, by upregulating α-KG levels [146].

4) Intrinsic effects of 2-HG in IDHm glioma tumor cells

Inside IDHm tumor cells, R-2HG promotes tumorigenesis by metabolic reprogramming that results in dysregulation of gene expression, DNA damage repair, inflammation, vascularization, intracellular trafficking, aging, and cell death.

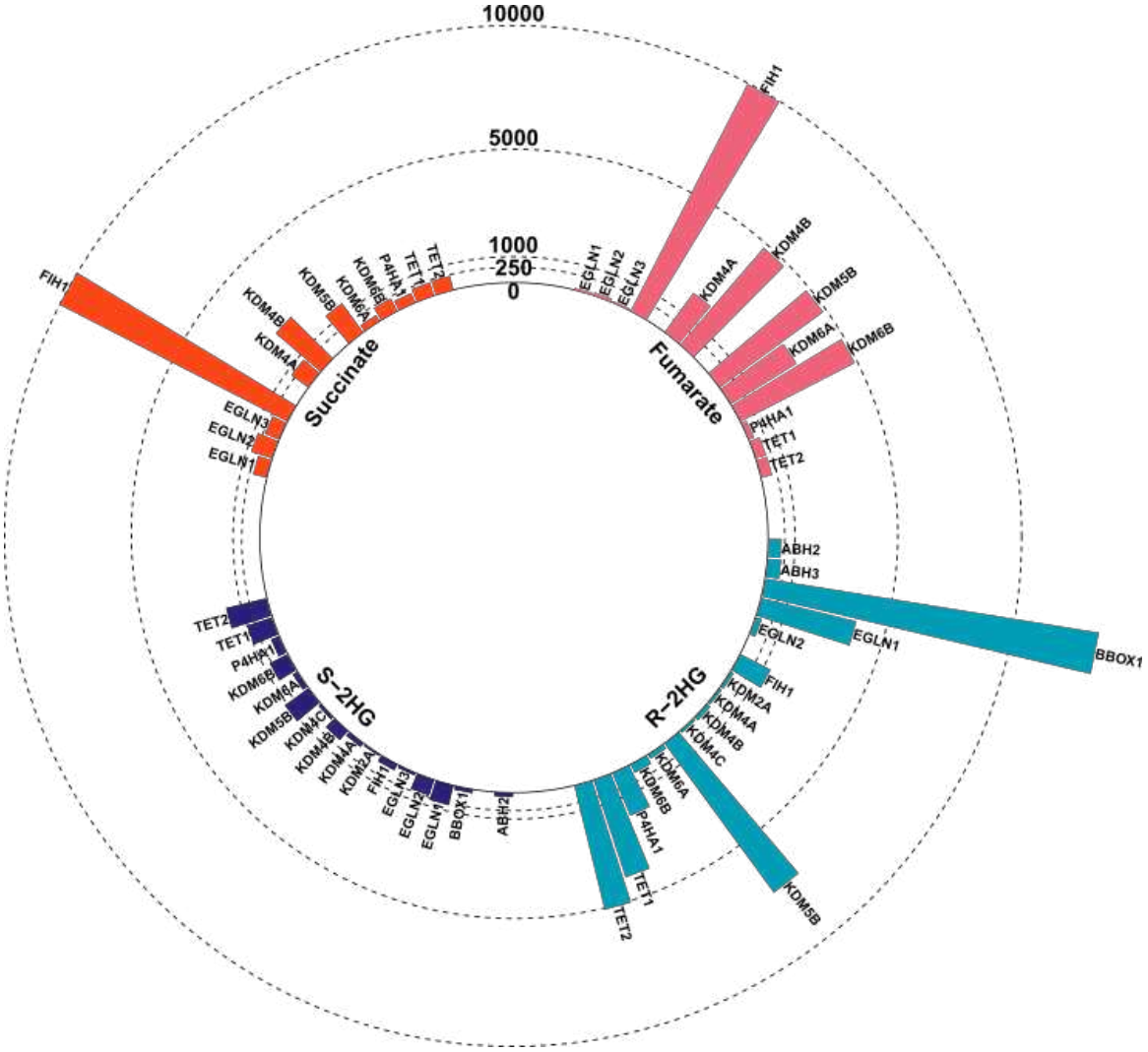

Figure 23| Inhibitory values of α-KGDD for α-KG analogs.

IC50 (μM) or *Ki values. In the case of divergent reported Km/IC50 values, the values presented are those determined by Losman et al. or are an average of all reported values. See Supplementary Table 4 for full values. Adapted from [133].

a. Epigenetic regulation of cell dedifferentiation

The precise mechanism underlying the pathogenic role of IDHm in diffuse gliomas remains unclear, although much has been learned regarding their biological effects. R-2HG and α-KG are structurally identical except that a hydroxyl group in R-2HG replaces the C2 carbonyl group of α-KG. Not surprisingly, considering the high levels of R-2HG generated in IDHm cells, this molecule competitively inhibits α-KGDDs. Thus, pathways that utilize α-KG as a substrate are perturbed in IDHm tumors, leading to epigenetic dysregulation with aberrant histone and DNA methylation, chromatin restructuring, blocking cellular differentiation, and other transformative mechanisms effects.

i) DNA hypermethylation

TET-mediated demethylation plays a critical role in the regulation of gene expression [147], DNA base excision repair [148], and chromosome replication [149], and deficiency of TET2 catalytic function could lead to oncogenesis through dysregulation of these processes. Interestingly, R-2HG is actually quite a poor TET inhibitor, with an IC50 value of about five mM (Supplementary Table 4). Nonetheless, a hypermethylated phenotype is consistently observed among many IDHm cancers [150], [151]. Two major types of hypermethylation are described in the literature: gene-specific hypermethylation in the CpG island of the promoter area and widespread (non-promoter) hypermethylation. We previously described the identification of a glioma CpG island methylator phenotype (cf page 71 Methylation profiling) [119], [152].

It has been shown that R-2HG inhibits the catalytic activity of TET2 and that its effects can be reversed in preclinical models [153]. IDHm is enriched in 5-mC content at the promoter of differentiation-associated genes and induced genes associated with stem cell [154], [155]. Furthermore, genomic hypermethylation and an associated inhibition of differentiation are induced by the expression of IDHm or the administration of D-2-HG in cell models, such as immortalized human astrocytes, human and mouse neural stem cells, human and mouse mesenchymal stem cells, mouse hepatoblasts, and mouse hematopoietic cells, but also human embryonic cells and mouse adipocytes [156]. Studies showed that the hypermethylation of CTCF-binding sites affects chromatin conformation and TAD boundary insulation, enabling promoter/enhancer interaction to drive the overexpression of PDGFRA, a known glioma oncogene [157] while blocking differentiation by disassociating SOX2 from putative enhancers [158]. Therefore, hypermethylation of certain regions correlates with cell malignant transformation and tumorigenesis. Specifically, the competitive inhibition of TET enzymes by R-2HG induces a hypermethylated state with low levels of 5hmC and elevated levels of 5mC [150], [159], [160], thus generating a hypermethylation signature characteristic of less differentiated cells.

The requirement for IDHm tumor cells to induce epigenetic hypermethylation and inhibit TET2 function is emphasized by the finding that in several IDHm AML patients who were successfully treated with an IDHm inhibitor (IDHi) but whose AML subsequently relapsed, a novel TET2 mutation that was not present at baseline emerged and DNA hypermethylation was maintained despite low D-2-HG levels [161]. Xenografts preclinical and *in vitro* mechanistic studies show that IDHi induced the expression of genes associated with both astrocytic and oligodendrocytic

differentiation (GFAP, AQP4, ATP1A2, PTGDS, and ZBTB16) [162]–[164]. This finding was recently demonstrated in human samples even though the number of treated patients was low [165]. However, not all epigenetic effects of IDHm are reversible, and the precise mechanisms of IDHi are still not yet understood.

In the context of IDHm gliomas, R-2HG may promote transformation by targeting other α-KGDDs. Indeed, several other enzymes besides TET2 have been proposed as potential tumor suppressors targeted by R-2HG, such as KDM enzymes which are significantly more sensitive to inhibition by R-2HG than TET2 (Supplementary Table 4) [133].

ii) Histones hypermethylation

In addition to DNA methylation, the methylation of lysine residues on histone proteins also contributes to alterations to chromatin structure and transcriptional regulation. However, it is complex to explain transcription activity by methylation changes in the respective gene or promoter loci because DNA methylation, which predominantly occurs at CpG islands, has variable effects on gene expression depending on the balance between activating histone H3 lysine 4 trimethylation (H3K4me3) and repressive histone H3 lysine 27 trimethylation (H3K27me3). Histone methylation events combine with other posttranslational modifications such as acetylation, phosphorylation, and ubiquitination, establishing a histone code responsible for recruiting the multiprotein complexes that epigenetically control transcription.

A paired RNA sequencing and methylation analysis revealed the significant changes in H3K27me3 dynamics, which probably reflects the R-2HG- mediated inhibition of KDMs, to the transcriptional alterations of glioma cells. The genes found to be most commonly dysregulated in glioma cells were the same that had bivalent H3K27me3 and H3K4me3 modifications in embryonic stem cells and neural progenitor cells. In tumor cells, CpG hypermethylation was present in genes also repressed in non-malignant brain cells. This finding suggests that further repression induced by IDHm via increased H3K27me3 limits epigenetic plasticity, thereby reinforcing the epigenetic state of glioma cells, restricting their ability to differentiate, and contributing to pathogenesis [21].

It is believed that KDM enzymes can function as tumor suppressors and that their inhibition by R-2HG could contribute to mutant IDH-mediated transformation.

However, little evidence currently exists to directly functionally implicate specific KDM enzymes in mutant IDH-mediated transformation [133]. Nonetheless, IDHm- mediated epigenetic dysregulation with subsequent effects on differentiation states can be observed in different cell types. For example, IDHm mouse hepatoblasts fail to differentiate into hepatocytes due to R-2HG- mediated silencing of the master transcriptional regulator HNF4α, which correlates with reduced H3K4me3 at the hepatocyte-specific promoter region of Hnf4a [166]. Moreover, in a mouse pre-adipocyte cell line, expression of IDHm causes a defect in the adipogenesis program owing to the downregulation of several transcription factors, including those encoded by Cebpa, Pparg, and Adipoq. Significantly, IDHm does not affect DNA methylation at the promoters of these genes but does increase H3K9me3 and H3K27me3 levels. Notably, short interfering RNA- mediated knockdown of KDM4C recapitulates this blockade of adipocyte differentiation [167]. Another study shows that expression of IDH1- R132C in human mesenchymal stem cells results in increased levels of H3K9me3 and H3K27me3 as well as H3K4me3, in association with upregulation of several early and late markers of chondrogenic differentiation and downregulation of osteogenic markers [168]. The differential effects on these markers illustrate gene-specific histone modifications. These findings might explain why IDH mutations are prevalent in chondrosarcomas but not in osteosarcomas.

Altogether, these results implicate histone methylation defects in IDHm-mediated impairments in cellular differentiation.

iii) RNA hypermethylation

FTO is an RNA N6-methyladenosine (m6A) demethylase, which mediates mRNA m6A modification and changes the stability of target RNAs. A high concentration of R-2HG induces cell-cycle arrest and apoptosis in R-2HG sensitive (without IDHm) AML via FTO/m6A mediated MYC inhibition [169]. Interestingly IDHm leukemia cells can tolerate this inhibitory activity. Furthermore, it was also shown that R-2HG abrogates FTO-mediated post-transcriptional upregulation of glycolytic genes and further suppresses aerobic glycolysis [170].

b. DNA repair

The ALKBH family, including ALKBH1- 8 and FTO, are a-KG-dependent DNA repair enzymes that oxidize the alkyl groups in cytotoxic lesions 1-methyladenine (m1A) and 3-methylcytosine (m3C) induced by alkylation agents. DNA repair deficiency

may help to accumulate mutations in the genome, thereby contributing to tumorigenesis.

Several studies have revealed that DNA repair pathways are altered with the presence of R-2HG, which might contribute to genomic instability, malignancy transformation, and sensitivity to genotoxic agents. First, it was shown that IDHm cells downregulate X-ray repair cross-complementing protein (XRCC), which results in DNA repair pathways inhibition [171]. Then, R-2HG was shown to increase the sensitivity of poly-ADP ribose polymerase (PARP) inhibitor through the suppression of homologous recombination [172] via inhibition of the histone demethylase KDM4B, which leads to increased H3K9me3 and thereby disrupts DNA damage signaling [173]. Moreover, IDHm cells can also harbor increased H3K9me3 and downregulation of the gene encoding the DNA damage sensor ATM, resulting in an impaired DNA damage response, irrespective of TET2 inhibition [174]. Finally, several other studies reported that R-2HG inhibits the mammalian alpha-ketoglutarate-dependent hydroxylase family homolog (ALKBH) enzymes and sensitizes IDHm cells to DNA alkylating agents, such as PCV regimen [175].

Even though most studies suggested that R-2HG suppresses DNA repair pathways, others indicated that IDHm cells could upregulate some DNA repair mechanisms and develop resistance to chemotherapeutic agents. For example, it was reported that IDHm induced RAD51-mediated TMZ resistance. Their study used immortalized, untransformed human astrocytes, which suggests that this process might occur in the early stage of glioma malignancy transformation. Still, the direct involvement of R-2HG in this process was not investigated [176]. Another study revealed that gliomas with IDH1 R132H, TP53, and ATRX inactivating mutations enhanced DDR via epigenetic upregulation of the ATM signaling pathway and elicited radioresistance. Inhibition of ATM or CHK1/2 restored the radiosensitivity [177]. As discussed above, R-2HG plays a critical role in inducing the hypermethylation phenotype, which elicits the epigenetic reprogramming of the cancer cells' transcriptome related to DNA repair pathways, but the detailed mechanisms still require further investigation.

c. Maturation of collagen

Researchers activated the expression of the IDHm during neuronal development in mice and observed that collagen synthesis and maturation were impaired, as measured by the level of soluble collagen present in the developing brain. Thus, the

basement membrane was disrupted, especially around blood vessels. This disruption likely contributes to the brain hemorrhage in these mutant mice. In addition, it has been previously shown that disruption of collagen folding by suppressing PHD activity leads to ER stress. Indeed, the levels of several ER stress-responsive genes were elevated in the brains of these IDHm mice.

d. Adaptation to hypoxia

Hypoxia response is largely mediated by Hypoxia-inducible transcription factors (HIF1–3). In normoxia, HIF is hydroxylated by HIF prolyl hydroxylases (PHD/EGLN). Subsequently, the hydroxylated HIF-a is recognized by von Hippel–Lindau (VHL) E3 ligase for degradation through the proteasome pathway. FIH can also hydroxylate HIF-a, resulting in its disability in interacting with transcription cofactors. HIF coordinates the response to hypoxia, ranging from forming new blood vessels to synthesizing red blood cells. HIF also regulates genes involved in glycolysis, glucose transporters, invasion factors, and survival factors. Although PHD/EGLN/FIH belong to the α-KGDD family, the influence of 2-HG on the HIF pathway seems debatable.

In IDHm glioma cell lines, Zhao *et al*. described that high concentrations of R-2HG suppress the activity of PHDs and FIHs, which reduces HIF-1 degradation, and increases HIF-1-dependent transcription [178]. It was also reported that L-2HG, a much more potent inhibitor, is synthesized primarily by cells in hypoxic microenvironments, and oxygen-starved tissue has a particular need for angiogenesis to combat hypoxia [179]. Koivunen *et al.* obtained similar results as the papers mentioned above, as they observed that L-2HG inhibited prolyl hydroxylase. Surprisingly, however, this research group also describes that instead of inhibiting, R-2HG is either related to the activation of PHDs [180] or is insufficient to affect HIF-1 [181]. The paper reports that HIF-1α levels were reduced in human IDHm tumors compared to IDHwt samples. Sun *et al*. also demonstrated that in U87 IDHm glioma cell line and IDHm patients, angiogenesis-related factors, including ANGPT1, PDGFB, and VEGFA, were downregulated, and promoter regions were also highly hyper-methylated [182]. This contradictory evidence suggests that the molecular mechanisms regarding how R-2HG impacts the hypoxia-sensing pathway are still to be fully characterized.

Overall, L-2HG partakes in acclimatizing hypoxia by regulating the activity of the HIF pathway. A study suggests that besides sensing oxygen directly, TET and KDM4C can sense changes in oxygen concentration indirectly through L-2HG. [183]**.** However,

in terms of D-2HG, there is no definitive evidence demonstrating D-2HG's contribution to the adaption to hypoxia.

EGLN enzymes were initially reported to be inhibited by R-2HG, implying that HIF acts as an oncogenic driver in IDHm tumors [184]. However, another study showed that R-2HG could potentiate EGLN activity, which blunts hypoxia-induced stabilization of HIFα [160], [185]. Moreover, HIF levels are relatively low in IDHm gliomas [186], [187]. It was also observed that loss of Hif1a potentiates tumor growth in an IDHwt orthotopic brain tumor mouse model, suggesting that HIF1α functions as a general tumor suppressor in brain tumors [188]. Two possible phenomena might explain why R-2HG is associated with enhanced EGLN activity. FirEGLN1 may stimulate rapid oxidation of R-2HG to α-KG, which is then decarboxylated to succinate by canonical EGLN1 activity [185]. Second, R-2HG can be converted to α-KG even in the absence of EGLN1 by prolonged incubation with high concentrations of iron and reducing agents [189].

e. Angiogenesis

Unlike HIF, endostatin is a natural inhibitor of angiogenesis, which ultimately reduces tumor vascularization and suppresses tumor growth. 2-HG can competitively inhibit the enzyme (PHD2) responsible for its synthesis, leading to lower concentrations of endostatin in IDHm gliomas [190]. The direct effect of 2-HG on endostatin was confirmed by the observation that 2-HG injection into cells decreased endostatin levels [153].

It was recently shown that R-2HG is imported into vascular endothelial cells and their mitochondria via the Na^+-dependent glutamate transporter SLC1A1. R-2HG remodels mitochondrial respiration by promoting mitochondrial Na+/Ca2+ exchange, which, in turn, activates the mitochondrial respiratory chain and fuels vascular endothelial cell migration in tumor angiogenesis. SLC1A1 deficiency in mice abolishes IDHm-promoted tumor angiogenesis as well as the therapeutic benefit of IDHi in solid tumors [191].

f. mTOR signaling

KDM4A reduces the ubiquitination of the DEP domain-containing mTOR interacting protein (DEPTOR) [95,98] which is an endogenous negative regulator of the mTOR pathway [96]. Therefore, the loss of DEPTOR by R-2HG blockade of KDM4A could enhance mTORC1/2 kinase activities [97]. The activated mTORC1/2 promotes cell

growth and survival [97]. An alternative mechanism of mTOR activation is mediated through the expression of Rictor, which is upregulated in IDHm patients' samples and cell lines [99].

Conversely, 2-HG was shown to inhibit ATP synthase, thereby inactivating mTOR and cell growth. This discovery uncovered the growth-suppressive effect of 2-HG on IDHm glioma [192] which was then followed by investigations on the role of FTO inhibition.

g. Metabolic reprogramming

The process of 2-HG's generation largely reprograms the metabolic landscape of IDHm cells. Briefly, 2-HG synthesis consumes the reducing equivalent NADPH and NADH, downregulates lipid synthesis, decreases glycolysis, stimulates glutamine metabolism, depletes the TCA flux, and impairs mitochondrial respiration.

Depletion of coenzymes, such as NADPH, impairs the regeneration of reduced glutathione (GSH), causing the accumulation of intracellular Reactive Oxygen Species (ROS) and elevated oxidative stress [193], [194]. Depletion of NADC by targeting nicotinamide phosphoribosyltransferase (NAMPT) prompted a synthetic lethality in IDHm cells [195]. Since NADC is a substrate for base excision repair (BER) mediated by PARP DNA repair machinery, IDHm glioma hardly sustains genomic integrity. This might explain the hypersensitivity of IDHm glioma to PARP inhibitors, which could synergize with a DNA alkylating agent such as TMZ [195]–[197]. Recent findings showed that the nuclear factor erythroid 2-related factor 2 (NFE2L2, also known as NRF2) plays a pivotal role in IDHm cells by elevating the transcriptional activation of cytoprotective genes to support *de novo* GSH synthesis and ROS scavenging [198]. Inhibiting Nrf2 by triptolide, a diterpenoid epoxide from *Tripterygium wilfordii*, compromised glutathione synthesis and caused synthetic lethality in IDHm glioma by inducing oxidative damage [198], [199]. The vulnerability to oxidative stress also derives from the potent inhibition of BCAT1/2, which lowers glutamate and prompts a dependence on the glutaminase to generate glutamate and downstream glutathione [200]. Hence, ablating glutaminase in IDHm glioma extensively sensitizes cells to oxidative damage and radiation [201].

Although multiple studies have revealed the metabolic stress in IDHm cells, the role of R-2HG in metabolic reprogramming in cancer cells is still controversial. For example, IDH mutation, but not 2-HG, was shown to prompt significant alterations in

the levels of NADP and NAD. Interestingly, IDH1 R132H mutation in normal astrocytes leads to increased expression of the NAD-synthesizing enzyme nicotinamide phosphoribosyltransferase (NAMPT), which could replenish the pool of NAD through the salvage pathway. The authors also suggest that these effects are not 2-HG mediated [202].

R-2HG also inhibits the mitochondrial electron transport chain by compromising the activity of cytochrome c oxidase (COX), resulting in a lower mitochondrial threshold to induce apoptosis, which has been shown to sensitize IDHm AML cells to the inhibitor of the anti-apoptotic protein BCL-2 [203]. Similarly, another study showed that R-2HG inhibits succinate dehydrogenase (SDH), which leads to the accumulation of succinate and finally induces the mitochondrial membrane localization of BCL-2 [204]. Another member of the BCL-2 family, Mcl-1, is downregulated in IDHm glioma, causing a dependence on the anti-apoptosis protein Bcl-xL and thus, the synthetic lethality of IDHm treated with Bcl-xL inhibitor [205]. These researches indicate that IDHm has a specific role in dictating cell death program, inducing a dependence on specific anti-apoptotic proteins, which might be potential targets.

In conclusion, epigenetic disarray, aberrant gene expression, blockade of differentiation, and altered metabolism all contribute to the transformed and tumorigenic state of IDHm cells. Additionally, the effects of IDHm are probably dependent on the cell type and genetic context, which render the comprehensiveness of these effects very difficult and still a matter of debate within the scientific community. Nonetheless, IDHm tumor cells may acquire the capacity to export R-2HG to evade the detrimental effects of intracellular R-2HG. The impact of this oncometabolite in the extracellular space is much less known. In order to understand the effects of R-2HG on the immune cells invading the tumor, we must first describe this atypical microenvironment in comparison with IDHwt tumors.

B. The immune microenvironment of IDHm gliomas in comparison with IDHwt gliomas

Deciphering the glioma tumor microenvironment has been the subject of vivid research. Only little was known three years ago when I began my Ph.D. project, and much has been done in the meantime. The first studies used bulk RNA-Seq of sorted non-tumoral cells, but the advent of scRNA-seq enabled a more accurate assessment

of the TME. It is comprised of numerous cell types: (i) tissue-resident cells such as neurons and astrocytes; (ii) myeloid cells such as resident microglia cells (MG); monocyte-derived macrophages (MDMs), monocytes, dendritic cells (DCs) and neutrophils; (ii) lymphoid cells and (iv) endothelial cells, pericytes, and fibroblasts. These cells are surrounded by a distinctive extra-cellular matrix (ECM). In this section, we will focus on the immune microenvironment. Noteworthy, the most limiting factor of a relevant quantification of immune cell types in glioma's TME is the variability of tumor sampling due to neurosurgeon techniques, localization of tumor resections, and, especially, the lack of uniform data collection. These limitations increase inter-studies variability and prevent the production of a uniform atlas of glioma's immune cells. A summary of the different immune clusters identified by scRNA-Seq in human samples is presented in Supplementary Table 5.

1) General immune landscape of gliomas

a. Evolution of technologies to study TME's composition

Because of the paucity of some immune cell types, such as T cells or granulocytes, traditional methods like immunofluorescence, flow cytometry, or even bulk RNA-Seq are not informative enough to fully characterize glioma's TME. scRNA-seq enables to determine the entire transcriptome of thousands of individual cells. Cytometry by time-of-flight (CyTOF) utilizes monoclonal antibodies conjugated with metal isotopes, which, due to minimal overlap between channels, allows evaluating more than 40 parameters in a single run. Cellular indexing of transcriptomes and epitopes by sequencing (CITE-seq) combines these two approaches by application of oligonucleotide-conjugated antibodies, of which the oligonucleotide tags are sequenced in parallel with transcriptome libraries, allowing simultaneous RNA and surface protein measurements. This relatively new method allows the identification of surface proteins and their level of expression, which enables a much more precise characterization of immune phenotypes. Additionally, spatial transcriptomics techniques are emerging and allow a quantitative transcriptome analysis with spatial resolution in tissue sections. In this approach, histological sections are positioned on arrayed reverse transcription primers with unique positional barcodes, allowing visualization of mRNAs' distribution within the tissue. More recently, spatial proteomics techniques combine spatial and protein information at the single-cell level.

b. Gliomas are immune desert tumors

Immunohistological staining of CD3+ T cells revealed that both IDHwt and IDHm gliomas are immune-desert tumors. Nevertheless, IDHwt is more infiltrated than IDHm (Figure 24 A). In 2018, Thorsson *et al.* published an extensive immunogenomic analysis of m over 10,000 tumors comprising 33 diverse cancer types using RNA-Seq data compiled by TCGA. The authors identified six immune subtypes: wound healing (C1), IFN-g dominant (C2), inflammatory (C3), lymphocyte depleted (C4), immunologically quiet (C5), and TGF-b dominant (C6). IDH1, ATRX, and CIC driver mutations correlate with C5, which consists mainly of LGG, while C4 is enriched in GBM. Importantly, chromosome 1p (including TNFRS9 and VTCN1) and 19q (including TGFB1) deletions associate with lower leukocyte fraction [12]. Therefore, there are differences between IDHwt and IDHm gliomas' microenvironment, even though both are defined as immune-desert.

c. Brain is shielded from immune infiltration

The brain was long believed to be an immunopriviledged site because of two morphological peculiarities: the absence of lymphatic vessels and the presence of the BBB. Two physical barriers regulate the homing of immune cells from the blood to the CNS: the BBB formed by the CNS parenchymal microvessels and the blood-CSF barrier formed by the choroid plexuses. The BBB is a selectively permeable barrier that protects the delicate (and non-regenerative) neural tissue from inflammatory damage. In experimental autoimmune encephalomyelitis, it has been demonstrated that mononuclear cells' diapedesis occurs via the transendothelial process of the cerebral venules, keeping the endothelial tight junctions intact [206].

However, this long-standing concept has been challenged and is now refuted. Indeed, CSF circulation was revised by the discoveries over the glymphatic system, involving paravascular routes where fluids are freely exchanged between the brain's cerebral interstitial fluid (ISF) and CSF without crossing the endothelial cell layer[207]. Meningeal lymphatic vessels receive CSF from the adjacent subarachnoid space and ISF via the glymphatic system, then transport the fluids into deep cervical lymph nodes via foramina at the skull base [208]. Thus, the BBB is not designed to keep leukocytes out of the brain but contributes to regulating immunoregulatory cells and molecules in the CNS microenvironment. Additionally, contiguous communication between the skull, bone marrow, and the brain provides an avenue for active traffic of myeloid cells to respond to emerging disturbances such as brain tumors. Indeed, brain tumors release signals into the CSF, which communicates with the skull bone marrow to

instruct cranial hematopoiesis [209]. This recent evidence further underscores the dynamic and unique nature of the brain immune system. The lack of DCs or other antigen-presenting cells (APCs) capable of conveying antigens to lymph nodes outside the CNS parenchyma makes the CNS hardly capable of constructing immune reactions.

The presence of the BBB can limit immune infiltration in gliomas. Nonetheless, during gliomagenesis, the growth of the tumor exerts physical pressure on the brain that can cause a disruption of the BBB and might facilitate the recruitment of immune cells to the TME. In a mouse model, it was shown that GBM cells displace astrocytic endfeet from endothelial or vascular smooth muscle cells and cause a focal breach in the BBB [210]. Clinical evidence also demonstrates a significant tumor burden with an intact BBB in all GBM [211].

2) Myeloid cells

a. Microglia and monocyte-derived macrophages

Tumor-associated macrophages and microglia cells (TAMs) represent up to 50% of the cells in the TME of gliomas (Figure 24 A).

i) Origins

During embryonic life, progenitor cells from the yolk sac migrate into the CNS and differentiate into parenchymal MG [212]. This brain-specific type of cell was preserved through the evolution of species to maintain CNS homeostasis, support maturation and functional adaptation of neuronal networks, and contribute to the elimination of apoptotic cells. Although studies in healthy adult mice did not detect extensive spatial heterogeneity, human MG cells display region-specific transcriptional programs. Moreover, MG cells' transcriptional programs diversify with age. Indeed, the comparison of MG from ten species identified greater microglial diversity in humans than in all other species analyzed, including macaque, marmoset, sheep, hamster, and mice [213]. Though some MG display remarkable longevity [214], the pool of these immune cells is sustained by modest local expansion throughout adult life with different proliferative rates depending on the brain region. During neuropathological conditions, specific MG clones expand to contend with CNS damage and subsequently decrease in cell number upon returning to homeostatic states [215]. Interestingly, neurological disorders are associated with changes in microglial activation states related to immune cell recruitment, cell debris removal, and cytokine production but typically not antigen presentation [216]. Although little is known about the proliferation

dynamics of MG under the influence of gliomas, MG and MDMs both have the proliferating capacity, which was assessed by Ki-67 expression [109].

Macrophages have two different origins: (i) tumor-infiltrating monocytes, which derive from hematopoietic stem cells; and (ii) tissue-resident macrophages, located in the perivascular, leptomeningeal, choroid plexus, and dural niches. Mice studies show that CNS-associated macrophages are diverse and long-lived. Some of these cell populations are replenished via local self-renewal, and others by bone-marrow macrophages [217]. Understanding the modulation of these macrophages by gliomas is an area of active investigation. The discovery that the skull and the vertebral bone marrow are prominent sources of monocytes implies that they contribute to the supply of MDMs in the TME. However, the extent of this contribution has not yet been defined [218]. Peripheral blood is still the best-known source of tumor-infiltrating myeloid cells. Particularly, relevant numbers of myeloid-derived suppressor cells (MDSCs) were found in matched peripheral blood and tumors of patients with grade 4 GBM [219]. MDSCs are myeloid progenitors at earlier stages of differentiation that develop and accumulate systemically and in the TME, where they promote an immunosuppressive milieu in support of gliomagenesis.

ii) Discriminating markers and localizations

One of the most significant challenges in understanding the functional role of the TAM is finding specific biomarkers able to distinguish between resident MG and infiltrating MDMs. Indeed, these two populations share positivity for CD45, CD68, IBA1, and to a lesser extent, TMEM119. Single-cell technologies have enabled exquisite characterizations of the multidimensional phenotypic states of TAMs and the validation that they are indeed distinct entities (Figure 24 B).

Müller *et al*. used TAMs' transcriptional profiles derived from a genetic lineage-tracing study to discriminate MG from MDMs in their scRNA-seq analysis of GBM samples. They determined P2RY12 and CD49d as good discriminating markers for MG and MDM, respectively. They demonstrated that although all TAMs show tumor-induced expression of human leukocyte antigen-DR (HLA-DR), its expression is higher in P2RY12- MDMs compared to P2RY12+ MG [220], [221]. This finding was confirmed by another study demonstrating significantly increased HLA-DR levels in MDMs versus MG both in IDHwt and IDHm gliomas. Globally, the expression of MHC-II molecules is higher in MDMs compared to MG [222].

Conversely, MG could be discriminated by the positivity for TMEM19, Sall1, and the low expression of CD206. Instead, MDMs express AHR, VDR, and high expression of CD206 [109]. The two transcriptomic signatures were then applied to estimate dominant populations across glioma anatomical regions in the dataset from the Ivy Glioblastoma Atlas Project [223]. The results showed that MG are enriched in the leading edge and adjacent white matter. In contrast, MDMs show increased accumulation in the areas containing hyperplastic blood vessels, microvascular proliferation, and peri-necrosis. Consistently, scRNA-seq on human GBM samples resected from a tumor core and tumor periphery demonstrated that MDMs predominate within the tumor core (69%). In contrast, MG are most abundant at the tumor edge (86%) [224]. Additionally, live *in vivo* 2-photon microscopy in mice models, showed that MDMs tend to be more enriched in the tumor core, while MG are typically found at the tumor periphery. The authors also demonstrated that MDMs are small and motile, while MG are large, sessile cells whose processes continuously extend and retract within tumors [225]. Peripheral monocyte infiltration occurs in the early phases of tumor development and is maintained by constant immune cell recruitment, as shown by the higher expression levels of MDMs genes compared to MG genes in advanced stages of gliomas irrespective of IDH mutational status [110]. The shift in the predominance of MG to MDMs suggests that they might compete for space in the TME. Indeed, it was documented that the blockade of monocyte infiltration increases MG cell numbers [226]. Subsequent studies show that TAMs from the periphery are enriched in the expression of pro-inflammatory interleukin IL1B and several cytokines (CCL2, CCL3, CCL4, TNF), as well as CSF1 and its receptor (CSF1R). However, core-derived TAMs present increased expression of pro-angiogenic VEGFA (vascular endothelial growth factor A), hypoxia-induced HIF1A, and anti-inflammatory interleukin IL1RN. These observations highlight tumor proximity's importance in expressing a distinct TAM phenotype. Interestingly, immune-checkpoint encoding genes CD274 (PD-L1), PDCD1LG2 (PD-L2), CD80, and CD86 (CTLA4 receptors) were expressed in both regions, with a slightly higher level in the periphery [224].

iii) IDHm vs. IDHwt

In 2020, two seminal studies by Swiss groups enabled for the first time a deep characterization of the TME of both IDHwt and IDHm gliomas, as well as brain metastases. These studies have shown that IDHwt gliomas have a very different myeloid cell composition and phenotype compared to those infiltrating IDHm gliomas. In IDHwt gliomas, MDMs comprise around 30% of TAMs, whereas, in IDHm gliomas, such cells occur at a very low number and harbor higher numbers of MG. Although not

abundant, monocytes represented the main myeloid cell population derived from the blood in IDHm gliomas. Their levels were comparable between IDHwt and IDHm gliomas indicating poor recruitment and, maybe, a deficient transition to tissue macrophages, although more evidence is needed to conclude.

We previously mentioned how IDH-A and IDH-O differ regarding genetic events and lineage origins. However, another study recently revealed that differences in bulk expression profiles are primarily explained by TME composition but not by distinct expression programs of glial lineages in the malignant cells. Indeed, they showed an overall increase in MG/MDMs infiltration in IDH-A compared to IDH-O. They also associated the MDM program, but not the MG program, with clinical grade and increased vascularity. These results suggest that MDMs infiltration is facilitated by the development of the disease, which is related to increased angiogenesis and alterations of the BBB [227].

Among the wide variety of TAMs' immune functions, immunosuppressive and tumor-supporting effects were particularly described. These functions are mediated by the secretion of glioma-derived factors, such as CSF-1, periostin, and NO. MDMs have been shown to produce anti-inflammatory cytokines such as IL-10, transforming growth factor-beta (TGF-β), IL-6, pleiotrophin, as well as molecules with tissue remodeling and angiogenesis properties such as VEGF, MMP2, MMP9, and versican-induced MT1-MMP. Functional transcriptomic profiles of MDMs described in the literature include: (i) interferon-related associated with increased expression of STAT1, IFIT2, ISG15, CXCL10; (ii) phagocytosis/lipid-related showing enhanced expression of GPNMB, LGALS3, FABP5, CD9; (iii) hypoxic characterized by induction of BNIP3, ADAM8, MIF, HILPDA; and (iv) immunosuppressive clusters [226], [228].

Recent studies identified molecular targets expressed by MDMs responsible for the induction of immunosuppression. The scavenger receptor MARCO was shown to be differentially expressed by MDMs from GBM compared to IDHm. These macrophages were associated with a mesenchymal profile and worse prognosis [229], [230]. In other studies, MDMs expressing CD73 in GBM were shown to have highly immunosuppressive and hypoxic gene signatures similar to the one displayed by MARCO-expressing MDMs [231], [232]. CD39 and CD73 are part of an immunosuppressive pathway that converts ATP to adenosine which binds to the A2a receptor (A2aR) on effector T cells rendering them exhausted. It was also shown that MDMs release several cytokines and ligands, such as oncostatin M (OSM), which binds to its cognate receptor and leukemia inhibitory factor receptor that signals through the

signal transducer and activator of transcript 3 pathway to induce the MES-like transcriptional program in glioma cancer cells (cf page 67 Heterogeneity of adult diffuse gliomas). Therefore, OSM induces the expression of MHC class I and II by glioma cells, resulting in increased susceptibility to T cell killing as shown by coculture assays [233]. Finally, the most extensive scRNA-Seq analysis to date identified S100A4 as a marker expressed by TAMs, which suppresses the immune response and promotes glioma growth [228].

Three findings support a more activated microglial phenotype in IDHwt glioma and brain metastases (BrM) than in IDHm glioma: (1) MG from IDHwt gliomas and BrMs express increased levels of CD14 and the scavenger receptor CD64; (2) MG from IDHwt gliomas and BrMs show an amoeboid morphology, associated with activation; and (3) MG from IDHm gliomas display a ramified morphology associated with homeostatic function [109], [110]. MG also develop specialized functions upon interaction with their TME. Clusters identified in the context of IDHm and GBM include (i) interferon-related associated with increased expression of IFIT1/3, CXCL10; (ii) phagocytic/lipid signatures, (iii) activated and homeostatic MG; and (iv) immunosuppressive clusters [226], [228]. Investigations on MG-specific targets are still lacking probably because these cells are sparse in the TME of GBM, the most studied type of glioma (Figure 24 C).

One of the objectives of my Ph.D. work was to characterize the myeloid compartment of both IDHm and IDHwt gliomas. Although other groups published results with more resolutive techniques, none thoroughly compared the MDMs and MG of IDHwt and IDHm, respectively, at the transcriptomic and epigenetic levels.

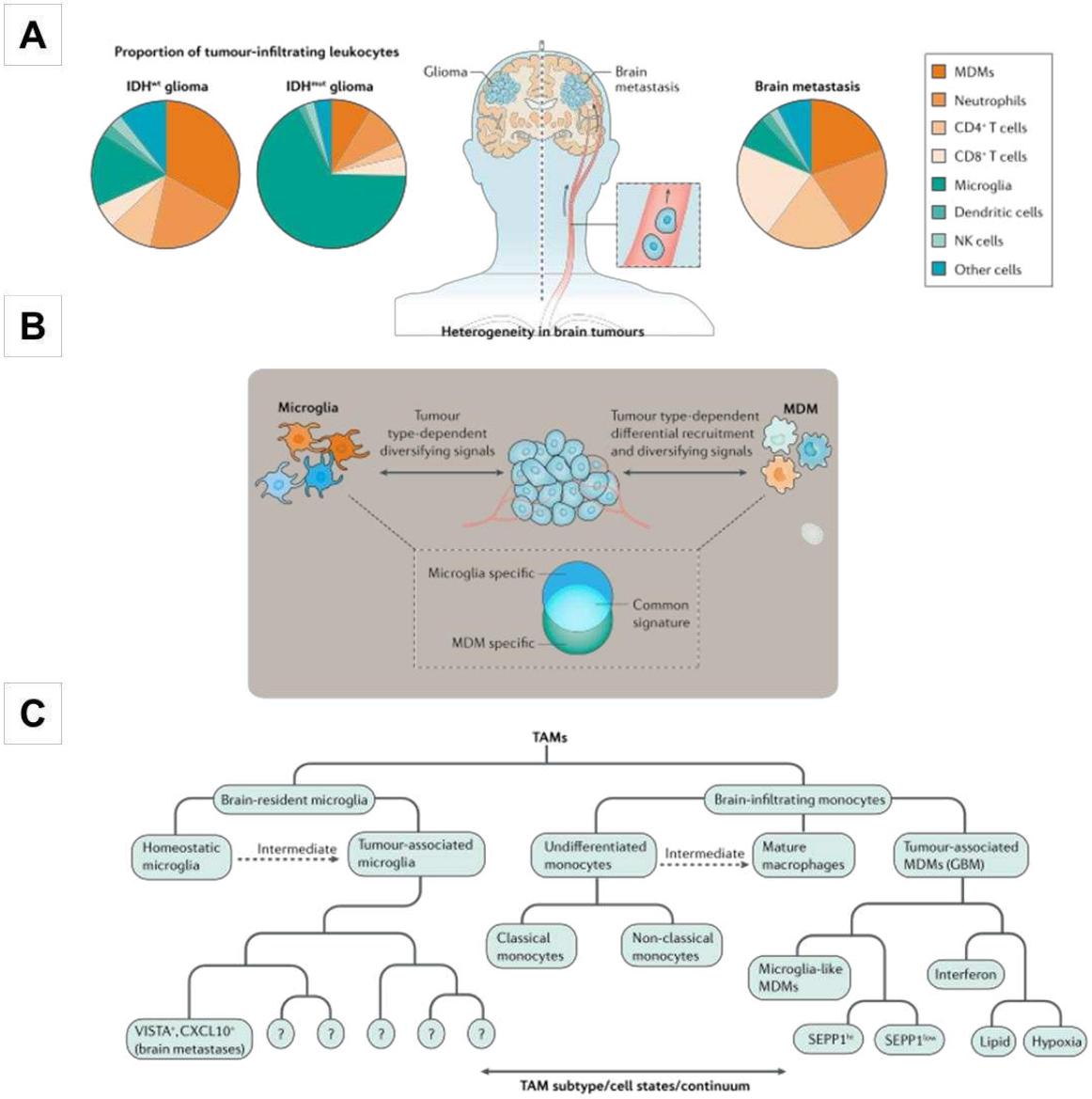

Figure 24| Gliomas' immune landscape.

A| Pie charts of the composition of immune cells in IDHwt and IDHm gliomas (left) and brain metastases (right) as determined by Friebel *et al.* [110] and Klemm *et al.* [109].The pie charts represent general trends from multiple tumors. **B|** Two main cell populations are resident microglia cells and infiltrating monocyte-derived-macrophages (TAMs) sharing transcriptomic similarities. **C|** Organizational structure for TAMs nomenclature. Notable subsets are listed from B. M. Andersen *et al.* GBM: glioblastoma; NK: natural killer. Adapted from [234].

b. Dendritic cells

Importantly, in brain tumors, it is suggested that DCs recognize and present tumor-derived antigens inside the brain tissue or in the draining lymphoid stations in order to elicit a specific T effector cell response against cancer cells [235].

Friebel *et al.* observed populations of cDC1, cDC2, and plasmocytoid DC (pDC) in both IDHwt and IDHm at similar frequencies. An increase in the relative frequencies of T cells, neutrophils, and pDCs correlated negatively with TAM/monocyte frequencies, whereas T cell frequencies positively correlated with pDCs and cDCs frequencies [110]. It is well known that tumor-derived factors affect infiltration, differentiation, recruitment, survival, and functions of DCs via diverse mechanisms. In GBM, FGL2 produced by tumor cells, interfered with GM-CSF signaling, blunting the differentiation of CD103+ cDC1s and consequently lowering the CD8+ T cell response [236]. PGE2 from glioma cells was found to increase the expression of IL-10 by DCs, in turn leading to the induction of Tregs response and reduced stimulation of effector T cells [237]. It was also shown that the TME of GBM induces overexpression of Nrf in DCs, which in turn results in the suppression of DCs maturation and the consequent decrease in effector T cell activation and that the inhibition of Nrf2 pathways rescued maturation of CD80+ and CD86+ DCs [238].

c. Myeloid-Derived Suppressor Cells (MDSCs)

MDSCs are a critical component of the suppressive network that supports tumor progression and contributes to therapy resistance. This population consists of two large groups of cells: granulocytic or polymorphonuclear MDSCs (PMN-MDSCs) and monocytic MDSCs (M-MDSCs). PMN-MDSCs are phenotypically and morphologically similar to neutrophils, whereas M-MDSCs are similar to monocytes. In humans, M-MDSCs are described as CD14+CD11b+CD33+HLA-DRlow/−CD15−, PMN-MDSCs as CD14−CD11b+CD33+HLA-DRlow/−CD15+ (or CD66+).

In glioma patients, the intratumoral and systemic blood frequency of MDSCs increases during progression and correlates with the grade and prognosis [239]. GBM patients with more prolonged survival also had reduced MDSCs levels, similar to LGG patients [219]. However, the role of MDSC in GBM recurrence is not well understood, and further studies are needed to clarify this critical point. In human gliomas, it is unclear whether there is the predominance of a specific subset of MDSCs.

PMN-MDSCs are very similar to neutrophils, but LOX1 marker seems to be specific to human PMN-MDSCs [240]. In GBM, Chai *et al.* reported that high presence of LOX1+PMNs but not LOX1-PMNs in the peripheral blood and tissue negatively correlated with the number of effector immune cells and was associated with an early recurrence and disease progression. LOX1+PMNs displayed a significant increase in

the expression of ROS, ARG1, and iNOS and the ability to suppress the proliferation of CD3+ T cell in an ARG1/iNOS-dependent manner [241].

d. Neutrophils

Neutrophils are growingly appreciated as a critical component of the TME. Neutrophils systemically and intratumorally accumulate in glioma patients, and a high frequency of neutrophils is correlated to a poor prognosis of GBM patients [242]. Moreover, their number also correlates with glioma grade and represents a negative prognostic parameter for resistant patients [243], [244]. Alghanri *et al.* used scRNA-Seq both in mice and humans and found that the granulocytes recruited to the TME of IDHm tumors are mainly neutrophils and preneutrophils, with a small fraction of PMN-MDSCs. More precisely, in fresh primary tumor samples, they found that the fraction of PMN-MDSCs (defined by the expression of IL1β, S100a8, S100a9, ARG1, and TGFβ1) accounted for nearly 23% of all immune cells in IDHwt tumors but only 3.75% of the total immune cells in IDHm tumors.

An *in vitro* coculture experiment with human glioma cells and a neutrophil progenitor cell line showed that neutrophils directly promoted GBM-initiating cells' proliferation and migration via the production of S100A4, which induced the transition to a mesenchymal phenotype. This was later linked to favoring cancer invasion and resistance to anti-VEGF therapies [245]. Furthermore, neutrophil extracellular traps (NETs) were shown to protect cancer cells in the brain and support the development of both primary tumor and metastasis niches [246]. Very interestingly, neutrophils isolated from GBM patients suppressed T cell function in an AARG1-dependent manner. Critically, T cell suppression could be reversed entirely through pharmacologic ArgI inhibition or with arginine supplementation [247]. A recent article showed that neutrophil-induced ferroptosis promoted tumor necrosis in GBM progression through a mechanism involving iron-dependent accumulation of lipid peroxides within the TME. Analyses of human GBMs supported that neutrophils and ferroptosis are associated with necrosis and predict poor survival in patients [248].

3) Lymphoid cells

a. NK cells

Innate lymphoid cells play a significant role in anti-tumor immunity and are potent regulators of the TME. Friedel et al.'s analysis of NK cells showed that the two main populations of CD56int/brightCD16− and CD56intCD16+ correspond to the

immature and cytotoxic NK cells, respectively. IDHwt gliomas are enriched in immature NK cells, whereas predominantly mature NK cells accumulate in the IDHm gliomas. Among the immature cluster, they also found a significant population of CD69+CD103+CD56+ cells, which closely resemble intraepithelial ILC1-like cells, whose number correlated with OS in IDHwt patients.

b. T cells

T cells were also dissected in these studies. Friedel *et al.* and Klemm *et al.* show no difference in the overall T cell infiltration rate between IDHwt and IDHm gliomas. However, Tregs were significantly more frequent in IDHwt gliomas, and T cell frequency positively correlated with pDCs and cDCs frequencies. In contrast, an increase in those populations was associated with decreased TAM/monocyte frequencies [109], [110]. Additionally, division of T cells into five functional subsets: naïve, central memory (CM), effector memory (EM), terminally differentiated effector memory (TEMRA), and non-circulating tissue-reside0000022nt (RM), according to the expression of five markers (CD45RA, CD45RO, CCR7, CD127, and CD103), enabled the authors to conclude that the majority of T cells found in GBMs were memory T cells. Moreover, CD8 RM and EM T cells had lower expression of proliferation and activation markers in IDHm compared to IDHwt gliomas. In contrast, IDH status did not affect the expression of co-stimulatory (ICOS, CD27, and CD137) and co-inhibitory receptors (2B4, TIGIT, and PD-1) [110].

Mathewson *et al.* investigated T cell subtypes by scRNA-Seq in a cohort of 26 primary and recurrent IDHwt and IDHm tumors. They first show that corticosteroid therapy with dexamethasone was associated with substantially reduced numbers of infiltrating T cells. Interestingly, the overall representation of clusters was similar in IDwt and IDHm gliomas. Both CD8 and CD4 T cells expressed an interferon signature, an effector memory signature, or a stress signature. The latter was not an artifact, as shown by the expression of these genes by RNA in situ hybridization. Several NK cell receptor genes, including KLRC2 (NKG2C protein), KLRC3 (NKG2E protein), KLRC1 (NKG2A protein), KLRD1 (CD94 protein), and KLRB1 (CD161 protein), were expressed by CD8 T cells with high cytotoxicity scores. This subset of CD8 T cells represents effectors that share transcriptional profiles with innate cells, despite having a diverse TCR repertoire. The authors postulated that inflammatory mediators induce the expression of these NK cell receptors in the TME. Mechanistic *in vitro* and *in vivo* studies demonstrated that the CD161 receptor inhibits T cell function and that the blockade of its liaison with its cognate receptor CD161, expressed by immunosuppressive myeloid and glioma cells,

was sufficient to restore an anti-tumoral immune response which increased survival in mice [249].

C. 2-HG is an immunometabolite

We discussed earlier how R-2HG drives tumorogenesis in IDHm glioma cells. In recent years, more knowledge has been acquired regarding its immunological effects. We now know that R-2HG mediates immune-related functions both in glioma tumor cells and immune cells present in the TME. These effects are summarized in Figure 25.

1) Immunological tumor cell-intrinsic effects

a. Decreased chemotaxis

TCGA data suggest that chemotaxis regulating genes are downregulated in IDHm compared to IDHwt. gliomas. Furthermore, CCL-2, CXCL-2, which are major myeloid chemoattractants, and C5a, a mediator of chemotaxis and cellular release reactions, were found downregulated at the mRNA and protein levels in IDHm tumors compared to IDHwt tumors, suggesting again that immune infiltration and chemotaxis are regulated by IDH mutation [250] This has been validated *in vitro* with Boyden chamber experiments using IDHm tumor cells and its conditioned media with different immune cells. An elegant study profiled cytokines known to influence myeloid differentiation in conditioned media collected from either IDHwt or IDHm cultured mouse glioma neurospheres. On the one hand, GM-CSF, CXCL1, CXCL10, IL-5, macrophage inflammatory protein 2, IL-6, and TNF–α were downregulated in IDHm conditioned media. On the other hand, G-CSF, Regulated on activation, normal T cell expressed and secreted (RANTES) (CCL5), IL-33, and Stem Cell Factor (SCF) were the only cytokines that were up-regulated in IDHm conditioned media. To investigate whether IDHm epigenetically regulated these cytokines, the authors performed a chromatin immunoprecipitation sequencing (ChIP-seq) from murine IDHwt and IDHm neurospheres. Only Csf3 showed a marked peak enrichment for H3K4me3, generally associated with transcriptional activation, around its promoter region. To confirm this result in humans, they again performed ChIP-seq analysis on SF10602 (patient-derived glioma cells expressing IDHm, inactivating mutations in ATRX and TP53) after treatment with vehicle or five µM of the IDHm inhibitor (AG1-5198) for seven days. Among all histone marks, they found a down-regulation of H3K4me3 deposition upstream of the transcriptional start site at the gene promoter region in SF10602

treated with AGI-5198 compared to the vehicle. To further validate this, the level of G-CSF was assessed by Elisa in human neurospheres and serum from IDHwt and IDHm patients. Results showed that G-CSF level was significantly higher in patients with IDHm gliomas compared to IDHwt patients. Blocking G-CSF in mice restored the inhibitory potential of PMN-MDSCs and accelerated tumor progression [251].

b. Evasion of immune surveillance

NKG2D receptors, expressed at the surface of NK cells, identify membrane-bound ULBP1 and ULBP3, which activate NK cells and cause target cell lysis. IDHwt tumors have significantly higher levels of ULBP1 and ULBP3 compared to IDHm tumors. The promoter methylation levels of ULBP1 and ULBP3 were also higher in IDHwt than in IDHm tumors, which correlated with transcript silencing. Treatment of IDHm tumor cells with decitabine restored the expression of ULBP1/3 and increased NK cell activation and subsequent NK-mediated cytotoxicity [252]. Conversely, higher DNA methylation levels of MHC-I HLA genes were observed in IDHm tumor cells than in IDHwt, which led to decreased MHC-I expression and upregulation of activated NK receptor recognized ligands, facilitating NK cells mediated lysis [253]. Additionally, 2-HG can activate NF-κB and regulate CX3CL1 expression, which leads to the recruitment of NK cells to the TME [254]. Both MHC-I and MHC-II molecules are downregulated in IDHm cells compared to IDHwt. It was also shown that 2-HG -mediated hypermethylation of the CD274 promoter decreases PD-L1 expression and reduces levels of inflammation [255].

2) Effects on immune cells in IDHm glioma's microenvironment

Study of the immunological effects of R-2HG is an active field of research. So far, R-2HG has been shown to modulate immunity in IDHm tumor cells by epigenetic alterations. However, the only described effects of R-2HG on human immune cells are mediated by metabolic alterations, raising the question as to whether R-2HG can really modify the epigenome of immune cells.

a. Inhibition of classical and alternative complement pathways

Zhang et al. showed that compared with IDHwt gliomas, IDHm tends to have lower complement depositing on the surface of tiny blood vessels and capillaries. In this study, 2-HG significantly reduced C3 deposition on cells through a dose-dependent approach, inhibited C3b (iC3b) complement-mediated phagocytosis and opsonization, and inhibited the assembling of C5 but not C3 convertases in the classical

complement activation pathway. Moreover, complement activation was inhibited by 2-HG, which reduced MAC-mediated brain cancer cell damage [256].

b. MDMs

Friedrich *et al.* explored the TME of human gliomas by single-cell RNA-sequencing and mass cytometry. They demonstrated that myeloid cells from IDHm gliomas showed reduced expression of antigen presentation-associated proteins, suggesting a more immunosuppressive phenotype in comparison with IDHwt. To further investigate the immunosuppressive effects of IDHm MDMs, the authors overexpressed WT or mutant IDH in the GL261 mouse glioma model. They used *ex vivo* cocultures to confirm that MDMs infiltrating IDHm gliomas suppress T cells via IDHm-derived R-2-HG. They found that following exposure to R-2-HG in MDMs, AHR translocated into the nucleus, resulting in an AHR-dependent increase of the anti-inflammatory cytokines IL-10 and TGF-β. Importantly, R-2-HG was not a direct inducer of AHR translocation. Instead, R-2-HG increased the tryptophan-2,3-dioxygenase (TDO)-2-mediated conversion of intracellular l-tryptophan (l-Trp) to the endogenous AHR ligand l-kynurenine (l-Kyn). In response, MDMs increased the uptake of l-Trp via the LAT-1/CD98 heterodimer, which was upregulated in MDMs from IDHm compared with IDHwt tumors. This unique susceptibility of MDMs could be partially overcome by using an AHR inhibitor in combination with an anti-PDL1 antibody inducing prolonged survival of IDHm, but not IDHwt, tumor-bearing mice [257].

c. Microglia

Only little is known about the effects of 2-HG on MG. A study published that 2-HG prevents LPS-induced activation of murine MG by affecting the AMPK/mTOR/NF-κB signaling pathway [258]. More evidence is needed to translate this finding into humans.

d. DCs

As professional APCs, DC play a key role in the initiation of antitumor immune responses but are also essential integrators of microenvironmental signals.

Yet, the effects of 2-HG on DCs are controversial. In 2018, Zhang *et al.* demonstrated that 2-HG in IDH mutant grade III and IV gliomas neither decreased the differentiation of DCs nor the functionality of differentiated DCs nor interfered with the processing or presentation of DC antigens [256]. In 2019, another study seemed to

show that 2-HG had no impact on cell viability but diminished CD83 expression after LPS stimulation. Furthermore, both R- and L-2HG significantly reduced IL-12 secretion but did not impact other cytokines such as IL-6, IL-10, or TNF. The two IL-12 subunits p35/IL-12A and p40/IL-12B genes were decreased in treated DCs. However, signaling pathways involved in LPS-induced cytokine expression (NFkB, Akt, p38) were not altered by R-2HG. 2-HG increased oxygen consumption and addition of the ATP synthase inhibitor oligomycin to DC cultures increased IL-12 secretion and partially reverted the effect of 2-HG [259].

In a more recent study, Friedrich *et al.* show that monocyte-derived DCs are differentially educated in IDHm and IDHwt tumors resulting in distinct phenotypical states. The phenotype of IDHm-educated DC is characterized as an intermediate state between immature monocyte-derived cells in early-stage gliomas, and the fully functional DC found in late-stage IDHwt tumors. Importantly, they demonstrate that paracrine R-2HG delays DC maturation and specifically suppresses MHC class I/II-mediated antigen (cross-)presentation and co-stimulation by IL-6, ultimately leading to reduced T cell activating capacities [260].

e. T cells

IFN-γ, as well as effector cytokine production, migration, and proliferation by activated T cells, were inhibited in a dose-dependent manner by 2-HG [256]. An orthotopic syngeneic glioma model also demonstrated that IDH1 R132H mutation decreased STAT1 protein expression via 2-HG, thus decreasing type 1-associated chemokines such as CXCL10 and, therefore, affecting CD8+ T cell infiltration [261]. The accumulation of intracellular 2-HG leads to increased apoptosis, decreased proliferation, and decreased Treg [262].

It was also reported that NFAT transcription and polyamine synthesis were disturbed after 2-HG uptake, thus reducing the ATP/ADP ratio and thereby inhibiting T cell activity and proliferation [263]. Very recently, a study showed that 20 mM of R-2HG inhibited lactate dehydrogenase (LDH) activity in T cells activated by CD3/CD28 ligation. This inhibition resulted in the perturbed glycolysis, shift to oxidative phosphorylation, and thus, less cytotoxic activity. By intracellular dosage of R-2HG by GC/MS and a mathematical approximation of a T cell volume, they estimated that 3 mM of R-2HG was found inside T cells when 20 mM was added in the culture medium (a concentration too low to inhibit TET enzymes, *cf* A.2) . Accumulation of R-2HG in IDHm tumor cells). Both these articles discarded any epigenetic effect of R-2HG since

the observations stated above were transient and lost when R-2HG was removed from the culture medium.

In mice, similar to L-2HG, R-2HG has also been demonstrated to mediate T cell differentiation. Tao Xu *et al.* showed that reprogramming of T helper 17 (TH17) cells towards induced regulatory T (iTreg) cells happens through increased transamination mainly catalyzed by GOT1 and leads to increased levels of 2-HG in differentiating TH17 cells. The 15N-labeling analysis demonstrated that R-2HG was largely derived from glutamine. This accumulation of 2-HG resulted in hypermethylation of the Foxp3 gene locus and inhibited Foxp3 transcription, which is essential for fate determination towards TH17 cells. Inhibition of the conversion of glutamate to α-ketoglutaric acid prevented the production of 2-HG, reduced methylation of the Foxp3 gene locus, and increased Foxp3 expression. This consequently blocked the differentiation of TH17 cells by antagonizing the function of transcription factor RORγt and promoted polarization into iTreg cells. Moreover, selective inhibition of GOT1 with (aminooxy)acetic acid ameliorated experimental autoimmune encephalomyelitis in a mouse model by regulating the balance between TH17 and iTreg cells [265]. Similarly, a particulate matter activated the expression of GOT1 in an AhR-dependent manner, thereby increasing the metabolic flux from glutamine to D-2HG, generating hypermethylation of Foxp3 loci, and finally disrupting Th17/Treg ratio. Interestingly, they used a GOT1 inhibitor and alleviated pulmonary inflammation in a mouse asthma model successfully and used shGot1 RNA, which significantly tempered experimental autoimmune encephalomyelitis severity in a mouse model [266].

Furthermore, high levels of 2-HG were found in T cells of IDHm AML patients, where it caused HIF-1α protein instability, which led to a metabolic shift toward oxidative phosphorylation, an increase in Tregs number, and a decrease in Th17 polarization [264].

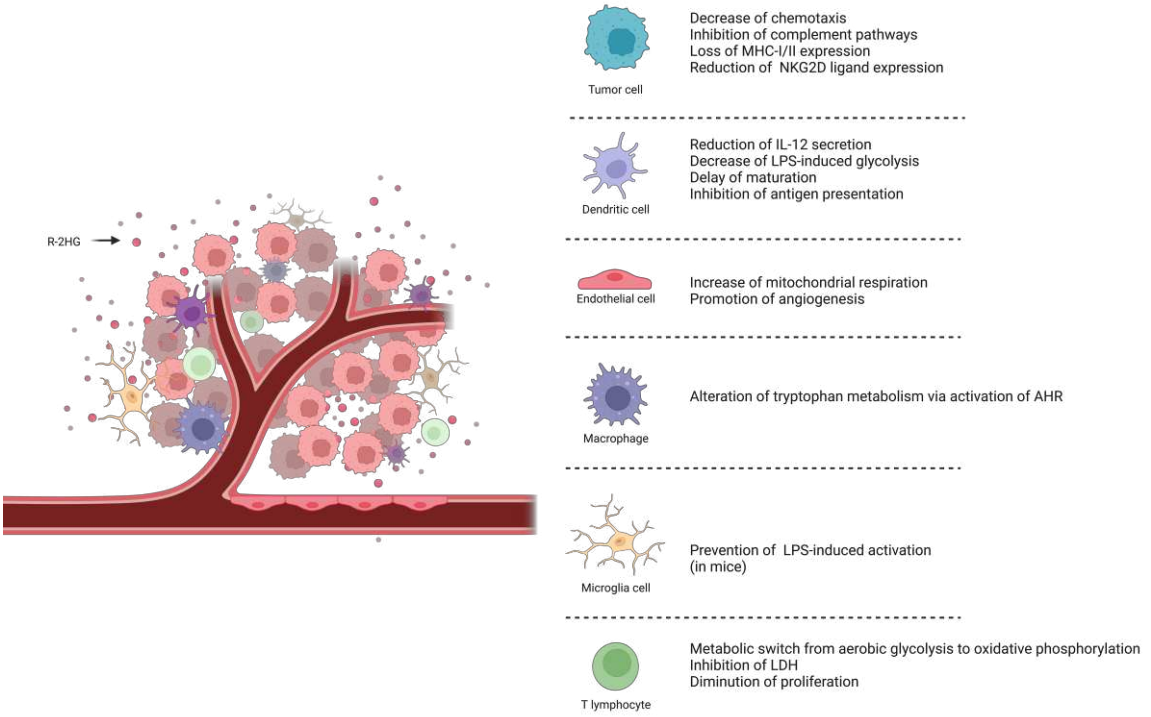

Figure 25| Summary of R-2HG immunological effects on glioma tumor cells and cells in their microenvironment.

From Q. Richard *et al.*, Curr Opin Neurol, 2022.

Overall, it seems that 2-HG educates the TME of IDHm glioma toward a more immunosuppressive phenotype in addition to driving tumorigenesis by blocking the differentiation of progenitor cells via epigenetic mechanisms. However, patients with IDHm still have a more favorable prognosis than IDHwt patients. While precise mechanisms of this prolonged overall survival are currently unknown, selective inhibitors targeting IDHm have decreased both R-2HG levels and tumor growth [267]. Interestingly, a recent study of IDH-O tumors from patients treated with IDHi showed a robust differentiation towards glial lineages, accompanied by a depletion of stem-like cells and a reduction of cell proliferation. However, the paucity of immune cells did not enable to characterize whether this therapy could have impacted the TME. The effects of R-2HG on the blockade of tumor cell differentiation and MHC I/II expression drove us to investigate whether R-2HG could also mediate these effects on immune cells.

PROJECT RATIONALE AND THESIS OBJECTIVES

A. Summary of the introduction

In this introduction, we first presented cancer as a disease defined by one or several hallmarks. One hallmark is tumor cells' capacity to escape the immune system's continuous attacks. Research in the field of cancer immunology led to what is now considered the fourth pillar of cancer treatment: immunotherapy. We detailed the cancer-immunity cycle to understand the specific roles of innate and adaptative immunity and described the concept of immunosurveillance and immunoediting, which ultimately results in cancer escape and progression. We concluded this first section with a survey of the current knowledge on the epigenetic mechanisms which control the lineage commitment, maintenance, and exhaustion of immune cells, especially T cells. We mainly focused on the role of TET-induced DNA demethylation and 5hmC marks deposition. Although the findings of this new research field are still under debate due to the labile composition of epigenetics and the lack of a relevant *in vivo* model, we mentioned a few studies which began harnessing immune epigenetics as a novel, innovative therapeutic approach. Importantly, *ex vivo* culture of CAR-T cells with the TET competitive inhibitor L-2HG resulted in less terminally differentiated, more cytotoxic, CAR-T cells.

This led us to introduce brain tumors and to focus on malignant adult diffuse gliomas, especially, IDHwt and IDHm gliomas. We described their similarities and differences in terms of epidemiology, treatments, and the heterogeneity of their clinical, histological, and molecular characteristics. More precisely, we described how the recent advances in sequencing technologies enabled the characterization of transcriptomic and methylation profiles, which goal is to categorize the inter- and intra-heterogeneity of gliomas in order to stratify patients for more relevant therapeutic strategies. These studies highlighted the crucial role of the interaction between glioma cells and their immune microenvironment in establishing immunosuppressive and more aggressive phenotypes.

In the last section, we described how IDHm amplifies the production of R-2HG. We compared the inhibition potency of R-2HG to other metabolites found in IDHm tumor cells toward α-KG dependent dioxygenases. Although R-2HG is a weak inhibitor, it shapes the epigenetic and metabolomic profiles of IDHm tumor cells. This oncometabolite is exported out of the tumor cell to flood the microenvironment. That is why we next described the immune microenvironment of both IDHwt and IDHm

gliomas and spotted the profound specificities in terms of cell types composition and phenotypes. Finally, we reported the immunological effects of 2-HG in tumor cells but also in the immune cells in which it can enter.

B. Project rationale

Intratumoral heterogeneity not only comprises genomic and epigenomic alterations of tumor cells but also changes in the immune context. Intratumoral heterogeneity of diffuse gliomas is increasingly recognized to play a prominent role in tumor evolution and resistance to therapies. More precisely, bulk tumor DNA methylome and abundance of tumor-associated TAMs have demonstrated a prognostic value. Reciprocal cross-talk between glioma tumor cells, myeloid cells, and T cells also contributes to the immune escape mechanisms of these tumors. Therefore, a thorough understanding of the sources and mechanisms leading to the intratumoral heterogeneity is fundamental for the identification of prognostic and predictive biomarkers, as well as for the design of relevant immune therapeutic strategies.

C. Scientific question and thesis objectives

Myeloid cells are the most abundant immune cell populations in gliomas. Epigenomic modifications drive their phenotypic states and immune functions in response to microenvironmental cues. However, the extent to which such modifications, particularly at the level of DNA methylation, contribute to the intratumoral heterogeneity and how they are connected with well-known transcriptional differences of myeloid cells between IDHm and IDHwt tumors has not yet been investigated. Moreover, while most immunosuppressive mechanisms and myeloid interactions have been reported in high-grade IDHwt gliomas, only little is known in IDHm tumors.

Besides investigation on myeloid cells, an improved understanding of the immune tumor environment requires advanced characterization of tumor-infiltrating lymphocytes. Initial deconvolution analyses applied to bulk transcriptome data from TCGA cohorts estimated that IDHm gliomas are enriched in CD4+ naïve T cells while memory T cells are reduced. Low numbers of immunosuppressive Tregs were also shown, particularly in IDH-O tumors. A recent scRNA-seq study of T cells from IDHm and IDHwt gliomas showed that they share similar phenotypes. Still, the total abundance of T cells and their cytotoxicity program remains higher in IDHwt tumors. Given the paucity of these cells, particularly in IDHm gliomas, more studies at single-

cell resolution are required to ascertain the differences in the T cell states between glioma subtypes.

Finally, recent studies suggested instructive roles for IDHm in shaping the TME. In agreement with this concept, it has been demonstrated that R-2HG released by IDHm glioma cells affects the metabolism of infiltrating macrophages and T cells. While these studies provided a mechanistic basis for the immunomodulatory effects of R-2HG, arguing against a simple reduction of immune cells recruitment by chemotactic factors, there is a dearth of knowledge about the possible impact on this oncometabolite on the epigenome of immune cells. It is now well described that differentiation of immune cells happens through widespread epigenomic modifications, including active demethylation via the DNA demethylase TET2, an enzyme that is expected to be inhibited by R-2HG. Therefore, more investigations are required to specify the roles of R-2HG as immune modulator of the TME of IDHm gliomas.

A detailed survey of the intratumoral heterogeneity in gliomas, differences in the immune TME between IDHm and IDHwt tumors, and cell-extrinsic roles of R-2HG is described in our review article (*cf* annex).

My thesis work aims to advance the characterization of TAMs and T lymphocytes in the immune tumor microenvironment of IDHm gliomas, with an emphasis on signaling pathways related to immune cell functions and epigenetic mechanisms that impact TAMs or T lymphocyte phenotypes.

To address these questions, my PhD work was divided into two main objectives:

1. To investigate the methylation changes that underlie CD11b+ cells functions in gliomas and determine their contribution to intratumoral heterogeneity, we:

- Performed a simultaneous profiling of bulk DNA methylome and transcriptome of CD11b+ and CD11b-cells isolated from human gliomas.
- Identified differentially methylated regions and differentially expressed genes between CD11b+ cells from IDHm and IDHwt gliomas.
- Investigated the contribution of DNA methylation changes to the transcriptional landscapes of CD11b+ cells and highlighted relevant pathways.
- Set up primary cultures of human CD14+ cells obtained from fresh leukapheresis blood and differentiated them into macrophages.
- Ascertained the uptake of non-permeable R-2HG by differentiating monocytes and macrophages using LC-MS and colorimetric assays.

- Assessed the effects of R-2HG on differentiating monocytes' expression of target genes.
- Evaluated the global 5mC and 5hmC methylation levels in immune cells and tumor cells from human samples, and *in vitro*, upon treatment with R-2HG, in differentiating monocytes.
- Analyzed the expression of ligand-receptor pairs between CD11b+and CD11b- cells specific to tumor types.

2. To evaluate differences in T cells phenotypes from glioma subtypes and find relevant potential targets for immune modulation, we:

- Performed an in-depth characterization of immune cells from human gliomas using a scRNA-seq approach.
- Projected our scRNA-seq data onto a reference map to identify and characterize T cell phenotypes.
- Highlighted an inhibitory program specific of IDHm glioma.
- Validated our findings with other scRNA-seq data and at the protein level.
- Set up primary cultures and differentiation assays of human CD14- cells obtained from fresh leukophoresis blood.
- Ascertained the uptake of non-permeable R-2HG by resting and stimulated CD14- using LC-MS.
- Evaluated the differences in global 5mC and 5hmC methylation levels of naïve T cells throughout their differentiation into effector cells caused by R-2HG treatment.
- Examined the effects of R-2HG treatment on T cell differentiation and expression of inhibitory receptors.

The following result section is divided in two parts according to the thesis objectives. The first part accounted for two years of my PhD. The last part accounted for one year of my PhD.

RESULTS

I) ANALYSIS OF THE TRANSCRIPTOME AND METHYLOME OF CD11B+ CELLS FROM IDHM AND IDHWT GLIOMAS

Before starting my PhD, it was decided to isolate CD11b+cells from human frozen IDHwt and IDHm gliomas in order to extract their RNA and DNA for bulk transcriptomic and methylome profiling (A). A few samples were already processed. My first goal was to increase the number of samples per group to perform fair comparisons matched by age and sex and to gain statistical power for the analysis. This resulted in the study described below.

A. Results

1) Study design

To explore tumor cells and immune cells diversity, we profiled bulk DNA methylome and/or transcriptome of CD11b- and CD11b+ cells isolated from 36 human frozen primary glioma resections (Figure 26 A). To avoid known biases, samples were matched by age and sex, and fully characterized for their clinical, pathological and genetic features (Table 1).

Table 1| Clinical and genetic details of the cohort

Sequencing	Status	Patient ID	Sex	Age at surgery	Histology	Grade	Tumor localization	Tumor hemisphere	Chemotherapy prior to surgery	Chemotherapy details	Corticotherapy prior to surgery	Corticotherapy details	Anti-epileptic	Relapse
DNA	IDHwt	N17-0071	F	69	Grade 4 Glioblastoma	4	Frontal	Right	NO		NO		NO ?	NO
DNA	IDH-O	N17-0199	F	60	Grade 3 Oligodendroglioma	3	Temporal	Right	NO		NO		Lamictal	YES
DNA	IDHwt	N17-0200	M	68	Grade 4 Glioblastoma	4	Temporal	Left	NO		NO		Trileptal, Depakine chrono	NO
DNA	IDH-O	N17-1314	F	31	Grade 3 Oligodendroglioma	3	Frontal	Left	YES	Temozolomide 24c	NO		Keppra + Lamictal	YES
DNA	IDH-A	N17-1610	M	25	Grade 3 Astrocytoma	3	Frontal	Right	NO		NO		Keppra	NO
DNA	IDHwt	N17-1698	M	51	Grade 4 Glioblastoma	4	Parietal	Left	NO		NO		Keppra	NO
DNA	IDH-A	N17-1710	M	29	Grade 2 Astrocytoma	2	Frontal	Right	NO		NO		Keppra	YES
DNA	IDH-A	N17-1743	M	22	Grade 2 Astrocytoma	2	Frontal	Left	NO		NO		Keppra	NO
RNA	IDH-A	N17-0552	F	47	Grade 2 Astrocytoma	2	Frontal	Left	NO		NO		NO	NO
RNA	IDH-A	N17-0608	M	46	Grade 3 Astrocytoma	3	Temporal	Right	NO		NO		Keppra	NO
RNA	IDH-A	N17-0739	F	60	Grade 3 Astrocytoma	3	Temporal	Right	NO		NO		Keppra	NO
RNA	IDH-O	N17-0742	F	28	Grade 3 Oligodendroglioma	3	Frontal	Right	NO		NO		NO	NO
RNA	IDHwt	N17-0746	M	69	Grade 4 Glioblastoma	4	Frontal	Left	NO		NO		Keppra	NO
RNA	IDHwt	N17-0815	M	61	Grade 4 Glioblastoma	4	Frontal	Left	NO		NO		NO	NO
RNA	IDHwt	N17-0823	M	36	Grade 4 Glioblastoma	4	Insulaire	Left	NO		YES	Solupred	NO ?	NO
RNA	IDHwt	N17-0851	M	44	Grade 4 Glioblastoma	4	Frontal	Left	NO		NO		Keppra	NO
RNA	IDH-O	N17-0928	M	54	Grade 3 Oligodendroglioma	3	Frontal-temporal	Left	NO		NO		Keppra	NO
RNA	IDH-A	N17-1031	F	30	Grade 2 Astrocytoma	2	Frontal	Left	NO		NO		Keppra	NO
RNA, DNA	IDH-O	N17-0149	M	25	Grade 2 Oligodendroglioma	2	Frontal	Right	NO		NO		Keppra	NO
RNA, DNA	IDH-O	N17-0427	M	61	Grade 3 Oligodendroglioma	3	Frontal	Left	NO		NO		Keppra	NO
RNA, DNA	IDH-A	N17-0482	M	52	Grade 3 Astrocytoma	3	Frontal	Right	YES	Temozolomide 12c	NO		NA	YES
RNA, DNA	IDH-A	N17-0682	M	50	Grade 3 Astrocytoma	3	Temporal	Left	NO		YES	Corticotherapy	Keppra	NO
RNA, DNA	IDH-O	N17-1030	F	59	Grade 3 Oligodendroglioma	3	Frontal	Right	NO		NO		Keppra	NO
RNA, DNA	IDH-O	N17-1103	F	63	Grade 2 Oligodendroglioma	2	Parietal	Right	NO		NO		Keppra	NO
RNA, DNA	IDHwt	N17-1319	F	62	Grade 4 Glioblastoma	4	Frontal	Right	NO		YES	NA	Keppra	NO
RNA, DNA	IDH-O	N17-1391	F	58	Grade 2 Oligodendroglioma	2	Frontal	Left	NO		NO		NO	NO
RNA, DNA	IDH-A	N17-1424	M	45	Grade 4 Glioblastoma	4	Frontal	Left	YES	Temozolomide 17c	NO		Gardenal	NO
RNA, DNA	IDHwt	N17-1452	F	55	Grade 4 Glioblastoma	4	Temporal	Right	NO		NO		Keppra	NO
RNA, DNA	IDH-O	N17-1517	F	33	Grade 2 Oligodendroglioma	2	Fronto-temporo-insulaire	Left	NO		NO		NO	NO
RNA, DNA	IDHwt	N17-1667	M	31	Grade 4 Glioblastoma	4	Frontal	Left	NO		NO		NO	YES
RNA, DNA	IDH-A	N17-1701	F	36	Grade 3 Astrocytoma	3	Temporal	Left	NO		NO		Keppra	NO
RNA, DNA	IDH-A	N17-1885	F	45	Grade 3 Astrocytoma	3	Frontal-temporal	Right	NO		YES	Solupred	NO	NO
RNA, DNA	IDH-O	N18-0149	M	31	Grade 2 Oligodendroglioma	2	Frontal	Left	NO		NO		NO	NO
RNA, DNA	IDHwt	N19-0471	M	60	Grade 4 Glioblastoma	4	Temporal	Left	NO		YES	NA	NO	NO
RNA, DNA	IDH-O	N17-0266	M	52	Grade 2 Oligodendroglioma	2	Frontal	Left	NO		NO		Keppra	NO
RNA, DNA	IDH-O	N17-1037	M	33	Grade 3 Oligodendroglioma	3	Frontal	Left	NO		YES	Cortancyl	Keppra	NO

Sequencing	Status	Patient ID	Status IDH1	Status IDH2	Status Chromosomes	Status P53	Status ATRX	Satut CIC	Satut TERT	Status BRAF	Status MDM2	Status FGFR	Status P16	Status EGFR
DNA	IDHwt	N17-0071	NORMAL	NORMAL	NA	OVEREXPRESSED	NORMAL	NA	NORMAL	NA	NA	NA	NA	NA
DNA	IDH-O	N17-0199	MUTANT R132H	NORMAL	LOSS 1P/19Q	NORMAL	NORMAL	MUTANT	NORMAL	NORMAL	NORMAL	NORMAL	NORMAL	NORMAL
DNA	IDHwt	N17-0200	NORMAL	NORMAL	NA	NA	NORMAL	NA	NA	NA	NA	NA	NA	AMPLIFIED
DNA	IDH-O	N17-1314	MUTANT R132H	NORMAL	LOSS 1P/19Q	NORMAL	NORMAL	MUTANT	MUTANT C228T	NORMAL	NORMAL	NORMAL	NORMAL	NORMAL
DNA	IDH-A	N17-1610	MUTANT R132H	NORMAL	NA	NORMAL	DIFFUSE LOSS OF NUCLEAR EXPRESSION	NA	NA	NA	NA	NA	NA	NA
DNA	IDHwt	N17-1698	NORMAL	NORMAL	GAIN 7P/7Q / LOSS SEMI 1P / LOSS 10P/10Q	NORMAL	NORMAL	NORMAL	MUTANT C228T	NORMAL	NORMAL	NORMAL	NORMAL	NORMAL
DNA	IDH-A	N17-1710	MUTANT R132H	NORMAL	NA	NORMAL	DIFFUSE LOSS OF NUCLEAR EXPRESSION	NA	MUTANT C228T	NA	NA	NA	NA	NA
DNA	IDH-A	N17-1743	MUTANT R132C	NORMAL	NORMAL	OVEREXPRESSED	DIFFUSE LOSS OF NUCLEAR EXPRESSION	NORMAL	NORMAL	NORMAL	NORMAL	NORMAL	NORMAL	NORMAL
RNA	IDH-A	N17-0552	MUTANT R132S	NORMAL	NA	NORMAL	DIFFUSE LOSS OF NUCLEAR EXPRESSION	NA	NA	NA	NA	NA	NA	NA
RNA	IDH-A	N17-0608	MUTANT R132H	NORMAL	NA	OVEREXPRESSED	DIFFUSE LOSS OF NUCLEAR EXPRESSION	NA	NA	NA	NA	NA	NA	NA
RNA	IDH-A	N17-0739	MUTANT R132H	NORMAL	NA	OVEREXPRESSED	DIFFUSE LOSS OF NUCLEAR EXPRESSION	NORMAL	NA	NA	NA	NA	NA	NA
RNA	IDH-O	N17-0742	NORMAL	MUTANT R172K	GAIN 17Q / LOSS 1P/19Q / LOSS SEMI 6P	NORMAL	NORMAL	MUTANT	MUTANT C228T	NORMAL	NORMAL	NA	NORMAL	NORMAL
RNA	IDHwt	N17-0746	NORMAL	NORMAL	NA	NA	NORMAL	NA	MUTANT C250T	NA	NA	NORMAL	NA	NORMAL
RNA	IDHwt	N17-0815	NORMAL	NORMAL	NA	NA	NORMAL	NA	MUTANT C228T	NA	NA	NORMAL	NA	AMPLIFIED
RNA	IDHwt	N17-0823	NORMAL	NORMAL	GAIN 1P/7P/7Q/19Q LOSS 10P/10Q / LOSS SEMI 9P	NORMAL	NORMAL	NORMAL	MUTANT C228T	NORMAL	NORMAL	MUTANT	DELETION	NORMAL
RNA	IDHwt	N17-0851	NORMAL	NORMAL	GAIN 19Q / LOSS SEMI 1Q/9P / LOSS 10P/10Q	NORMAL	NORMAL	NORMAL	MUTANT C250T	NORMAL	NORMAL	NA	DELETION	AMPLIFIED
RNA	IDH-O	N17-0928	MUTANT R132H	NORMAL	LOSS 1P/19Q	NORMAL	NORMAL	NORMAL	MUTANT C228T	NORMAL	NORMAL	NA	NORMAL	NORMAL
RNA	IDH-A	N17-1031	MUTANT R132G	NORMAL	GAIN 1P/19Q/10P	OVEREXPRESSED	DIFFUSE LOSS OF NUCLEAR EXPRESSION	NORMAL	NORMAL	NORMAL	NORMAL	NA	NORMAL	NORMAL
RNA, DNA	IDH-O	N17-0149	MUTANT R132H	NORMAL	LOSS 1P/19Q	NORMAL	NORMAL	NORMAL	MUTANT C228T	NORMAL	NORMAL	NA	NORMAL	NORMAL
RNA, DNA	IDH-O	N17-0427	MUTANT R132H	NORMAL	LOSS 1P/19Q	NORMAL	NORMAL	MUTANT	MUTANT C250T	NORMAL	NORMAL	NA	NORMAL	NORMAL
RNA, DNA	IDH-A	N17-0482	MUTANT R132H	NORMAL	GAIN 19P / LOSS SEMI 19Q	NORMAL	NORMAL	NA	NORMAL	NA	NA	NA	NORMAL	NORMAL
RNA, DNA	IDH-A	N17-0682	MUTANT R132G	NORMAL	NA	OVEREXPRESSED	DIFFUSE LOSS OF NUCLEAR EXPRESSION	NORMAL	NA	NA	NA	NA	NA	NA
RNA, DNA	IDH-O	N17-1030	MUTANT R132H	NORMAL	LOSS 1P/19Q	NORMAL	NORMAL	MUTANT	MUTANT C228T	NORMAL	NORMAL	NA	NORMAL	NORMAL
RNA, DNA	IDH-O	N17-1103	MUTANT R132H	NORMAL	LOSS 1P/19Q	NORMAL	NORMAL	NORMAL	MUTANT C228T	NORMAL	NORMAL	NA	NORMAL	NORMAL
RNA, DNA	IDHwt	N17-1319	NORMAL	NORMAL	NA	NORMAL	NORMAL	NORMAL	MUTANT C228T	NORMAL	NORMAL	NORMAL	NA	NA
RNA, DNA	IDH-O	N17-1391	MUTANT R132H	NORMAL	LOSS 1P/19Q	NORMAL	NORMAL	MUTANT	MUTANT C228T	NORMAL	NORMAL	NA	NORMAL	NORMAL
RNA, DNA	IDH-A	N17-1424	MUTANT R132H	NORMAL	GAIN 1P/1Q/7Q/10P/10Q/19P LOSS SEMI 7P/9P	OVEREXPRESSED	DIFFUSE LOSS OF NUCLEAR EXPRESSION	NORMAL	NORMAL	NORMAL	NORMAL	NA	NORMAL	NORMAL
RNA, DNA	IDHwt	N17-1452	NORMAL	NORMAL	GAIN 1P / LOSS SEMI 7P/7Q / LOSS 10P/10Q/19P/19Q	NORMAL	NORMAL	NORMAL	MUTANT C250T	NORMAL	NORMAL	NORMAL	NORMAL	AMPLIFIED
RNA, DNA	IDH-O	N17-1517	MUTANT R132H	NORMAL	GAIN 7Q / LOSS 1P/19Q	NORMAL	NORMAL	NORMAL	MUTANT C228T	NORMAL	NORMAL	NORMAL	NORMAL	NORMAL
RNA, DNA	IDHwt	N17-1667	NORMAL	NORMAL	NOE	MUTANT	NORMAL	NORMAL	NORMAL	NORMAL	NORMAL	NORMAL	NORMAL	NORMAL
RNA, DNA	IDH-A	N17-1701	MUTANT R132H	NORMAL	NA	OVEREXPRESSED	NORMAL	NA	NA	NA	NA	NA	NA	NA
RNA, DNA	IDH-A	N17-1885	NORMAL	MUTANT R172M	NOE	OVEREXPRESSED	DIFFUSE LOSS OF NUCLEAR EXPRESSION	NORMAL	NORMAL	MUTANT	NORMAL	NA	NORMAL	NORMAL
RNA, DNA	IDH-O	N18-0149	MUTANT R132H	NORMAL	LOSS 1P/19Q	NORMAL	NORMAL	MUTANT	MUTANT C228T	NORMAL	NORMAL	NA	NORMAL	NORMAL
RNA, DNA	IDHwt	N19-0471	NORMAL	NORMAL	LOSS 9P/10P/10Q	NORMAL	NORMAL	NORMAL	MUTANT C250T	NORMAL	NORMAL	NORMAL	DELETION	NORMAL
RNA, DNA	IDH-O	N17-0266	MUTANT R132H	NORMAL	LOSS 1P/19Q	NORMAL	NORMAL	MUTANT	MUTANT C250T	NORMAL	NORMAL	NA	NORMAL	NORMAL
RNA, DNA	IDH-O	N17-1037	MUTANT R132H	NORMAL	LOSS 1P/19Q	NORMAL	NORMAL	NORMAL	MUTANT C228T	NORMAL	NORMAL	NA	NORMAL	NORMAL

To assess the degree of contamination in the CD11b+ fractions by CD11b- cells, we quantified the amount of IDH1 R132H (Figure 26 B) and TERT C228T/C250T (Figure 26 C) mutant and wildtype sequences (copies/µL) using the sensitive droplet digital PCR method. The mutant over wildtype concentration ratios was used to estimate the level of contamination in each sample. All samples were below a threshold of 5%, with the exception of two IDH1 R132H mutated patient samples, corresponding to a rare glioblastoma and to a tumor with no histological particularity. Both samples were excluded from the analysis. Two other samples harboring the IDH R172M and IDH R132G mutations were not analyzed for lack of validated probes. Moreover, two IDHwt samples did not carry any TERT mutation and could not be analyzed either.

This result demonstrates that we obtained CD11b+ fractions with at least 95% purity for downstream analyses and, at the same time, rules out the possibility that CD11b+ cells, from our study cohort, harbor the IDH1 R132H mutation in a significant percentage, as previously reported [268].

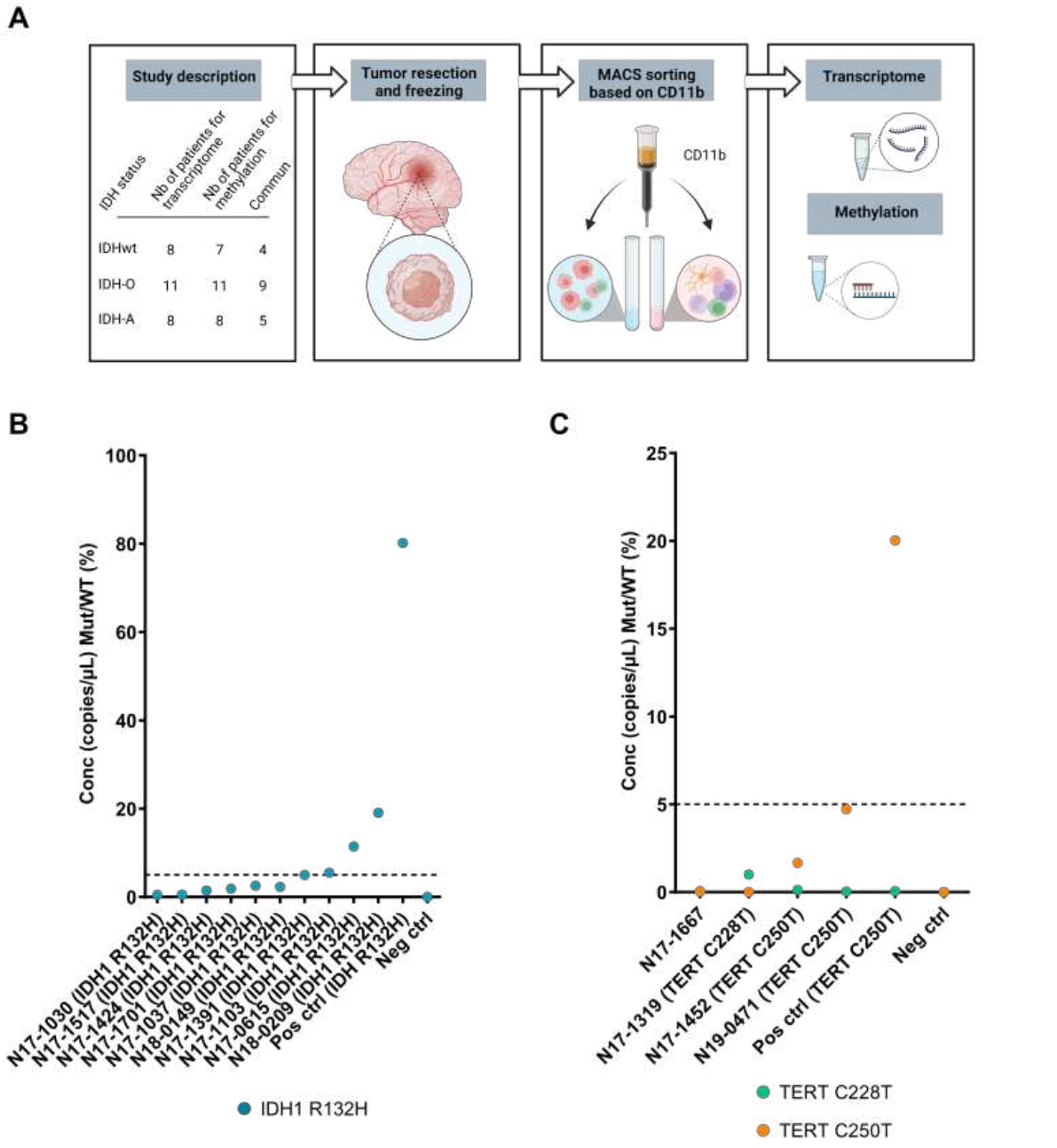

Figure 26| Study design and estimation of contamination in CD11b+ samples.

A| Graphical abstract of the study design. Concentration ratios of mutant over WT DNA (copies/µL) for **B|** IDH1R132H (blue) and **C|** TERT C228T (green) and C250T (orange). Patient IDs are given on the x axis with the mutation for which their tumor cells are positive in parenthesis. The horizontal dash line represents the threshold of 5%.

2) DNA methylome profiling of CD11b- cells from IDHm and IDHwt gliomas

To verify the DNA methylation status of our samples, we first profiled CD11b- cells from 17 patient samples (Table 1). In addition to CpG sites, four sets of genomic regions are covered by bisulfite sequencing: genes, promoters, CpG islands, and tiling

regions of 5000 bp. Methylation value distributions across all probes confirmed that CD11b- cells from IDHm samples display a hypermethylation phenotype, as shown by the area under curve (Figure 27 A). Reduction of the high-dimensional expression space using PCA clearly separate IDHm and IDHwt samples, yet with a higher degree of heterogeneity in IDH-A samples (Figure 27 B) as previously reported [119], [269]–[271].

In total, 87886 methylated regions (adjusted FDR ≤ 0,05, adjusted p-value ≤ 0,05), distributed across four genomic regions, were found between CD11b- cells of IDHm and IDHwt gliomas. We observed more significantly hypermethylated regions (|Δβ value|>0,2; adjusted FDR ≤ 0,05; adjusted p-value ≤ 0,05) than hypomethylated regions in IDHm samples compared to IDHwt samples, consistent with a hypermethylator phenotype in IDHm tumor cells (Figure 27 C).

To gain insight into the biological functions of the differentially methylated promoters, we performed pathway analyses in Metascape. In the list of promoters hypermethylated in IDHm samples / hypomethylated in IDHwt samples, we observed an enrichment of processes related to leukocyte activation (GO0045321), regulation of mononuclear cell migration (GO0071675), and positive regulation of MHC I molecules (GO0054345) (Figure 27 D). In the list of promoters hypermethylated in IDHwt samples / hypomethylated in IDHm samples, we observed strong molecular signatures of genes putatively involved in the maintenance of a stem-cell phenotype of AML tumor cells (M9377), genes with high-CpG-density promoters bearing the repressive H3K27me3 in embryonic stem cells (M2000) and in neural precursor cells (M1932) (Supplementary Figure 4).

Because R-2HG has been shown to influence antigen presentation through gene DNA methylation of MHC I/II, we sought to evaluate the promoters involved in the positive regulation of MHC I molecules (GO0054345) signature cited above. We found that CIITA mainly contributed to this signature and that its promoter was largely hypermethylated in CD11b- cells of IDHm gliomas compared with IDHwt gliomas (Figure 27 E).

Here we confirm the global hypermethylation phenotype observed in IDHm samples compared to IDHwt samples. As previously shown, hypermethylated regions in IDHm samples are involved in chemotaxis [250], whereas hypomethylated regions are involved in the maintenance of a stemness program [156]. In addition to gene hypermethylation, we found that hypermethylation of CIITA promoter may also influence MHC I/II gene expression in CD11b- cells.

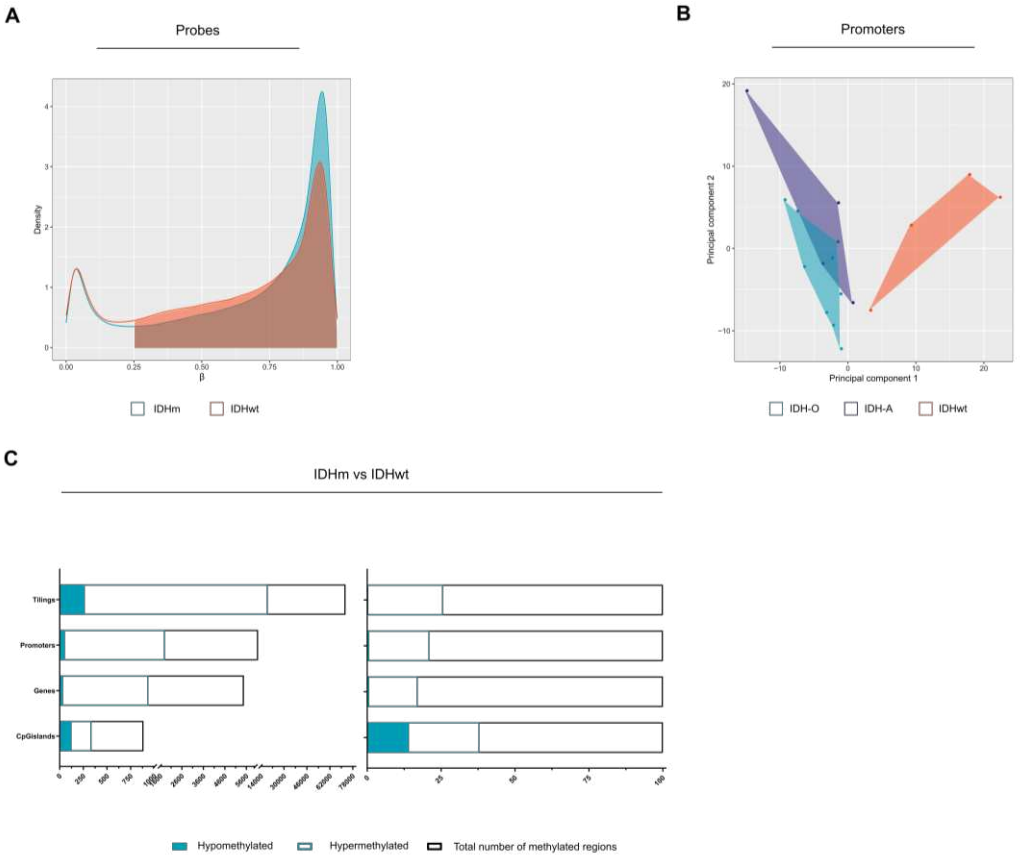
A
Probes
Density
β
IDHm
IDHwt
B
Promoters
Principal component 2
Principal component 1
IDH-O
IDH-A
IDHwt
C
IDHm vs IDHwt
Tilings
Promoters
Genes
CpGislands
Hypomethylated
Hypermethylated
Total number of methylated regions
D
Hypermethylated promoters in IDHm
GO:0050911: detection of chemical stimulus involved in sensory perception of smell
GO:0042742: defense response to bacterium
GO:0031424: keratinization
GO:0002250: adaptive immune response
M7977: GSE25123 CTRL VS ROSIGLITAZONE STIM PPARG KO MACROPHAGE UP
GO:0071675: regulation of mononuclear cell migration
GO:0006959: humoral immune response
GO:0002819: regulation of adaptive immune response
GO:0050778: positive regulation of immune response
GO:0045345: positive regulation of MHC class I biosynthetic process
M6916: GSE6674 UNSTIM VS ANTI IGM STIM BCELL DN
GO:0042445: hormone metabolic process
M8335: GSE24574 BCL6 HIGH TFH VS TCONV CD4 TCELL DN
M6235: GSE22601 DOUBLE NEGATIVE VS CD8 SINGLE POSITIVE THYMOCYTE UP
GO:0045321: leukocyte activation
GO:0002523: leukocyte migration involved in inflammatory response
GO:0006968: cellular defense response
M7541: GSE21546 UNSTIM VS ANTI CD3 STIM SAP1A KO AND ELK1 KO DP THYMOCYTES DN
GO:0051930: regulation of sensory perception of pain
M6722: GSE6259 FLT3L INDUCED VS WT SPLENIC DC 33D1 POS DN
-log10(P)
E
Hypermethylated promoters
IDHwt
IDHm
−log10 (comb.p.adj.fdr)
CIITA
Mean beta values

Figure 27| Methylation landscape of CD11- fractions of IDHm and IDHwt samples.

A| Density plot of methylation values (β values), color-coded by IDH status. **B|** PCA projection of CD11b- cell promoters from 17 patient samples. PCA projection is shown by IDH status. **C|** Bar chart of significantly hypermethylation regions (Δβ value>0,2; adjusted FDR ≤ 0,05; adjusted p-value ≤ 0,05) and hypomethylated regions (Δβ value<0,2; adjusted FDR ≤ 0,05; adjusted p-value ≤ 0,05) of all methylated regions. Absolute number is represented on the left and relative number (% of methylated regions) is represented on the right. **D|** Barplot representation of pathway enrichment across promoters hyermethylated in IDHm samples colored by p-values. Log10(P) is the p-value in log base 10. **E|** Volcano plot of differentially methylated promoters. The x-axis represents the mean difference in means across all promoters. The y-axis represents the combined p-value adjusted by FDR.

3) DNA methylome profiling of CD11b+ cells from IDHm and IDHwt gliomas

CD11b+ cells constitute up to 50% of the tumor mass. As for all cells, their phenotype and functions are largely determined by epigenomic modifications in response to microenvironmental cues. However, the extent to which methylome profiles of CD11b+ cells may contribute to the distinctive methylation patterns of bulk IDHm and IDHwt gliomas is an area of active investigation. Thus, we profiled CD11b+ cells from 26 patient samples (Table 1). Methylation value distributions across all probes shows a relatively higher methylation pattern in CD11b+ cells from IDHm samples compared to IDHwt samples, as shown by the area under curve (Figure 28 A). We reduced the high-dimensional expression space using PCA. Unlike for CD11b- cells, PC1 and PC2 did not enable a clear separation of CD11b+ cells from IDHm and IDHwt samples. Similar to CD11b- cells, there is a substantial heterogeneity of methylome data in CD11b+ cells from IDHmut tumors (Figure 28 B).

To deeper explore the differences of CD11b+ cells' methylation patterns from IDHm and IDHwt samples, we performed a differential methylation analysis. In total, 95126 methylated regions (adjusted FDR ≤ 0,05, adjusted p-value ≤ 0,05), distributed across four genomic regions, were found between CD11b+ cells of IDHm and IDHwt gliomas. Similar to CD11b- cells, we observed more significantly hypermethylated regions (|Δβ value|>0,2; adjusted FDR ≤ 0,05; adjusted p-value ≤ 0,05) than hypomethylated regions in IDHm samples compared to IDHwt samples, except for CpG islands (Figure 28 C).

To gain insight into these differentially methylated promoters, we performed pathway analyses in Metascape. First, we looked at promoters hypermethylated in IDHm samples / hypomethylated in IDHwt samples. Similar to what was observed in CD11b- cells, we also observed, in CD11b+ cells, an enrichment of gene ontology pathways related to regulation of leukocyte activation (GO0002694), cytokine

production (GO0001819), leukocyte migration (GO0050900). In addition, we observed an enrichment of gene ontology pathways related to regulation of IL-6 production (GO0032675) and immune cell differentiation (GO1902107) (Figure 28 D). We also noted strong molecular signatures of genes expressed by stimulated mature immune cells such as macrophages (M8643), monocytes (M4458), and DCs (M6816). After that, we looked at promoters hypomethylated in IDHm samples / hypermethylated in IDHwt samples. We observed that they concerned genes involved in the positive regulation of epithelial cell migration (GO0010634). Interestingly, we found a significant enrichment of molecular signatures from stimulated memory CD8 T cells (M3664) and cytotoxic Th1 cells (M2527) (Supplementary Figure 5).

Although antigen presentation was not a pathway present in the list of differentially methylated promoters, we still observed that CIITA promoter was hypermethylated in CD11b+ cells of IDHm gliomas compared to IDHwt gliomas as shown by the volcano plot (Figure 28 D).

In conclusion, DNA methylation may be a mechanism that underlie differences in CD11b+ cells functions.

Tiling intergenic regions, located over a window of 5 kb distance from transcriptional start sites, harbor important regulatory elements such as enhancers. Transcription factors (TFs) bind to DNA sequence motifs on enhancers to control cell-type specific transcriptional programs and such binding could be affected by methylation status. DNA hypomethylation is a universal feature of active enhancers [272]. That is why, we sought to examine motifs for TFs enriched in these regions. To this end, we applied the Locus Overlap Analysis (LOLA) algorithm, which tests for enrichment analysis at genomic region sets and regulatory elements. Strikingly, we found an overrepresentation of binding sites for core TFs involved in immune cell differentiation and inflammation. More precisely, PU.1, CEBPα, and CEBPβ binding sites at both promoters and tilings were hypermethylated in CD11b+ cells from IDHm samples or hypomethylated in CD11b+ cells from IDHwt samples (Figure 28 E). Differential genomic occupancy of PU.1, influenced by chromatin landscapes, and cooperative binding with CEBPβ have been shown to influence differential education between MG and MDMs [273], [274]. Here we observe that distinct transcriptional networks between MG and MDMs are also influenced by DNA methylation. This hypermethylation may affect the binding of those TFs rendering CD11b+ cells of IDHm gliomas hyporeactive. In contrast, these motifs are hypomethylated in CD11b+ cells

from IDHwt, which is consistent with the fact that these cells preserve an intact pro-inflammatory program.

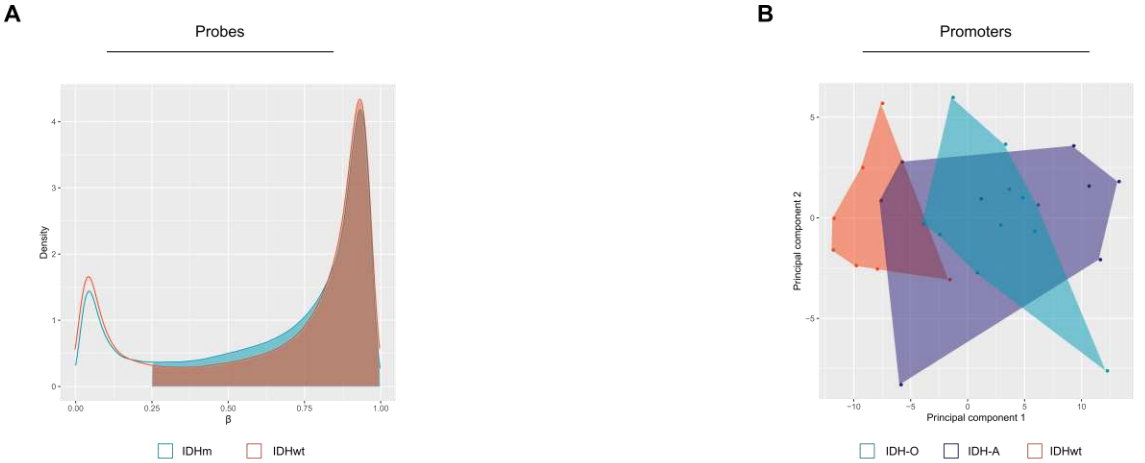

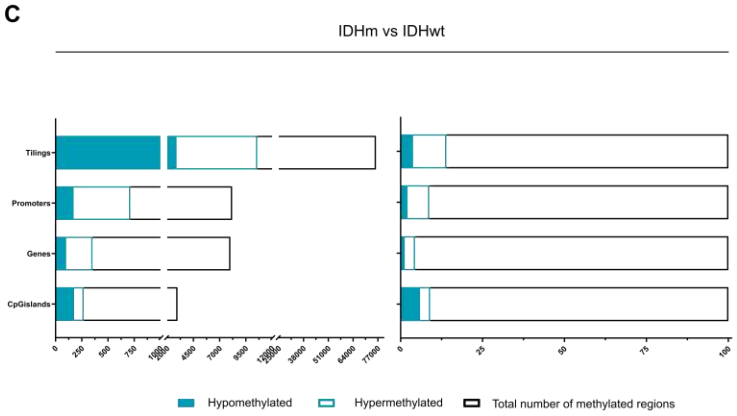

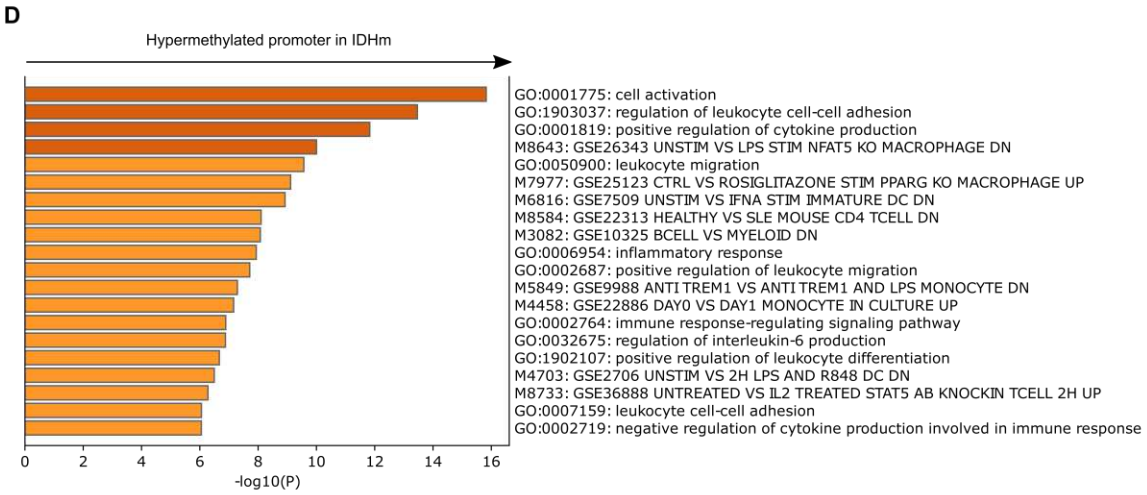

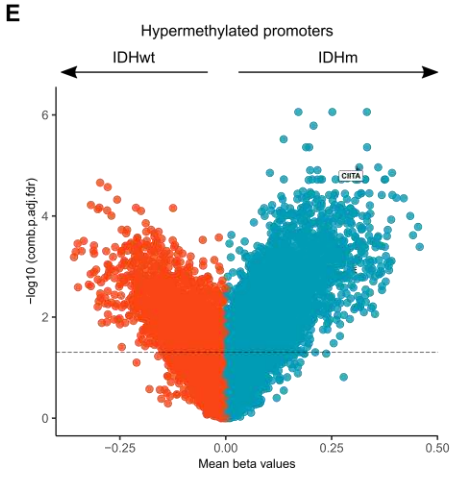

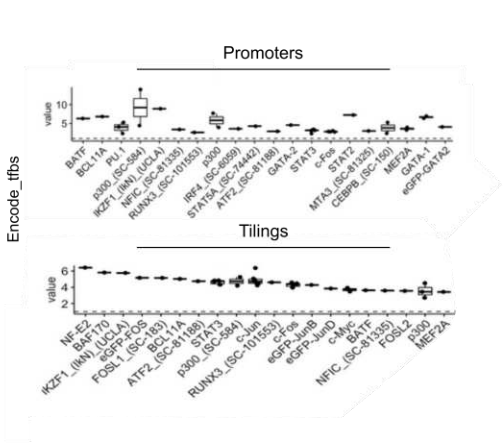

Figure 28| Methylation landscape of CD11b+ fractions of IDHm and IDHwt samples.

A| Density plot of methylation values (β values), color-coded by IDH status. **B|** PCA projection of CD11b+ cell promoters from 26 patient samples. PCA projection is shown by IDH status. **C|** Bar chart of significantly hypermethylation regions (Δβ value>0,2; adjusted FDR ≤ 0,05; adjusted p-value ≤ 0,05) and hypomethylated regions (Δβ value<0,2; adjusted FDR ≤ 0,05; adjusted p-value ≤ 0,05) of all methylated regions. Absolute number is represented on the left and relative number (% of methylated regions) is represented on the right. **D|** Barplot representation of pathway enrichment across promoters hypermethylated in IDHm samples, colored by p-values. Log10(P) is the p-value in log base 10. **E|** Volcano plot of differentially methylated promoters. The x-axis represents the mean difference in means across all promoters. The y-axis represents the combined p-value. **F|** Enrichment analysis of transcription factor binding sites overlapping hypermethylated CpGs at promoters and tiling regions (binned into 1-kilobase) in CD11b+ cells from IDHm vs IDHwt gliomas. The encode_tfbs was used.

4) Transcriptomic landscape of CD11b+ cells from IDHm and IDHwt gliomas

To investigate the phenotypes and functions of CD11b+ cells in human gliomas, we performed bulk RNA-seq of 28 human samples (Table 1). We first reduced the high-dimensional expression space using PCA and observed a clear separation between samples from IDHwt and IDHm gliomas (Figure 29 A). To ascertain that IDH status was the limiting factor, we computed a heatmap with the z-score normalized gene expressions of all samples with their genetic biomarkers. We observed that TP53, ATRX, CIC, TERT, P16 and EGFR status, as well as sex, grade, relapse and glucocorticoid intake had no impact on samples clustering. Interestingly, one IDH-A patient harbored a BRAF V600E mutation and had a very distinct gene expression pattern than the other samples (Supplementary Figure 6).

To gain molecular insights into tumor-specific features of CD11b+ cells, we performed differential expression analysis. We found more upregulated genes in IDHm samples compared to IDHwt samples (2714 genes upregulated, 1404 genes down, FDR<0,05, |logFC|>1) (Figure 29 B, C). This observation confirms that CD11b+ cells from human gliomas adopt different transcriptional programs according with the IDH status.

To determine whether CD11b+ cells are associated with particular molecular or signaling pathways, we performed pathway analyses with differentially expressed genes from IDHm and IDHwt samples in Metascape. First, we looked at genes upregulated in IDHm samples / downregulated in IDHwt samples. We found an enrichment of cellular movement related ontologies (GO0098609, GO0034330, GO0030029, etc...) and less differentiated CD4 and CD8 T cells (M7501, M8469, M8465, M4305) (Figure 29 D).

We then looked at genes downregulated in IDHm samples / upregulated in IDHwt samples. We observed a strong induction of antigen response (M11884) and mesenchymal genes from an IDHwt glioma dataset (M2122). Immunologic signatures consisted of genes related to antigen-experienced memory T cells (M11884) and to monocytes (M4945) (Figure 29 D).

The lower expression of CIITA in IDHm samples is shown in Figure 29 C.

Altogether, these data suggest that the CD11b+ fraction from IDHm samples is enriched in resident cells with strong expression of adhesion molecules and less differentiated T cells, while CD11b+ cells from IDHwt samples are defined by a strong mesenchymal macrophage signature, monocytes and antigen experienced, effector T cells. The CD11b+ fractions of IDHm and IDHwt gliomas is therefore composed of very distinct cell types.

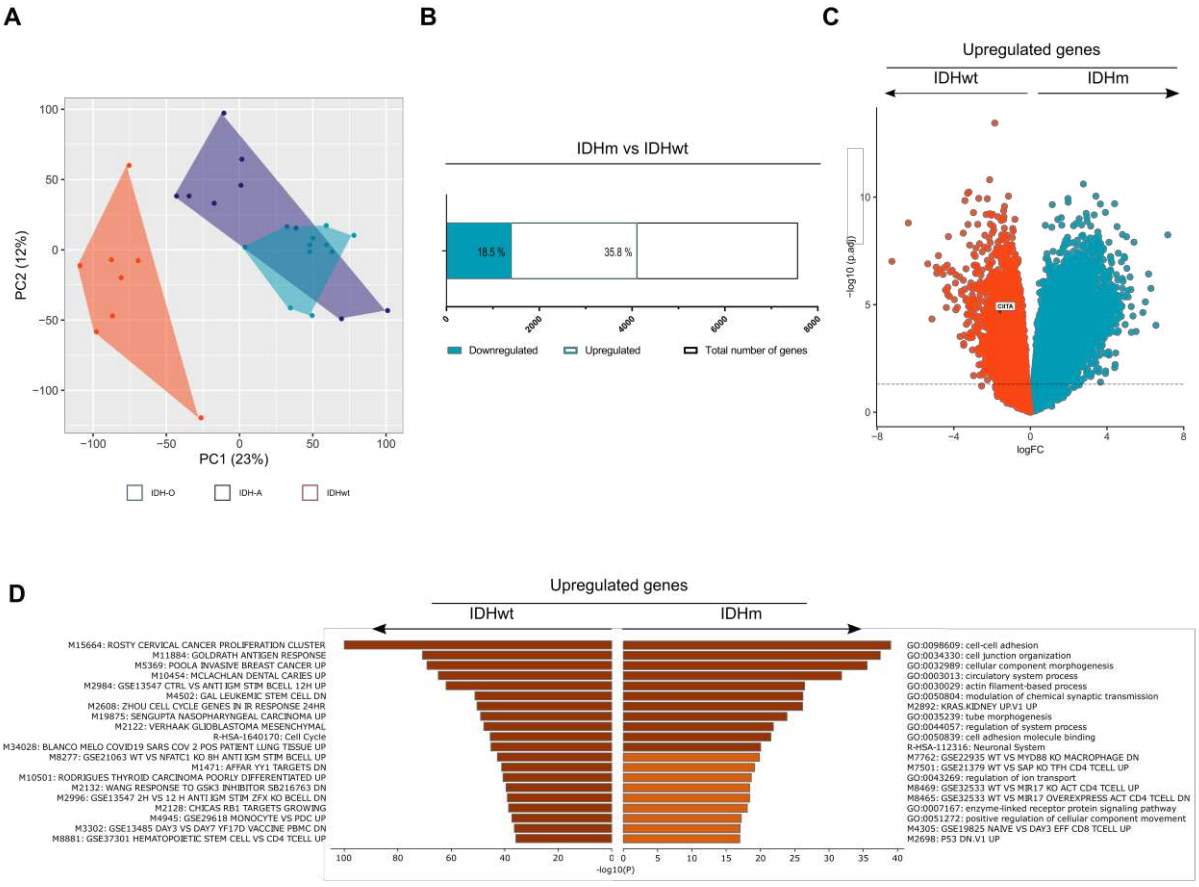

Figure 29| Transcriptomic landscape of CD11b+ fractions of IDHm and IDHwt samples.

A| PCA projection CD11b+ cell fractions from 28 patient samples. PCA projection is shown by IDH status. **B|** Number of differentially expressed genes between IDHm and IDHwt sample and **C|** volcano plot of their distribution. Genes with a |logFC| > 1, FDR<0.05, and adjusted p-value <0.05 are highlighted in red.

D| Barplot representation of pathway enrichment across upregulated genes in IDHm samples (right) and IDHwt samples (left), colored by p-values. Log10(P) is the p-value in log base 10.

5) Integrative methylome/transcriptome analysis of CD11b+ cells from IDHm and IDHwt gliomas

DNA hypermethylation mostly drives gene silencing to engage cellular states in both normal and cancer cells. Considering that CD11b+ cells from IDHm glioma samples exhibited a global hypermethylation, we prioritized the analysis to downregulated genes in CD11b+ cells from IDHm samples. In order to investigate the contribution of DNA methylation changes to the transcriptional landscapes displayed by CD11b+ cells, we cross matched the lists of differentially methylated promoters with differentially expressed genes in a series of 18 samples for which we obtained both data sets (Table 1). This approach allows to identifying genes whose dysregulated expression may be explained by a corresponding change in DNA methylation. We found 40 downregulated genes whose promoters were hypermethylated in IDHm samples (Bonferroni corrected p-value, Fisher's test = 2.9e-12) and11 upregulated genes whose promoters were hypomethylated in IDHm samples (Bonferroni corrected p-value, Fisher's test = 0.006). We also found an overlap of 11 overexpressed genes whose promoters were hypermethylated (Bonferroni corrected p-value, Fisher's test = 0.045). No significant overlap was found in the list of downregulated genes whose promoters were hypomethylated (Figure 30 A).

To gain insight into the functions of these genes, we performed gene set enrichment analysis in Metascape. The 40 genes exhibiting downregulation and hypermethylation in CD11b+ cells from IDHm gliomas pointed to the regulation of cytokine production (GO0001819) and the positive regulation of immune response (GO0050778) (Figure 30 B). The 14 genes exhibiting upregulation and hypomethylation in CD11b+ cells from IDHm gliomas pointed out to the positive regulation of epithelial cell migration (GO0010634) (Figure 30 C).

However, some of these genes were present only either in the comparison of IDH-A vs. IDHwt or IDH-O vs. IDHwt. For instance, CXCL10 is a gene downregulated, whose promoter is hypermethylated in the comparison of IDHm vs. IDHwt samples. However, it is only found in the comparison of IDH-O vs. IDHwt and not IDH-A vs. IDHwt samples. Alternatively, TESPA1 is a gene downregulated, whose promoter is hypermethylated in the comparison of IDHm vs. IDHwt samples. However, it is only found in the comparison of IDH-A vs. IDHwt and not IDH-O vs. IDHwt samples (Figure 30 D and E). To explore whether these genes, in immune cells, could be regulated by

the environment or the contact with IDHm tumor cells, we focused on the genes that were downregulated and whose promoters were hypermethylated in both IDH-A and IDH-O compared to IDHwt samples. We found 14 genes.

Altogether, these results suggest that expression of a few genes such as OSM and CIITA, in CD11b+ cells, is related to DNA methylation of their promoters.

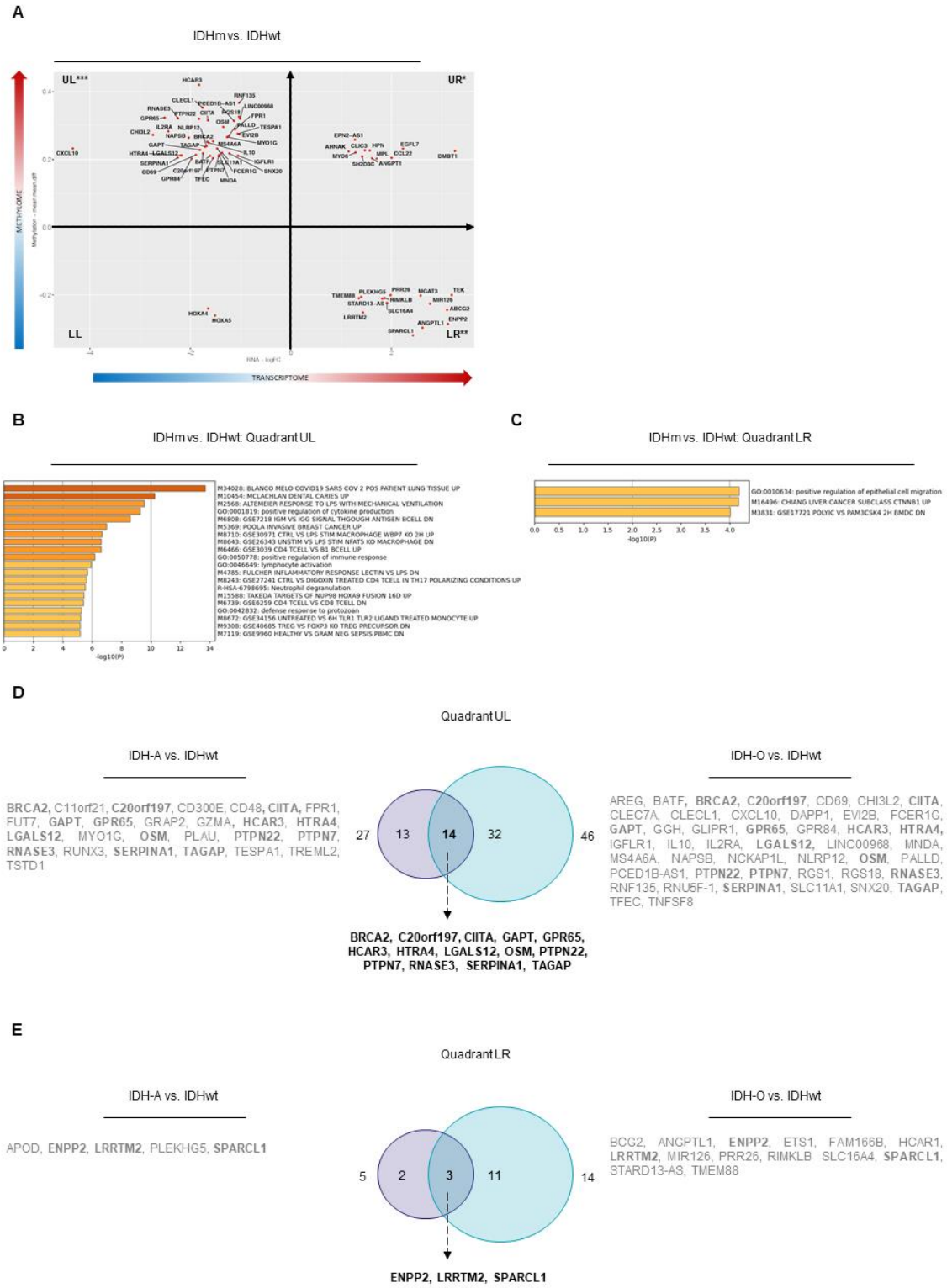

Figure 30| Integrative analysis of transcriptomic and methylation data from CD11b+ cells of IDHm and IDHwt gliomas.

A| Quadrant plot with RNA expression (logFC) in the x-axis and DNA methylation (Δ β values) in the y-axis. Plot is divided into four quadrants: UL (upper-left) for hypermethylated promoters / downregulated genes in IDHm samples; UR (upper-right) for hypermethylated promoters / upregulated genes in IDHm samples; LR (lower-right) for hypomethylated promoters / upregulated genes in IDHm samples; and LL (lower-left) for hypomethylated promoters / downregulated genes in IDHm samples. Stars represent Fisher's test with Bonferroni corrected p-values. **B|** Barplot representation of pathway enrichment across

hypermethylated promoters / downregulated genes in IDHm samples, colored by p-values. Log10(P) is the p-value in log base 10. **C|** Barplot representation of pathway enrichment across hypomethylated promoters / upregulated genes in IDHm samples, colored by p-values. Log10(P) is the p-value in log base 10. **D|** Venn diagram of downregulated / hypermethylated genes in IDH-A vs. IDHwt samples (left) and IDH-O vs. IDHwt samples (right).

6) 2-HG effects on OSM and CIITA expression

Overproduction of R-2HG by IDHm tumor cells causes DNA hypermethylation via inhibition of the methylcytosine dioxygenase TET2 leading to a global epigenetic reprogramming. R-2HG has been shown to accumulate at milimolar level in the TME of IDHm gliomas. To determine whether R-2HG is taken up by primary immune cells and induces the hypermethylation-mediated downregulation of OSM and CIITA, we isolated CD14+ cells from human buffy coats. CD14+ cells were cultured with CSF-1 for two days or for seven days to obtain fully differentiated macrophages. R-2HG as added for two more days and the intracellular concentration of 2-HG was assessed by LC-MS. We found that R-2HG uptake was concentration dependent. Interestingly, macrophages' uptake was higher than differentiating monocytes/macrophages (Figure 31 A).

According to a public single-cell database, OSM is highly expressed in macrophages. It is also expressed, although at lower level, in granulocytes, T cells and DCs. According to the same public single-cell database, CIITA is highly expressed in monocytes, B cells, macrophages and microglia cells (Figure 31 B).

To evaluate whether R-2HG had a direct influence on OSM and CIITA mRNA expression, we cultured CD14+ cells for one and two days with R-2HG at 1 and 5 mM and performed qRT-PCR. We found that R-2HG did not decrease the mRNA expression of both OSM (Figure 31 C) nor CIITA (Figure 31 D). Surprisingly, R-2HG increased the expression of CIITA at day 2 compared to untreated cells. Interestingly, our team performed an RNA-Seq analysis of murine microglia cells treated with 15 mM R-2HG for 72h. They found that CIITA was significantly downregulated in treated samples (logFC = -2.39, p-value = 0,000338) (Figure 31 E). This suggest that R-2HG might have cell-specific effects in addition to time and concentration-dependent effects.

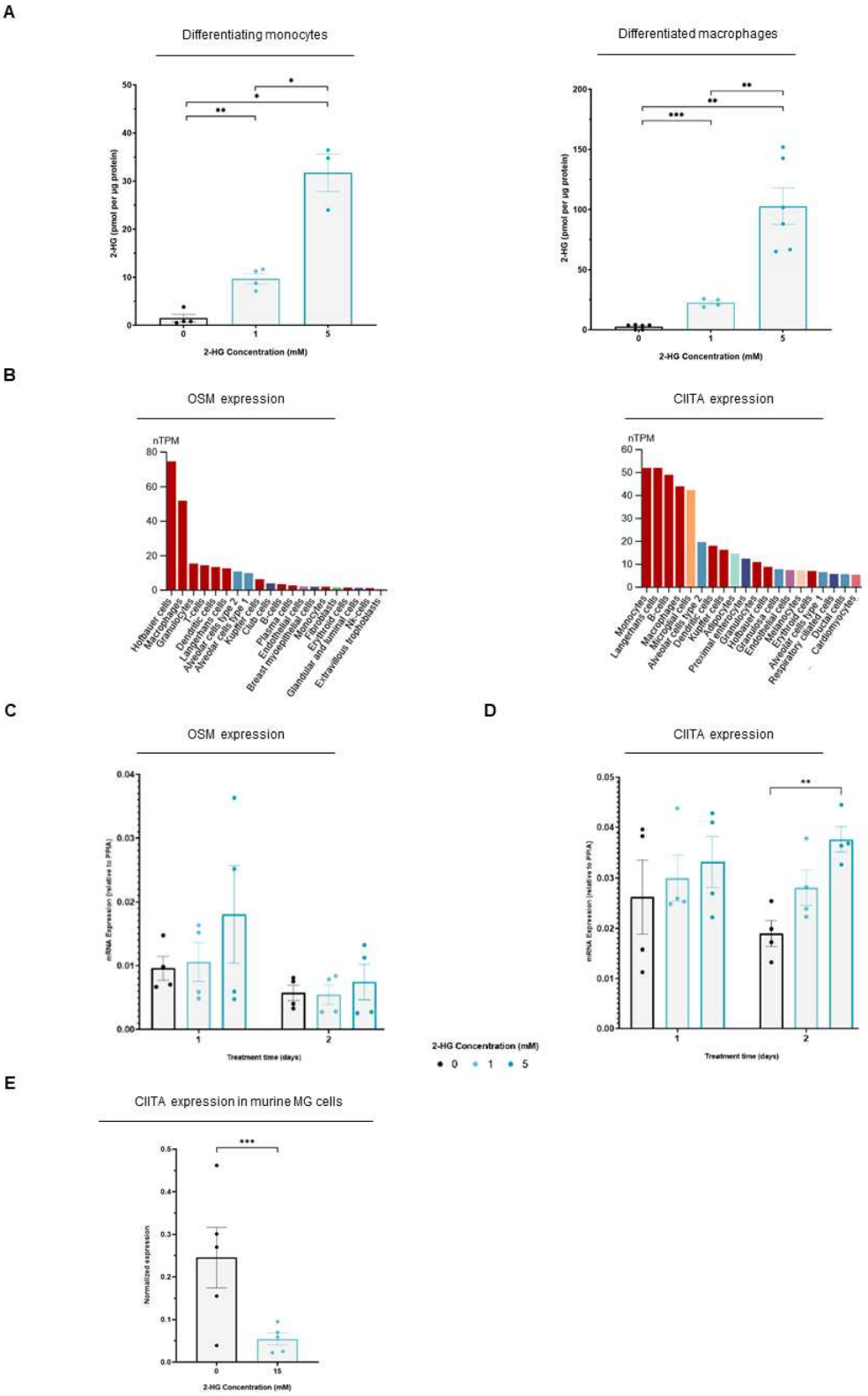

Figure 31| Evaluation of R-2HG effects on OSM and CIITA expression.

A| Intracellular quantification of 2-HG was performed by GC-MS in differentiating monocytes/macrophages and fully differentiated macrophages untreated or treated with 1 or 5 mM R-2HG for two days. T-test with Welch correction **B|** OSM and CIITA expressions assessed in the protein atlas database (https://www.proteinatlas.org/). **C|** qRTPCR analysis of OSM and **D|** CIITA mRNA expression relative to PPIA in differentiating monocytes/macrophages after treatment by R-2HG during

the indicated times. T-test with Welch correction. **E|** Normalized count for CIITA in murine microglia cells treated with 15mM 2-HG for 72h.

7) Heterogeneity of CD11b+ cells fractions

Transcriptomic signatures found in our analysis of CD11b+ cells involved T cells in IDHm samples. Current RNA-seq methods for determining the TME composition either use a deconvolution approach (e.g. CIBERSORT, CIBERSORTX, TIMER, MCP-counter) or a GSA analysis (GSEA or GSVA) on curated gene lists. GSA methods compute enrichment scores based on the ranked expression of a curated gene list which was previously associated with a specific cell type. Such enrichment scores allow for inter-sample comparison of the size of specific immune cell populations but are typically not directly interpretable as relative fractions of different cell types [275]. Therefore, it is possible to infer whether a sample or a group of samples is more enriched in a cell type as another. But it is not possible to know whether a cell type is more abundant than another. We chose to use the most differentially and uniquely expressed genes of clusters identified in single cell RNA-Seq studies as signatures.

The choice of the curated gene lists is critical to have the most precise representation of the different cell types in bulk RNA-Seq samples. First, we used the latest published scRNA-Seq dataset, made with an integrated analysis of 201986 human glioma, immune, and other stromal cells. The heatmap of the mean expression shows that myeloid cell signatures were more enriched in the CD11b+ fraction of IDHwt samples compared to IDHm samples, whereas oligodendrocyte and endothelial cell signatures seemed enriched in IDHm samples compared to IDHwt samples. We also noticed an enrichment of T cells both in IDHwt and IDH-O samples but not in IDH-A samples (Figure 32 A).

Deeper analysis of the myeloid cluster revealed that the microglia signatures were relatively equivalent between gliomas. Macrophages were relatively more enriched in IDHwt and IDH-O samples compared to IDH-A samples (Figure 32 B). These results were unexpected since the literature agrees that IDHwt gliomas are enriched in macrophages and IDHm gliomas are enriched in MG cells. These differences might be due to the integration of the data from this article.

Then, we used our scRNA-Seq study that will be described in the second part of the results. This study was conducted with human tumor samples that were processed the same way as for the bulk RNA-Seq study at the exception that the CD45+/CD11b+ cell fraction was FACS sorted instead of magnetically separated. Moreover, two patient

samples were present in both bulk CD11b+ RNA-Seq and scRNA-Seq studies. Therefore, this dataset was the closest possible from the bulk RNA-Seq data in terms of tumor samples and processing. From the scRNA-Seq study, we highlighted three populations of MG cells; four populations of infiltrating myeloid cells that probably are constituted by DCs, monocytes, MDMs; five populations of lymphoid cells (T and NK cells); and one population of B cells. Consistent with the literature [109], [110], we found that the CD11b+ fraction from IDHm tumor was mainly composed of MG cells, while the CD11b+ fraction from IDHwt tumor was mainly composed of infiltrating myeloid cells. We noted a slight infiltration of myeloid cells in IDH-O samples as well (Figure 32 C). These results demonstrate that the cell type composition of our CD11b+ fractions from IDH-O, IDH-A, and IDHwt samples are very heterogenous.

Very interestingly, we observed a significant enrichment of T and NK cells signatures in IDH-O samples. To investigate whether this enrichment came from NK cells, which are known to be CD11b+, or T cells, which have been shown to upregulate CD11b, we evaluated the expression of known T cell markers (CD3, CD8 and CD4). We detected a significant enrichment for these genes in IDH-O samples and, to a lesser extent, in IDHwt samples (Figure 32). Since the expression of CD8 was much higher than CD4 expression, we sought to evaluate the cytotoxic potential of the putative CD11b+ CD8 T cells present in our samples. The expression of granzyme B (GZMB) and perforin 1 (PRF1) was significantly higher in the CD11b+ fraction of IDH-O compared to both IDH-A and IDHwt samples. Noteworthy, the RNA expression of these cytotoxic molecules was comparable in the CD11b- fractions of IDH-O and IDHwt samples, and it was significantly higher compared to IDH-A samples (Figure 32 E). Therefore, the CD11b+ fractions of our IDH-O samples seem to contain cytotoxic CD8 T cells. They may drive the different T cell-related signatures observed in the differential analysis of CD11b+ cells.

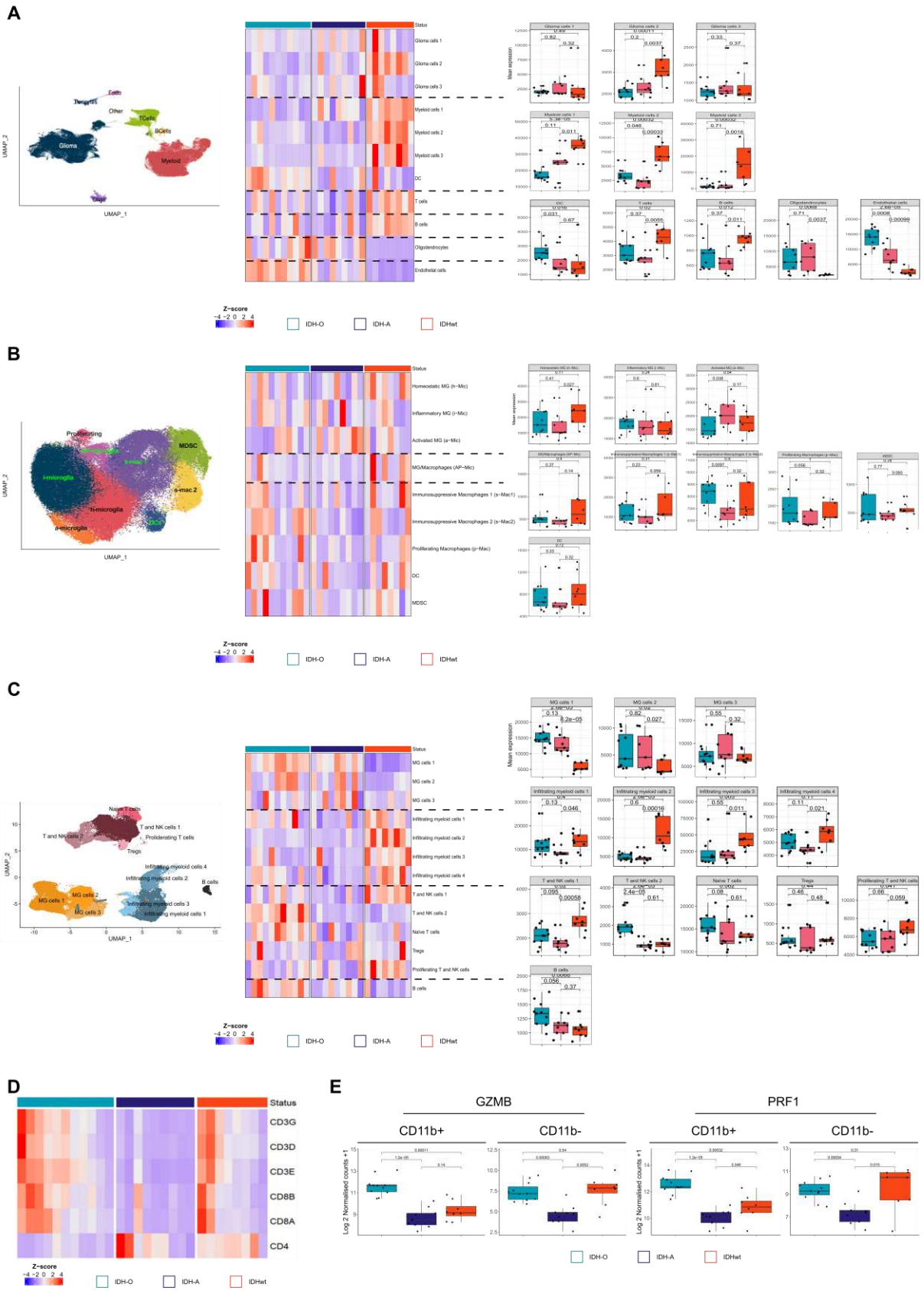

Figure 32| Transcriptomic heterogeneity of CD11b+ fractions of IDHm and IDHwt gliomas.

A| UMAP projections of 201,986 single cells from 18 patients showing the composition of different cell types in human gliomas., color coded by cluster assignment (left). Heatmap showing the average expression of normalized counts for different signatures. Gene expression values were centered, scaled,

and transformed to a scale from −4 to 4 (middle). Boxplots of the same average expression, per cell type signature and IDH status (right). From [228]. **B|** UMAP projections of myeloid cells showing the composition of different cell types in human gliomas., color coded by cluster assignment (left). Heatmap showing the average expression of normalized counts for different signatures. Gene expression values were centered, scaled, and transformed to a scale from −4 to 4 (middle). Boxplots of the same average expression, per cell type signature and IDH status (right). From [228]. **C|** UMAP projection of 61532 single CD45+/CD11b+ cells from 9 patients shown by cluster annotation (left). Heatmap showing the average expression of normalized counts for different signatures. Gene expression values were centered, scaled, and transformed to a scale from −4 to 4 (middle). Boxplots of the same average expression, per cell type signature and IDH status (right). **D|** Heatmap showing the average expression of normalized counts for CD3, CD8, and CD4 genes. Gene expression values were centered, scaled, and transformed to a scale from −4 to 4. **E|** Boxplots of the average expression of GZMB and PRF1 in CD11b+ and CD11b- cells, per IDH status.

8) Identification of Ligand-Receptor pairs between CD11b+ and CD11- cells

The heterogeneity of tumor cells and CD11b+ cells from IDH-A, IDH-O, an IDHwt leas to differential cross-talk between these two fractions. Recent studies highlighted cross-talk reciprocal interactions between immune cells and glioma cells from IDHwt tumors leading to either immunosuppressive or immunostimulatory effects [228], [249], [276], [277]. Here we leveraged our transcriptome data from CD11b- and CD11b+ cells from matched samples to infer potential Ligand-Receptor (L-R) pair interactions that could be specific to tumor types or expressed in common between IDH-A and IDH-O samples. We applied the computational pipeline single-cell Tumor Host Interaction (scTHI) developed by our collaborators [278]. This function uses a dataset generated from scRNA-seq experiments to identify L-R pairs that are significantly enriched in a given dataset. L-R pairs were considered specific of a glioma type if the pair was expressed in at least 80% of the samples from this glioma type.

We found 97 L-R pairs specifically expressed in IDHwt, 107 L-R pairs specifically expressed in IDH-O, and 22 L-R pairs specifically expressed in IDH-A gliomas. Of note, 43 L-R pairs were common between IDH-O and IDH-A samples (Figure 33 A). The complete list of L-R pairs is presented in Supplementary Table 6 (confidential data).

To investigate the functions of the specific L-R pairs, we performed gene set enrichment analysis in Metascape. Pathways related to integrin cell surface interactions were the distributed across all samples regardless of the glioma type (Figure 33 B, C). In IDHwt gliomas, we observed a strong enrichment of signatures related to inflammation (GO0006954), mesenchymal state (M2122, M5930), and complement system (WP2806) (Figure 33 B). Complement activation promotes a wide range of glioma malignant behaviors including tumor cell growth, migration, invasion, EMT, and

angiogenesis [279]. L-R pairs common in IDHm samples were related to cell migration and Notch signaling pathway (Figure 33 C).

To perform a more comprehensive analysis of the impact of the identified L-R pairs on clinical outcomes of patients, Cox proportional-hazards regression models were applied to TCGA cohort using the complete list of significant L-R pairs expressed per tumor type. The list of L-R pairs with prognostic value is presented in Supplementary Table 7 (confidential data).

Together, these results uncovered novel L-R pairs specific to glioma types that could be used for prognostic and even therapeutic purposes.

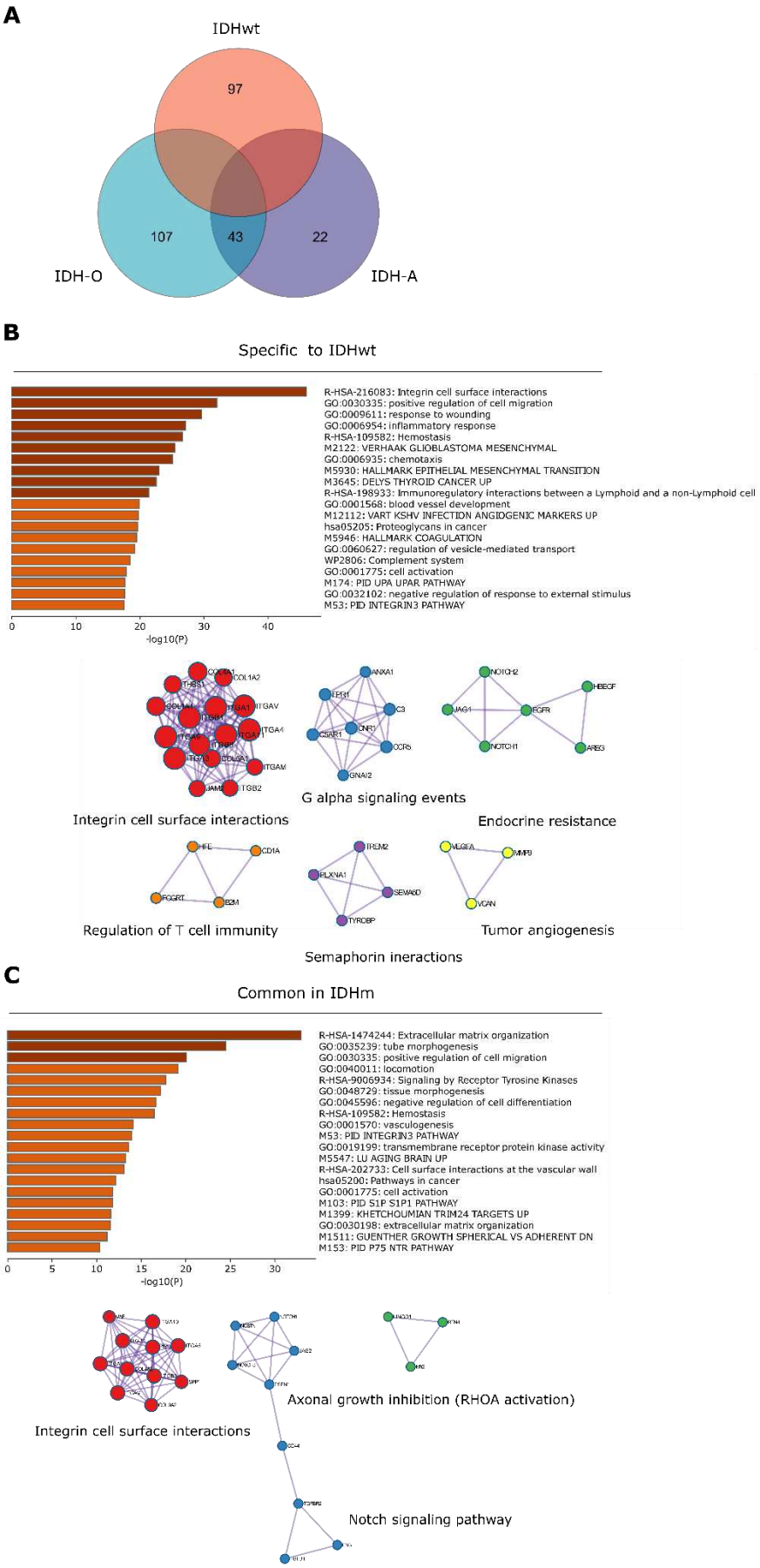
A
IDHwt
97
107
43
22
IDH-O
IDH-A
B
Specific to IDHwt
R-HSA-216083: Integrin cell surface interactions
GO:0030335: positive regulation of cell migration
GO:0009611: response to wounding
GO:0006954: inflammatory response
R-HSA-109582: Hemostasis
M2122: VERHAAK GLIOBLASTOMA MESENCHYMAL
GO:0006935: chemotaxis
M5930: HALLMARK EPITHELIAL MESENCHYMAL TRANSITION
M3645: DELYS THYROID CANCER UP
R-HSA-198933: Immunoregulatory interactions between a Lymphoid and a non-Lymphoid cell
GO:0001568: blood vessel development
M12112: VART KSHV INFECTION ANGIOGENIC MARKERS UP
hsa05205: Proteoglycans in cancer
M5946: HALLMARK COAGULATION
GO:0060627: regulation of vesicle-mediated transport
WP2806: Complement system
GO:0001775: cell activation
M174: PID UPA UPAR PATHWAY
GO:0032102: negative regulation of response to external stimulus
M53: PID INTEGRIN3 PATHWAY
0
10
20
30
40
-log10(P)
Integrin cell surface interactions
G alpha signaling events
Endocrine resistance
Regulation of T cell immunity
Tumor angiogenesis
Semaphorin ineractions
C
Common in IDHm
R-HSA-1474244: Extracellular matrix organization
GO:0035239: tube morphogenesis
GO:0030335: positive regulation of cell migration
GO:0040011: locomotion
R-HSA-9006934: Signaling by Receptor Tyrosine Kinases
GO:0048729: tissue morphogenesis
GO:0045596: negative regulation of cell differentiation
R-HSA-109582: Hemostasis
GO:0001570: vasculogenesis
M53: PID INTEGRIN3 PATHWAY
GO:0019199: transmembrane receptor protein kinase activity
M5547: LU AGING BRAIN UP
R-HSA-202733: Cell surface interactions at the vascular wall
hsa05200: Pathways in cancer
GO:0001775: cell activation
M103: PID S1P S1P1 PATHWAY
M1399: KHETCHOUMIAN TRIM24 TARGETS UP
GO:0030198: extracellular matrix organization
M1511: GUENTHER GROWTH SPHERICAL VS ADHERENT DN
M153: PID P75 NTR PATHWAY
0
5
10
15
20
25
30
-log10(P)
Integrin cell surface interactions
Axonal growth inhibition (RHOA activation)
Notch signaling pathway

Figure 33| Analysis of Ligand-Receptor pairs in CD11b- and CD11+ fractions.

A| Venn diagram of the number of L-R pairs specific to either IDHwt, IDH-O, IDH-A samples and common between IDH-O and IDH-A samples. **B|** Barplot representation of pathway enrichment across L/P specific to IDHwt samples, color-coded by p-values. Log10(P) is the p-value in log base 10. Protein-protein Interaction Enrichment Analysis showing network of the subset of proteins that form physical interactions with at least one other member in the list. **C|** Barplot representation of pathway enrichment across L/P common between IDH-O and IDH-A samples, color-coded by p-values. Log10(P) is the p-value in log base 10. Protein-protein Interaction Enrichment Analysis showing network of the subset of proteins that form physical interactions with at least one other member in the list.

B. Discussion

It is increasingly recognized that intratumoral heterogeneity of diffuse gliomas is a key factor to explain variations in both tumor progression and the response to therapies. Diffuse gliomas have been classified into six distinct tumor subtypes (LGm1–LGm6) by bulk DNA methylation analysis. LGm1–LGm3 are enriched for IDHm tumors and show genome-wide hypermethylation, while LGm4–LGm6 are enriched for IDHwt tumors [119]. A recent study used a novel technological approach combining joint methylomics and transcriptomics analysis at the single cell level to evaluate the intratumoral heterogeneity of both IDHm and IDHwt gliomas. Understanding the cellular and molecular heterogeneity of TME of these tumors is also fundamental for the design of efficient therapeutic strategies. Interestingly, they found that pseudo-bulk analysis of all immune cells classified them into LGm6, a subtype associated with either GBM or pilocytic astrocytoma-like gliomas, suggesting that the TME may contribute to bulk subtype assignments to LGm6 [280]. However, this study did not address the differences, at the level of DNA methylation, from immune cells between IDHm and IDHwt gliomas.

CD11b+ cells are highly abundant cell populations in gliomas and, as such, have been suggested as a promising prognostic marker and therapeutic target [220], [228]. CD11b+, especially macrophages, are highly plastic cells, and their phenotype upon microenvironmental stimuli is driven by epigenomic modifications [281]–[283]. In this study, we performed a simultaneous profiling of the transcriptome and methylome of CD11b+/- cells from IDHm and IDHwt gliomas. In line with previous studies, we found that CD11b+ cells from these tumors exhibit differences in expression signatures of the inflammatory response, regulation of MHC molecules, mesenchymal-like phenotype, proliferation and hypoxia, further emphasizing that CD11b+ cells are very different according to glioma subtypes. In addition, we revealed for the first time that these cells also undergo significant differences in their methylation profiles. Similar to CD11b- cells, CD11b+ cells from corresponding tumors exhibit a bias towards more

hypermethylated regions. This finding confirms that the methylome of CD11b+ immune cells contributes to changes in bulk methylome of gliomas for which a prognostic value has been reported [269], [270], [284].

Our integrative transcriptome/methylome analysis showed that methylation levels at promoters are tightly connected with a fraction of the transcriptional differences observed between CD11b+ cells of IDHm and IDHwt samples. A study found that macrophages induce a transition of IDHwt cells into mesenchymal-like (MES-like) state by the secretion of OSM that interacts with its receptors (OSMR or LIFR) in complex with GP130 on IDHwt cells and activates STAT3 [276]. In our study, we found that OSM in CD11b+ cells of IDHwt tumors is hypomethylated and overexpressed compared to IDHm tumors. Therefore, it is possible to assume that the demethylation of OSM promoter in macrophages enables its expression and production which participate in the acquisition of the MES-like phenotype of IDHwt gliomas. A recent study revealed that the MES program is specific of IDHwt gliomas and not found in IDHm gliomas [285]. More evidence is needed to conclude whether OSM expression, in MDMs of IDHwt gliomas, is driven by DNA hypomethylation and/or whether OSM expression, in MG of IDHm gliomas, is prevented by DNA hypermethylation.

One defining feature of IDHm gliomas is the fact that these tumors are immune desert with very little expression of MHC-I/II molecules [276], [286]. Class II transactivator (CIITA) is a transcriptional coactivator that regulates γ-IFN-activated transcription of MHC-I/II genes [287]. Genetically modifying cold tumor cells to express CIITA resulted in infiltration of immune cells and tumor rejection in mice [288]. CIITA was shown to be expressed in mice MDMs and repressed in mice MG by chromatin remodeling [274]. Here we propose a complementary approach to CIITA's regulation by DNA methylation both in CD11b- and CD11b+ cells of IDHm gliomas. More evidence is needed to conclude that DNA methylation controls CIITA expression and therefore MHC I/II expression. Noteworthy, if CIITA promoter hypermethylation may be mediated by R-2HG in tumor cells, the difference that we observed in CD11b+ cells may come from a differential methylation pattern in human MG and MDMs like in mice.

The overproduction of R-2HG in IDHm tumor cells is responsible for a global hypermethylation, through the inhibition of α-ketoglutarate-dependent enzymes such as the DNA demethylase TET2 . High concentrations of R-2HG have been estimated to be present in the TME [132] and were detected in CD11b+ cells of a mouse model of IDHm glioma [289] . Here, we show that R-2HG penetrates inside primary human

monocytes/macrophages. SCL13A3 is a transporter involved in the uptake of R-2HG in primary T cells [263]. Specific transporters mediating this intake in human monocytes/macrophages remains unknown. Notably, TET inactivation leads to enhancer hypermethylation, reduction of enhancer activity and impaired differentiation of ESCs [290]. Thus, it is plausible that inhibition of TET by R-2HG accounts for the hypermethylated promoters and enhancers that affect the binding of TFs involved in immune cells differentiation and expression of markers such as OSM and CIITA. Here we did not observe such a relationship. However, more experiments are needed to conclude on R-2HG effects on DNA hypermethylation in these cells. Another possible explanation is that the epigenetic differences observed in immune cells, particularly myeloid cells, from IDHm and IDHwt gliomas are due to other microenvironmental factors. In this regard, a recent study showed that type I proinflammatory cytokines, such as GM-CSF and IFNγ, control complementary differentiation programs in monocyte [291].

Two papers were published at the same time detailing the composition of the IDHm and IDHwt TMEs. They uncovered that the majority of immune cells were composed of resident MG in IDHm tumors, while infiltrating MDMs were the most abundant immune cell type in IDHwt tumors. While MG from IDHm gliomas are close to resting MG from non-tumor tissues, MDMs are highly immunosuppressive in IDHwt tumors [109], [110]. Recent scRNA-seq studies confirmed these findings and further identified subsets of MDMs displaying mesenchymal-like and hypoxia signatures and subsets of inflammatory microglial cells as strong predictors of glioma aggressiveness regardless of the IDH status [226], [228], [276]. These two cell populations, along with monocytes, DCs, NKs and granulocytes are known to express CD11b. We did not find granulocytes in our deconvolution analysis because these cells do not resist freezing and thawing. In addition to this already high degree of cells heterogeneity, we found a very surprising high CD8 cytotoxic T cell signature in the CD11b+ fraction of IDH-O samples. CD11b is not a canonical marker for T cells. However, it was first described in 1992 in mouse lymphocytic choriomeningitis virus infection model, in a subpopulation of cytotoxic CD8+ T cells that include both the active virus-specific and the virus-specific memory populations [292]. Later, it was discovered that this subset could actually constitute an intermediate phenotype, between memory- and effector-type T cells in the human CD8+CD28+ T cell subset and that the presence of this marker on antigen-specific CD8+ T cells signified recent activation [293], [294]. We also found a very high cytotoxic signatures in IDH-O samples, which was not found in IDH-A or IDHwt, which suggest that CD11b+ CD8 T cells might be cytotoxic. Altogether, the studied CD11b+ fractions were very different in terms of cell composition. Moreover,

the high heterogeneity between IDH-A and IDH-O samples also complicated the comparative analysis and made the evaluation of IDH mutation's role very difficult.

C. Limitations and prospects

Recently, a study showed that pseudo-bulk analysis of all immune cells classified them into the LGm6 subtype [280]. By applying the same classifier to the pseudo-bulk DNA methylation profiles of CD11b+ cells, we could observe whether IDHm and IDHwt samples are assigned to different DNA methylation subtypes.

It is now well known that MG and MDMs are very distinct cells that mainly populate IDHm and IDHwt tumors, respectively. scRNA-seq profiling of human gliomas' TME highlighted subtypes of MG and MDMs in both IDHm and IDHwt gliomas, although at very different proportions. Previous studies in mouse IDHwt glioma models revealed differences in expression and chromatin landscapes related to distinct activation patterns of MG and MDMs, such as accessible chromatin and subsequent preferential expression of CIITA in MDMs compared to MG [274] . This study is the first, to our knowledge, to show that the differential gene expression pattern of CD11b+ cells of IDHm and IDHwt gliomas is also governed by DNA methylation. However, the biggest limitation of this study is the significant differences in cell types composition in the CD11b+ fraction. Thus, it is impossible to ascertain whether the observed differences come from different cell types or the IDHm. That is why, careful considerations were made not to attribute any effect to TAMs but to CD11b+ cells. It is now recognized that P2RY12+TMEM119+CD49d- cells can discriminate between MG and MDMs (which would be P2RY12-TMEM119-CD49d+). It is therefore possible to use FACS to isolate these different cell populations and then use bisulfite sequencing. This would enable to really infer the methylation status of the same populations and compare IDHm and IDHwt gliomas with more precision. A recent study even used single cell methylation profiling coupled with scRNA-Seq [285].

Moreover, experiments in mouse models indicate that MDMs compete with resident MG for the niche during glioma progression [226]. A study in IDHwt tumors highlighted phenotypic differences depending on the regional localization of cells within the tumor, with pro-inflammatory MDMs in the core and anti-inflammatory MG at the periphery [295]. Therefore, single-cell or even single molecule approaches combined with spatial resolution [296], [297] will be required for a thorough characterization of specific cell subsets including MG and MDMs.

To confirm L-R pairs, we plan on using immunohistochemistry on FFPE tissue sections.

Only little is known about the epigenetic effects of R-2HG on myeloid cells. However, evidence indicates that TET2 mediated DNA demethylation is involved during monocyte to macrophage differentiation [298], [299]. We are actively working on evaluating the phenotypic effects of R-2HG treatment *in vitro* during monocytes to macrophages differentiation and to study the enzymatic activity of TET2 during this process. As for the expression of OSM and CIITA, we did not observe any effect on monocytes to macrophages. differentiation, but these experiments need to be reproduced. In addition to qRTPCR, it would be interesting to use an immunoprecipitation assay to look at the enrichment of 5mC and 5hmC in specific genes such as OSM and CIITA in human MDMs and MG, respectively upon treatment with R-2HG. Nevertheless, what is necessary is to quantify the amount of αKG and R-2HG since R-2HG is a weak antagonist of αKG-dependent dioxygenases and even a small concentration of αKG may be sufficient for these enzymes to still work.

Evaluating the relationship between CIITA promoter methylation and MHC-I/II molecules expression may be possible by introducing methylation through CRISPR-Cas9. This would be essential to understand why IDHm gliomas are so cold tumors. In this peculiar context of lack of antigen presentation, we asked how T cells could behave and what were the differences between T cells from IDHwt and IDHm gliomas. Investigations of T cells are described in the second section of the results.

D. Conclusion

In conclusion, our results indicate that CD11b+ cells of human gliomas display substantial differences in their methylome and transcriptome landscapes according to the IDH status, reinforcing the concept that the TME is instructed by glioma cells. In addition, our findings confirm the contribution of epigenetic states in CD11b+ cells to the intratumoral heterogeneity of gliomas.

E. Methods

a. Prospective human tumor tissue collection

Fresh patient tumor samples were selected from the Pitié-Salpêtrière tumor bank Onconeurotek and reviewed by our senior pathologist (FB) to validate histological features and confirm patients' diagnosis. Collection of tumor samples and clinical-

pathological information were obtained upon patients' informed consent and ethical board approval, as stated by the Declaration of Helsinki. Molecular characterizations were performed as previously described (Clinical, molecular, and radiomic profile of gliomas with FGFR3-TACC3 fusions.)

b. Human tumor tissue processing and CD11b sorting

Tumor tissues were transported on ice in HBSS (Gibco) immediately following surgical resection, rinsed in HBSS to remove visible blood clots and to reduce blood leukocytes contamination, and cut using scalpels into approximately 2 to 5 mm diameter pieces. Tumor pieces were then submerged in cryotubes containing 1 mL of freezing medium consisting of 70% DMEM/F-12 (Gibco), 20% FBS and 10% DMSO (Sigma-Aldrich). Cryotubes were quickly placed at -80°C in a freezing container (Corning) to allow for slow freezing. Cryopreserved samples were stored at -80 °C (maximum 30 days) or in liquid nitrogen at -160 °C until analysis.
The day of analysis, tumor pieces were quickly thawed and rinsed in DMEM/F-12. After, they were mechanically disrupted into small fragments with scalpels and further digested for 5 to 10 min at 37°C in a HBSS-papain based lysis buffer (Worthington) containing DNAse (0.01%, Worthington) and L-Cystein (124 µg/mL, Sigma). Enzymatic digestion was inhibited by adding ovomucoid (70 µg/mL, Worthington). Afterward, the homogenates were filtered through a 70 µm on top of a 30 µm strainer (Miltenyi) to remove residual clumps and centrifuged at 300 g for 10 min at 4°C. Cell pellets were resuspended in cold HBSS and a debris removal step was performed according to the manufacturer's instructions (Miltenyi). After the last centrifugation, single cell suspensions were magnetically labeled with CD11b MicroBeads, human and mouse according to the manufacturer's instructions (Miltenyi). Both CD11b+ and CD11b- fractions were collected and each fraction sample was divided in half. Pellets were either stored at -80°C directly or resuspended in the homogenization buffer of the Maxwel RSC simplyRNA Cells Kit (Promega, AS 1390) and stored at -80°C until ribo/nucleic acids extraction.

c. RNA and DNA isolation

RNA and DNA from CD11b+ and CD11b- cells were extracted using the Maxwel RSC simplyRNA Cells Kit (Promega, AS 1390) and Maxwell RSC Blood DNA Kit (Promega, AS 1400), respectively, according to the manufacturer's instructions. RNA and DNA of some CD11b+ and CD11b- samples were coeluted using the AllPrep

DNA/RNA Micro Kit (Qiagen, 80284) and AllPrep DNA/RNA Mini Kit (Qiagen, 80204), respectively.

d. Digital droplet PCR assay

Digital droplet PCR (ddPCR) was performed for IDH1R132H, TERTC228T, and TERTC250T mutations. The ddPCR technology uses a combination of microfluidics and surfactant chemistries to divide PCR samples into water-in-oil droplets, which support PCR amplification of the template molecules. Following PCR, each droplet is read to determine the fraction of PCR-positive droplets in the original sample. This system included an automated droplet generator, which fractionates samples into ~20,000 droplets, and a reader from Bio-Rad (Bio-Rad, Hercules (CA), United States, QX200 Automated Droplet Generator and QX200 Droplet Reader, 1864002 and 1864003, respectively). Two sets of primers and probes and ddPCR™ Supermix for Probes (No dUTP) were used for quantification of absolute copy number by ddPCR. All primer and probes were obtained from Bio-Rad. Sequence and other information about primers and probes are available at www.bio-rad.com with following ID numbers: IDH1 p.R132H Hsa, Human (Ref: 10031246 UniqueAssayID: dHsaCP2000055), IDH1 WT for p.R132H Hsa, Human (Ref: 10031249 UniqueAssayID: dHsaCP2000056), TERT C228T_113 Hsa, Human (Ref: 12009308 UniqueAssayID: dHsaEXD72405942), TERT C250T_113 Hsa, Human (Ref: 12003908 UniqueAssayID: dHsaEXD46675715). Data were then analyzed using Poisson statistics to determine the target DNA template concentration in the original sample. 3 ng of input DNA was used when possible. Positive controls consisted of tumor DNA from the CD11b- fractions and negative controls contained water instead of DNA. Manufacturer's instructions were followed.

e. Bulk RNA-Seq and analysis

The quantity and quality of the total RNAs extracted were assessed by the Tapestation 2200 (Agilent), and sequenced with the Illumina Novaseq 6000 Sequencing system with 200 cycles cartridge, to obtain 2*60 million reads 100bases / RNA. Library preparations were done following the manufacturer's instructions with Kapa mRNA Hyper prep (Roche). Quality of raw data was evaluated with FastQC. Poor quality sequences were trimmed or removed with Fastp software to retain only good quality paired reads. Star v2.5.3a was used to align reads on the GRCh38 reference genome using default parameters except for the maximum number of multiple alignments allowed for a read which was set to 1. Quantification of gene and isoform abundances were done with rsem 1.2.28 on RefSeq catalogue, prior to normalisation with edgeR

bioconductor package. Finally, differential analysis was conducted with the glm framework likelihood ratio test from edgeR. Multiple hypothesis adjusted p-values were calculated with the Benjamini-Hochberg procedure to control FDR. Functional enrichment analysis was performed with clusterProfiler (v3.14.3) bioconductor package on the differentially deregulated genes with over-representation analysis (enricher function).

f. Bulk DNA methylome profiling

Genomic DNA was quantified by Quant-iT dsDNA Broad range Assay (Thermo Fisher Scientific, Waltham, MA, USA) in a Tecan SPARK microplate Reader (TECAN, Switzerland). Bisulfite modification was performed using Zymo EZ-96 DNA Methylation kit as describe in protocol according the manufacturer's recommendations for Infinium assay (Zymo Research, catalog number: D5004). Total DNA (500 ng) from each sample was sodium bisulfite converted. After conversion DNA was eluted in 15 µL of M-Elution Buffer and 1 µL was used to determine concentration using Nanodrop. DNA concentration of each sample was adjusted to 50ng/µL with M-elution Buffer or concentrated using speed vaccum. A quantity corresponding to 300 ng (or a volume of 6 µL equivalent of 300 ng) of converted DNA for each sample was used as template on the infinium Methylation EPIC 850 K arrays following the manufacturer's recommendations (Illumina, catalogue Number). Briefly, bisulfite converted DNA is whole genome amplified, fragmented and hybridized to BeadChip. After hybridization, unhybridized and no specifically hybridized DNA is washed away, and the captured product is extended with labels fluorescent coupled to nucleotides. Finally, the BeadChip are scanned with high resolution Illumina scanner (iScan) which acquired light images emitted from fluorophores. The intensities are measured and the methylation signals are extracted and recorded as raw data (IDAT). Quality data was performed using Genome Genome Studio software 2011.1 with methylation module v1.9 (Illumina, San Diego, CA, USA) by checking the percentage of correctly detected CpG with p-value cut-off at 1 % and 5 %, as well as the sample-dependent and independent controls probes which are present on the BeadChip. The methylation module allows beta values extraction and provides clustering for infinium Methylation EPIC data. Beta value is the ratio between methylated and unmethylated allele to estimate the methylation level of the CpG locus. Here, the CpG success detection rate higher than 96 % for all samples. This array examines methylation status of over to 850 000 CpG sites across whole genome. This assay was performed by the P3S plateform (Sorbonne University).

DNA profiling analysis of CD11b- and CD11b+samples were performed in RnBeads without and with filtering of the X chromosome, respectively.

g. Pathway and process enrichment analysis

Upregulated gene list in IDHm samples and upregulated gene list in IDHwt samples were used in Metascape for enrichment analysis (https://metascape.org). Briefly, for each given gene list, pathway and process enrichment analysis were carried out with the following ontology sources: KEGG Pathway, GO Molecular Functions, GO Biological Processes, Immunologic Signatures, Oncogenic Signatures, Reactome Gene Sets, Hallmark Gene Sets, Canonical Pathways, Chemical and Genetic Perturbations, BioCarta Gene Sets, WikiPathways and PANTHER Pathway. All genes in the genome have been used as the enrichment background. Terms with a p-value < 0.01, a minimum count of 3, and an enrichment factor > 1.5 (the enrichment factor is the ratio between the observed counts and the counts expected by chance) are collected and grouped into clusters based on their membership similarities. More specifically, p-values are calculated based on the cumulative hypergeometric distribution2, and q-values are calculated using the Benjamini-Hochberg procedure to account for multiple testings3. Kappa scores4 are used as the similarity metric when performing hierarchical clustering on the enriched terms, and sub-trees with a similarity of > 0.3 are considered a cluster. The most statistically significant term within a cluster is chosen to represent the cluster.

h. Isolation of primary human immune cells for *in vitro* culture

Peripheral blood mononuclear cells (PBMCs) were isolated from fresh leukapheresis blood buffy coats provided by the *Etablissement Français du Sang* (EFS). PBMCs were isolated by density gradient centrifugation using Human Pancoll, density 1.077 g/ml (Dutscher). Human CD14- cells were purified using CD14 MicroBeads Miltenyi) following the manufacturer's instructions. Ten million cells were submerged per cryotubes containing 200 µL of freezing medium consisting of 90% FBS and 10% DMSO (Sigma-Aldrich). Cryotubes were quickly placed at -80°C in a freezing container (Corning) to allow for slow freezing. Cryopreserved samples were stored at -80 °C (maximum 30 days) or in liquid nitrogen at -160 °C until analysis.
When needed, cells were quickly thawed, rinsed in RPMI-1640 medium (Gibco), and seeded at a density of 1 million cells/mL of RPMI-1640 medium (Gibco) supplemented with 10% FBS 1% penicillin/streptomycin (Thermo Fisher Scientific), 5 mM HEPES, 2 mM Glutamax, 5 mM non-essential amino acids, 5 mM sodium pyruvate. CD14+ cells were

cultured with 50 ng/mL of recombinant human M-CSF (Peprotech), CD14- cells were cultured with 10 ng/mL of recombinant human IL-2 (Peprotech). The next day, cells were treated with 5 mM D-α-Hydroxyglutaric acid disodium salt (Sigma-Aldrich) for the indicated time.

i. RNA isolation, cDNA synthesis and quantitative real-time PCR

Total RNA was purified using the Maxwell RSC simplyRNA Cells Kit (Promega), and 300 µg of RNA was reverse transcribed to complementary DNA using the Maxima First Strand cDNA Synthesis Kit (Thermo Fisher Scientific). Assays were run in triplicate on a Light Cycler 480 instrument (Roche) using the LightCycler 480 SYBR Green Master 2X (Roche). Human OSM mRNA was amplified using primers 5′- ATGGGGGTACTGCTCACAC -3′ and 5′- CGGTACTCTTTCGAGCAGC -3′, human CIITA mRNA was amplified using primers 5′- CCCGAGCAAACATGACAGAG -3′ and 5′- CCTGCAGTGAGCGGTAGAAC -3′, and human PPIA mRNA was amplified using primers 5′- ATGCTGGACCCAACACAAAT -3′ and 5′- TCTTTCACTTTGCCAAACACC -3′. All primers were verified for the production of a single specific PCR product with a melting curve program. The relative expression level of target mRNAs was calculated using the $2^{-\Delta\Delta Ct}$ method, normalized to the housekeeping gene PPIA.

j. Intracellular quantification of 2-HG

Cells were cultured for two days as previously described. Dry pellets were stored at -80°C until analysis. Dry pellets were lysed in water and the solution was divided in half for 2-HG measurement and protein quantification. NaCl was added and samples were acidified using HCl. A liquid-liquid extraction of organic acids with ethylacetate was performed. 3 extractions were performed, organic phases were pooled, dried under nitrogen stream at 30 °C. Then samples were derivated by a standard syliliation protocol (BSTFA [N,Obis[trimethylsilyl]trifluoroacetamide] and 1%TMCS(Trimethylchlorosilane)) under anhydrous conditions using pyridine. Chromatographic separation was performed with a TR-5MS (30m x 0.25 mm x 0.25 mm) column from Thermo Scientific (Waltham, Massachusets, USA). Spectral data acquisitions were performed using XCalibur software (Thermo Electron Corporation, Austin, TX, USA)..Sample were placed 30 min at 80°C, and then injected into the GC system. Quantification were performed using internal standard 2-hydroxyglutaric acid-D3 from Cambridge isotope laboratories (Tewksbury, Massachusetts, USA) on a gas chromatography-mass spectrometry (GC-MS) using a Focus GC DSQ II (Thermo

Electron Corporation, Austin, TX, USA). This assay was performed at the *Hôpital Trousseau* (Sorbonne University).

Proteins were quantified using a Pierce™ BCA Protein Assay Kit (Thermo Fisher Scientific) according to the manufacturer's instructions.

II) SINGLE-CELL ANALYSIS REVEALS AN ALTERNATIVE IMMUNE CHECKPOINT AXIS IN IDH-MUTANT GLIOMAS

1) Summary

Gliomas are the most frequent malignant diffuse brain tumors in adults. The remarkable intratumoral heterogeneity of these tumors is one reason why they still carry bleak prognoses. During the last twenty years, immunotherapy has provided unprecedented benefits in multiple cancers but remains ineffective in gliomas, mainly because of the paucity of T cells and the low expression of classical immune checkpoints. In this study, we explore T cells of human gliomas at the single-cell level. We describe more naïve T cells in isocitrate dehydrogenase mutated (IDHm) patients and identify NKG2A/CD94 as a candidate inhibitory receptor. Moreover, we reveal a TCR-independent activation pathway in T cells from IDHm gliomas. This work accentuates the need to better characterize the phenotypic heterogeneity of immune cells in gliomas and provides this dataset as a mean to discover new therapeutic targets to improve anti-glioma immunity.

2) Keywors

Gliomas, scRNAseq, T cells, NKGG2A, 2-HG

3) Highlights

- Single-cell analysis highlights fundamental differences in T cells from IDHm and IDHwt gliomas
- T cells from IDHm gliomas are less differentiated than T cells from IDHwt gliomas
- NKG2A+ CD8+ T cells represent a major cluster in IDHm gliomas
- NKG2A associates with better survival in IDHm gliomas
- NKG2A is highly is acquired after a state of exhaustion in T cells from IDHm gliomas
- NKG2A+ CD8+ T cells retain cytotoxic functions

4) Introduction

Diffuse gliomas are the most common primary brain tumors and are characterized by the absence or presence of mutations in the genes encoding for the metabolic enzymes isocitrate dehydrogenase 1 and 2 (IDHwt and IDHm, respectively).

The remarkable intratumoral heterogeneity of these tumors prevents the success of standard therapies (e.g. surgery followed by radiation and chemotherapy). In this context, immunotherapy offers a promising treatment option since the vast repertoire of immune cells provides sufficient diversity, adaptability, and cytotoxicity to compete with this complexity.

The success of immunotherapies involving immune checkpoint blockade (ICB) targeting PD1 and/or CTLA-4 or chimeric antigen receptor (CAR)-T cells transfer in other types of cancer has led to their evaluation in brain malignancies. However, recent phase 3 clinical trials all failed to demonstrate benefit of ICB in newly diagnosed [104] and recurrent IDHwt tumors [105], [106]. Results in IDHm gliomas are not yet available, although one phase 2 clinical trial showed no improvement of overall survival [107]. Investigations on subsets of patients which may respond to ICB are currently being conducted [108]. Aside from tumor-intrinsic mechanisms, limitations to immunotherapy efficacy include abundant immunosuppressive myeloid cells and the paucity of tumor infiltrating lymphocytes, expressing low levels of classical immune checkpoint receptors [109]–[111]. In addition, IDH mutation leads to the overproduction and release of the immuno-oncometabolite R-2-hydroxyglutarate (R-2HG), which induces an immunosuppressive phenotype in T cells trough modulation of their metabolism [263], [300], [301] and, indirectly, in myeloid cells [286]. Another defining feature of IDHm gliomas is the low expression of MHC-I/II molecules by tumor cells and cells of the tumor microenvironment (TME) [287], [293]. In this context of lack of antigen presentation, it is necessary to better characterize gliomas' infiltrating T cells and discover more specific inhibitory molecular targets, which can be modulated to boost anti-tumor immunity.

Recent studies using high-dimensional profiling techniques have begun to explore the immune landscapes of human gliomas with a focus on tumor associated myeloid cells (TAMs) [109], [110], [226], [228], [257], [302], which have led to investigational therapies aiming at reeducating TAMs to a more antitumorigenic state [303]. More recently, single-cell RNA-sequencing (scRNA-Seq) enabled the discovery of expression programs and functional states of glioma-infiltrating T cell populations. In particular, it was reported that the NK gene KLRB1 (encoding CD161) [249] and S100A4 [228] are receptors driving T cell inhibition. Much less is known about T cells' phenotypes and their inhibitory receptors in IDHm gliomas as the low number of this crucial cell population precludes their analysis. A profound understanding of the immune ecosystem of IDHm gliomas is fundamental for the development of specific therapies to treat these tumors.

Herein, we interrogate the cellular and molecular phenotypes of the lymphocytic compartment of IDHm gliomas in comparison to IDHwt tumors at the single-cell resolution. This scRNA-Seq study, to our knowledge, contains the highest number of T cells from primary IDHm and IDHwt patients. This degree of precision allows us to highlight the presence of γδT cells and to reveal previously undisclosed fundamental differences in T cells from these gliomas. Tumor cells and antigen presenting cells of IDHm gliomas have significantly reduced expression of MHC-I/II molecules, potentially limiting CD8 T cell responses to the tumor. This lack of antigen presentation leads to more naïve T cells in IDHm tumors compared to IDHwt tumors. Nonetheless, we provide evidence of the presence of a subset of NKG2A-expressing CD8 T cells which can overcome this evasion strategy through TCR-independent cytotoxic functions, partly due to their increased expression of activating receptors, such as the DNAX accessory molecule (DNAM)-1/CD226 and NKG2D /KLRK1.

5) Results

a. Comparative analysis of IDHm and IDHwt diffuse gliomas' immune landscapes

To map the heterogeneity of glioma's TME, we used multicolor fluorescence activated cell sorting (FACS) to analyze 61532 CD45+/CD11b+ cells, which passed QC steps, from 3 IDHwt, 3 astrocytomas (IDH-A) and 3 oligodendrogliomas (IDH-O) human frozen primary tumor resections (Figure 34 A, Supplementary Table 5). Unsupervised clustering using Louvain community detection revealed four main clusters with very distinct gene expression patterns (Figure 34 B). Unique marker gene expression analysis identified a cluster of microglia cells (MG cells, expressing P2YR12, SERPINE1 and TMEM119), infiltrating myeloid cells (expressing CXCL8, PLAUR and CD163), lymphoid cells (expressing CD3E, CD8A, CD4 and NCR1), and B cells (expressing CD79A and CD19) (Figure 34 C). Consistently with previous studies, IDHwt TME consisted mostly of infiltrating myeloid cells (60% of CD45+ cells), while IDHm TME contained mainly MG cells (64% of CD45+ cells). More lymphoid cells were present in IDHwt (38% of CD45+ cells) compared to IDHm samples (26% of CD45+ cells). B cells were present in IDHwt and IDHm samples at similar low frequency (1% of CD45+ cells) (Figure 34 D).

To gain insights into differences between immune cells from IDH and IDHwt gliomas, we performed a differential expression. It revealed an enrichment of antigen presentation in IDHwt samples (Supplementary Figure 7 A). Therefore, we compared the expression of genes encoding HLA class I and II between the immune cell clusters.

We found that expression levels of HLA-A, HLA-B, and HLA-C were higher in T cells and lower in IDHm samples compared to IDHwt samples (Supplementary Figure 7 B). Additionally, we found that expression levels of HLA-II genes were higher in infiltrating myeloid cells and lower in IDHm samples compared to IDHwt samples (Supplementary Figure 7 C).

Notably, the final number of lymphoid cells analyzed was 8224 cells for primary IDHwt patients and 7804 cells for IDHm patients (Figure 34 E, Supplementary Table 9). Further sub-clustering of lymphoid cells did not show any difference in NK cells' frequency between the two gliomas. Interestingly, a cluster of γδT cells, defined by the preferential expression of TRGV9 and TRDV2 (Figure 34 F), was found mostly in IDHwt samples (4.3% of lymphoid cells) compared to IDHm samples (1.3% of lymphoid cells). Additionally, CD4 T cells were more abundant than CD8 T cells in IDHwt samples (62 % and 18% of lymphoid cells, respectively), while the opposite was true in IDHm samples (29 % and 55% of lymphoid cells, respectively) (Figure 34 G).

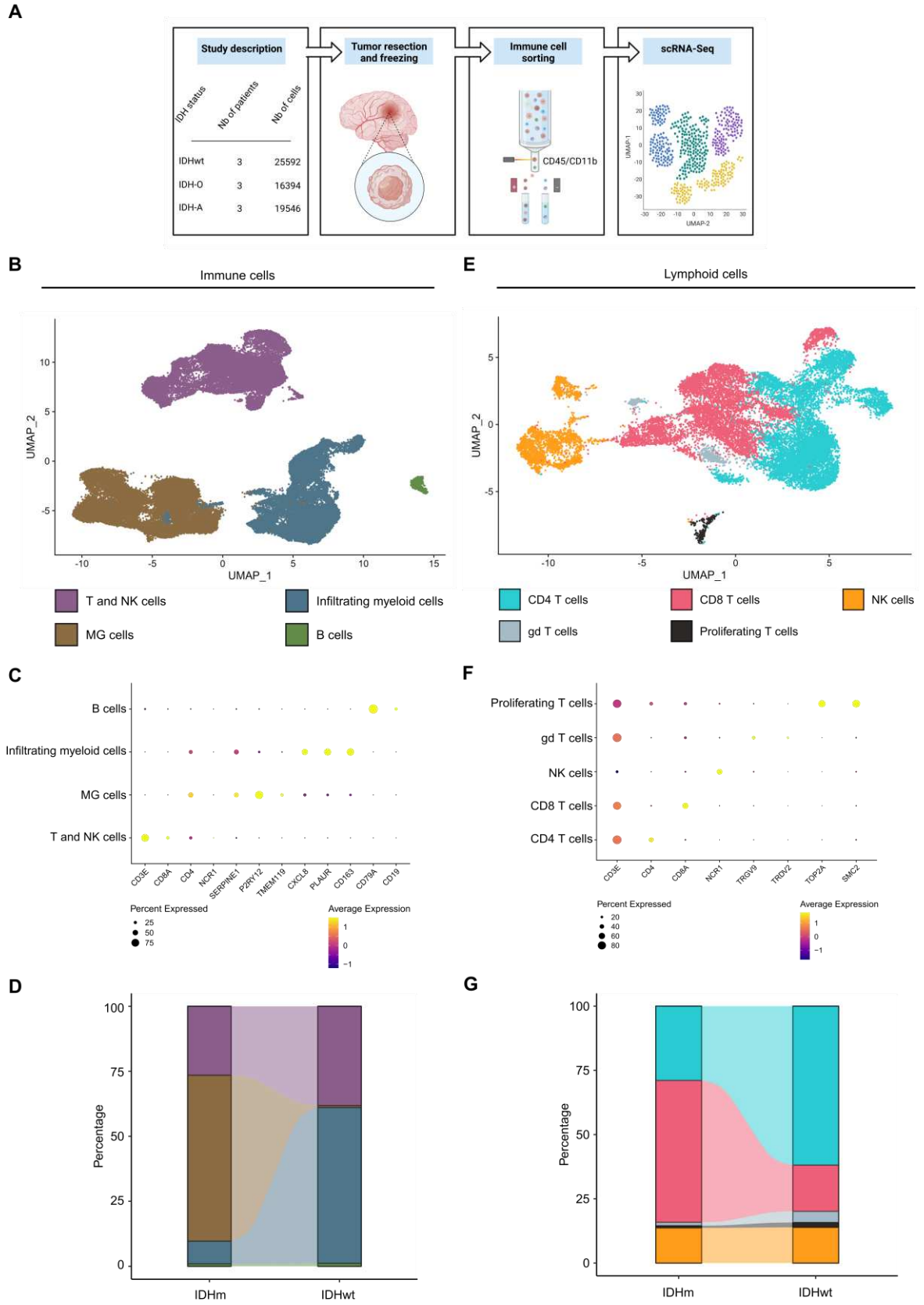

Figure 34| Single-cell transcriptome analysis of immune cells from IDHm and IDHwt human gliomas.

A| Graphical summary of the study design. **B|** UMAP projection of 61532 single CD45+/CD11b+ cells from 9 patients shown by cluster annotation (numbers of cells per cluster are presented in Supplementary Table 9). **C|** Dot plot showing marker gene expression for different cell types (MG, Infiltrating myeloid, T and NK, and B cells). Dot sizes indicate the percentage of cells in each cluster expressing the gene and colors indicate average expression levels. **D|** Alluvial plot showing the percentage of cells in each cluster from IDHm and IDHwt patients separately, color-coded for cluster annotations. **E|** UMAP projection of 16028 lymphoid cells from 9 patients shown by cluster annotation (numbers of cells per cluster presented in Supplementary Table 9). **F|** Dot plot showing marker gene expression for different cell types (CD4 T cells, CD8 T cells, γδT cells, Proliferating T cells, and NK cells). Dot sizes indicate the percentage of cells in each cluster expressing the gene and colors indicate average expression levels. **G|** Alluvial plot showing the percentage of cells in each cluster from IDHm and IDHwt patients separately, color-coded for cluster annotations. UMAP: Uniform manifold approximation and projection; MG: Microglia cells; IDHm: Isocitrate dehydrogenase-mutated; IDHwt: Isocitrate dehydrogenase wild-type; γδT cells: gamma-delta T cells.

b. Comparative analysis of IDHm and IDHwt diffuse gliomas' T cells

To elucidate T cells heterogeneity, we extracted T cells from the data presented above, performed *de novo* clustering, and identified 13 major sub-clusters across IDHwt and IDHm samples, including the cluster of γδT cells (7) (Figure 35 A). Cell numbers in each cluster is presented in Figure 35 B.

We annotated the T cell type or state represented by each cluster by considering the cluster's differentially expressed genes. Remarkably, we found a cluster of CD8 T cells expressing high levels of KLRC1 (encoding NKG2A), an intracytoplasmic tyrosine-based inhibitory motifs (ITIM)-bearing receptor, which binds to CD94 to induce T cell inhibition [305]. KLRD1 (encoding CD94) was also highly expressed in this cluster but was not specific to it. Nevertheless, the co-expression of these two genes suggests that inhibition may be active in these T cells. In line with previous findings [249], we confirmed high expression of KLRB1 (encoding CD161), an inhibitory NK receptor, in the most abundant cluster of T cells from IDHwt gliomas. Furthermore, we found that this same cluster expressed high levels of S100A4, a receptor also described as a major negative regulator of T cell functions [228] (Figure 35 C).

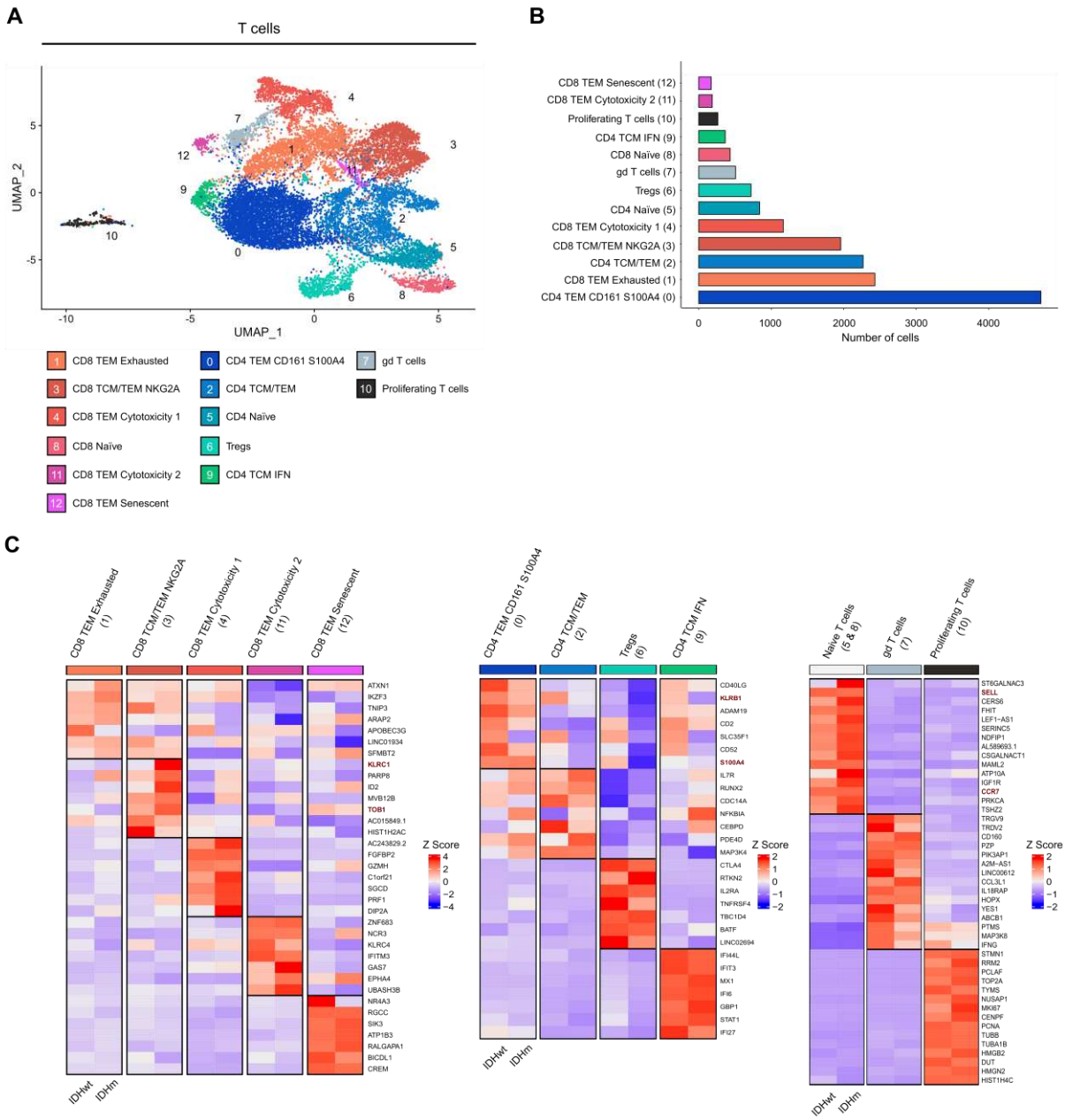

Figure 35| Phenotypic heterogeneity of T cells from IDHm and IDHwt gliomas.

A| UMAP projection of 16028 single T cells from 9 patients shown by cluster annotation. **B|** Bar plot representation of number of cells in each cluster. **C|** Heatmap showing relative expression of the 7 or 15 most differentially expressed genes for each cluster, separately for IDHwt and IDHm patients, ranked by log2FC. Gene expression values were centered, scaled, and transformed to a scale from either −4 to 4 or -2 to 2. KLRC1, TOB1, and KLRB1, S100A4, and SELL, CCR7 genes are bolded red. UMAP: Uniform manifold approximation and projection; TCM: Central memory T cell; TEM: Effector memory T cell; γδT cells: gamma-delta T cells; Tregs: Regulatory T cells; IDHm: Isocitrate dehydrogenase-mutated; IDHwt: Isocitrate dehydrogenase wild-type.

c. T cells from IDHm and IDHwt gliomas harbor different maturation phenotypes

To annotate T cell phenotypes, usually defined at the protein level, we projected our dataset onto a CITE-seq reference of 162,000 PBMCs measured with 228 antibodies [304]. This enabled us to distinguish between naïve, central memory (CM) and effector memory (EM) T cells, and to annotate clusters more precisely (Supplementary Figure 8). The different clusters spanned distinct T cell states. We found more naïve CD8 (8) and CD4 T cells (5) in IDHm samples compared to IDHwt samples. Moreover, we also found more CD8 and CD4 T cells exhibiting mix features of CM and EM (3, 2, respectively) in IDHm samples compared to IDHwt samples. A small cluster of CD4 TCM enriched in IFN related genes (9) was less enriched in IDHm samples than in IDHwt samples. As regards to more differentiated T cells, a cluster of CD4 T cells exhibiting inhibitory NK receptors (0), regulatory T cells (Tregs, 6), CD8 exhausted T cells (1), CD8 cytotoxic T cells (11) and CD8 senescent T cells (12) were less present in IDHm samples than in IDHwt samples. Alternatively, a large cluster of cytotoxic T cells (4) was predominant in IDHm samples compared to IDHwt samples (Figure 36 A).

To determine whether T cells are associated with particular molecular or signaling pathways, we performed Gene Ontology pathway analyses with differentially expressed genes of T cells from IDHm and IDHwt samples. We found that T cells from IDHwt samples showed strong ATP synthesis signatures, consistent with more differentiated cells and regulation of leukocyte activation signatures, consistent with a major cluster of inhibited T cells. T cells from IDHm samples exhibited cell activation signatures but also regulation of cell activation signatures mainly driven by KLRC1 (Figure 36Figure 35 B).

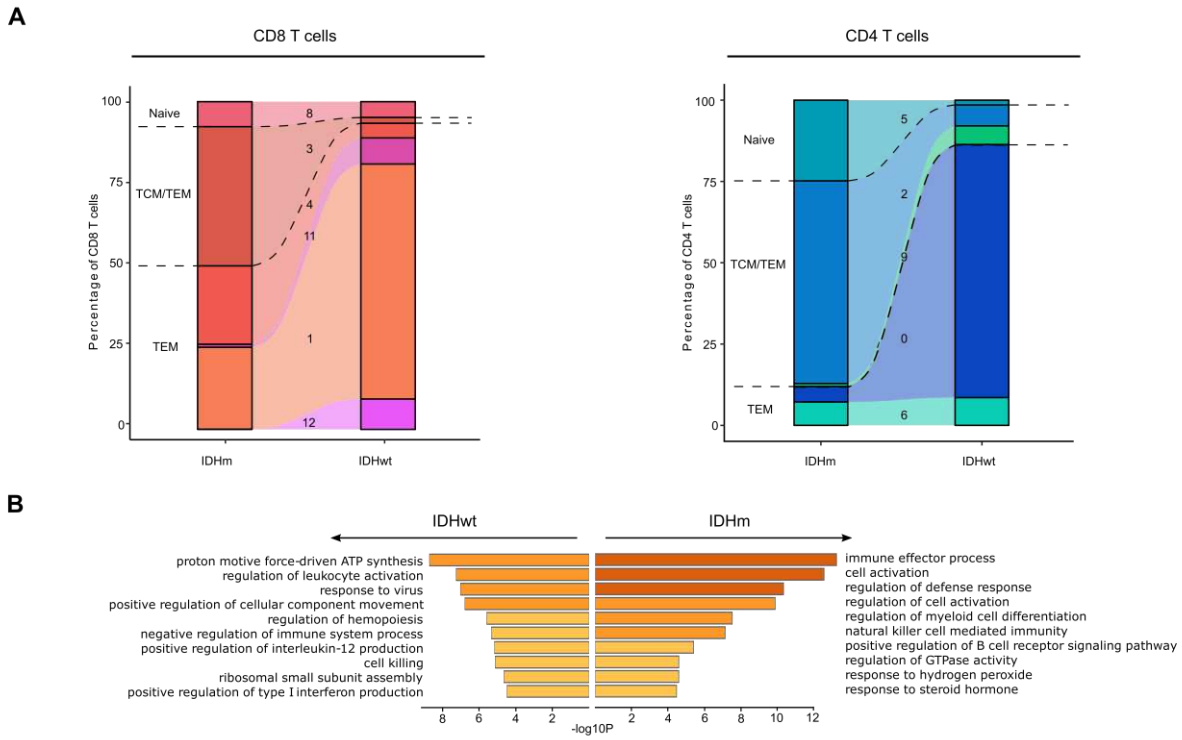

Figure 36| Differences of T cells proportion between IDHm and IDHwt gliomas.

A| Alluvial plot showing the percentage of CD8 (left) and CD4 (right) T cells in each cluster from IDHm and IDHwt patients separately, color-coded for cluster annotations. A bar graph showing the numbers of cells in each cluster from all patients is on the right. **B|** Barplot representation of pathway enrichment across genes upregulated in IDHwt (left) and IDHm (right) samples, color-coded by p-values. Log10(P) is the p-value in log base 10. TCM: Central memory T cell; TEM: Effector memory T cell; IDHm: Isocitrate dehydrogenase-mutated; IDHwt: Isocitrate dehydrogenase wild-type.

In all T cells of our study, KLRC1 and KLRD1 are significantly more expressed in IDHm samples compared to IDHwt samples (log2FC of 0.99 and 1.2, respectively), while KLRB1 and S100A4 are significantly less expressed in IDHwt (log2FC of 1.1 and 0.81, respectively) (Figure 37 A). Importantly, it is challenging to infer the impact of these two cluster signatures on TCGA data because most of the highlighted genes are not specific to these clusters. For instance, KLRC1 is also expressed by NK cells and γδT cells, which we have shown to be present in the TME of IDHwt and IDHm gliomas. To circumvent this limitation, we interrogated normalized TCGA bulk RNA-seq profiles to the T cell signal per tumor, as described by Mathewson *et al.* [249]. We confirmed the differential expression of KLRC1 and KLRB1 in IDHm and IDHwt samples, respectively (log2FC of 0.72 and 0.42, respectively) (Figure 37 B).

To validate the robustness of this finding, we leveraged public scRNA-Seq data of glioma's immune cells where we could isolate αβT cells. We scored each αβT cell across 3 publicly available datasets for the unique cluster signatures of: naïve T cells (5 & 8), CD4 TEM CD161 S100A4(0, enriched for KLRB1), CD8 TCM/TEM NKG2A (3,

enriched for KLRC1). Similar to our study, the scores of the CD8 TCM/TEM NKG2A (3) and naïve T cells (5 & 8) clusters were significantly higher in IDHm patients than in IDHwt patients, except for the Abdelfattah *et al.* dataset where it did not reach significance. Alternatively, the score of the CD4 TEM CD161 S100A4(0) cluster was significantly lower in IDHm patients than in IDHwt patients, except for the Alghamri *et al.* dataset where it did not reach significance. (Figure 37 C).

We further confirmed the phenotypes and inhibitory receptors at the protein level. Because tissue sections only enable a small representation of gliomas' specific immune cells (about 2% of Dapi+ cells are CD3+, Supplementary Figure 12), we developed an innovative approach combining immune cell sorting from whole frozen tumor samples coupled with multiplex immunofluorescence. This approach enabled to quantify the expression of: CD3, CD4, CD8, CD45RA, CCR7, CD161, and NKG2A at the same time. *This experiment is ongoing.*

Overall, we hope that this study demonstrates, at the transcriptomic and proteomic levels, the enrichment of naïve T cells and the presence of CD8 T cells expressing NKG2A in IDHm gliomas.

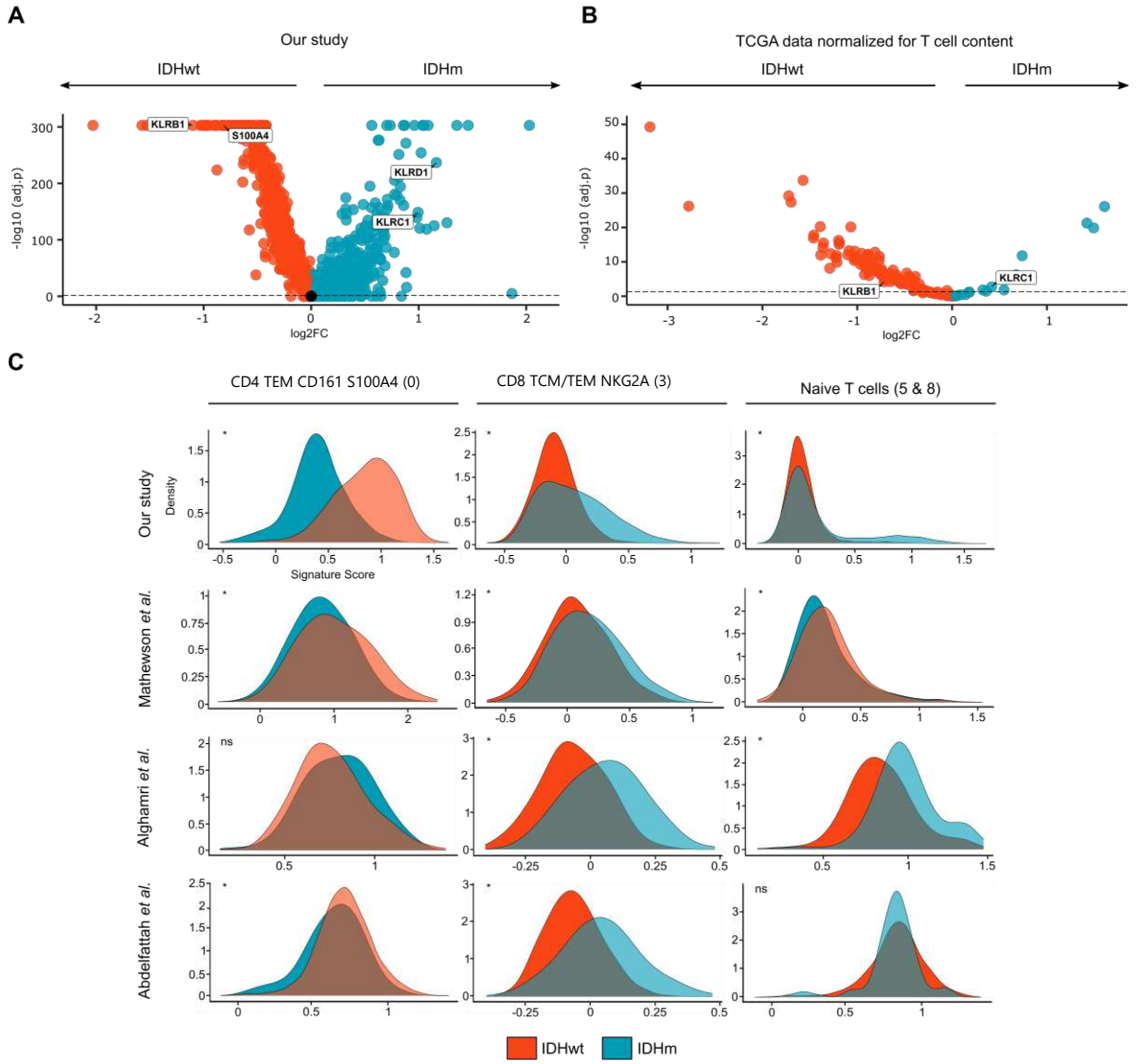

Figure 37| Expression of different inhibitory receptors in T cells from IDHwt and IDHm patients.

A| Volcano plots comparing gene expressions in IDHwt (left) versus IDHm (right). Genes are color-coded with respect to the glioma group. Select genes are highlighted. **B|** Analysis of TCGA datasets from IDHwt and IDHm for expression of T cell-specific genes. T cell-specific genes, the selection of glioma patients with a sufficient T cell signal (129 of 148 IDHwt and 161 of 428 IDHm samples), and the normalization of the total T cell signal (average expression of CD2, CD3D, CD3E, and CD3G) were made as described in [249]. Volcano plots comparing gene expressions in IDHwt (left) versus IDHm (right). Genes are color-coded with respect to the glioma group. Select genes are highlighted. **C|** Expression of gene signatures in αβT cells from our study (16028 αβT cells), Mathewson *et al.* (8252 αβT cells) [249], Alghamri *et al.* (947 αβT cells) [251], and Abdelfattah *et al.* (6980 αβT cells) [228]. Extreme values were chosen to belong to the 9th decile, and Pearson's Chi-squared test with Yates' continuity correction was performed. Cluster designation corresponds to Figure 35 A. TCM: Central memory T cell; TEM: Effector memory T cell; IDHm: Isocitrate dehydrogenase-mutated; IDHwt: Isocitrate dehydrogenase wild-type.

d. NKG2A expression associates with better survival in IDHm gliomas

NKG2A engages the non-classical HLA-E molecule expressed by a variety of cells, including tumor cells, T cells and microglia cells [307]–[309]. To determine the

clinical relevance of the NKG2A-mediated inhibition of T cells, we examined the association between the expression of HLA-E and patient survival in TCGA. We found that HLA-E expression was associated with significantly worse overall survival in IDHm patients (p-value=0.045) but not in IDHwt patients (p-value=0.08) (Figure 38 B). Importantly, multivariate analysis of HLA-E expression, Karnofsky Performance Status (KPS), age, and tumor grade showed that HLA-E expression was not an independent prognostic indicator (multivariate Cox regression analysis p-value=0.252) (Supplementary Figure 11). Based on the increased interest into NKG2A function in CD8 T cells and the emerging data in clinical trials of NKG2A blockade in other tumor types, we also evaluated the effect of KLRC1 gene expression on the survival of IDHm glioma patients in TCGA. Interestingly, higher KLRC1 expression significantly associated with better overall survival (Figure 38 C). To better distinguish the effect of KLRC1 expressed by NK or T cells on survival, we stratified patients based on NCR1 (NKp46) (Figure 38 D) or CD8A (Figure 38 E). We found that the protective effect of KLRC1 was lost only in $CD8A^{high}$ patients.

Overall, these results suggest a detrimental role for NKG2A on CD8 T cells in IDHm gliomas.

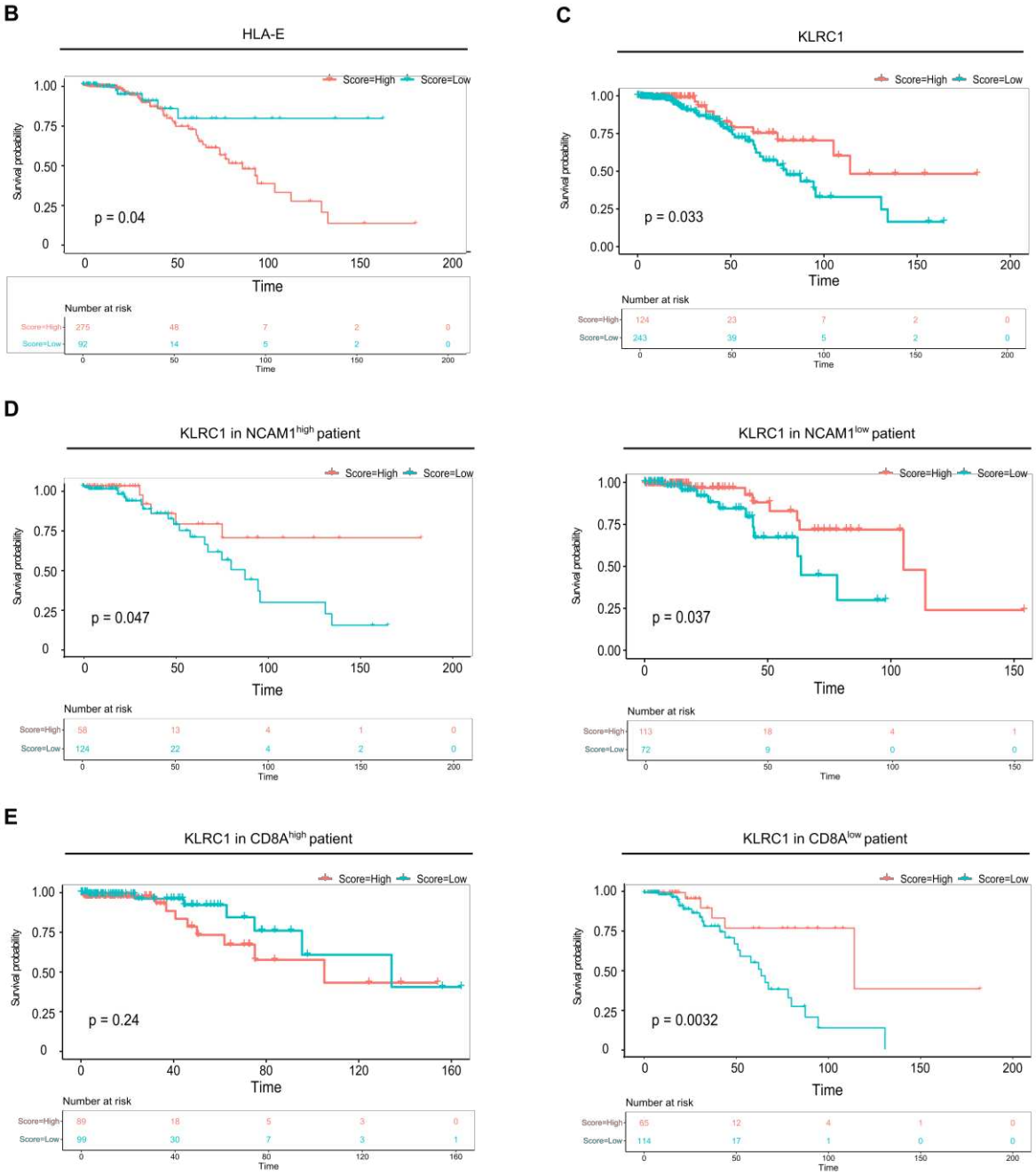

Figure 38| Improved overall survival in NKG2A+ (KLRC1high) IDHm patients.

Kaplan-Meier survival curves of the TCGA IDHm cohort showing associations between HLA-E and KLRC1 (NKG2A) expression and overall survival in **B|** and **C|** respectively. Kaplan-Meier survival curves of the TCGA IDHm cohort showing associations between KLRC1 (NKG2A) expression and overall survival in patients with **D|** NCAM1Ahigh/low (Nkp46) gene expression or **E|** CD8Ahigh/low (CD8) gene expression.

e. NKG2A defines a subset of TRM CD8 T cells that retain TCR-independent cytotoxic functions in IDHm gliomas

Projection of our datasets onto a reference map revealed that NKG2A was restricted to the memory CD8 T cell compartment, with highest expression of CM and EM features (Figure 39 A).

We then performed pseudotime analysis to evaluate the phenotypic diversity of CD8 T cells from IDHm gliomas. Pseudotime analysis predicts phenotypic relatedness and assigns a trajectory for visualization. We observed that NKG2A acquisition is defined by a branch point derived from a subset of exhausted CD8 T cells (1), suggesting that exhaustion markers are acquired before NKG2A during chronic activation, in line with recent findings. Globally, well-known co-inhibitory receptors (PDCD1, CTLA4, HAVCR2, LAG3, TIGIT, BTLA and VSIR) expression was low, except for CTLA4 and TIGIT which expression was restricted to Tregs (6) (Supplementary Figure 10). Interestingly, the cluster of CD8 cytotoxic T cells was also defined by a branch point derived from the same subset of exhausted CD8 T cells (Figure 39 B). The numbers of cells in each cluster according to their pseudotime are detailed in Supplementary Figure 9.

To better understand the phenotype of CD8 T cells that may be engaged independent of MHC-I, we sought to compare cluster 3 (CD8 TCM/TEM NKG2A) to the other CD8 T cells in IDHm gliomas. We found that NKG2A+ CD8 T cells displayed higher levels of the activating NK receptors NKG2D and DNAM-1 (CD226), the canonical NK-lineage marker CD56, as well as the resident-memory (TRM) markers CD69, ITGA1 (CD49a), and ITGAE (CD103). In addition, NKG2A+ CD8 T cells also expressed the highest levels of the anti-proliferation transcription factor TOB1. Strikingly, expression of CD28 was downregulated on NKG2A+ CD8 T cells (Figure 39 C).

Because this cluster expressed high levels of activating receptors, we asked whether NKG2A+ CD8 T cells could still retain cytotoxic capacities. We found that both GZMB and PRF1 were highly expressed by these cells (Figure 39 D).

Collectively, the data suggest that NKG2A marks an alternative path of differentiation by CD8 T cells in IDHm gliomas defined by a progressive loss of TCR co-stimulation, anti- proliferation, and tissue-residency, divergent from pathways associated with exhaustion. These T cells still possess a high cytolytic payload, reinforcing the need to test NKG2A blocking antibody in IDHm gliomas.

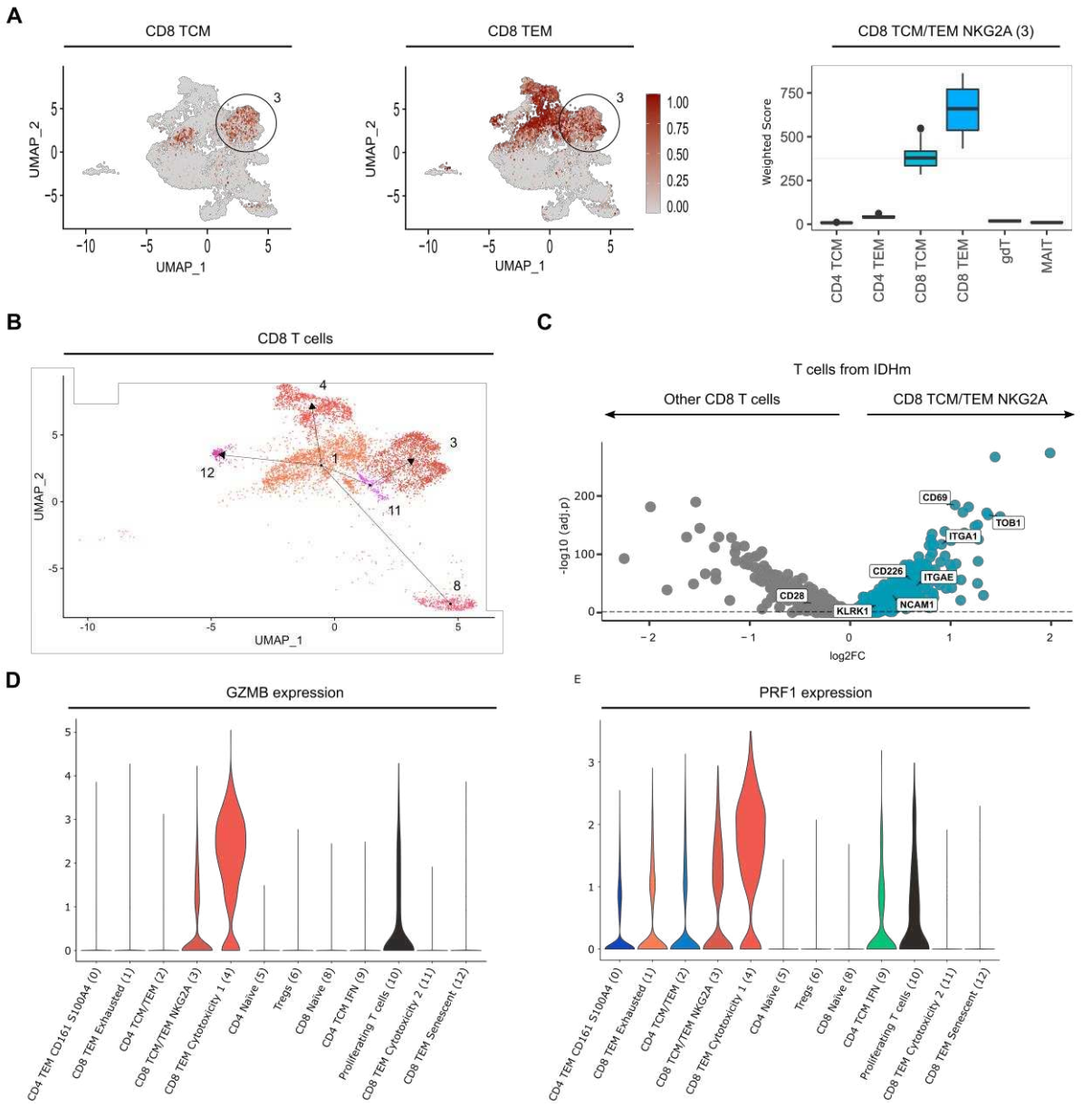

Figure 39| Investigations on NKG2A+ CD8 T cells from IDHm gliomas.

A| UMAP of T cells with TCM and TEM prediction scores. Boxplot on the right represents the weighted score i.e. the prediction score multiplied by the number of cells in each predicted cluster. **B|** T cell trajectories suggested by the Slingshot pseudotime analysis for CD8 T cells. The overlaid lines represent the lineages found by the algorithm. **C|** Volcano plots comparing gene expressions in CD8 TCM/TEM NKG2A (cluster 3) on the right versus all other CD8 T cells, on the left, in IDHm gliomas. Genes are color-coded with respect to the cluster group. Select genes are highlighted. **D|** Violin plots showing GZMB and PRF1 expression levels in human glioma-associated T cells

f. R-2HG does not affect the phenotypes of T cells during stimulation

Overproduction of R-2HG by IDHm tumor cells causes a metabolic disruption in T cells, which hinders TCR-triggering signaling. However, proper TCR triggering, in addition to costimulation signals are essential for T cells to differentiate. In IDHm tumor cells, R-2HG causes DNA hypermethylation via inhibiting methylcytosine dioxygenase

TET2, leading to a global epigenetic reprogramming. Functional and phenotypic changes during T cell differentiation are well characterized, but the epigenetic states that underlie these changes are poorly understood. Nevertheless, it was described that, upon TCR triggering, TET proteins turn on the expression of lineage specifying transcription factors that govern cell differentiation resulting in a peak of 5hmC. Then, 5hmC and 5mC levels gradually diminish as the cell identity is established [34]. Therefore, we asked whether altered TCR triggering by R-2HG also alters TET2-mediated 5hmC content leading to the observed defect of maturation. Therefore, we asked whether R-2HG decreases T cell maturation which may account for the high number of naïve T cells observed in IDHm gliomas compared to IDHwt gliomas.

To determine if R-2HG was taken up by primary immune cells, we isolated CD14- cells from human buffy coats, cultured them *in vitro* for two days with R-2HG, and quantified the total amount of intracellular 2-HG by GC-MS. Cells were either unstimulated or stimulated with CD3/CD28 ligation beads. Stimulation of T cells for two days seemed to increase, although not statistically, the amount of total 2-HG compared to unstimulated T cells. Here, we validated the uptake of R-2HG by T cells (Figure 40 A).

To evaluate the functional implications of R-2HG on the maturation phenotypes of T cells, we induced the differentiation of pan T cells with an acute CD3/CD28 ligation and followed markers of maturation for seven days by flow cytometry. The proportion of naïve CD8 T cells (CD45RA+CCR7) at days 2 was significantly higher in cells treated with R-2HG compared to untreated cells. Alternatively, the proportion of CD8 TEM (CD45-CCR7-) and TEMRA cells (CD45+CCR7-) were higher in the untreated group (Figure 40 B). To make sure that these differences were not due to a heterogenous population of T cells at the beginning of the assay, we also induced the differentiation of isolated naive T cells with chronic stimulations but did not observe any effect of R-2HG in T cell differentiation.

Altogether, 5 mM of R-2HG DID not significantly delay T cell differentiation in our setting.

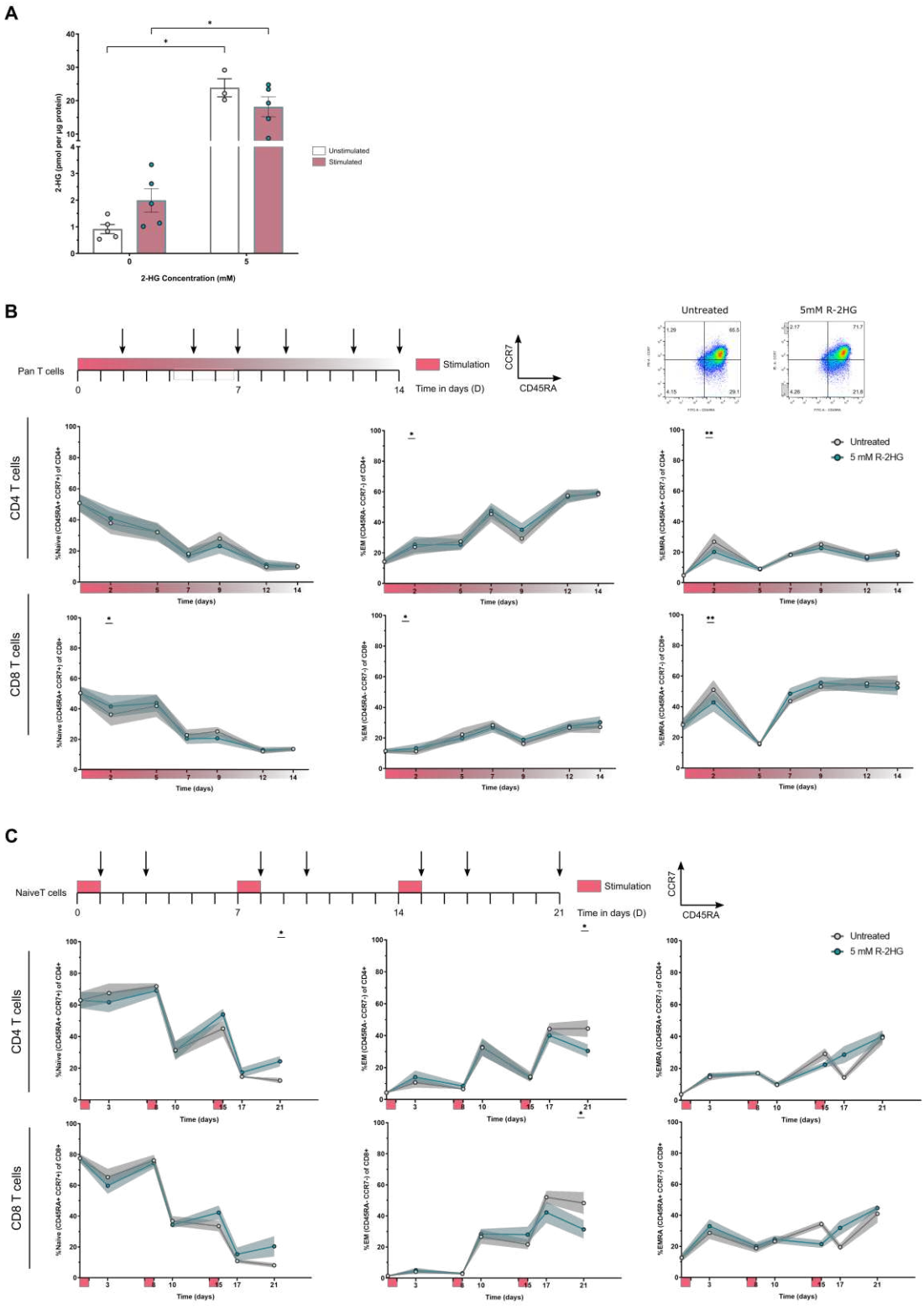

Figure 40| R-2HG does not delay T cell differentiation.

A| Intracellular measurement of 2HG in human CD14- cells. Cells were unstimulated or stimulated with aCD3/CD28 beads at a bead-to-cell ratio of 1:2 for the duration of the assay. Cells were incubated without or with 5mM R-2HG for the duration of the assay. **B|** Schematic overview of the *in vitro* assay. Pink bars represent the duration of T cells stimulation. Vertical arrows represent time of harvest for flow cytometry analysis. Representative dot plots from flow cytometry analysis of CD8 T cells. Flow cytometric analysis of CD45RA and CCR7 proteins on the surface of CD4 (top) and CD8 (bottom) T cells stimulated

with aCD3/CD28 beads at a bead-to-cell ratio of 1:2. Cells were incubated without or with 5mM R-2HG for the duration of the assay. **C|** Schematic overview of the *in vitro* assay. Pink bars represent the duration of T cells stimulation. Vertical arrows represent time of harvest for flow cytometry analysis. Representative dot plots from flow cytometry analysis of CD8 T cells. Flow cytometric analysis of CD45RA and CCR7 proteins on the surface of CD4 (top) and CD8 (bottom) T cells stimulated with aCD3/CD28 beads at a bead-to-cell ratio of 1:2. Cells were incubated without or with 5mM R-2HG for the duration of the assay. Experiments in (A) were performed on five different donors, experiments in (B) was performed on six different donors, and experiment in (C) was performed on four different donors. *p < 0.05, **p < 0.01, ***p < 0.001, all error bars denote SEM. Paired t-test (D). TCM: Central memory T cell; TEM: Effector memory T cell; TEMRA: Effector memory RA T cell.

To evaluate the kinetic of 5hmC during T cell differentiation, we induced T cell differentiation with an acute CD3/CD28 ligation and quantified the amount of 5hmC, 5mC, and cytosine contents by HPLC-MS. 5hmC levels at day two were similar to baseline. However, we observed a drastic decrease at seven days of stimulation. We noticed a trend toward more 5hmC in treated cells after seven days of stimulation (Figure 41 A). These data confirm that 5hmC and 5mC amount significantly decrease upon stimulation in effector cells. The lower proportion of TEM cells (CD45-CCR7-) at day seven in treated CD8 and CD4 T cells observed earlier may account for the relatively higher amount of 5hmC at this time point However, we did not observe a peak of 5hmC on day two compared to baseline. *Quantifying 5hmC by HPLC-MS in the same setting but before two days of stimulation is underway*.

Then, we isolated pan T cells from blood PBMCs and sorted naïve and non-naïve T cells. We induced T cell differentiation by stimulating these cell populations with acute CD3/CD28 ligation Noteworthy, we found that TET2 mRNA expression showed a similar trend in stimulated pan T cells and in stimulated non-naïve T cells. More precisely, TET2 mRNA expression slowly decreased from baseline to reach significantly lower levels at 24h. No difference was observed in both unstimulated pan T cells and non-naïve T cells treated with R-2HG compared to untreated cells. On the contrary, stimulation of naïve T cells resulted in a maximal TET2 mRNA expression at 1.5h and slowly decreased to also reach significantly lower levels compared to the starting time at 24h post-stimulation. Interestingly, naïve T cells treated with R-2HG did not exhibit this rapid and transient peak, although statistical difference was not reached (Figure 41 B).

Altogether, these data do not support the hypothesis that R-2HG exposure induces profound epigenetic reprogramming of T cells during TCR stimulation, but more experimental evidence is needed to conclude.

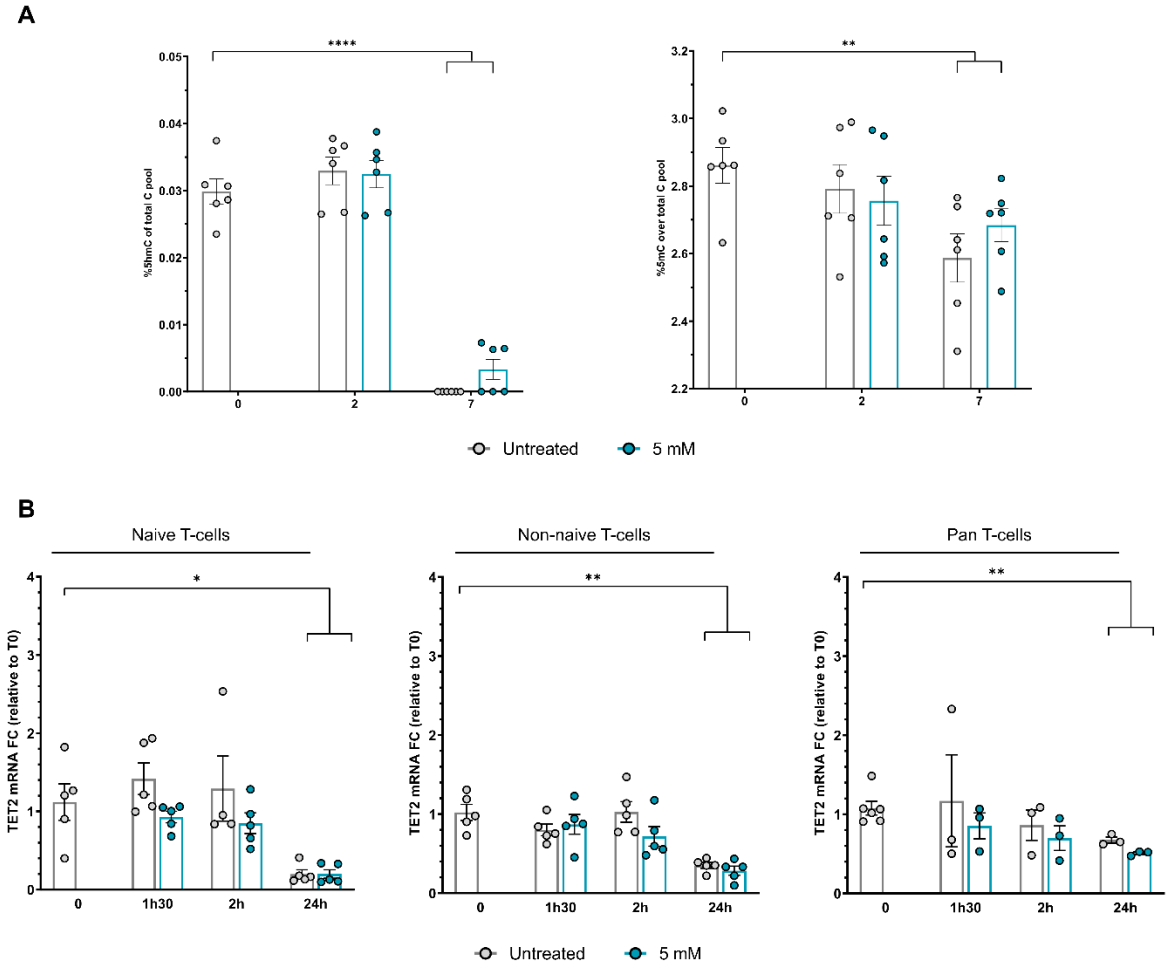

Figure 41| R-2HG delays T cell differentiation through epigenetic mechanisms.

A| Percentage of 5hmC and 5mC (of the sum of 5hmC, 5mC, and C) on the left and right, respectively, at day 0, 2, and 7 in CD14- cells stimulated with aCD3/CD28 beads at a bead to cell ratio of 1:2. Cells were incubated without or with 5mM R-2HG for the duration of the assay. **B|** qRTPCR analysis of TET2 and GAPDH in naïve, non-naïve, or pan T cells stimulated with aCD3/CD28 beads at abead-to-celll ratio of 1:2. Cells were incubated without or with 5mM R-2HG for the duration of the assay. Experiments in (A) were performed on six different donors, and experiments in (C) were performed on five or six different donors. *p < 0.05, **p < 0.01, ***p < 0.001, all error bars denote SEM. Mann-Whitney with Welch correction (A, B). FC: Fold change.

g. R-2HG effect on NKG2A expression

Altered and/or chronic TCR stimulus, as well as a normal antigenic stimulus in the absence of costimulation, induce, in T cells, a state of anergy, which leads to the failure to synthesize IL-2 and other functional cytokines. TOB1 has been shown to be a marker of anergy. Therefore, we asked whether R-2HG increases the expression of NKG2A in T cells, which may account for the large cluster of T cells expressing high levels of NKG2A and TOB1 observed in IDHm gliomas gliomas.

We chronically stimulated naive T cells in presence of low dose IL-7/IL-2 or IL-7 only. We observed that NKG2A expression on CD8 T cells increased only after the second stimulation and was higher in cells treated with R-2HG. The expression of NKG2A on CD8 T cells was abrogated when IL-2 was removed from the culture medium. These results are still preliminary and need to be reproduced. The optimization of an *in vitro* system to harvest NKG2A+ CD8 T cells would be useful to study the killing of IDHm glioma cells derived from patients in the presence of NKG2A blocking antibody (monalizumab).

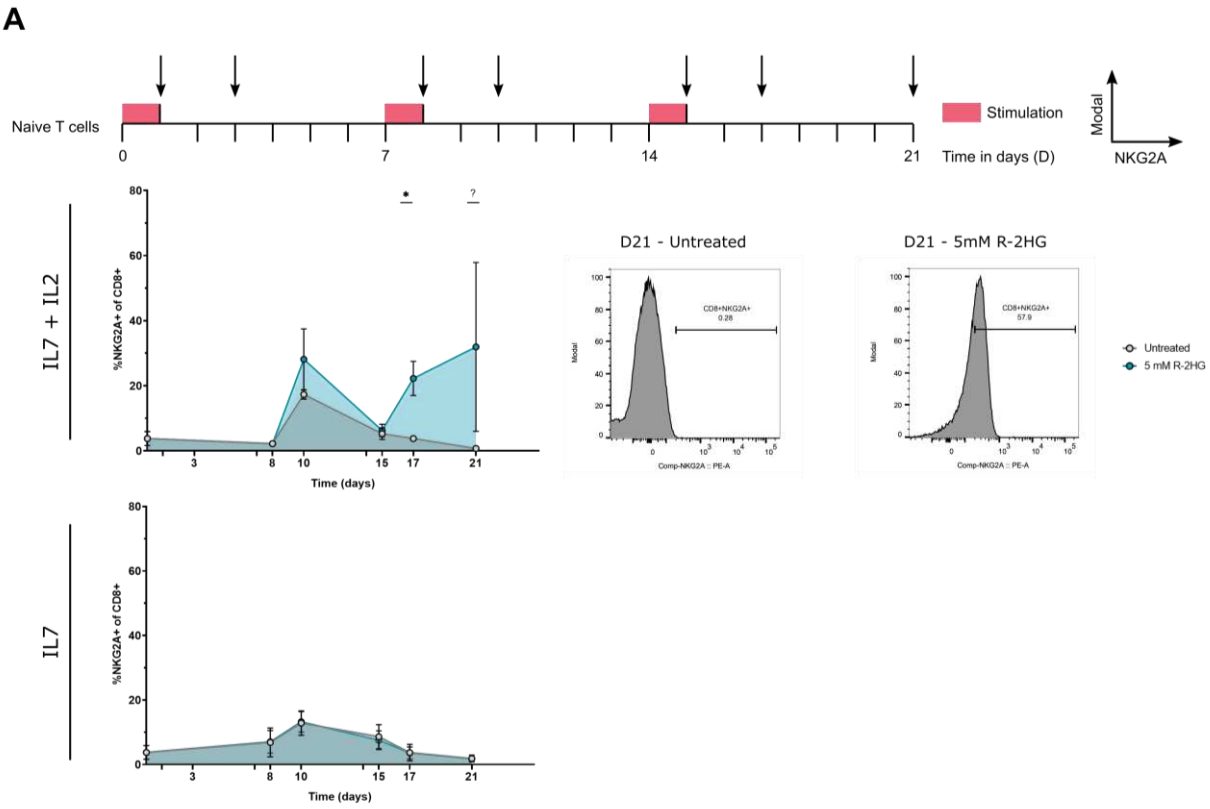

6) Discussion

It is recognized that inter- and intra-individual molecular and cellular heterogeneity of immune cells in the TME is a critical hurdle for the clinical response to cancer immunotherapies. The paucity of T cells, as well as the lack of classical immune checkpoint receptors expression underpin the failure of immunotherapy both in IDHm and IDHwt patients. In the last couple of years, the advent of highly resolutive sequencing techniques such as scRNA-Seq enabled the investigation of the myeloid compartment that can constitute more than half of the cells in the TME of diffuse gliomas. Descriptive analysis of T cells has also begun but only with a small number of

cells, especially in IDHm samples. Therefore, the extent to which T cells from IDHm and IDHwt patients differ has not yet been addressed.

Gain-of-function mutations in IDH in gliomas result in the overproduction of R-2HG, an oncometabolite that promotes tumorigenesis through epigenetic alterations. One of these alterations is the inhibition of DNA demethylation through competitive inhibition of TET proteins [159], [310]. Mathematical models showed that R-2HG concentration in the TME of IDHm gliomas exceeds three mM [132] raising the question as to whether R-2HG could affect the function of immune cells as well. Studies have shown that R-2HG, taken up by T cells, induces an immunosuppressive phenotype through the alteration of their metabolism and subsequent suppression of early TCR signaling events [263] [301]. When stimulated by TCR triggering and costimulation molecules, such as CD28, naïve CD8, and CD4 T cells engage in differentiation programs toward memory and effector functions. Culture of naïve CD8 T cells from mice with the cell-permeable form of L-2HG decreased phenotypic effector markers [63]. Moreover, enrichment of naïve T cells has already been observed in the bulk analysis of human IDHm gliomas compared to IDHwt gliomas [263], but the opposite was observed in a recent scRNA-Seq study [228]. However, this scRNA-Seq study only contained 147 T cells from IDHm gliomas, while it contained 4968 T cells from primary IDHwt gliomas. In the present study, exploratory analysis of 7804 T cells from IDHm gliomas and 8224 T cells from IDHwt gliomas confirmed that the proportion of naïve and central memory T cells is higher in IDHm patients compared to IDHwt patients. Therefore, we asked whether suppression of TCR signaling by R-2HG decreased the maturation of T-cells. In our setting, we did not show an impact of R-2HG on T cell differentiation.

Despite the increasing discoveries related to TET proteins, the precise mechanisms of TET functions in immune cells remain elusive. Nonetheless, it was shown that transient exposure to antigen causes a peak of TET2-induced 5hmC which precedes T cell lineage specifications and that 5hmC levels decreases afterward. Global levels of 5mC also decreases following stimulation [34], [50]. Moreover, studies have shown an increase of L-2HG rapidly after T cells stimulation. Here, we observed an increase of global 2-HG after 2 days of stimulation, but we cannot attribute this increase to the S- or R- enantiomer. In addition to the aforementioned effects on TCR signaling, we hypothesized that the observed delay of maturation following stimulation could be due to a modification of 5hmC deposition via inhibition of TET2 by R-2HG. Already published results show that exposure to R-2HG did not result in profound epigenetic reprogramming in human T cell when looking at global DNA methylation array and

histone methylation analyses [263]. Culture of naïve CD8 T cells from mice with the cell permeable form of L-2HG altered 5hmC levels but only after seven days of stimulation. In this study, we confirmed that the induction of differentiation of T cells through the stimulation of CD3/CD28 in presence of IL-2 resulted in a drastic decrease of 5hmC and, a lower decrease of 5mC. Of note, R-2HG did not alter the levels of 5hmC nor 5mC during differentiation. However, one study showed that stimulation of naïve T cells resulted in a peak of 5hmC from 30 minutes to 2 hours after stimulation only and showed a peak of TET2 mRNA expression only after 2 hours of stimulation. TET2 mRNA expression levels were not significantly different than baseline after 4 hours of stimulation. These results suggest that the peak of TET2/5hmC is very rapid and transient after stimulation. The discordant timing of 5hmC induction versus TET2 gene expression is still poorly understood. However, we did not observe any statistical increase in TET2 mRNA expression following stimulation but only a slight tendency. No effect of R-2HG was also observed. We will send samples stimulated at earlier time points than two hours to our collaborators for the dosages of 5hmC. Moreover, we are currently working on an assay to quantify the activity of TET2. These two assays might give us more reliable results on whether R-2HG can epigenetically rewire T cells.

In conclusion, in our setting, we show preliminary results that discard DNA methylation changes in primary T cells due to the presence of 5 mM of R-2HG in the culture medium. The absence of TET enzymes inhibition most likely come from the presence of αKG, the natural substrate of TET enzymes, in these primary cells. In IDHm tumor cells, αKG is converted to R-2HG, resulting in a high R-2HG/αKG ratio which enable the competitive inhibition of these enzymes. We quantified the amount of R-2HG in primary T cells and we are currently working on also quantifying the amount of αKG. These data suggest that the reason why naïve T cells subsist in IDHm TME lies elsewhere.

Antigen presenting cells (APCs), in IDHm gliomas, express lower levels of MHC-I/II molecules compared to their counterparts in IDHwt gliomas. In the previous study, we hypothesized that the downregulation of MHC-I/II molecules may be attributed to CIITA promoter hypermethylation both in CD11b- and CD11b+ cells. In addition, APCs in gliomas have been described to lack expression of costimulatory receptors, such as CD80, CD86, and CD40 [317]. A recent study shows that monocyte-derived DCs in IDHm tumors are characterized as an intermediate state between immature monocyte-derived cells in early-stage gliomas and the fully functional DC found in late-stage IDHwt tumors. Importantly, they demonstrate that paracrine R-2HG specifically suppresses MHC class I/II-mediated antigen (cross-)presentation and co-stimulation

by IL-6, which ultimately leads to reduced T cell activating capacities [260]. These data demonstrate that the TME of IDHm gliomas is poorly capable of inducing T cell activation and is most likely the reason why more naïve T cells are observed in IDHm gliomas compared to IDHwt gliomas.

The cluster of TEM inhibited 2 (3), expressing high levels of NKG2A also expresses high levels of TOB1. TOB1 (also known as transducer of ERBB2,1) is a member of the TOB/BTG antiproliferative protein family and is constitutively expressed in naïve primary human CD4 and CD8 T cells. Upon T cell activation, TOB1 is rapidly downregulated. Importantly, TOB1 downregulation requires full T cell activation with TCR triggering and costimulation. Naïve T cells only activated through the TCR[5] fail to downmodulate TOB1 levels, which results in a lack of proliferation and cytokine production. In other words, TOB1 is expressed in unstimulated naïve T cells and anergic T cells where it is necessary for the maintenance of quiescence. T cells that lack TOB1 due to gene silencing are fully activated by TCR triggering alone, both in terms of proliferation and effector function, suggesting that TOB1 acts as a rheostat and increases the threshold for naïve T cells to become activated [306], [313]. Although TOB1 is associated with T helper 17 cell–related autoimmunity, its role in modulating other subsets of T cell, such as CD8 T cells–mediated immune responses remains poorly understood. In accordance with the TOB1 gene silencing studies performed *in vitro*, Tob1-deficient mice develop severe CNS autoimmunity and display an increased infiltration of Th1 and Th17 cells in the CNS, while the proportional number of infiltrating Tregs decreases [314]. Data from human studies also imply that TOB1 is required to dampen T cell activity, because downregulation of TOB1 gene expression is correlated with the progression of multiple sclerosis [315]. Interestingly, TOB1 was also shown to impair IL-2 production in Th17 cells, to block the expression of cell cycle genes, and to suppress Th17-cell proliferation through several pathways, including transcription, translation initiation, and mRNA decay [313], [316]. The highlighted cluster of TEM inhibited 2 (3) does not express features of naïve T cells and was associated with a TCM/TEM phenotype. Altogether, the expression of TOB1 reveals a defect in IL-2 production and/or a stimulation without costimulation in these T cells, which may explain the high expression of KLRC1 and KLRD1, encoding NKG2A and CD94, respectively. This suggest that, in our study, T cells from this major cluster in IDHm gliomas may be anergic.

[5] Activation by TCR triggering without costimulation generate T cells defined as anergic.

Importantly, this study reveals for the first time, to our knowledge, a large cluster of T cells in IDHm samples expressing high levels of KLRC1 and KLRD1 (encoding NKG2A and CD94, respectively). These results clearly highlight the differences between specific T cell subtypes and underscore the need for more precise targeted immune therapies in glioma. The surface inhibitory receptor NKG2A forms heterodimers with the invariant CD94 chain and is expressed on cytotoxic CD8 T cells to engage the non-classical HLA-E molecule in different cancers [307], [308]. Blocking antibody targeting NKG2A unleashed the reactivity of these effector cells resulting in tumor control in multiple mouse models, and is currently being investigated in late clinical trial (NCT04590963, NCT05221840) [311]. A very recent article revealed the presence of NKG2A+ CD8 T cells in bladder cancer. Similar to us, they showed that NKG2A is acquired by CD8 T cells after other exhaustion markers, in line with recent findings [305], alongside with the enrichment of TRM markers; TOB1 expression, and a strong downregulation of CD28, suggestive of a specialization of NKG2A+ CD8 T cells toward TCR-independent activation. This subset of CD8 T cells still harbor a heavy cytotoxic payload, which suggest that TCR independent, innate-like functions, may be partly mediated through DNAM-1 and NKG2D, two activating receptors highly expressed by these cells. NKG2A, although universally defined as an inhibitory receptor, also correlated with better survival in non-muscle-invasive bladder cancer patients. Here, we showed that the protective effect of NKG2A is lost only in patients with a high CD8 T cell content. Moreover, the pseudotime analysis revealed that NKG2A+ CD8 T cells were distinct of cytotoxic CD8 T cells. highlight the inhibitory function of this receptor on CD8 T cells of IDHm gliomas. Altogether, these data show that NKG2A is an alternative immune checkpoint axis that defines inhibited anti-tumor functions by NKG2A+ CD8 T cells in IDHm gliomas. Blocking NKG2A by monalizumab may reactivate NKG2A+ CD8 T cells which could increase the release of cytotoxic molecules.

7) Limitations and prospects

The low and highly variable number of T cells in IDHm gliomas (we obtained about 2461 T cells per IDH-O patients and only 140 T cells per IDH-A patients in our scRNA-Seq analysis) make their isolation, and, therefore, the analysis of subpopulations' phenotypes and functions by classical assays very challenging. Nonetheless, the development of droplet-based microfluidics allows the phenotyping of single-cell by microscopy[318] and the development of single-cell cytotoxic assays [319]. These technologies could be helpful to validate the expression of NKG2A/CD94 in T cells from IDHm gliomas and to study the efficacy of NKG2A blockade by monalizumab. Unfortunately, IDH-O patient-derived cell lines hardly grow *in vitro,* and

IDHm patient-derived cell lines do not grow well in immunocompetent mice, which means that the only option to study T cells *in vivo* would be to use genetically engineered mice models [251]. However, the observations made in our study have yet to be confirmed in these animal models.

Typical *in vivo* responses of naïve CD8 T cells to antigen involve up-regulation of a wide variety of cell-surface molecules. For most of these markers, it is well accepted that their up-regulation during the immune response is TCR-dependent and amplified by CD28-dependent costimulation and contact with growth factors, especially IL-2. However, the requirements for inducing NKG2A/CD94 expression are quite different. Although a couple of articles describe *in vitro* systems to increase NKG2A on CD8 T cells, they have contrasting results. One showed that induction of NKG2A/CD94 expression was only possible with CD3 activation alone, or with CD3/CD28 activation in the absence of IL-2. Indeed, CD28 costimulation had a negative effect on the expression of NKG2A/CD94, because of the high levels of IL-2 in the cultures, with IL-2 synthesis being much higher after combined CD3/CD28 ligation than with CD3 ligation alone [312]. Another very recent article, showed that induction of NKG2A on CD8 T cells was possible with CD3/CD28 ligation in the presence of low dose cytokines (IL2 10 UI/mL and IL7 10 ng/mL). However, these articles agree that chronic stimulations are required and that TGFβ1 increases NKG2A expression. In this study, we evaluated the expression of NKG2A on T cells after repeated TCR stimulation with CD3/CD28 ligation in the presence of IL-7 or IL-7 and IL-2. We are working on improving this assay by using CD3 ligation alone and adding TGFβ1 in the culture medium. Optimizing an *in vitro* system to increase NKG2A expression on CD8 T cells will be necessary to test the efficacy of monalizumab with IDHm glioma cells from patients in coculture experiments.

To test the hypothesis that glioma tumors cells and other APCs from IDHm tumors induce anergic T cells and therefore, the overexpression of NKG2A, it may be possible to isolate APCs cells from tumor resections and to coculture them with naïve T cells isolated from healthy blood. T cell stimulation or anergy can be evaluated by the presence of maturation and activation markers by flow cytometry.

Owing to substantial advances in microscopy, mass spectrometry, and machine learning applications for data analysis, spatial proteomic is now available [320]. We could apply this technology to confirm the co-expression of NKG2A/CD94 as well as the marker of anergy TOB1 and markers of maturation such as CD45RA, CCR7, etc. This

would enable the phenotyping of T cells, at the protein level, on gliomas tissue slides, along with the investigation of the expression of HLA-E, the ligand of NKG2A.

The evaluation of the modulation of epigenetics by R-2HG requires highly sensitive techniques at the nucleotide resolution. However, we tried more easily available ELISA assays to quantify the amount of 5hmC [321] and 5mC [322] in primary human T cells. Values of 5hmC were below the limit of detection and could not be interpreted. We did not observe a decrease of 5mC following stimulation, and no effect of R-2HG was observed. We tried to use a more sensitive approach and to immunoprecipitate hydroxymethylated DNA [323] followed by qPCR of specific genes, but the absence of qPCR primers targeting positive and negative regions on the human genome prevented monitoring the success of the immunoprecipitation. These setbacks prompted us to collaborate with a team in the USA to quantify the amount of 5hmC and 5mC by HPLC-MS. Unfortunately, this analysis took four months and the latest hypothesis (samples stimulated within only two hours) is yet to be tested. In recent years, several techniques have been developed for the sequencing of DNA epigenetic modification of 5-hmC at the nucleotide level [324]. It is certain that evaluation of DNA methylation status after treatment by R-2HG would benefit from such assays. Finally, the evaluation of TET2 activity by an ELISA assay is under investigation.

8) Methods

a. Prospective human tumor tissue collection

Fresh patient tumor samples were selected from the Pitié-Salpêtrière tumor bank Onconeurotek and reviewed by an expert neuro-pathologist (FB) to validate histological features and confirm patients' diagnoses. Collection of tumor samples and clinical-pathological information were obtained upon patients' informed consent and ethical board approval, as stated by the Declaration of Helsinki. Molecular characterizations were performed as previously described (Clinical, molecular, and radiomic profile of gliomas with FGFR3-TACC3 fusions.)

b. Human tumor tissue processing and single-cell isolation for Fluorescence Activated Cell Sorting (FACS)

Tumor tissues were transported on ice in HBSS (Gibco) immediately following surgical resection, rinsed in HBSS to remove visible blood clots and to reduce blood leukocytes contamination, and cut using scalpels into approximately 2 to 5 mm diameter pieces. Tumor pieces were then submerged in cryotubes containing 1 mL of

freezing medium consisting of 70% DMEM/F-12 (Gibco), 20% FBS and 10% DMSO (Sigma-Aldrich). Cryotubes were quickly placed at -80°C in a freezing container (Corning) to allow for slow freezing. Cryopreserved samples were stored at -80 °C (maximum 30 days) or in liquid nitrogen at -160 °C until analysis.

The day of analysis, tumor pieces were quickly thawed and rinsed in DMEM/F-12. Next, they were mechanically disrupted into small fragments with scalpels and further digested for 5 to 10 min at 37°C in a HBSS-papain based lysis buffer (Worthington) containing DNAse (0.01%, Worthington) and L-Cystein (124 µg/mL, Sigma). Enzymatic digestion was inhibited by adding ovomucoid (70 µg/mL, Worthington). Afterward, the homogenates were filtered through a 70 µm on top of a 30 µm strainer (Miltenyi) to remove residual clumps and centrifuged at 300 g for 10 min at 4°C. Cell pellets were resuspended in cold HBSS and a debris removal step was performed according to the manufacturer's instructions (Miltenyi). After the last centrifugation, single cell suspensions were stained with a fixable viability dye 488/515 (1/1000; Ozyme) and Fc-blocked in D-PBS (Gibco) with Human TruStain FcX reagent (Biolegend) for 10 min on ice. Cell suspensions were subsequently stained with direct fluorophore-conjugated antibodies specific for CD45 (2D1, PE/Cyanine7, 1/50; Biolegend) and CD11b (M1/70, PE/Cyanine7, 1/200; Biolegend) for 30 min on ice. Cells were then washed with D-PBS and sorted using the S3e cell sorter (Biorad). Live cells were collected in D-PBS + 0.1% BSA precoated tubes, centrifuged and resuspended in D-PBS + 0.1% BSA at a concentration of about 1200 cells/µL.

c. Preparation and sequencing of scRNA-seq libraries using the 10X Genomics platform and subsequent analysis

Cell suspensions were loaded with the Chromium Next GEM Chip G Single Cell Kit (10X Genomics, #PN-1000120) and a library was generated using Chromium Next GEM Single Cell 3' Reagent Kits v3.1 (10X Genomics, #20012850). The library was sequenced on an Illumina NovaSeq 6000 instrument using a 100 cycle S2 flow cell in XP mode, with the following parameters: 2050 million reads depth, 200 Gbases per run and 50 000 reads per cell. Raw Illumina sequencing reads were aligned to GRCh38 genome (refdata-gex-GRCh38-2020-A) using Cell Ranger (v. 6.1.1, 10x Genomics) including intronic reads with default parameters. Matrix files were loaded using the Seurat Read10X function. Downstream analysis was performed with Seurat (v.4.0.6). Cells with > 10% of unique molecular identifiers (UMIs) coming from mitochondrial genes; > 20000 and < 1000 UMIs per cell; > 5000 and < 500 genes per cell were filtered out. A cluster of 742 cells identified by the expression of common oligodendrocyte markers (PLP1, MOBP, TF) and cells identified as doublets were removed. All samples

were merged together for downstream analysis. No integration step was needed, as no batch effects were observed among the samples. Size normalization (natural-log transformed) for each cell was performed using the Seurat NormalizeData function with the default scale factor of 10,000. Feature selection was performed using FindVariableFeatures ('vst' selection method) to identify 2000 highly variable features within each patient sample. Next, ScaleData was used to center the expression vectors and scale the mean and variance of each feature across cells. After that, the high-dimensional expression space was reduced using PCA. The number of informative components of each dataset was inferred from a jackstraw plot of each principal component. The component space was used to construct a neighborhood graph of cells using the FindNeighbors function with a k of 40 followed by the graph-based Louvain clustering method with a resolution of 0.4. Cell clusters were embedded in 2D and visualized using the RunUMAP function. Subsetting of T and NK cells was performed based on CD3E and NCR1 expression, respectively.

d. Cell types and cell states identification

First, global cell types represented by each cluster were annotated by considering the known cell type markers CD3D, CD3E, CD3G, CD4, CD8A, CD8B for CD4+ and CD8 T cells respectively; CCR7, SELL for naïve T cells; TRDC, TRGV9, TRDV2 for γδ T cells; and FOXP3 for CD4+ Tregs. Second, cell phenotypes (i.e. naïve, T_{CM}, T_{EM}) were obtained by an unsupervised projection of our single cell dataset onto a CITE-seq reference dataset of 162,000 PBMC measured with 228 antibodies, as described in https://satijalab.org/seurat/articles/multimodal_reference_mapping.html Only cells with a prediction score >0.6 were kept. However, in some cases, very few cells were predicted to belong to a cluster with a high prediction score. To remove this confounding factor, the prediction score was then multiplied by the number of cells predicted in each cluster to obtain a weighted prediction score. Third, cluster genes were obtained using the function FindAllMarkers, with a Wilcoxon rank sum test while adjusting p values for multiple hypothesis testing with the Bonferroni correction and a log2FC threshold of 0.25. To identify enriched molecular pathways, each gene list was analyzed in IPA (v. 76765844) and inserted into the Metascape (https://metascape.org) online tool with default parameters.

e. Cluster-specific gene signatures generation and analysis in additional scRNA-seq glioma datasets

To obtain cluster-specific gene signatures, the function FindAllMarkers was used on αβ T cells clusters as previously described but with a log2FC threshold of 0.5. Non-unique genes (i.e. genes present with a log2FC>0.5 in other clusters) were removed from the cluster-specific signature of interest.

To examine gene expression signatures within single cells in diffuse gliomas, raw data from immune cell sorted scRNA-Seq from the literature were retrieved, loaded using the Seurat Read10X function and processed as closely as possible to the original papers. Levels of specific signatures using AddModuleScore were scored. All genes were binned into 25 bins based on their average expression across all cells, and for each gene in a signature, a random set of 20 genes was chosen from the same average expression bin as that gene.

f. Human tumor tissue processing and single-cell isolation for cytospin

Tumor tissue samples were processed as described above. After the last centrifugation, single cell suspensions were magnetically sorted using CD45 (TIL) MicroBeads (Miltenyi) following the manufacturer's instructions. CD45+ cells were then washed and fixed with the Foxp3 / Transcription Factor Staining Buffer Set (Thermo Fisher Scientific) for 15min on ice. After that, cell suspensions were washed twice in PBS +1% BSA (Sigma-Aldrich) + 2 mM EDTA (Thermo Fisher Scientific). 200 µL of cells were pipetted into the cytofunnel and centrifuged at 500 rpm for 7min with the Cytospin 4 (Thermo Fisher Scientific). Cells were fixed again for 15min at 4°C and slides were then placed in PBS at 4°C overnight until multiplex immunofluorescence stainings.

g. Multiplex immunohistofluorescence assay

Multiplexed immunohistofluorescence was performed according to Akoya Biosciences/PerkinElmer's protocol on 4 µm thick FFPE human tumor sections, using the following antibodies: CD3 (F7.2.38, 1/50; Dako). Opal fluorophore 690 (1/80; Akoya Biosciences) was used for tyramide signal amplification. Slides were counterstained with spectral 4',6-diamidino-2-phenylindole (DAPI) and cover-slipped. Image acquisistion was done on the Mantra workstation (Akoya Biosciences), and the multispectral images obtained were unmixed using spectral libraries that were previously built from images stained for each fluorophore. Image analysis was performed using the inForm Advanced Image Analysis software (InForm 2.4.1; Akoya Biosciences).

h. Isolation of CD14- cells for *in vitro* culture

Primary human T cells were isolated from fresh leukophoresis blood buffy coats provided by the *Etablissement Français du Sang* (EFS). Briefly, PBMCs were isolated by density gradient centrifugation using Human Pancoll, density 1.077 g/ml (Dutscher). Human CD14- cells were isolated using CD14 MicroBeads (Miltenyi) following the manufacturer's instructions. Ten million cells were submerged per cryotubes containing 200 µL of freezing medium consisting of 90% FBS and 10% DMSO (Sigma-Aldrich). Cryotubes were quickly placed at -80°C in a freezing container (Corning) to allow for slow freezing. Cryopreserved samples were stored at -80 °C (maximum 30 days) or in liquid nitrogen at -160 °C until analysis.

i. Intracellular quantification of 2-HG

Unstimulated or activated CD14- cells were cultured for 48 hours with 0, 1, or 5 mM D-α-Hydroxyglutaric acid disodium salt (Sigma-Aldrich). Cells were pelleted and the media was removed following careful centrifugation at 500g for 5 min. Following the same procedure, 2 washes with ice-cold PBS were performed to ensure that all 2HG-containing media was removed. Dry pellets were stored at -80°C until extraction of intracellular metabolites.

Dry pellets were lysed in water and the solution was divided in half for 2-HG measurement and protein quantification. NaCl was added and samples were acidified using HCl. A liquid-liquid extraction of organic acids with ethylacetate was performed. 3 extractions were performed, organic phases were pooled, dried under nitrogen stream at 30 °C. Then samples were derivated by a standard sylilation protocol (BSTFA [N,Obis[trimethylsilyl]trifluoroacetamide] and 1%TMCS(Trimethylchlorosilane)) under anhydrous conditions using pyridine. Chromatographic separation was performed with a TR-5MS (30m x 0.25 mm x 0.25 mm) column from Thermo Scientific (Waltham, Massachusets, USA). Spectral data acquisitions were performed using XCalibur software (Thermo Electron Corporation, Austin, TX, USA)..Sample were placed 30 min at 80°C, and then injected into the GC system. Quantification were performed using internal standard 2-hydroxyglutaric acid-D3 from Cambridge isotope laboratories (Tewksbury, Massachusetts, USA) on a gas chromatography-mass spectrometry (GC-MS) using a Focus GC DSQ II (Thermo Electron Corporation, Austin, TX, USA).

Proteins were quantified using a Pierce™ BCA Protein Assay Kit (Thermo Fisher Scientific) according to the manufacturer's instructions.

j. Isolation and activation of naïve T cells for flow cytometry analysis

Naïve T cells were isolated from CD14- cell stock solutions by negative selection using the Naïve Pan T Cell Isolation Kit (Miltenyi). Following isolation, naïve T cells were platted in 24-wells plates at a concentration of 0.5×10^6 cells/well, and activated with αCD3/αCD28 coated human Dynabeads (Thermo Fisher Scientific) at a bead-to-cell ratio of 1:2, and cultured in RPMI-1640 medium (Gibco, A10491-01) supplemented with 10% heat inactivated FBS, 1% penicillin/streptomycin (Thermo Fisher Scientific), and 75 µM 2-Phospho-L-ascorbic acid trisodium salt (Sigma-Aldrich). Plates were centrifuged for 1 minute at 1000 rpm to initiate cell and bead contacts.

After 24 hours of stimulation, beads were removed and cells were transferred to fresh 24-wells plates at a concentration of 0.5×10^6 cells/well in the presence of recombinant human cytokines IL-7 (2 ng/mL; Peprotech) alone or in addition to human recombinant IL-2 (10 ng/mL; Peprotech). Cells were cultured in RPMI-1640 medium (Gibco, A10491-01) supplemented with 10% heat inactivated FBS, 1% penicillin/streptomycin (Thermo Fisher Scientific), and 75 µM 2-Phospho-L-ascorbic acid trisodium salt (Sigma-Aldrich). Every 3 to 4 days cells were split and cytokines and medium refreshed or harvested for subsequent stimulation. 5 mM D-α-Hydroxyglutaric acid disodium salt (Sigma-Aldrich) was added to the medium of treated cells during the whole assay.

k. Flow cytometry analysis

Single cell suspensions were stained with a fixable live-dead stain (Zombie Aqua, BioLegend), FC-blocked for 15 min (Human TruStain FcX, BioLegend) at room temperature, and then incubated with fluorophore-conjugated antibodies directed against extracellular markers (see below) for 20 min on ice in PBS +1% BSA (Sigma-Aldrich) + 2 mM EDTA (Thermo Fisher Scientific). Cells were then washed with FACS buffer. Fixation and permeabilization were performed using Foxp3 / Transcription Factor Staining Buffer Set (Thermo Fisher Scientific). Briefly, cells were fixed for 30 min on ice, washed twice and stored at 4 °C in the dark until analysis or permeabilized, stained for intracellular markers (see below), washed twice, and analyzed right away. FCM acquisition was completed on a MacsQuant 10 (Miltenyi) and analysis of FCM data was performed with FlowJo v10.8.0 (BD).

Antibodies used: CD3 (UCHT1, APC/Cyanine7, 1/50; Biolegend), CD8 (SK1, PerCP, 1/50; Biolegend), CD4 (OKT4, APC, 1/50; Biolegend), CD45RA (HI100, FITC, 1/50; Biolegend), CCR7 (G043H7, PE, 1/50; Biolegend), NKG2A (S19004C, PE,1/50; Biolegend), CD161 (HP-3G10, Bv421, 1/50; Biolegend).

l. Culture of T cells for qRT-PCR

Naïve and non-naïve T cells were isolated from CD14- cell stock solutions by negative and positive selection, respectively, using the Naïve Pan T Cell Isolation Kit (Miltenyi). Following isolation, naïve T cells, non-naïve T cells, and pan CD14- cells were platted in 24-wells plates at a concentration of 0.5×10^6 cells/well, and activated with αCD3/αCD28 coated human Dynabeads (Thermo Fisher Scientific) at a bead-to-cell ratio of 1:2, and cultured in RPMI-1640 medium (Gibco, A10491-01) supplemented with 10% heat inactivated FBS, 1% penicillin/streptomycin (Thermo Fisher Scientific), 75 µM 2-Phospho-L-ascorbic acid trisodium salt (Sigma-Aldrich),and human recombinant IL-2 (10 ng/mL; Peprotech). Plates were centrifuged for 1 minute at 1000 rpm to initiate cell and bead contacts. 5 mM D-α-Hydroxyglutaric acid disodium salt (Sigma-Aldrich) was added to the medium of treated cells during the whole assay.

m. RNA isolation, cDNA synthesis and quantitative real-time PCR

Total RNA was purified using the Maxwell RSC simplyRNA Cells Kit (Promega), and 300 µg of RNA was reverse transcribed to complementary DNA using the Maxima First Strand cDNA Synthesis Kit (Thermo Fisher Scientific). Assays were run in triplicate on a Light Cycler 480 instrument (Roche) using the LightCycler 480 SYBR Green Master 2X (Roche). Human TET2 mRNA was amplified using primers 5′-CAGCCTTCACACACAAAGCA -3′ and 5′- CTGGCATCCATCGCAAAGTG -3′, and human GAPDH mRNA was amplified using primers 5′- GCATCTTCTTTTGCGTCGCC -3′ and 5′-ATCCGTTGACTCCGACCTTC -3′. All primers were verified for the production of a single specific PCR product with a melting curve program. The relative expression level of TET2 mRNA was calculated using the $2^{-\Delta\Delta Ct}$ method [325], normalized to the housekeeping gene GAPDH.

n. Statistical Analysis

Statistical comparisons were performed using GraphPad Prism v9.3.0 (GraphPad Software, La Jolla, CA) or R. Data are presented as mean with standard error to the mean (SEM) unless otherwise in the figures or in the figure legends. The respective number of replicates (n) is indicated in the figures or in the figure legends. *p*-Values were determined by an appropriate statistical test such as Wilcoxon-Mann-Whitney with Welch correction t-test as indicated in the figure legends. *p*-Values unless otherwise specified (*, $p<0.05$; **, $p<0.01$; ***, $p<0.001$).
The detailed list of materials used is available in Supplementary Table 10.

III) SUPPLEMENTARY INFORMATION

Supplementary Table 1| Therapeutic targets directed toward tumor-associated immune and stromal cells in interventional clinical trials or approved by the FDA.

Target	Drug name	Drug type	Mechanism	Current status
			TAMs	
CSF1R	Various, including BLZ945, edicotinib, emactuzumab, and PLX3397	Neutralizing antibodies and small-molecule inhibitors	Reduces macrophage survival or leads to macrophage reeducation	Several phase I and II studies ongoing, some reporting lack of efficacy. PLX3397 approved for TGCT patients
CCL2	Carlumab	Neutralizing antibody	Limiting monocyte and macrophage recruitment to the TME	Phase I trials completed; drug has been discontinued
CCR2	MLN1202, PF-04136309 and TAK202	Neutralizing antibodies	Limiting monocyte recruitment and infiltration into the TME	Clinical trials in phase I and II; few trials terminated
CD40	Chi Lob 7/4, CP-870,893, and dacetuzumab	Agonistic antibodies	To activate host APCs to induce clinically meaningful antitumor T-cell responses in patients	Clinical trials in phases I and II
CD47	CC-90002, magrolimab, and ZL-1201	Neutralizing antibodies	Interfere with recognition of CD47 by the SIRPα receptor on macrophages	Clinical trials in phase I and few in phase II; studies are at an early stage
SIRPα	TTI-621 and TTI-622	Recombinant fragment fusion proteins	Acts by binding to CD47 and preventing it from delivering an inhibitory "do not eat" signal to macrophages	Clinical trials in phase I
PI3Kγ	Eganelisib	Small-molecule inhibitor	Leads to macrophage reeducation into antitumoral phenotypes	Several clinical trials in phases I and II
TREM2	PY314	Neutralizing antibody	Leads to macrophage reeducation into antitumoral phenotypes	One clinical trial in phase I
			DCs	
FLT3L	CDX-301 (FLT3L)	Recombinant cytokine	Expansion of DCs and infiltration in the TME	Clinical trials ongoing in phases I and II
GM-CSF	GM-CSF, GM-CSF vaccines, leucine, and sangramostin	Cytokine	Booster of antitumor immunity by promoting differentiation of DCs	Several clinical trials ongoing in phases I and II and few trials in phase III
			Immune checkpoint blockade	
CTLA4	Ipilimumab	Neutralizing antibody	Blocking of the inhibitory signal CTLA4, allowing CTLs to destroy tumor cells	Several clinical trials ongoing in phases I, II, and III. FDA-approved immunotherapy for patients with melanoma
PD-L1	Atezolizumab, avelumab, and durvalumab	Neutralizing antibodies	Binds to PD-L1 to stop the interaction between PD-1 and PD-L1 in order to restore antitumor T-cell functions	Several clinical trials ongoing in phases I and II. FDA-approved immunotherapy for several cancers, including urothelial carcinoma, advanced renal carcinoma, and non–SCLC
PD-1	Various, including nivolumab, PDR001, and pembrolizumab	Neutralizing antibodies	Binds to the PD-1 receptor and blocks its interaction with PD-L1 and PD-L2, releasing PD-1 pathway–mediated inhibition of antitumor responses	Several clinical trials ongoing in phases I and II. FDA-approved immunotherapy for a number of cancers, including squamous cell lung cancer, non-SCLC, head and neck cancer, renal cell cancer
			Immune checkpoint blockade	
LAG3	Various, including FS118, GSK2831781, IMP321, IMP761, LAG525, and relatlimab	Blocking and antagonistic bispecific antibodies	Blocking MHC-II–LAG3 interaction	Clinical trials ongoing in phases I and II
TIM3	Various, including cobolimab, INCAGN2390, MBG453, and Sym023	Antagonistic antibodies	Binding to TIM3 expressed on specific T cells, including TILs, thereby preventing T-cell inhibition	Clinical trials ongoing in phases I and II
TIGIT	Various, including tiragolumab, AB154, or BMS-986207	Blocking antibodies	Binding to TIGIT to prevent interaction with its ligands	Clinical trials ongoing in phases I–III; tiragolumab granted FDA BTD in combination with atezolizumab
			Tumor vasculature	
VEGF/VEGFR	Various, including aflibercept, bevacizumab, and ramucirumab	Neutralizing antibodies, fusion protein (VEGF-TRAP)	Antiangiogenic therapy	FDA-approved; clinical trials ongoing in phases I–III
VEGFR/other RTKs	Various, including pazopanib, sorafenib, and sunitinib	Small-molecule inhibitors	Antiangiogenic therapy	FDA-approved; clinical trials ongoing in phases I–III
ANG2–TIE2	Various, including MEDI3617, rebastinib, and trebananib	Neutralizing antibody/peptibody, small-molecule inhibitor	Antiangiogenic therapy	Clinical trials ongoing in phases I–II; clinical trials in phase III completed or terminated (negative outcome)
			ECM and CAFs	
HA	PEGPH20	PEGylated enzyme	Degradation of HA	Clinical trials ongoing in phases I and II; terminated phase III clinical trial (negative outcome)
LOXL2	Simtuzumab	Blocking antibody	Destabilization of collagen networks	Clinical trials in phase II completed or terminated (negative outcome)
Fibrosis	Various, including losartan, metformin, and pirfenidone	Small-molecule inhibitors	Collagen and HA reduction	FDA approved; clinical trials ongoing in phases I–III
FAK	Various, including defactinib (VS-6063, PF-04554878) and GSK-2256098	Small-molecule inhibitors	Prevents integrin signaling	Clinical trials ongoing in phases I and II
CTGF	Pamrevlumab (FG-3019)	Blocking antibody	Prevents integrin signaling	Clinical trials ongoing in phases I–III
FAP-expressing cells	PT630, RO6874281, and sibrotuzumab	Blocking antibody, small-molecule inhibitors, fusion protein	Interferes with CAF function, promotes T cell responses	Clinical trials ongoing in phases I and II
TGFβ	Various, including galunisertib	Small-molecule inhibitors and blocking antibodies	Prevents CAF activation and interferes with CAF signaling	Clinical trials ongoing in phases I and II
FGFR	Erdafitinib (JNJ-42756493)	Small-molecule inhibitor	Prevents CAF activation	Clinical trials ongoing in phases I–III
Hedgehog	Various, including saridegib and vismodegib	Small-molecule inhibitors	Prevents/reduces CAF activation	Clinical trials ongoing in phases I and II
ROCK	AT13148	Small-molecule inhibitor	Interferes with CAF function	Clinical trials in phase I completed
CXCR4	AMD3100	Small-molecule inhibitor	Interferes with CAF signaling	Clinical trials ongoing in phases I–III
Vitamin D	Paricalcitol	Small-molecule agonist	Induces CAF normalization	FDA approved; clinical trials ongoing in phases I and II
Vitamin A metabolism	ATRA	Vitamin A metabolite	Induces CAF normalization	FDA approved; clinical trials ongoing

Data collected from http://clinicaltrials.gov, accessed in December 2020. From [326].

Supplementary Table 2| Molecular markers for the diagnosis and treatment of adult diffuse gliomas.

Molecular marker	Biological function of affected genes	Diagnostic roles
IDH1 R132 or IDH2 R172 mutation	Gain-of-function mutation	Distinguishes diffuse gliomas with IDH mutation from IDH-wild-type glioblastomas and other IDH-wild-type gliomas
1p/19q codeletion	Inactivation of putative tumour suppressor genes on 1p (such as *FUBP1*) and 19q (such as *CIC*)	Distinguishes oligodendroglioma, IDH-mutant and 1p/19q-codeleted from astrocytoma, IDH-mutant
Loss of nuclear ATRX	Cell proliferation and promotion of cellular longevity by alternative lengthening of telomeres	Loss of nuclear ATRX in an IDH-mutant glioma is diagnostic for astrocytic lineage tumours
Histone H3 K27M mutation	Histone H3.3 (*H3F3A*) or histone H3.1 (*HIST1H3B/C*) missense mutation affecting epigenetic regulation of gene expression	Defining molecular feature of diffuse midline glioma, H3 K27M-mutant
Histone H3.3 G34R/V mutation	Histone mutation affecting epigenetic regulation of gene expression	Defining molecular feature of diffuse hemispheric glioma, H3.3 G34-mutant
MGMT promoter methylation	DNA repair	None, but is a predictive biomarker of benefit from alkylating chemotherapy in patients with IDH-wild-type glioblastoma
Homozygous deletion of *CDKN2A/CDKN2B*	Encode cyclin-dependent kinase inhibitors 2A and 2B and tumour suppressor ARF, which function as regulators of Rb1 and p53-dependent signalling	A marker of poor outcome and WHO grade 4 disease in IDH-mutant astrocytomas
EGFR amplification	Cell proliferation, invasion and resistance to induction of apoptosis	*EGFR* amplification occurs in ~40–50% of glioblastoma, IDH wild type Molecular marker of glioblastoma, IDH wild type, WHO grade 4 (REF.[5])
TERT promotor mutation	Cell proliferation; promotes cellular longevity by increasing TERT expression	*TERT* promoter mutation occurs in ~70% of glioblastoma, IDH wild type and >95% of oligodendroglioma, IDH-mutant and 1p/19q-codeleted Molecular marker of glioblastoma, IDH wild type, WHO grade 4 (REF.[5])
+7/−10 cytogenetic signature	Gain of chromosome 7 (harbouring genes encoding, among others, PDGFA and EGFR) combined with loss of chromosome 10 (harbouring genes including *PTEN* and *MGMT*)	Molecular marker of glioblastoma, IDH wild type, WHO grade 4 (REF.[5])
BRAF^{V600E} mutation	Oncogenic driver mutation leading to MAPK pathway activation	Rare in adult diffuse gliomas but amenable to pharmacological intervention

From [327].

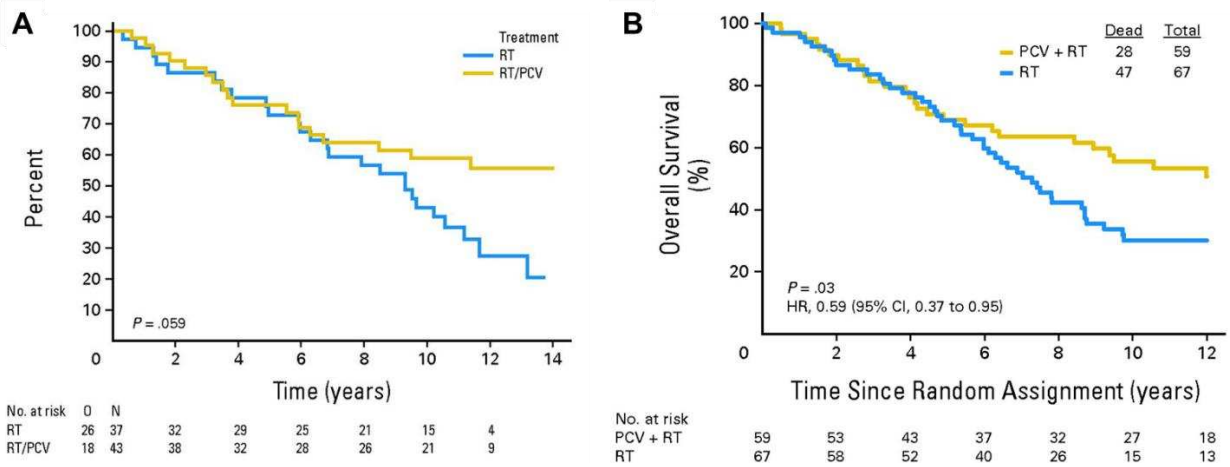

Supplementary Figure 1| Kaplan-Meier estimates of overall survival by treatment for patients with grade 3 IDH-O.

A| Kaplan-Meier survival curves from [100] In the 80 patients with a 1p/19q codeletion, OS is increased, with a trend toward more benefit from adjuvant PCV (OS not reached in the RT/PCV group v 112 months in the RT group; HR, 0.56; 95% CI, 0.31 to 1.03). **B|** Kaplan-Meier survival curves from [101]. Median survival of patients treated with PCV plus RT is twice that of patients receiving RT (14.7 *v* 7.3 years; HR = 0.59; 95% CI, 0.37 to 0.95; *P* = .03).

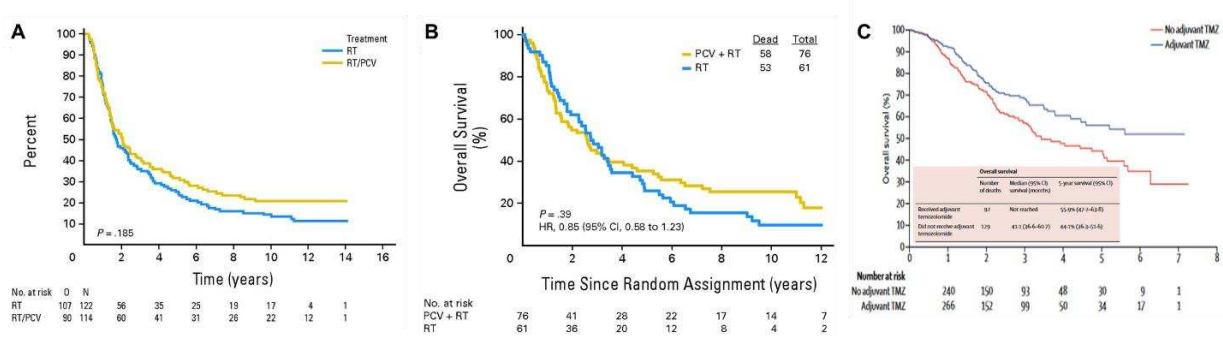

Supplementary Figure 2| Kaplan-Meier estimates of overall survival by treatment for patients with grade 3 IDH-A.

A| Kaplan-Meier survival curves from [100], **B|** Kaplan-Meier survival curves from [101]. Only a trend toward a benefit of RT plus PCV compared to RT alone is observed. **C|** Kaplan-Meier survival curves from [328]. Interim analysis showing an overall survival at five years of 55.9% (95% CI 47.2- 63.8) with adjuvant TMZ and a 44.1% (36.3-51.6) without adjuvant TMZ.

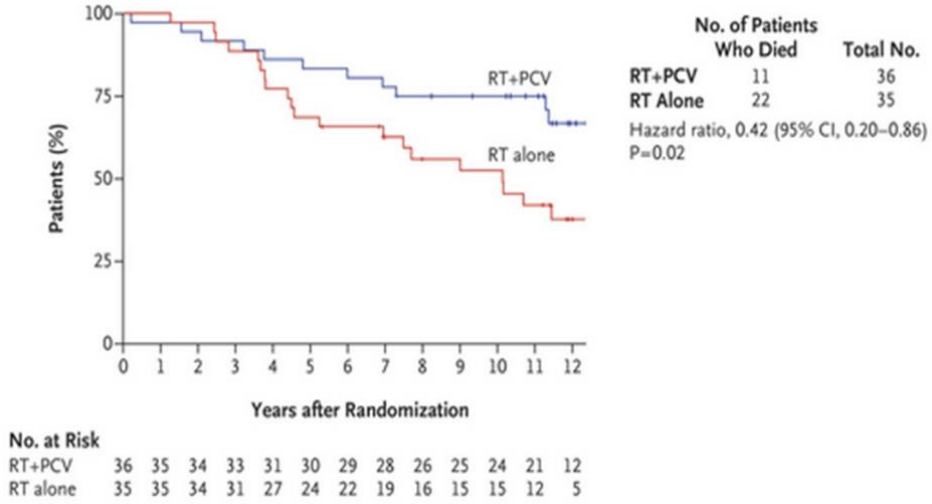

Supplementary Figure 3| Kaplan-Meier estimates of overall survival by treatment for patients with grade 2 IDHm gliomas.

A| Kaplan-Meier survival curves from [103]. Radiation therapy plus chemotherapy increases overall survival compared to radiation therapy alone (P=0.02).

Supplementary Table 3| Km values of α-KGDD for co-substrates.

Target	Substrate	Km value (µM)
	Fe2+	10
EGLN1	Fe2+	0,05
EGLN2	Fe2+	0,05
EGLN3	Fe2+	0,1
FIH1	Fe2+	0,5
KDM4A	Fe2+	0,1
KDM4B	Fe2+	0,1
KDM5B	Fe2+	0,1

KDM6A	Fe2+	0,1
KDM6B	Fe2+	6
P4HA1	Fe2+	2
PLOD1	Fe2+	2
TET1	Fe2+	5
TET2	Fe2+	4
ABH2	αKG	4
BBOX1	αKG	200
EGLN1	αKG	135,5
EGLN2	αKG	2
EGLN3	αKG	10
FIH1	αKG	87,5
KDM2A	αKG	6
KDM4A	αKG	15,5
KDM4B	αKG	6
KDM4C	αKG	7
KDM5B	αKG	10
KDM5C	αKG	5
KDM6A	αKG	9
KDM6B	αKG	29
P4HA1	αKG	20
PHYH	αKG	120
PLOD1	αKG	100
TET1	αKG	55
TET2	αKG	60
BBOX1	O2	55
EGLN1	O2	156
EGLN2	O2	230
EGLN3	O2	230
FIH1	O2	165
KDM4A	O2	112,5
KDM4B	O2	150
KDM4C	O2	160
KDM5A	O2	90
KDM5B	O2	40
KDM5C	O2	35
KDM5D	O2	25

KDM6A	O2	200
KDM6B	O2	25
P4HA1	O2	40
PHYH	O2	95
PLOD1	O2	45
TET1	O2	15,15
TET2	O2	15,25

Supplementary Table 4| IC50 values of α-KGDD for inhibitors.

Target	Inhibitor	IC50 value (μM)
EGLN1	Fumarate	80
EGLN2	Fumarate	120
EGLN3	Fumarate	60
FIH1	Fumarate	10000
KDM4A	Fumarate	1900
KDM4B	Fumarate	5000
KDM5B	Fumarate	5000
KDM6A	Fumarate	3000
KDM6B	Fumarate	5000
P4HA1	Fumarate	190
TET1	Fumarate	390
TET2	Fumarate	400
EGLN1	Succinate	510
EGLN2	Succinate	830
EGLN3	Succinate	570
FIH1	Succinate	10000
KDM4A	Succinate	800
KDM4B	Succinate	2300
KDM5B	Succinate	1400
KDM6A	Succinate	270
KDM6B	Succinate	550
P4HA1	Succinate	400
TET1	Succinate	540
TET2	Succinate	570
ABH2	R-2HG	460
ABH3	R-2HG	500

BBOX1	R-2HG	13200
EGLN1	R-2HG	3800
EGLN2	R-2HG	210
FIH1	R-2HG	1300
KDM2A	R-2HG	110
KDM4A	R-2HG	81
KDM4B	R-2HG	150
KDM4C	R-2HG	80
KDM5B	R-2HG	7235
KDM6A	R-2HG	180
KDM6B	R-2HG	350
P4HA1	R-2HG	1800
TET1	R-2HG	4000
TET2	R-2HG	5000
ABH2	L-2HG	150
BBOX1	L-2HG	140
EGLN1	L-2HG	785
EGLN2	L-2HG	630
EGLN3	L-2HG	90
FIH1	L-2HG	245
KDM2A	L-2HG	50
KDM4A	L-2HG	157,5
KDM4B	L-2HG	450
KDM4C	L-2HG	95
KDM5B	L-2HG	1115
KDM6A	L-2HG	180
KDM6B	L-2HG	750
P4HA1	L-2HG	310
TET1	L-2HG	1000
TET2	L-2HG	1600

Supplementary Table 5 | Summary of single cell RNA-Seq data on IDHm and IDHwt immune cells.

First author	Tumor type	Clusters	Annotation	Effect to OS	Top 10 DE genes										
Abdelfattah	Primary + Recurrent	C1			CCL3	APOC1	C1QB	C1QA	C1QC	CCL3L1	SPP1	APOC2	CD74	HLA-DRA	vs. All
		C4			S100A9	S100A8	LYZ	AREG	THBS1	C15orf48	IL1R2	FCN1	S100A12	VCAN	
		C7			TGFBI	IBSP	FN1	HMGB2	MKI67	PCLAF	S100A4	H2AFZ	HIST1H4C	RNASE1	
		C3			CCL5	IL32	IL7R	CD2	GZMA	GZMK	CD52	NKG7	CD3D	LTB	
		MC1	inflammatory MG		CCL3L1	CCL4L2	CCL4	CCL3	EGR3	IL1B	EGR2	CD83	BTG2	CH25H	vs. Myeloid
		MC2	homeostatic MG	Better OS	HLA-DRB5	HBB	MT3	C1orf61	APOC2	GNLY	C3	GPR34	LTC4S	ITM2B	
		MC6	Isupp MG		ISG15	CXCL10	IFIT1	IFIT3	IFI6	IFI44L	MX1	IFIT2	IFI27	IFITM3	
		MC7	activated MG	Better OS	XIST	SPRY1	SRGAP2	TRA2B	SLC1A3	PDK4	AC020916.1	AC253572.2	CACNA1A	MALAT1	
		MC8	DC		AREG	HLA-DQA1	S100B	FCER1A	HLA-DPB1	PPA1	HLA-DRB1	HLA-DPA1	HLA-DQB1	JAML	
		MC4	MDSC		MT1G	MT1X	MT2A	MT1H	MT1E	C15orf48	CSTB	MIF	BNIP3	G0S2	
		MC3	Isupp MDM	Worse OS	RNASE1	SELENOP	CXCL2	CTSD	CXCL3	GPNMB	TGFBI	CD163	LGALS3	GCHFR	
		MC5	Isupp MDM	Worse OS	S100A9	S100A8	VCAN	LYZ	THBS1	TIMP1	S100A12	FCN1	AREG	IL1R2	
		MC9	proliferating MDM		HIST1H4C	STMN1	MKI67	TOP2A	HIST1H1D	TUBB	H2AFZ	CENPF	PCLAF	HIST1H1E	
		TC1	CD8		GZMH	CD8B	CD8A	NKG7	CCL5	GZMK	CCL4	IFNG	GZMA	GZMB	vs. T cells
		TC2	CD8		GZMK	CCL5	GZMA	ITM2C	GZMH	IFNG	APOBEC3G	HLA-DPB1	CCL4	APOE	
		TC6	CD8		IL7R	KLRB1	FKBP11	XCL1	ANXA1	HSPA6	GPR171	KLF2			
		TC4	Tregs		IL2RA	FOXP3	TNFRSF4	LTB	CTLA4	BATF	TNFRSF18	RTKN2	TIGIT	UGP2	
		TC5	CD4		G0S2	GNLY	C15orf48	KLRB1	CCL20	MT2A	CXCR6	CSF2	RBPJ	TNFRSF4	
		TC3	Naive		IL7R	KLF2	CCR7	ANXA1	MAL	RPS6	RPS20	EEF1B2	RPS8	RPS3A	
		TC7	NK		KLRC1	TYROBP	XCL1	XCL2	KLRD1	AREG	GNLY	TRDC	FCER1G	IGFBP2	
		TC8	NK		GNLY	FGFBP2	GZMB	PTGDS	KLRD1	PRF1	FCGR3A	SPON2	TYROBP	KLRF1	
Antunes	Primary	TAM1			MT1G	SEPP1	CXCL3	ADM	BNIP3	SDS	CXCL2	ADAMDEC1	PLIN2	MT1X	vs. All
		TAM2			DHRS9	CH25H	SYNDIG1	TMEM119	RP11-552D4.1	CX3CR1	AP005530.2	GLDN	P2RY12	LINC01235	
		prol. TAM			TK1	UBE2C	MKI67	TOP2A	TYMS	KIAA0101	CDK1	CENPF	RRM2	BIRC5	
		DC			FCER1A	CD1C	CLEC10A	CD1E	PKIB	JAML	CD207	CD1A	C15orf48	AREG	
		Monocyte			S100A12	FCN1	S100A9	S100A8	EREG	IL1R2	VCAN	TIMP1	CFP	THBS1	
		TC3			GZMH	GZMK	NKG7	CD8A	CD8B	CCL5	CST7	GZMA	FGFBP2	CTSW	
		TC4			CD40LG	KLRB1	IL2	IL7R	LTB	CD2	SPOCK2	TRAC	CD3D	IFNG	
		TC7			IL7R	LTB	CCR7	MAL	HBB	CD3E	KLRB1	LEF1	TRAC	TRAT1	
		TC10			ISG20	LAG3	IFITM1	ISG15	CD2	GZMK	IFIT3	OASL	NT5C3A	GBP1	
		NK9			UBE2C	TYMS	RRM2	KIAA0101	TRAV14DV4	TRBV19	STMN1	MKI67	CD8A	CD8B	
		NK11			GNLY	KLRC1	KRT81	XCL2	KRT86	TRDC	GZMB	CTSW	TNFRSF18	KLRD1	
		Mg-TAM1			GRID2	ACY3	DHRS9	HBB	CLEC9A	ADRB2	HCG22	P11-489O18.	IPCEF1	AP005530.2	vs. Myeloid
		Mg-TAM2			IBSP	TSPAN13	TNFRSF11B	HAMP	IL21R	SELENBP1	PLTP	RNASE3	AP000439.1	ARG2	
		Phago-Lipid Mg-TAM			LRRC39	MYOZ1	OLFM2	RAMP1	LINC01235	MATK	LILRA4	S100A1	FABP3	LPL	
		IFN Mg-TAM			IFIT1	IFIT3	CXCL10	RSAD2	ISG15	ETV7	IFIT2	ZBP1	IFITM1	USP18	
		Mg-TAM5			BAG3	DNAJA4	HSPA6	SERPINH1	ZC3H12A	DNAJB4	IRAK2	DNAJB1	ZFAND2A	IL1A	
		Transitory Mo-TAM			MARCO	ANPEP	CXCL1	CXCL3	EREG	MCEMP1	TIMP1	CD300E	CXCL2	VCAN	
		IFN Mo-TAM			CXCL11	CXCL10	APOBEC3A	GBP1	CCL8	IFITM1	IFIT1	GBP4	ISG20	HAPLN3	
		SEPP1+ Mo-TAM			SEPP1	ADAMDEC1	IL2RA	PKIB	MRC1	ALDH1A1	JAML	SLC40A1	CLEC10A	AREG	
		Hypoxic Mo-TAM			MT1H	MT1G	SLC2A1	ENO2	EGLN3	BNIP3	SLC6A8	ADM	AK4	HILPDA	
		Lipid Mo-TAM			ACP5	ALDH1A1	HTRA4	LGALS3	GCHFR	ADAMDEC1	AC079767.4	RP11-212I21.1	SDS	TSPAN4	
		prol. TAM12			RRM2	FAM111B	TYMS	UHRF1	TK1	CENPM	PKMYT1	CLSPN	KIAA0101	CDT1	
		prol. TAM13			CDC20	ASPM	UBE2C	HMMR	PLK1	CCNB1	TOP2A	CENPF	MKI67	BIRC5	
		Monocyte			S100A12	FCN1	CFP	LGALS2	CDA	FAM65B	IL1R2	S100A9	S100A8	PADI4	
		Unknown			HBB	CYP19A1	SLPI	ADSSL1	MARCKSL1	CRYBB1	MIF	GNG10	SHISA4	MAGOHB	
Mathewson	Primary + Recurrent	CD8	Chemokine-IFNg		CRTAM	CCL4L1	CCL4L2	CCL3	HLA-DQB1	CCL4	RGS1	HLA-DRA	GZMK	HLA-DQA1	vs. CD8 T-cells
		CD8	Cytotoxicity-NK		FGFBP2	FCGR3A	GNLY	SPON2	CX3CR1	S1PR5	GZMB	GPR56	KLRC3	KLRC1	
		CD8	Effector Memory		CCR7	SELL	GPR183	IL7R	KLRB1	LMNA	CCR6	SATB1	CD55	AREG	
		CD8	Interferon		RRM2	STMN1	KIAA0101	IFI6	RSAD2	PCNA	CD38	TUBB	MCM7	DNPH1	
		CD8	ND		CISH	OC10013023:	BCYRN1	GIMAP2	GIMAP5	LUC7L3	XIST	ZEB2	ISG15	SLC2A3	
		CD8	Stress		HSPA6	HSPA1A	HSPA1B	HSPA7	DNAJB1	ZFAND2A	DNAJA4	HSPH1	DNAJB4	HSP90AA1	
		CD4	Cytotoxicity_Chemokine		CCL4	CCL4L1	CCL4L2	NKG7	GZMH	GZMK	CCL5	CRTAM	SLAMF7	IL10	vs. CD4 T-cells
		CD4	Effector Memory		CAPG	CTSH	OC10012842(	HOPX	LGALS1	KLRB1	DPP4	DHRS3	CISH	S100A11	
		CD4	Interferon		IFIT3	RSAD2	IFI6	ISG15	IFIT1	MX1	USP18	OASL	OAS1	PLSCR1	
		CD4	Memory		CCR7	SELL	LEF1	TCF7	TXK	CD55	AREG	MAL	PLAC8	S1PR1	
		CD4	Stress		HSPA6	HSPA1A	HSPA1B	DNAJB1	HSPA7	DNAJA4	ZFAND2A	DNAJB4	HSPB1	HSPH1	
		CD4	Treg		CCR8	FOXP3	TNFRSF18	LAYN	IL2RA	FANK1	RRM2	TNFRSF9	STMN1	ACP5	
Alghamri	Primary	C1	PMN-MDSC IDHm		CCL3	CCL4	vIL1β	S100a8	S100a9	ARG1	TGFβ1				
		C2			HLA-A	HLA-DRA									
		C3	Granulocytes		CSF3R	NEAT1									
		C4	MG		C1Qc	AIF1									
		C5	PMN-MDSC IDHwt		IL1β	S100a8	S100a9	ARG1	TGFβ1						

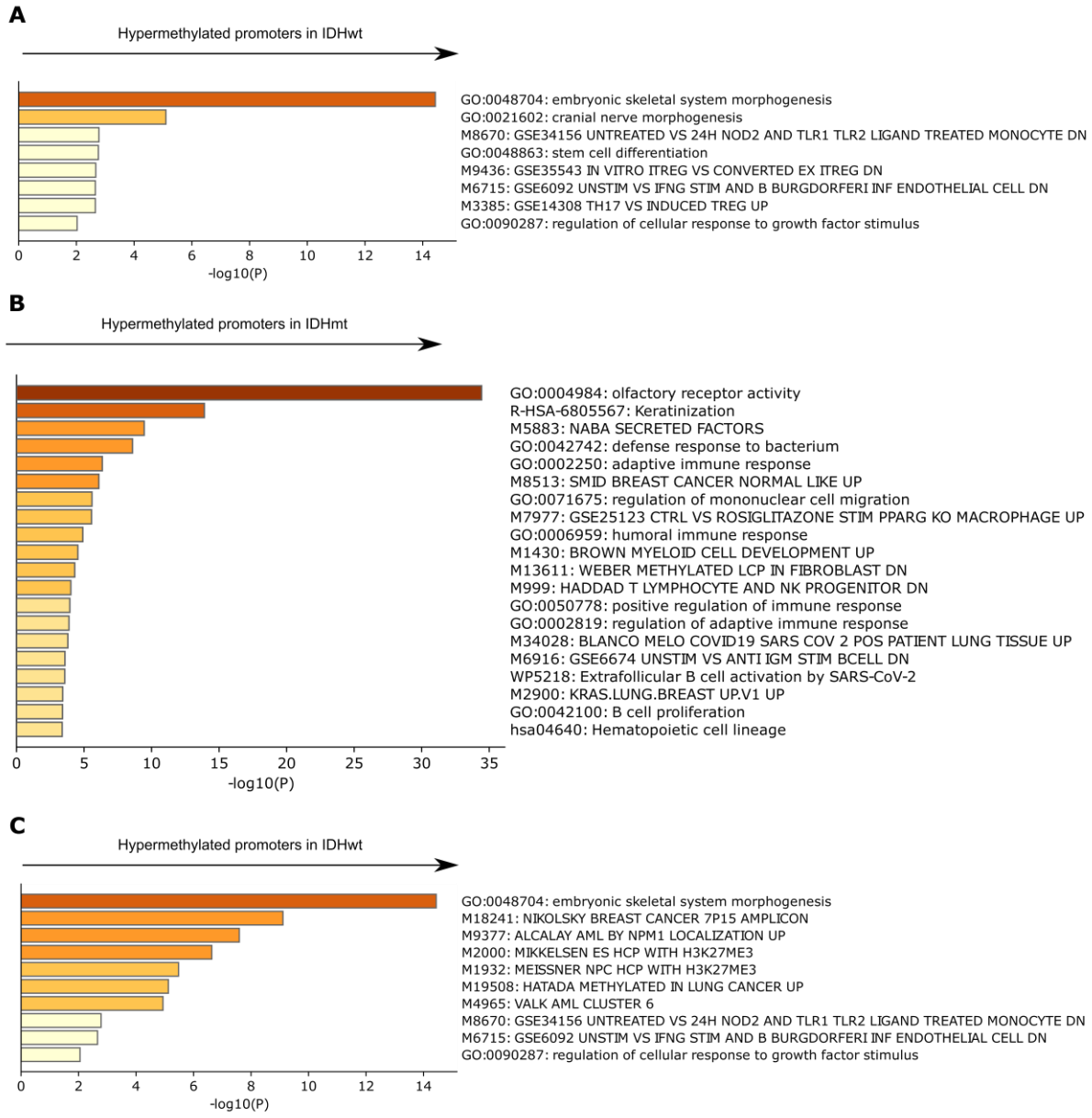

Supplementary Figure 4| Pathways analysis of differentially methylated promoters in CD11b- cells

A| Barplot representation of pathway enrichment across promoters hyermethylated in IDHwt samples colored by p-values. Log10(P) is the p-value in log base 10. **B|** Barplot representation of pathway enrichment across promoters hyermethylated in IDHm samples with more signatures, colored by p-values. Log10(P) is the p-value in log base 10. **C|** Barplot representation of pathway enrichment across promoters hyermethylated in IDHwt samples with more signatures, colored by p-values. Log10(P) is the p-value in log base 10.

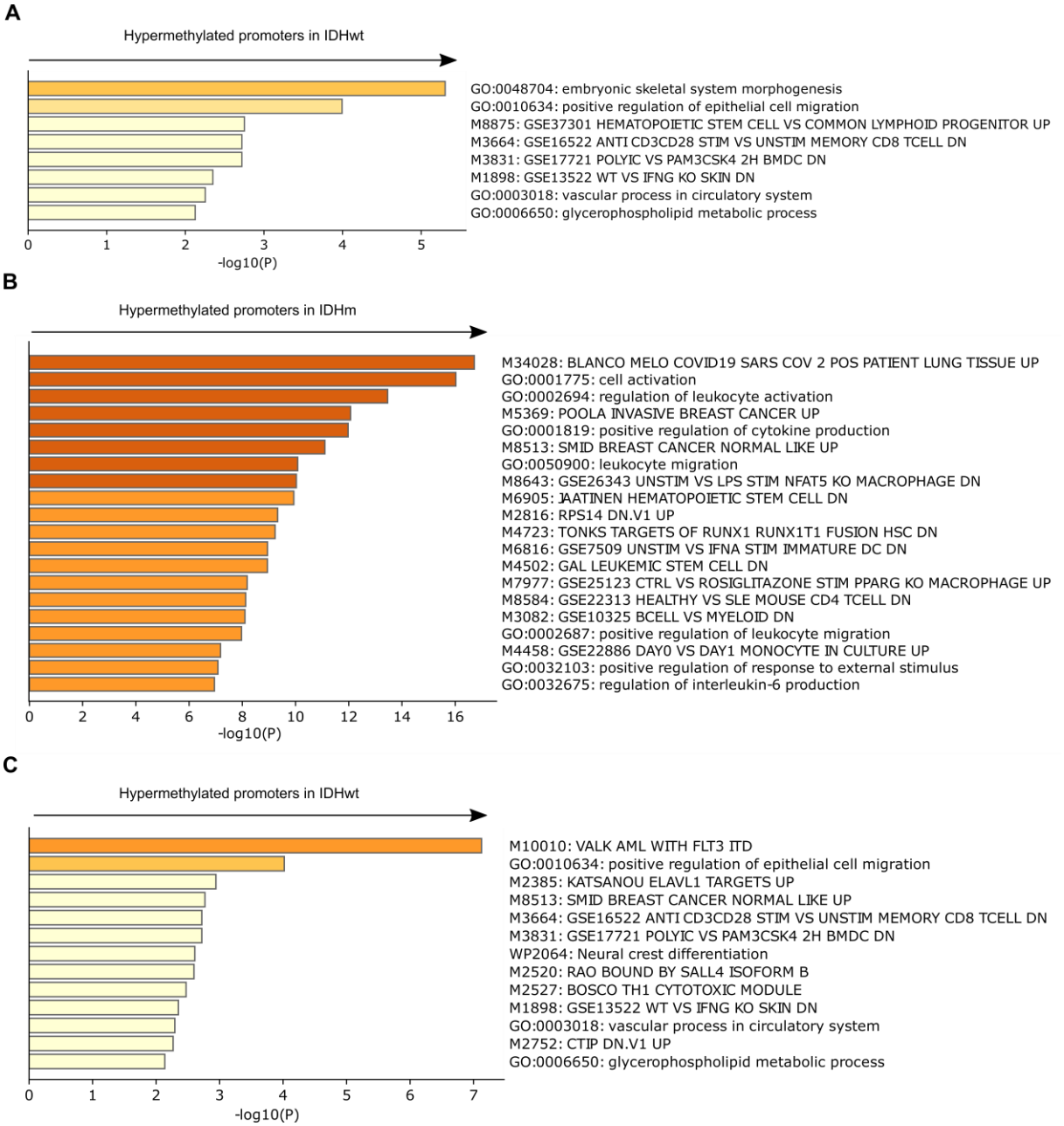

Supplementary Figure 5| Pathways analysis of differentially methylated promoters in CD11b+ cells

A| Barplot representation of pathway enrichment across promoters hyermethylated in IDHwt samples colored by p-values. Log10(P) is the p-value in log base 10. **B|** Barplot representation of pathway enrichment across promoters hyermethylated in IDHm samples with more signatures, colored by p-values. Log10(P) is the p-value in log base 10. **C|** Barplot representation of pathway enrichment across promoters hyermethylated in IDHwt samples with more signatures, colored by p-values. Log10(P) is the p-value in log base 10.

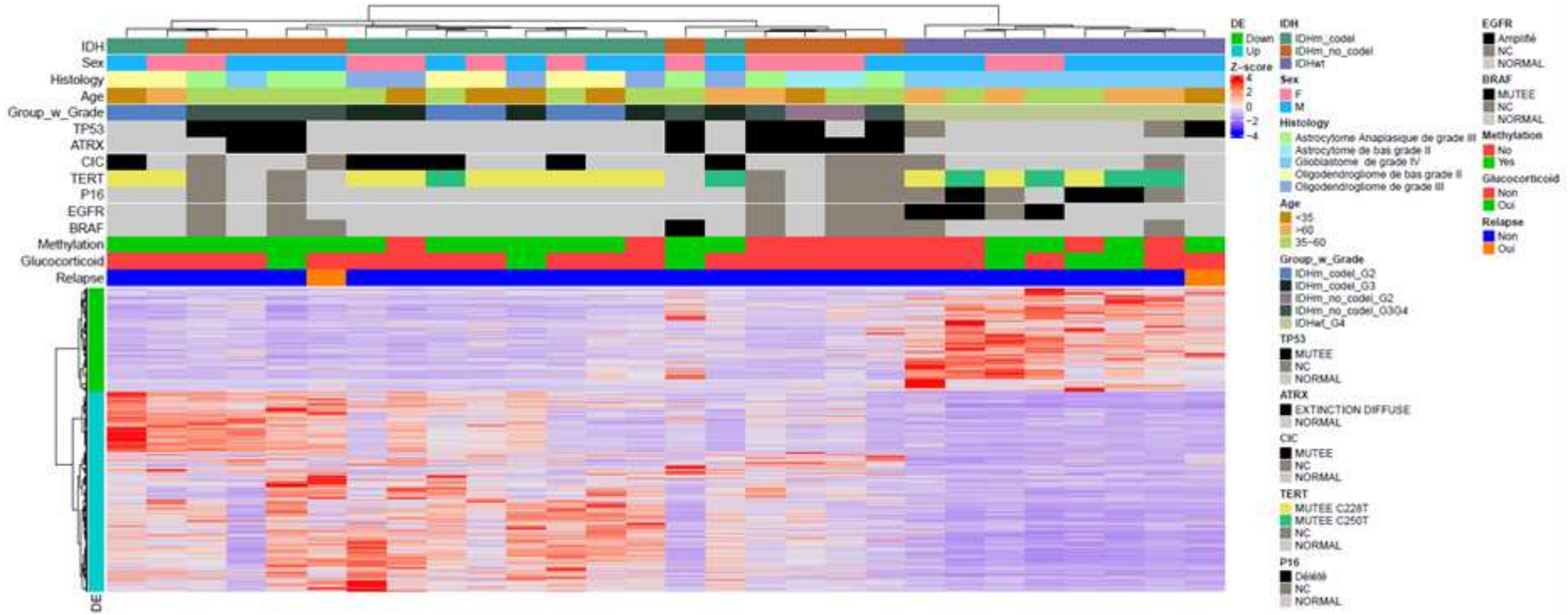

Supplementary Figure 6| Clinical and genetic characteristics of the patients.

Heatmap showing relative gene expression of CD11b+ cells per sample with their molecular and genetic characteristics.

Supplementary Table 6| List of Ligand-Receptor pairs.

Specific IDHwt	score	Specific IDH-A	score	Specific IDH-O	score	Common IDHmut-IDH-O	score
EGFR_VCAN	0,030336	NRCAM_CNTN2	0,298158	COL18A1_KDR	0,211452	TIMP3_KDR	0,0820175
EGFR_HBEGF	0,076183	FGFR2_CD83	0,344113	PLAUR_FN1	0,22759	KDR_TIMP3	0,1133925
EGFR_AREG	0,089424	TF_TFR2	0,413226	ITGB1_THBS1	0,307146	CAV1_APP	0,153243
PTPRZ1_MDK	0,116675	DLL3_NOTCH1	0,427716	TFRC_TF	0,314973	NCSTN_APP	0,2089225
EGFR_ICAM1	0,143625	CNTN2_NRCAM	0,44512	KDR_COL18A1	0,323008	ITGB1_TGM2	0,2162235
C3_LRP1	0,168976	PDGFRA_PDGFB	0,524536	ITGB1_HSPG2	0,330847	MAG_COL9A2	0,2244165
TIMP1_CD63	0,20752	EDIL3_ITGAV	0,529152	ITGB1_COL4A1	0,333345	SPP1_S1PR1	0,262053
PTPRZ1_CNTN1	0,20817	VCAN_EGFR	0,55699	COL13A1_FN1	0,347754	LRPAP1_SORT1	0,3213825
C3_ITGB2	0,226292	FGF1_NRP1	0,600344	HSPG2_ITGB1	0,36144	TGM2_ITGB1	0,3372215
LRP1_LPL	0,233366	FGFR2_FGF1	0,618288	SORBS1_INSR	0,363164	COL18A1_ITGB1:ITGA1	0,3627168
MDK_LRP1	0,235455	SPP1_ITGA9	0,663552	ITGA2B_FN1	0,37047	ITGB1_COL18A1	0,3639885
LPL_LRP1	0,248818	OMG_TNFRSF1B	0,69242	VEGFB_FLT1	0,416784	NRXN2_AFDN	0,41679
VEGFA_NRP1	0,266473	NCAM1_GFRA1	0,736736	GNAI2_CAV1	0,426525	APOD_LEPR	0,426696
CD63_TIMP1	0,281175	MAG_COL9A3	0,77389	NAMPT_INSR	0,436514	SEMA3B_NRP1	0,463565
TNFRSF1A_GRN	0,282282	NCAM1_BDNF	0,82812	FLT1_VEGFB	0,47712	LRP4_AGRN	0,4934375
LRP1_SERPINA1	0,31414	CNTN2_CNTN1	1,042587	ITGA6_THBS1	0,478023	LAMA5_BCAM	0,577286
CD44_LGALS9	0,328812	KCNJ10_IL16	1,246728	TGM2_ADGRG1	0,491344	SPP1_ITGB1:ITGA9	0,5801515
LRP1_PLAU	0,3318	SPP1_ITGAV:ITGB3	1,682552	ITGB1_ADAM15	0,500322	PSEN1_NOTCH1	0,6572615
VCAN_CD44	0,337725	MAG_COL9A1	2,090344	APOE_SCARB1	0,51765	GAS6_MERTK	0,6603
ITGB8_COL4A1	0,352869	TGFB3_TGFBR2	2,280978	CD47_THBS1	0,531354	ADAM15_ITGB1	0,665254
LRP1_SERPING1	0,357448	COL16A1_ITGB1:ITGA11	3,258801	PGF_FLT1	0,566124	COL18A1_ITGA5	0,6805335
GPC1_VEGFA	0,396417	CD47_SIRPB1:TYROBP	5,359879	ITGB1:ITGA10_COL4A1	0,56653	SEMA3B_NRP2	0,70718
PTN_PTPRZ1	0,402944			ITGB1:ITGA6_LAMC1	0,5967	COL18A1_ITGB1:ITGA10	0,723328
COL1A2_CD44	0,403975			ITGAV_ADAM15	0,59892	NOTCH1_JAG2	0,7497135
CD9_HBEGF	0,433125			JAG1_NOTCH3	0,600327	ITGB1:ITGA1_COL9A2	0,946761
SERPING1_LRP1	0,444978			INSR_SORBS1	0,60187	COL4A5_ITGB1:ITGA1	1,0050545
ICAM1_ITGB2	0,45175			PIGF_FLT1	0,602741	NOTCH1_PSEN1	1,0213215
COL1A1_CD93	0,468026			CD46_JAG1	0,619357	SPP1_CD44	1,080352
ITGB8_TGFB1	0,479451			ITGA1_COL4A1	0,622502	PSEN1_NOTCH3	1,128443
ICAM3_ITGB2	0,482176			PDGFRB_PDGFB	0,676998	TYRO3_GAS6	1,1313525
TNC_ITGB1	0,496672			ITGAV:ITGB3_VWF	0,717288	COL9A2_ITGB1:ITGA1	1,1477313
VCAM1_ITGB2	0,506944			BCAM_LAMA5	0,727904	COL9A2_ITGB1:ITGA10	1,1671975
HMGB1_THBD	0,515268			PODXL_SELL	0,732641	CALM2_MYLK2	1,1718785
CNR1_GNAI2	0,542922			ADGRG1_TGM2	0,739011	PTGDR_GNAS	1,1798235
CR1_C1QA	0,549072			NOTCH3_JAG1	0,74023	BMP7_ENG	1,181473
THBS1_LRP1	0,560972			PTPRB_PTN	0,772188	PDGFRA:PDGFRB_PDGFB	1,2423323
PDGFB_LRP1	0,5723			ITGA5_COL18A1	0,82302	ADAM15_ITGAV	1,2818715
MCAM_WNT5A	0,610296			NOTCH3_PSEN1	0,83664	LINGO1_RTN4	1,3385475
ANTXR1_WNT5A	0,640487			ICAM1_ITGAX	0,842776	TGFBR2_TGFB1	1,376621
ARF1_PLD2	0,662232			COL5A3_ITGB1:ITGA10	0,866304	ITGB1:ITGA10_COL9A2	1,3850168
MMP9_LRP1	0,67738			COL6A2_ITGB1:ITGA1	0,900237	COL4A5_ITGB1:ITGA10	1,5150627
VEGFA_NRP2	0,693328			FLT1_PGF	0,91296	SORT1_BDNF	1,53913
ABCA1_PLTP	0,72384			EGFR_DCN	0,91332	VWF_ITGAV:ITGB3	1,7197378
COL4A1_ITGB8	0,72624			CALM2_PDE1C	0,915621		
C3_ITGB2:ITGAM	0,740036			ITGB1:ITGA1_COL6A1	0,917865		
TSHR_CALR	0,757071			APOE_LRP8	0,95567		
TNC_ITGB1:ITGA4	0,7984185			SELL_PODXL	0,956524		
ICAM2_ITGB2	0,801834			JAG2_NOTCH3	0,958867		
HP_ITGB2	0,834438			ITGB1:ITGA1_COL6A2	0,9791835		
MRC2_LGALS9	0,839978			THBS2_ITGB1	0,996455		
TFPI_LRP1	0,844526			NOTCH3_JAG2	1,022322		
CALR_ITGA3	0,85332			CSF1_SLC7A1	1,089585		
GPC3_CD81	0,866291			LRP2_SERPINE1	1,091944		
TNFRSF1B_GRN	0,883688			LAMB1_ITGB1	1,145907		
COL4A1_ITGB1:ITGA11	0,887835			ADAM15_ITGA5	1,20393		
LGALS9_LRP1	0,914972			F11R_AFDN	1,233428		
CD44_HBEGF	0,945			CD93_COL4A2	1,237464		
NOTCH1_PLXNA1	0,967439			ITGAV_NID1	1,23836		
PLAU_LRP1	0,977984			TBXA2R_GNAI2	1,260225		
PTN_PTPRS	0,985248			IL6ST_EBI3	1,275756		
ICAM5_ITGB2	0,995148			COL20A1_ITGB1:ITGA1	1,285497		
ICAM4_ITGB2	1,01541			ITGB1:ITGA7_LAMC1	1,29675		
SEMA6D_TYROBP	1,025916			COL4A5_CD93	1,31252		
CALR_TSHR	1,050192			SPP1_ITGA4	1,31345		
VCAN_ITGA4	1,0604			COL18A1_ITGB1:ITGA2	1,3174265		
NID1_ITGAV	1,082164			ITGB1:ITGA10_COL6A2	1,3203325		
PLTP_ABCA1	1,094096			ITGAV_MFGE8	1,328405		
ANXA1_FPR1	1,119176			EFNB2_PECAM1	1,338715		
SDC3_COL5A1	1,124048			ITGB1_LAMA2	1,378722		
LTF_LRP1	1,150372			GNAI2_ADORA1	1,39438		
GNAI2_CCR5	1,16025			ITGB1:ITGA1_COL5A3	1,404405		
NRP2_VEGFA	1,20162			ITGB1:ITGA1_COL1A2	1,442415		
SDC3_PTN	1,23876			MYLK2_CALM1	1,447875		
C3_ITGAM	1,25378			COL6A2_ITGB1:ITGA10	1,470464		
F8_LRP1	1,27632			ITGB1:ITGA2_COL18A1	1,502601		
COL1A1_ITGB1	1,2831			JAG2_NOTCH1	1,523092		
C5AR1_GNAI2	1,34537			GNAI2_TBXA2R	1,523964		
C1QB_LRP1	1,348386			IL6ST_OSM	1,531411		
JAG1_NOTCH2	1,401332			GNAI2_PTPRU	1,612926		
GNAI2_EDNRA	1,413326			MYLK_CALM3	1,625348		
VEGFA_KDR	1,44723			COL7A1_ITGB1:ITGA1	1,675236		
TNC_ITGB1:ITGA9	1,602965			P2RY12_GNAI2	1,687248		
FZD3_WNT5A	1,619838			THBS2_ITGA6	1,702527		
LRP1_MDK	1,629138			COL9A3_ITGB1:ITGA1	1,7354775		
LIPC_LRP1	1,69836			COL18A1_ITGB1:ITGA11	1,82312		
GPC1_COL18A1	1,702881			CLCF1_IL6ST	1,848936		
SERPINA1_LRP1	1,72103			ITGB1:ITGA10_COL6A1	1,999225		
GAS6_AXL	1,752054			FPR1_GNAI2	2,094696		
HFE_B2M	1,9866			ITGB1:ITGA10_COL5A3	2,150799		
PLXNA1_NOTCH1	2,520795			FLT1:KDR_VEGFB	2,273841		
CD1A_B2M	2,666895			VEGFB_FLT1:KDR	2,360526		
JAM2_ITGB1:ITGA4	3,2938765			ITGB1:ITGA10_COL1A2	2,385435		
GP1BA_ITGB2:ITGAM	3,852092			ITGB1:ITGA11_COL18A1	2,4139585		
ALB_B2M:FCGRT	3,928331			COL7A1_ITGB1:ITGA10	2,426164		
ITGB1:ITGA1_COL8A2	3,960669			EBI3_IL6ST	2,433268		
SEMA6D_PLXNA1:TREM2:TYROBP	4,2307417			ITGB1:ITGA2_COL4A2	2,5623		
F10_ITGB2:ITGAM	4,662478			PECAM1_EFNB2	2,624239		
				ITGB1:ITGA1_COL16A1	2,7230985		
				ITGB1:ITGA3_THBS1	2,821959		
				COL4A3_ITGB1:ITGA1	2,8505285		
				COL3A1_ITGB1:ITGA1	2,872337		
				PGF_FLT1:KDR	3,170908		
				ITGB1:ITGA2_COL4A1	3,481975		
				COL1A1_ITGB1:ITGA1	3,539137		
				COL4A4_ITGB1:ITGA1	3,624264		
				COL5A1_ITGB1:ITGA1	3,716901		
				ITGB1:ITGA11_COL4A2	4,2042		

List of L-R pairs. The score reflects the average expression of L-R pairs and the percentage of cells that express the interaction pair. Lower score reflects the higher probability to express the L-R pairs. Partner A (from CD11- cells) is on the left, partner B (from CD11b+cells) is on the right of each pair.

Supplementary Table 7| Cox proportional-hazards regression models in TCGA data.

IDHwt Specific L-R				
	beta	HR (95% CI for HR)	wald.test	p.value
ITGA9	-0,14	0.87 (0.78-0.97)	6,5	1,10E-02
LTF	0,06	1.1 (1-1.1)	9	2,60E-03
AREG	0,069	1.1 (1-1.1)	4,6	3,10E-02
MMP9	0,07	1.1 (1-1.1)	9,2	2,40E-03
COL1A1	0,079	1.1 (1-1.2)	5,5	1,90E-02
THBS1	0,085	1.1 (1-1.2)	4,7	3,00E-02
CR1	0,098	1.1 (1-1.2)	7,2	7,20E-03
VEGFA	0,11	1.1 (1-1.2)	7	8,20E-03
ICAM4	0,11	1.1 (1-1.2)	4,7	3,10E-02
COL1A2	0,12	1.1 (1-1.2)	8,3	3,90E-03
NID1	0,14	1.1 (1-1.3)	4,4	3,70E-02
COL8A2	0,14	1.1 (1-1.3)	5,9	1,50E-02
ICAM1	0,15	1.2 (1-1.3)	7,5	6,20E-03
C3	0,15	1.2 (1-1.3)	5,4	2,00E-02
FPR1	0,15	1.2 (1.1-1.3)	10	1,20E-03
JAG1	0,15	1.2 (1-1.3)	4,4	3,50E-02
VCAM1	0,16	1.2 (1.1-1.3)	11	9,20E-04
TNFRSF1B	0,16	1.2 (1-1.4)	4,4	3,60E-02
LPL	0,17	1.2 (1.1-1.3)	10	1,60E-03
TNC	0,18	1.2 (1.1-1.3)	9,1	2,60E-03
HBEGF	0,19	1.2 (1-1.4)	5,3	2,10E-02
ITGA11	0,19	1.2 (1.1-1.4)	7,5	6,20E-03
CCR5	0,19	1.2 (1.1-1.4)	11	7,60E-04
C5AR1	0,19	1.2 (1.1-1.3)	14	1,60E-04
PLAU	0,2	1.2 (1.1-1.3)	18	2,00E-05
SERPING1	0,2	1.2 (1.1-1.4)	9,7	1,90E-03
ITGAM	0,2	1.2 (1.1-1.4)	7,5	6,20E-03
ANXA1	0,2	1.2 (1.1-1.4)	13	2,80E-04
SERPINA1	0,21	1.2 (1.1-1.4)	15	9,30E-05
GPC1	0,21	1.2 (1.1-1.5)	7,1	7,80E-03
C1QA	0,21	1.2 (1.1-1.4)	14	2,20E-04
MCAM	0,21	1.2 (1-1.5)	4,9	2,70E-02
MRC2	0,21	1.2 (1.1-1.4)	7,5	6,20E-03
TFPI	0,21	1.2 (1.1-1.4)	16	7,20E-05
C1QB	0,21	1.2 (1.1-1.4)	14	2,10E-04
TREM2	0,21	1.2 (1.1-1.4)	11	8,50E-04
TYROBP	0,22	1.2 (1.1-1.4)	12	5,00E-04
ITGB2	0,23	1.3 (1.1-1.4)	11	8,00E-04
LGALS9	0,23	1.3 (1.1-1.5)	8,1	4,40E-03
PLTP	0,23	1.3 (1.1-1.5)	8,6	3,40E-03
ITGA3	0,23	1.3 (1.1-1.4)	14	1,60E-04
B2M	0,24	1.3 (1.1-1.5)	7,7	5,50E-03
NRP1	0,25	1.3 (1.1-1.5)	9,8	1,70E-03
TIMP1	0,26	1.3 (1.1-1.5)	17	3,60E-05
ABCA1	0,26	1.3 (1.1-1.5)	11	1,00E-03
HFE	0,27	1.3 (1.1-1.5)	13	3,10E-04
CD44	0,29	1.3 (1.2-1.5)	19	1,10E-05
TGFB1	0,29	1.3 (1.1-1.6)	8,9	2,90E-03
MDK	0,3	1.4 (1.2-1.6)	19	1,70E-05
ITGAV	0,3	1.4 (1.1-1.7)	6,8	9,20E-03
ICAM3	0,33	1.4 (1.1-1.8)	7,6	5,90E-03
CD81	0,35	1.4 (1-2)	4	4,40E-02
ITGB1	0,36	1.4 (1.1-1.8)	9,5	2,10E-03
TNFRSF1A	0,39	1.5 (1.2-1.8)	17	4,50E-05
FCGRT	0,39	1.5 (1.2-1.8)	13	3,30E-04
CD63	0,4	1.5 (1.2-1.9)	13	3,40E-04
GRN	0,43	1.5 (1.2-1.9)	15	1,20E-04
ARF1	0,47	1.6 (1.1-2.4)	5	2,60E-02
CALR	0,47	1.6 (1.2-2.2)	9,1	2,50E-03

IDH-O Specific L-R				
	beta	HR (95% CI for HR)	wald.test	p.value
LRP2	-0,15	0.86 (0.74-1)	4	4,70E-02
SELL	-0,27	0.77 (0.62-0.95)	5,9	1,50E-02
SPP1	-0,32	0.73 (0.56-0.96)	5,2	2,20E-02
P2RY12	-0,5	0.61 (0.47-0.79)	14	2,30E-04
PGF	-0,52	0.59 (0.43-0.82)	9,7	1,80E-03
COL4A5	-0,56	0.57 (0.4-0.82)	9,3	2,30E-03
TF	-0,62	0.54 (0.41-0.72)	18	1,80E-05
ADORA1	-0,63	0.53 (0.31-0.91)	5,3	2,10E-02
ITGAX	-0,68	0.51 (0.33-0.79)	9,2	2,40E-03
APOE	-0,99	0.37 (0.24-0.58)	19	1,50E-05
MFGE8	-1,1	0.35 (0.2-0.59)	15	1,20E-04
SERPINE1	0,28	1.3 (1-1.7)	5	2,50E-02
COL3A1	0,3	1.3 (1-1.7)	5,4	2,00E-02
COL4A4	0,31	1.4 (1-1.8)	4,4	3,60E-02
COL4A3	0,32	1.4 (1.1-1.8)	5,7	1,70E-02
COL4A1	0,39	1.5 (1.1-1.9)	8,2	4,10E-03
ICAM1	0,4	1.5 (1.1-2.1)	5,2	2,30E-02
COL5A1	0,4	1.5 (1.1-2)	7,6	5,70E-03
CLCF1	0,42	1.5 (1.2-2)	9,4	2,20E-03
COL4A2	0,44	1.6 (1.2-2.1)	8,8	3,00E-03
CD93	0,47	1.6 (1.2-2.2)	8,1	4,30E-03
HSPG2	0,49	1.6 (1.2-2.2)	10	1,20E-03
DCN	0,52	1.7 (1.1-2.7)	4,7	3,00E-02
COL6A2	0,53	1.7 (1.2-2.4)	10	1,40E-03
PECAM1	0,53	1.7 (1-2.9)	3,9	4,90E-02
COL1A2	0,54	1.7 (1.1-2.6)	6,9	8,80E-03
CAV1	0,57	1.8 (1.2-2.5)	10	1,60E-03
ITGA10	0,57	1.8 (1.2-2.7)	7,3	6,90E-03
FN1	0,6	1.8 (1.1-3.1)	4,7	3,00E-02
LAMC1	0,6	1.8 (1-3.3)	3,9	4,80E-02
LAMB1	0,63	1.9 (1.3-2.8)	10	1,60E-03
ITGA1	0,67	2 (1.2-3.1)	7,7	5,60E-03
ITGA5	0,67	2 (1.3-3)	9,8	1,80E-03
ITGB3	0,68	2 (1.4-2.8)	16	5,40E-05
NAMPT	0,74	2.1 (1.3-3.2)	11	9,80E-04
PTPRU	0,74	2.1 (1.1-4.1)	4,8	2,80E-02
BCAM	0,75	2.1 (1-4.4)	4	4,50E-02
F11R	0,75	2.1 (1.2-3.8)	6,2	1,30E-02
VWF	0,76	2.1 (1.4-3.2)	13	3,10E-04
LAMA2	0,83	2.3 (1.4-3.9)	9,8	1,80E-03
ITGA3	0,86	2.4 (1.6-3.6)	16	5,20E-05
PDGFRB	0,88	2.4 (1.3-4.4)	7,9	5,00E-03
TGM2	0,99	2.7 (1.4-5.2)	9,1	2,50E-03
ITGB1	1,1	3.1 (1.4-6.8)	7,9	4,90E-03
PODXL	1,4	4 (1.6-10)	8,7	3,10E-03
ADAM15	1,8	6.2 (1.8-21)	8,4	3,70E-03

IDH-A Specific L-R				
	beta	HR (95% CI for HR)	wald.test	p.value
ITGA9	-0,25	0.78 (0.62-0.98)	4,5	0,035
NRCAM	-0,38	0.68 (0.47-0.99)	4	0,046
CNTN2	0,15	1.2 (1-1.3)	5,1	0,024
MAG	0,19	1.2 (1.1-1.4)	7,3	0,0071
PDGFRA	0,26	1.3 (1.1-1.6)	6,2	0,012
SPP1	0,3	1.4 (1.1-1.6)	12	0,00053
COL9A3	0,36	1.4 (1.2-1.7)	14	0,00023

Survival analysis in TCGA datasets of IDHwt (left), IDH-O (middle), and IDH-A (right) gliomas. Negative beta values mean positive effect on survival, while positive beta values mean negative effect on survival.

Supplementary Table 8| Clinical data of the glioma cohort.

Expérience	Status	Patient_ID	Sex	Age at surgery	Histology	Grade	Status IDH1	Status IDH2	Status Chromosomes	Status P53	Status ATRX	Satut CIC	Satut TERT	Status BRAF	Status MDM2	Status FGFR	Status P16	Status EGFR
RNA, DNA, Single Cell RNA	IDHm_codel	N17-0266	M	52	Grade 2 oligodendroglioma	2	MUTANT R132H	WT	LOSS 1P/19Q	WT	WT	MUTANT	MUTANT C250T	WT	WT	NA	WT	WT
RNA, DNA, Single Cell RNA	IDHm_codel	N17-1037	M	33	Grade 3 oligodendroglioma	3	MUTANT R132H	WT	LOSS 1P/19Q	WT	WT	WT	MUTANT C228T	WT	WT	NA	WT	WT
Single Cell RNA	IDHm_no_codel	20EN00876	F	26	Grade 3 astrocytoma	3	MUTANT R132H	WT	NO	WT	EXTINATION DIFFUSE	WT	WT	WT	WT	WT	NA	WT
Single Cell RNA	IDHwt	20EN01001	M	65	Grade 4 glioblastoma	4	WT	WT	NA	NA	NA	NA	NA	NA	NA	NA	NA	NA
Single Cell RNA	IDHm_no_codel	20EN01526	M	32	Grade 2 astrocytoma	2	MUTANT R132H	WT	NO	SUREXPRIMEE	EXTINATION DIFFUSE	WT	WT	WT	WT	WT	NA	WT
Single Cell RNA	IDHwt	21EN00260	M	20	Grade 4 glioblastoma	4	WT	WT	NO	SUREXPRIMEE	EXTINATION DIFFUSE	WT	WT	WT	WT	WT	NA	WT
Single Cell RNA	IDHm_codel	21EN00559	F	25	Grade 2 oligodendroglioma	2	MUTANT R132H	WT	LOSS 1P/19Q	NA	WT	WT	MUTANT C250T	WT	WT	WT	NA	WT
Single Cell RNA	IDHm_no_codel	N19-0506	M	38	Grade 3 astrocytoma	3	MUTANT R132H	WT	NO	SUREXPRIMEE	EXTINATION DIFFUSE	WT	WT	WT	WT	WT	NA	WT
Single Cell RNA	IDHwt	N19-1109	M	41	Grade 4 glioblastoma	4	WT	WT	GAIN 7P/7Q/19P/19Q / LOSS P9/10P/10Q	WT	WT	WT	MUTANT C228T	WT	WT	WT	NA	AMPLIFIED

Expérience	Status	Patient_ID	Tumor localization	Tumor hemisphere	Chemotherapy before surgery	Corticotherapy before surgery	Corticotherapy details	Antiepileptic	Antiepileptic details	Relapse
RNA, DNA, Single Cell RNA	IDHm_codel	N17-0266	Frontal	Left	NO	NO	NO	YES	Keppra	NO
RNA, DNA, Single Cell RNA	IDHm_codel	N17-1037	Frontal	Left	NO	YES	Cortancyl 40	YES	Keppra	NO
Single Cell RNA	IDHm_no_codel	20EN00876	Temporal	Right	NO	YES	Corticotherapy 1mg/kg	YES	Rivotril + Keppra	NO
Single Cell RNA	IDHwt	20EN01001	Parieto-occipital	Right	NO	NO	NO	YES	Keppra	NO
Single Cell RNA	IDHm_no_codel	20EN01526	Frontal-temporal	Left	NO	NO?	NO	NO?	NO	NO
Single Cell RNA	IDHwt	21EN00260	Frontal	Right	NO	NO	NO	YES	Keppra	NO
Single Cell RNA	IDHm_codel	21EN00559	Frontal	Left	NO	NO?	NO	YES	Keppra	NO
Single Cell RNA	IDHm_no_codel	N19-0506	Frontal	Left	NO	NO?	NO	NO?	NO	NO
Single Cell RNA	IDHwt	N19-1109	Frontal	Right	NO	Probably YES	NO	NO	NO	NO

Supplementary Table 9| Number of cells in our study and publicly available scRNA-Seq datasets.

Study	IDH status	Nb of patients	Nb of cells				Nb of cells / patients				Nb of cells recovered				Nb of cells recovered / patients			
			All cells	Tumor cells	Immune cells	**T cells**	All cells	Tumor cells	Immune cells	T cells	All cells	Tumor cells	Immune cells	**T cells**	All cells	Tumor cells	Immune cells	T cells
Abdelfattah	IDHwt recurrent	5	87880	30652	57228	**13368**	17576	6130	11446	2674	99714			**13429**	19943	0	0	2686
	IDHwt initial	11	94450	40019	54431	**4968**	8586	3638	4948	452	99737			**6849**	9067	0	0	623
	IDH-A	1	7608	2691	4917	**19**	7608	2691	4917	19	8227			**19**	8227	0	0	19
	IDH-O	1	12048	8402	3646	**128**	12048	8402	3646	128	13023			**112**	13023	0	0	112
Alghamri	IDHwt initial	8			9765				1221				11988	**737**			1499	92
	IDH-A	10			17452				1745				21559	**210**			2156	21
Mathewson	IDHwt recurrent	12												**2838**				237
	IDHwt initial	4												**657**				164
	IDHm	15												**4757**				317
Our study	IDHwt initial	3			25592	**8224**			8531	2741								
	IDH-A	3			19546	**421**			6515	140								
	IDH-O	3			16394	**7383**			5465	2461								

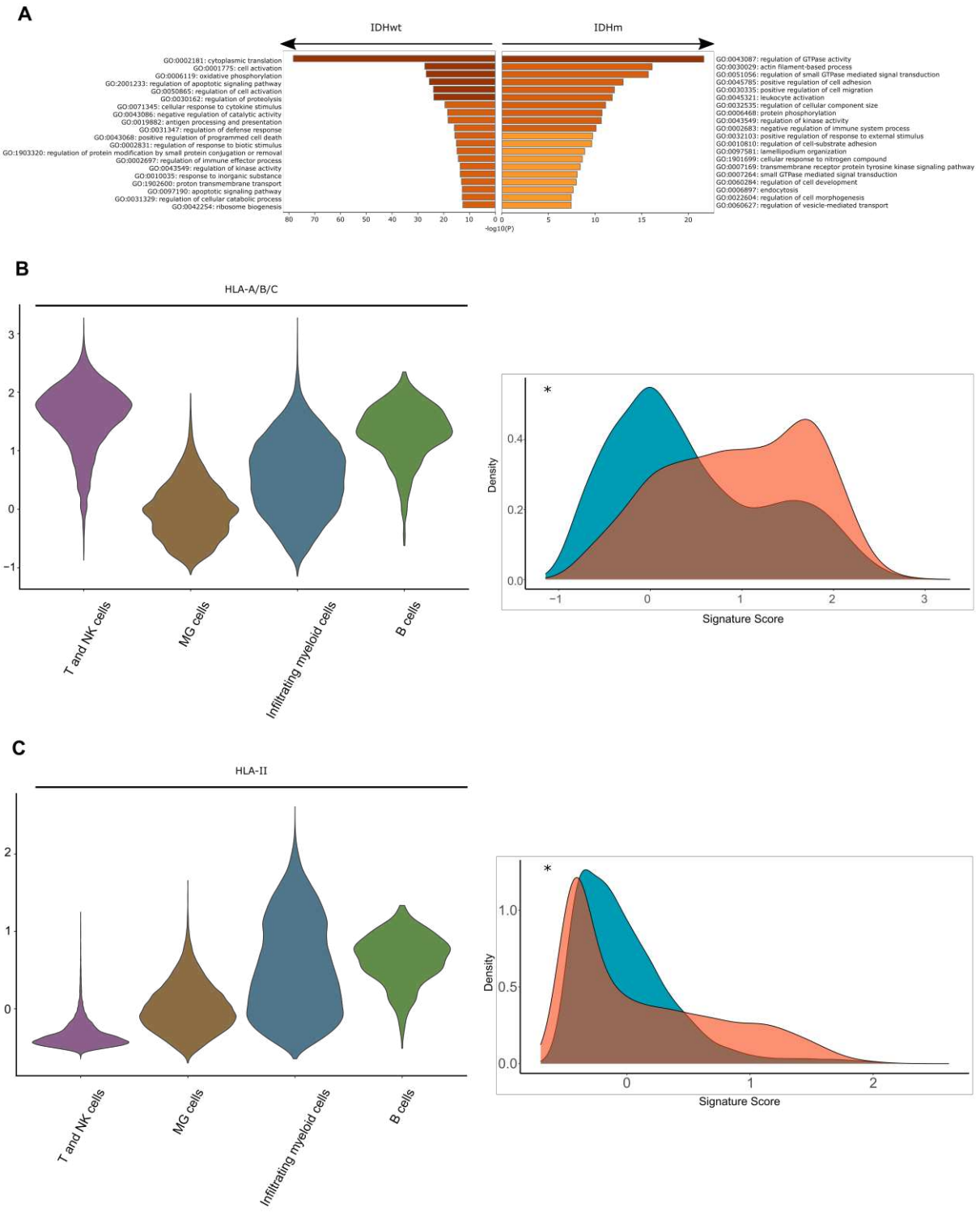

Supplementary Figure 7| Differential expression analysis of immune cells from IDHwt and IDHm human gliomas.

A| Barplot representation of pathway enrichment across genes upregulated in IDHwt (left) and IDHm (right) samples, color-coded by p-values. Log10(P) is the p-value in log base 10. **B|** Violin plots showing HLA-A/B/C expression levels in human glioma-associated immune cells. Expression of HLA-A/B/C gene signatures in immune cells. Extreme values were chosen to belong to the 9th decile, and Pearson's Chi-squared test with Yates' continuity correction was performed. Cluster designation corresponds to Figure 35 A. **C|** Violin plots showing HLA-II expression levels in human glioma-associated immune cells.

Expression of HLA-II gene signatures in immune cells. Extreme values were chosen to belong to the 9th decile, and Pearson's Chi-squared test with Yates' continuity correction was performed. Cluster designation corresponds to Figure 35 A.

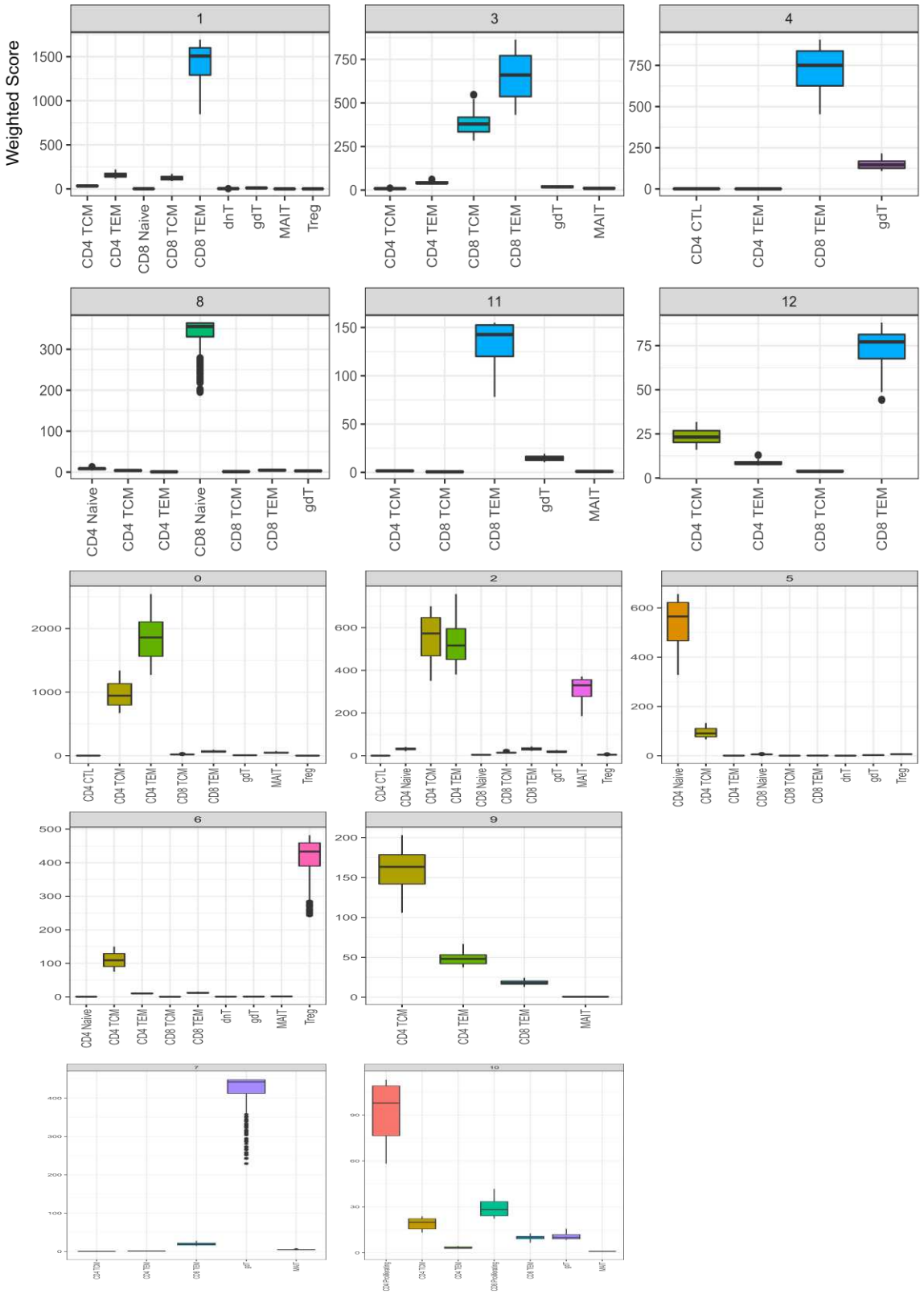

Supplementary Figure 8| Weighted scores of T cells projection.

Boxplot of the weighted score of each cell projection. The projection score was multiplied by the number of cells in the predicted cluster.

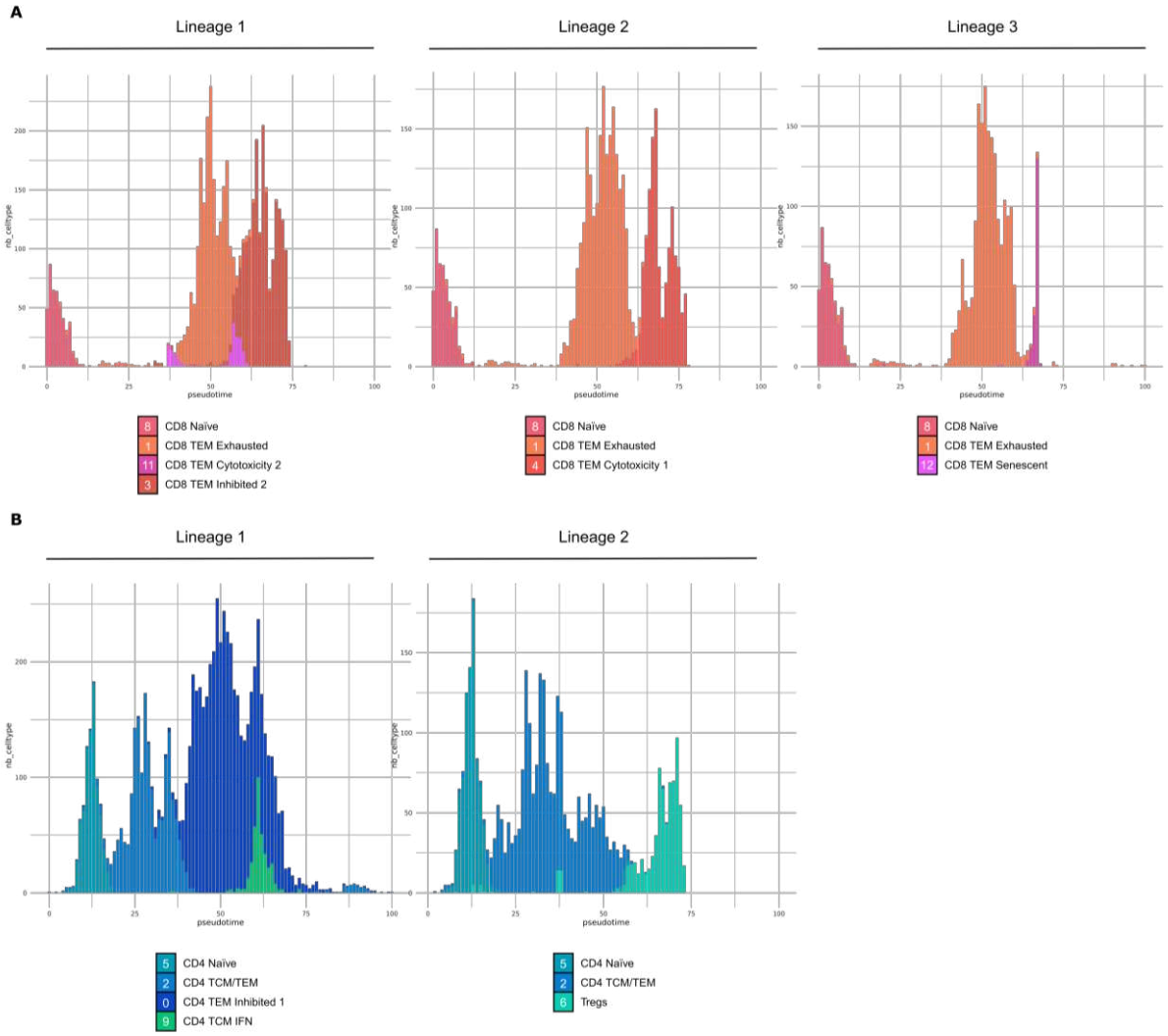

Supplementary Figure 9| Number of cells per cluster according to their pseudotime.

Histogram of the number of cells color-coded per cluster according to the pseudotime that Slingshot calculated in their lineage for **A|** CD8 T cells and **B|** CD4 T cells.

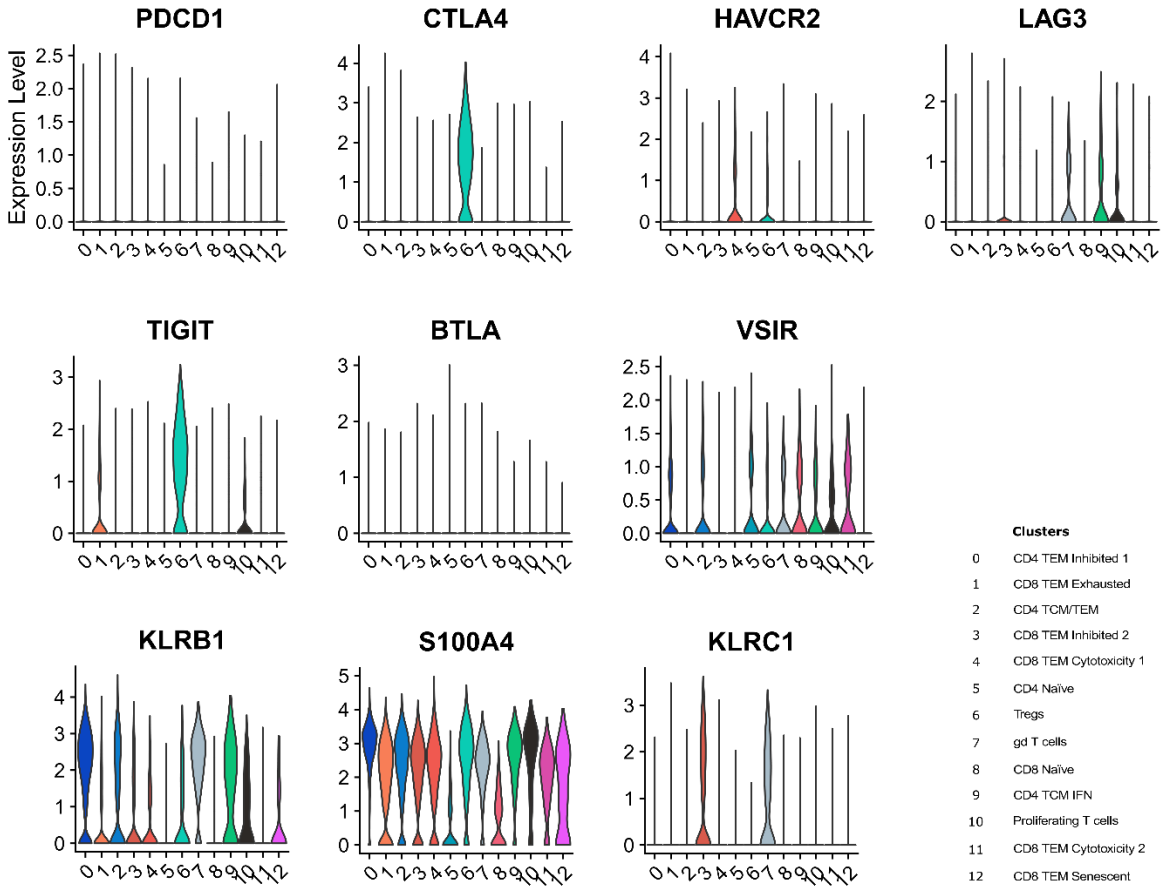

Supplementary Figure 10| Expression of classical immune checkpoints in T cells.

Violin plots of the expression of classical immune checkpoints in each T cell cluster. KLRB1, S100A4, and KLRC1 are represented for comparison purposes.

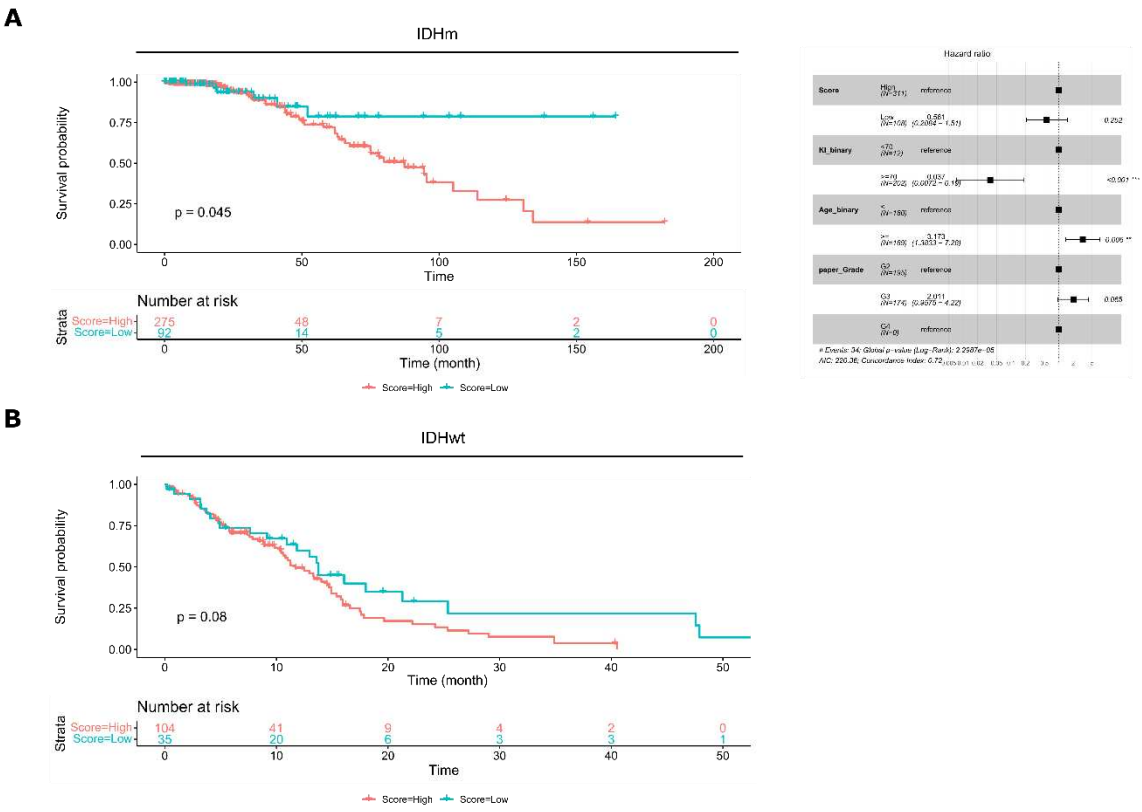

Supplementary Figure 11| Survival analysis of HLA-E expression in IDHm and IDHwt samples from TCGA.

A| Kaplan–Meier survival curves generated with HLA-E using 367 primary IDHm patients from TCGA dataset (left). Multivariate Cox regression analysis using 419 primary IDHm patients from TCGA dataset (right). **B|** Kaplan–Meier survival curves generated with HLA-E using 139 primary IDHwt patients from TCGA dataset.

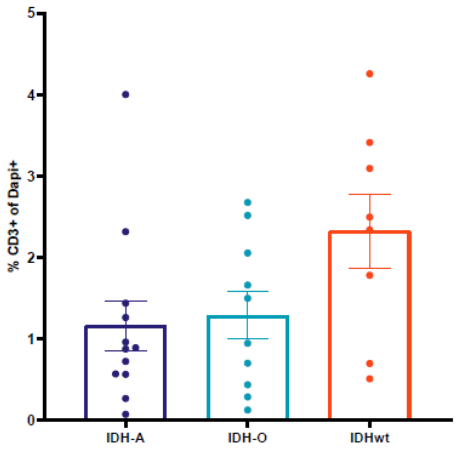

Supplementary Figure 12| Quantification of T cells in IDHm and IDHwt glioma FFPE slides.

Quantification of CD3+ cells of Dapi+ cells in FFPE slides of 12 IDH-A tumor sections, 10 IDH-O tumor sections, and 8 IDHwt tumor sections.

Supplementary Table 10| List of materials.

Materials	Supplier	Reference
Human TruStain FcX	BioLegend	422301
PE/Cyanine7 anti-mouse/human CD11b Antibody	BioLegend	101216
PE/Cyanine7 anti-mouse/human CD45 Antibody	BioLegend	
FITC anti-human CD45RA Antibody	BioLegend	304106
PerCP anti-human CD8 Antibody	BioLegend	344708
PE anti-human CD197 (CCR7) Antibody	BioLegend	353204
APC/Cyanine7 anti-human CD3 Antibody	BioLegend	300426
APC anti-human CD4 Antibody	BioLegend	317416
PE Donkey anti-rabbit IgG (minimal x-reactivity) Antibody	BioLegend	406421
FITC anti-human/mouse Granzyme B Recombinant Antibody	BioLegend	372206
Brilliant Violet 421™ anti-human CD25 Antibody	BioLegend	302630
Zombie Aqua™ Fixable Viability Kit	BioLegend	423101
FITC Mouse IgG1, κ Isotype Ctrl (ICFC) Antibody	BioLegend	400137
PerCP Mouse IgG1, κ Isotype Ctrl Antibody	BioLegend	400147
Brilliant Violet 42 Mouse IgG1, κ Isotype Ctrl Antibody	BioLegend	400157
APC/Cyanine7 Mouse IgG1, κ Isotype Ctrl Antibody	BioLegend	400127
PE Mouse IgG1, κ Isotype Ctrl (ICFC) Antibody	BioLegend	400139
APC Mouse IgG2b, κ Isotype Ctrl Antibody	BioLegend	400321
PE anti-human FOXP3 Antibody	BioLegend	320108
Corning® CoolCell™ LX Cell Freezing Container	Corning	CLS432002-1EA
PANCOLL Humain - densité 1,077 g/ml - 500 ml	Dutscher	P04-60500
MACS Debris Removal Solution	Miltenyi	130-109-398
CD14 MicroBeads, human	Miltenyi	130-050-201
Naive Pan T Cell Isolation Kit, human	Miltenyi	130-097-095
CD45 (TIL) MicroBeads	Miltenyi	130-118-780
Live-or-Dye™ 488/515 Fixable Viability Dye	Ozyme	BTM32004-T
Recombinant Human IL-2	Peprotech	200-02
Maxwell RSC simplyRNA Cells Kit	Promega	AS1390
LightCycler 480 SYBR Green Master 2X	Roche	4887352001
L-cystein	Sigma	C7880-100g
DMSO	Sigma-Aldrich	D8418-50ML
D-α-Hydroxyglutaric acid disodium salt	Sigma-Aldrich	H8378
2-Phospho-L-ascorbic acid trisodium salt	Sigma-Aldrich	49752
Bovine Serum Albumin solution	Sigma-Aldrich	A7979
Pénicilline-streptomycine (10 000 U/ml)	Thermo Fisher Scientific	15140122
Dynabeads™ Human T-Activator CD3/CD28 for T Cell Expansion and Activation	Thermo Fisher Scientific	11132D
Maxima First Strand cDNA Synthesis Kit	Thermo Fisher Scientific	K1642
UltraPure 0.5M EDTA，pH 8.0	Thermo Fisher Scientific	15575020
Foxp3 / Transcription Factor Staining Buffer Set	Thermo Fisher Scientific	00-5523-00
Pierce™ BCA Protein Assay Kit	Thermo Fisher Scientific	23225
Papain	Worthington	WOLS03126
DNAse	Worthington	LS002139
Ovomucoid	Worthington	LS003085

IV) REFERENCES

[1] L. Weiss, "Early Concepts of Cancer," *Cancer and Metastasis Reviews 2000 19:3*, vol. 19, no. 3, pp. 205–217, 2000, doi: 10.1023/A:1010698321682.

[2] D. Hanahan and R. A. Weinberg, "The hallmarks of cancer," *Cell*, vol. 100, no. 1. Cell, pp. 57–70, Jan. 07, 2000. doi: 10.1016/S0092-8674(00)81683-9.

[3] D. Hanahan and R. A. Weinberg, "Hallmarks of cancer: The next generation," *Cell*, vol. 144, no. 5. Cell, pp. 646–674, Mar. 04, 2011. doi: 10.1016/j.cell.2011.02.013.

[4] D. Hanahan, "Hallmarks of Cancer: New Dimensions," *Cancer Discovery*, vol. 12, no. 1. American Association for Cancer Research Inc., pp. 31–46, Jan. 01, 2022. doi: 10.1158/2159-8290.CD-21-1059.

[5] B. Vogelstein and K. W. Kinzler, "Cancer genes and the pathways they control," *Nature Medicine*, vol. 10, no. 8. Nature Publishing Group, pp. 789–799, Aug. 30, 2004. doi: 10.1038/nm1087.

[6] C. Neftel *et al.*, "An Integrative Model of Cellular States, Plasticity, and Genetics for Glioblastoma," *Cell*, vol. 178, no. 4, pp. 835-849.e21, Aug. 2019, doi: 10.1016/j.cell.2019.06.024.

[7] A. Marusyk, V. Almendro, and K. Polyak, "Intra-tumour heterogeneity: A looking glass for cancer?," *Nature Reviews Cancer*, vol. 12, no. 5. Nature Publishing Group, pp. 323–334, May 19, 2012. doi: 10.1038/nrc3261.

[8] T. Mazor *et al.*, "DNA Methylation and Somatic Mutations Converge on the Cell Cycle and Define Similar Evolutionary Histories in Brain Tumors," *Cancer Cell*, vol. 28, no. 3, pp. 307–317, Sep. 2015, doi: 10.1016/j.ccell.2015.07.012.

[9] A. Marusyk, M. Janiszewska, and K. Polyak, "Intratumor Heterogeneity: The Rosetta Stone of Therapy Resistance," *Cancer Cell*, vol. 37, no. 4. Cell Press, pp. 471–484, Apr. 13, 2020. doi: 10.1016/j.ccell.2020.03.007.

[10] H. Salmon, R. Remark, S. Gnjatic, and M. Merad, "Host tissue determinants of tumour immunity," *Nat Rev Cancer*, vol. 19, no. 4, pp. 215–227, Mar. 2019, doi: 10.1038/s41568-019-0125-9.

[11] J. Galon *et al.*, "Type, density, and location of immune cells within human colorectal tumors predict clinical outcome," *Science (1979)*, vol. 313, no. 5795, pp. 1960–1964, Sep. 2006, doi: 10.1126/science.1129139.

[12] V. Thorsson *et al.*, "The Immune Landscape of Cancer," *Immunity*, vol. 48, no. 4, pp. 812-830.e14, Apr. 2018, doi: 10.1016/j.immuni.2018.03.023.

[13] J. Zhang, D. Huang, P. E. Saw, and E. Song, "Turning cold tumors hot: from molecular mechanisms to clinical applications," *Trends in Immunology*, vol. 43, no. 7. Elsevier Ltd, pp. 523–545, Jul. 01, 2022. doi: 10.1016/j.it.2022.04.010.

[14] G. P. Dunn, L. J. Old, and R. D. Schreiber, "The Three Es of Cancer Immunoediting," *http://dx.doi.org/10.1146/annurev.immunol.22.012703.104803*, vol. 22, pp. 329–360, Mar. 2004, doi: 10.1146/ANNUREV.IMMUNOL.22.012703.104803.

[15] P. Sharma and J. P. Allison, "Immune checkpoint targeting in cancer therapy: toward combination strategies with curative potential," *Cell*, vol. 161, no. 2, pp. 205–214, Apr. 2015, doi: 10.1016/J.CELL.2015.03.030.

[16] I. Mellman, G. Coukos, and G. Dranoff, "Cancer immunotherapy comes of age," *Nature*, vol. 480, no. 7378, pp. 480–489, Dec. 2011, doi: 10.1038/NATURE10673.

[17] D. S. Chen and I. Mellman, "Oncology meets immunology: the cancer-immunity cycle," *Immunity*, vol. 39, no. 1, pp. 1–10, Jul. 2013, doi: 10.1016/J.IMMUNI.2013.07.012.

[18] C. G. Drake, E. Jaffee, and D. M. Pardoll, "Mechanisms of immune evasion by tumors," *Adv Immunol*, vol. 90, pp. 51–81, 2006, doi: 10.1016/S0065-2776(06)90002-9.

[19] L. Laurent *et al.*, "Dynamic changes in the human methylome during differentiation," *Genome Res*, vol. 20, no. 3, pp. 320–331, Mar. 2010, doi: 10.1101/gr.101907.109.

[20] R. Lister *et al.*, "Human DNA methylomes at base resolution show widespread epigenomic differences," *Nature*, vol. 462, no. 7271, pp. 315–322, Nov. 2009, doi: 10.1038/nature08514.

[21] F. Court *et al.*, "Transcriptional alterations in glioma result primarily from DNA methylation-independent mechanisms," *Genome Res*, vol. 29, no. 10, pp. 1605–1621, 2019, doi: 10.1101/gr.249219.119.

[22] M. Tahiliani *et al.*, "Conversion of 5-methylcytosine to 5-hydroxymethylcytosine in mammalian DNA by MLL partner TET1," *Science (1979)*, vol. 324, no. 5929, pp. 930–935, May 2009, doi: 10.1126/science.1170116.

[23] S. Ito, A. C. D'Alessio, O. v. Taranova, K. Hong, L. C. Sowers, and Y. Zhang, "Role of Tet proteins in 5mC to 5hmC conversion, ES-cell self-renewal and inner cell mass specification," *Nature*, vol. 466, no. 7310, pp. 1129–1133, Aug. 2010, doi: 10.1038/nature09303.

[24] Y. F. He *et al.*, "Tet-mediated formation of 5-carboxylcytosine and its excision by TDG in mammalian DNA," *Science (1979)*, vol. 333, no. 6047, pp. 1303–1307, Sep. 2011, doi: 10.1126/science.1210944.

[25] S. Ito *et al.*, "Tet proteins can convert 5-methylcytosine to 5-formylcytosine and 5-carboxylcytosine," *Science (1979)*, vol. 333, no. 6047, pp. 1300–1303, Sep. 2011, doi: 10.1126/science.1210597.

[26] W. A. Pastor, L. Aravind, and A. Rao, "TETonic shift: Biological roles of TET proteins in DNA demethylation and transcription," *Nature Reviews Molecular Cell Biology*,

vol. 14, no. 6. Nature Publishing Group, pp. 341–356, Jun. 23, 2013. doi: 10.1038/nrm3589.

[27] S. Cortellino *et al.*, "Thymine DNA glycosylase is essential for active DNA demethylation by linked deamination-base excision repair," *Cell*, vol. 146, no. 1, pp. 67–79, Jul. 2011, doi: 10.1016/j.cell.2011.06.020.

[28] A. Tsagaratou *et al.*, "Dissecting the dynamic changes of 5-hydroxymethylcytosine in T-cell development and differentiation," *Proceedings of the National Academy of Sciences*, vol. 111, no. 32, pp. E3306–E3315, Aug. 2014, doi: 10.1073/pnas.1412327111.

[29] C. E. Nestor *et al.*, "Rapid reprogramming of epigenetic and transcriptional profiles in mammalian culture systems," *Genome Biol*, vol. 16, no. 1, p. 11, Feb. 2015, doi: 10.1186/s13059-014-0576-y.

[30] M. R. Branco, G. Ficz, and W. Reik, "Uncovering the role of 5-hydroxymethylcytosine in the epigenome," *Nat Rev Genet*, vol. 13, no. 1, pp. 7–13, Jan. 2012, doi: 10.1038/nrg3080.

[31] J. L. Sardina *et al.*, "Transcription Factors Drive Tet2-Mediated Enhancer Demethylation to Reprogram Cell Fate," *Cell Stem Cell*, vol. 23, no. 5, pp. 727-741.e9, Nov. 2018, doi: 10.1016/j.stem.2018.08.016.

[32] K. D. Rasmussen *et al.*, "TET2 binding to enhancers facilitates transcription factor recruitment in hematopoietic cells," *Genome Res*, vol. 29, no. 4, pp. 564–575, Apr. 2019, doi: 10.1101/gr.239277.118.

[33] A. Tsagaratou, C. W. J. Lio, X. Yue, and A. Rao, "TET methylcytosine oxidases in T cell and B cell development and function," *Frontiers in Immunology*, vol. 8, no. MAR. Frontiers Research Foundation, p. 220, Mar. 31, 2017. doi: 10.3389/fimmu.2017.00220.

[34] C. E. Nestor *et al.*, "5-Hydroxymethylcytosine Remodeling Precedes Lineage Specification during Differentiation of Human CD4+ T Cells," *Cell Rep*, vol. 16, no. 2, pp. 559–570, Jul. 2016, doi: 10.1016/j.celrep.2016.05.091.

[35] L. Vincenzetti, C. Leoni, M. Chirichella, I. Kwee, and S. Monticelli, "The contribution of active and passive mechanisms of 5mC and 5hmC removal in human T lymphocytes is differentiation- and activation-dependent," *Eur J Immunol*, vol. 49, no. 4, pp. 611–625, Apr. 2019, doi: 10.1002/eji.201847967.

[36] A. Tsagaratou *et al.*, "TET proteins regulate the lineage specification and TCR-mediated expansion of iNKT cells," *Nat Immunol*, vol. 18, no. 1, pp. 45–53, Jan. 2017, doi: 10.1038/ni.3630.

[37] V. S. Nair, M. H. Song, M. Ko, and K. I. Oh, "DNA demethylation of the Foxp3 enhancer is maintained through modulation of ten-eleven-translocation and

DNA methyltransferases," *Mol Cells*, vol. 39, no. 12, pp. 888–897, Dec. 2016, doi: 10.14348/molcells.2016.0276.

[38] R. Yang *et al.*, "Hydrogen Sulfide Promotes Tet1- and Tet2-Mediated Foxp3 Demethylation to Drive Regulatory T Cell Differentiation and Maintain Immune Homeostasis," *Immunity*, vol. 43, no. 2, pp. 251–263, Aug. 2015, doi: 10.1016/j.immuni.2015.07.017.

[39] X. Yue *et al.*, "Control of Foxp3 stability through modulation of TET activity," *Journal of Experimental Medicine*, vol. 213, no. 3, pp. 377–397, Mar. 2016, doi: 10.1084/jem.20151438.

[40] H. Nakatsukasa *et al.*, "Loss of TET proteins in regulatory T cells promotes abnormal proliferation, Foxp3 destabilization and IL-17 expression," *Int Immunol*, vol. 31, no. 5, pp. 335–347, Apr. 2019, doi: 10.1093/intimm/dxz008.

[41] X. Yue, C. W. J. Lio, D. Samaniego-Castruita, X. Li, and A. Rao, "Loss of TET2 and TET3 in regulatory T cells unleashes effector function," *Nat Commun*, vol. 10, no. 1, pp. 1–14, Dec. 2019, doi: 10.1038/s41467-019-09541-y.

[42] R. Yang *et al.*, "Hydrogen Sulfide Promotes Tet1- and Tet2-Mediated Foxp3 Demethylation to Drive Regulatory T Cell Differentiation and Maintain Immune Homeostasis," *Immunity*, vol. 43, no. 2, pp. 251–263, Aug. 2015, doi: 10.1016/j.immuni.2015.07.017.

[43] P. D. Issuree *et al.*, "Stage-specific epigenetic regulation of CD4 expression by coordinated enhancer elements during T cell development," *Nat Commun*, vol. 9, no. 1, p. 3594, Dec. 2018, doi: 10.1038/s41467-018-05834-w.

[44] R. S. Akondy *et al.*, "Origin and differentiation of human memory CD8 T cells after vaccination," *Nature*, vol. 552, no. 7685, pp. 362–367, Dec. 2017, doi: 10.1038/nature24633.

[45] B. Youngblood *et al.*, "Effector CD8 T cells dedifferentiate into long-lived memory cells," *Nature*, vol. 552, no. 7685, pp. 404–409, Dec. 2017, doi: 10.1038/nature25144.

[46] A. N. Henning, C. A. Klebanoff, and N. P. Restifo, "Silencing stemness in T cell differentiation," *Science*, vol. 359, no. 6372. American Association for the Advancement of Science, pp. 163–164, Jan. 12, 2018. doi: 10.1126/science.aar5541.

[47] N. P. Restifo and L. Gattinoni, "Lineage relationship of effector and memory T cells," *Current Opinion in Immunology*, vol. 25, no. 5. Elsevier Ltd, pp. 556–563, Oct. 01, 2013. doi: 10.1016/j.coi.2013.09.003.

[48] E. Teixeiro *et al.*, "Different T cell receptor signals determine CD8+ memory versus effector development," *Science (1979)*, vol. 323, no. 5913, pp. 502–505, Jan. 2009, doi: 10.1126/science.1163612.

[49] T. C. Wirth *et al.*, "Repetitive antigen stimulation induces stepwise transcriptome diversification but preserves a core signature of memory CD8+ T cell differentiation," *Immunity*, vol. 33, no. 1, pp. 128–140, Jul. 2010, doi: 10.1016/j.immuni.2010.06.014.

[50] A. N. Henning, R. Roychoudhuri, and N. P. Restifo, "Epigenetic control of CD8+ T'cell differentiation," *Nature Reviews Immunology*, vol. 18, no. 5. Nature Publishing Group, pp. 340–356, May 01, 2018. doi: 10.1038/nri.2017.146.

[51] H. A. Abdelsamed *et al.*, "Human memory CD8 T cell effector potential is epigenetically preserved during in vivo homeostasis," *Journal of Experimental Medicine*, vol. 214, no. 6, pp. 1593–1606, Jun. 2017, doi: 10.1084/jem.20161760.

[52] R. Fonseca *et al.*, "Developmental plasticity allows outside-in immune responses by resident memory T cells," *Nat Immunol*, vol. 21, no. 4, pp. 412–421, Apr. 2020, doi: 10.1038/s41590-020-0607-7.

[53] M. Sade-Feldman *et al.*, "Defining T Cell States Associated with Response to Checkpoint Immunotherapy in Melanoma," *Cell*, vol. 175, no. 4, pp. 998-1013.e20, Nov. 2018, doi: 10.1016/j.cell.2018.10.038.

[54] A. Schietinger *et al.*, "Tumor-Specific T Cell Dysfunction Is a Dynamic Antigen-Driven Differentiation Program Initiated Early during Tumorigenesis," *Immunity*, vol. 45, no. 2, pp. 389–401, 2016, doi: 10.1016/j.immuni.2016.07.011.

[55] S. Kurtulus *et al.*, "Checkpoint Blockade Immunotherapy Induces Dynamic Changes in PD-1 – CD8 + Tumor-Infiltrating T Cells," *Immunity*, vol. 50, no. 1, pp. 181-194.e6, Jan. 2019, doi: 10.1016/j.immuni.2018.11.014.

[56] M. Singer *et al.*, "A Distinct Gene Module for Dysfunction Uncoupled from Activation in Tumor-Infiltrating T Cells," *Cell*, vol. 166, no. 6, pp. 1500-1511.e9, Sep. 2016, doi: 10.1016/j.cell.2016.08.052.

[57] G. P. Mognol *et al.*, "Exhaustion-associated regulatory regions in CD8+ tumor-infiltrating T cells," *Proc Natl Acad Sci U S A*, vol. 114, no. 13, pp. E2776–E2785, Mar. 2017, doi: 10.1073/pnas.1620498114.

[58] M. Philip *et al.*, "Chromatin states define tumour-specific T cell dysfunction and reprogramming," *Nature*, vol. 545, no. 7655, pp. 452–456, May 2017, doi: 10.1038/nature22367.

[59] C. A. Klebanoff *et al.*, "Memory T cell-driven differentiation of naive cells impairs adoptive immunotherapy," *Journal of Clinical Investigation*, vol. 126, no. 1, pp. 318–334, Jan. 2016, doi: 10.1172/JCI81217.

[60] Y. Xu *et al.*, "Closely related T-memory stem cells correlate with in vivo expansion of CAR.CD19-T cells and are preserved by IL-7 and IL-15," *Blood*, vol. 123, no. 24, pp. 3750–3759, Jun. 2014, doi: 10.1182/blood-2014-01-552174.

[61] J. Feucht *et al.*, "Calibration of CAR activation potential directs alternative T cell fates and therapeutic potency," *Nat Med*, vol. 25, no. 1, pp. 82–88, Jan. 2019, doi: 10.1038/s41591-018-0290-5.

[62] Y. Kagoya *et al.*, "BET bromodomain inhibition enhances T cell persistence and function in adoptive immunotherapy models," *Journal of Clinical Investigation*, vol. 126, no. 9, pp. 3479–3494, Sep. 2016, doi: 10.1172/JCI86437.

[63] P. A. Tyrakis *et al.*, "S-2-hydroxyglutarate regulates CD8+ T-lymphocyte fate," *Nature*, vol. 540, no. 7632, pp. 236–241, Dec. 2016, doi: 10.1038/nature20165.

[64] I. P. Foskolou *et al.*, "The S enantiomer of 2-hydroxyglutarate increases central memory CD8 populations and improves CAR-T therapy outcome," *Blood Adv*, vol. 4, no. 18, pp. 4483–4493, Sep. 2020, doi: 10.1182/BLOODADVANCES.2020002309.

[65] J. A. Fraietta *et al.*, "Disruption of TET2 promotes the therapeutic efficacy of CD19-targeted T cells," *Nature*, vol. 558, no. 7709, pp. 307–312, Jun. 2018, doi: 10.1038/s41586-018-0178-z.

[66] "BIennIal report," 2020, Accessed: Mar. 20, 2022. [Online]. Available: http://apps.who.int/bookorders.

[67] Q. T. Ostrom, G. Cioffi, K. Waite, C. Kruchko, and J. S. Barnholtz-Sloan, "CBTRUS Statistical Report: Primary Brain and Other Central Nervous System Tumors Diagnosed in the United States in 2014–2018," *Neuro Oncol*, vol. 23, no. Supplement_3, pp. iii1–iii105, Oct. 2021, doi: 10.1093/neuonc/noab200.

[68] Q. T. Ostrom, G. Cioffi, K. Waite, C. Kruchko, and J. S. Barnholtz-Sloan, "CBTRUS Statistical Report: Primary Brain and Other Central Nervous System Tumors Diagnosed in the United States in 2014-2018," *Neuro Oncol*, vol. 23, no. 12 Suppl 2, pp. III1–III105, Oct. 2021, doi: 10.1093/neuonc/noab200.

[69] B. Malmer, R. Henriksson, and H. Grönberg, "Familial brain tumours - Genetics or environment? A nationwide cohort study of cancer risk in spouses and first-degree relatives of brain tumour patients," *Int J Cancer*, vol. 106, no. 2, pp. 260–263, Aug. 2003, doi: 10.1002/ijc.11213.

[70] I. Baldi, A. Huchet, L. Bauchet, and H. Loiseau, "Épidémiologie des glioblastomes," *Neurochirurgie*, vol. 56, no. 6. Neurochirurgie, pp. 433–440, Dec. 2010. doi: 10.1016/j.neuchi.2010.07.011.

[71] Q. T. Ostrom *et al.*, "The epidemiology of glioma in adults: A state of the science review," *Neuro-Oncology*, vol. 16, no. 7. Oxford University Press, pp. 896–913, 2014. doi: 10.1093/neuonc/nou087.

[72] G. Cairncross *et al.*, "Phase III trial of chemoradiotherapy for anaplastic oligodendroglioma: Long-term results of RTOG 9402," *Journal of Clinical Oncology*, vol. 31, no. 3, pp. 337–343, Jan. 2013, doi: 10.1200/JCO.2012.43.2674.

[73] M. A. Vogelbaum *et al.*, "Phase II trial of pre-irradiation and concurrent temozolomide in patients with newly diagnosed anaplastic oligodendrogliomas and mixed anaplastic oligoastrocytomas: long term results of RTOG BR0131," *J Neurooncol*, vol. 124, no. 3, pp. 413–420, Sep. 2015, doi: 10.1007/s11060-015-1845-7.

[74] M. J. van den Bent *et al.*, "Adjuvant procarbazine, lomustine, and vincristine chemotherapy in newly diagnosed anaplastic oligodendroglioma: Long-term follow-up of EORTC brain tumor group study 26951," *Journal of Clinical Oncology*, vol. 31, no. 3, pp. 344–350, Jan. 2013, doi: 10.1200/JCO.2012.43.2229.

[75] J. E. Eckel-Passow *et al.*, "Glioma Groups Based on 1p/19q, *IDH* , and *TERT* Promoter Mutations in Tumors," *New England Journal of Medicine*, vol. 372, no. 26, pp. 2499–2508, Jun. 2015, doi: 10.1056/NEJMoa1407279.

[76] A. L. Cohen, S. L. Holmen, and H. Colman, "IDH1 and IDH2 mutations in gliomas," *Curr Neurol Neurosci Rep*, vol. 13, no. 5, p. 345, 2013, doi: 10.1007/s11910-013-0345-4.

[77] "Comprehensive, Integrative Genomic Analysis of Diffuse Lower-Grade Gliomas," *New England Journal of Medicine*, vol. 372, no. 26, pp. 2481–2498, Jun. 2015, doi: 10.1056/NEJMoa1402121.

[78] M. Weller *et al.*, "EANO guidelines on the diagnosis and treatment of diffuse gliomas of adulthood," *Nature Reviews Clinical Oncology 2020 18:3*, vol. 18, no. 3, pp. 170–186, Dec. 2020, doi: 10.1038/s41571-020-00447-z.

[79] Y. Jiao *et al.*, "Frequent ATRX, CIC, FUBP1 and IDH1 mutations refine the classification of malignant gliomas," *Oncotarget*, vol. 3, no. 7, pp. 709–722, 2012, doi: 10.18632/oncotarget.588.

[80] B. Wiestler *et al.*, "ATRX loss refines the classification of anaplastic gliomas and identifies a subgroup of IDH mutant astrocytic tumors with better prognosis," *Acta Neuropathol*, vol. 126, no. 3, pp. 443–451, Sep. 2013, doi: 10.1007/s00401-013-1156-z.

[81] M. Shirahata *et al.*, "Novel, improved grading system(s) for IDH-mutant astrocytic gliomas," *Acta Neuropathol*, vol. 136, no. 1, pp. 153–166, Apr. 2018, doi: 10.1007/S00401-018-1849-4.

[82] R. Appay *et al.*, "CDKN2A homozygous deletion is a strong adverse prognosis factor in diffuse malignant IDH-mutant gliomas," *Neuro Oncol*, vol. 21, no. 12, pp. 1519–1528, Dec. 2019, doi: 10.1093/NEUONC/NOZ124.

[83] M. E. Hegi *et al.*, "*MGMT* Gene Silencing and Benefit from Temozolomide in Glioblastoma," *New England Journal of Medicine*, vol. 352, no. 10, pp. 997–1003, Mar. 2005, doi: 10.1056/NEJMoa043331.

[84] C. L. Maire and K. L. Ligon, "Molecular pathologic diagnosis of epidermal growth factor receptor," *Neuro-Oncology*, vol. 16, no. Suppl 8. Oxford University Press, pp. viii1–viii6, Sep. 12, 2014. doi: 10.1093/neuonc/nou294.

[85] H. Arita *et al.*, "Upregulating mutations in the TERT promoter commonly occur in adult malignant gliomas and are strongly associated with total 1p19q loss," *Acta Neuropathol*, vol. 126, no. 2, pp. 267–276, Aug. 2013, doi: 10.1007/s00401-013-1141-6.

[86] J. E. Eckel-Passow *et al.*, "Glioma Groups Based on 1p/19q, *IDH* , and *TERT* Promoter Mutations in Tumors," *New England Journal of Medicine*, vol. 372, no. 26, pp. 2499–2508, Jun. 2015, doi: 10.1056/NEJMoa1407279.

[87] R. Stupp *et al.*, "Radiotherapy plus Concomitant and Adjuvant Temozolomide for Glioblastoma," *New England Journal of Medicine*, vol. 352, no. 10, pp. 987–996, Mar. 2005, doi: 10.1056/NEJMoa043330.

[88] R. Stupp *et al.*, "Effects of radiotherapy with concomitant and adjuvant temozolomide versus radiotherapy alone on survival in glioblastoma in a randomised phase III study: 5-year analysis of the EORTC-NCIC trial," *Lancet Oncol*, vol. 10, no. 5, pp. 459–466, May 2009, doi: 10.1016/S1470-2045(09)70025-7.

[89] L. Bauchet *et al.*, "Oncological patterns of care and outcome for 952 patients with newly diagnosed glioblastoma in 2004," *Neuro Oncol*, vol. 12, no. 7, pp. 725–735, Jul. 2010, doi: 10.1093/neuonc/noq030.

[90] S. Scoccianti *et al.*, "Patterns of care and survival in a retrospective analysis of 1059 patients with glioblastoma multiforme treated between 2002 and 2007: A multicenter study by the central nervous system study group of Airo (Italian association of radiation oncology)," *Neurosurgery*, vol. 67, no. 2. Neurosurgery, pp. 446–458, Aug. 2010. doi: 10.1227/01.NEU.0000371990.86656.E8.

[91] A. S. Darefsky, J. T. King, and R. Dubrow, "Adult glioblastoma multiforme survival in the temozolomide era: A population-based analysis of Surveillance, Epidemiology, and End Results registries," *Cancer*, vol. 118, no. 8, pp. 2163–2172, Apr. 2012, doi: 10.1002/cncr.26494.

[92] D. R. Johnson and B. P. O'Neill, "Glioblastoma survival in the United States before and during the temozolomide era," *J Neurooncol*, vol. 107, no. 2, pp. 359–364, Apr. 2012, doi: 10.1007/s11060-011-0749-4.

[93] M. Koshy *et al.*, "Improved survival time trends for glioblastoma using the SEER 17 population-based registries," *J Neurooncol*, vol. 107, no. 1, pp. 207–212, Mar. 2012, doi: 10.1007/s11060-011-0738-7.

[94] P. A. Rønning, E. Helseth, T. R. Meling, and T. B. Johannesen, "A population-based study on the effect of temozolomide in the treatment of glioblastoma

multiforme," *Neuro Oncol*, vol. 14, no. 9, pp. 1178–1184, Sep. 2012, doi: 10.1093/neuonc/nos153.

[95] K. R. Yabroff, L. Harlan, C. Zeruto, J. Abrams, and B. Mann, "Patterns of care and survival for patients with glioblastoma multiforme diagnosed during 2006," *Neuro Oncol*, vol. 14, no. 3, pp. 351–359, Mar. 2012, doi: 10.1093/neuonc/nor218.

[96] R. Dubrow *et al.*, "Time trends in glioblastoma multiforme survival: The role of temozolomide," *Neuro Oncol*, vol. 15, no. 12, pp. 1750–1761, Dec. 2013, doi: 10.1093/neuonc/not122.

[97] F. Graus *et al.*, "Patterns of care and outcome for patients with glioblastoma diagnosed during 2008-2010 in Spain," *Neuro Oncol*, vol. 15, no. 6, pp. 797–805, Jun. 2013, doi: 10.1093/neuonc/not013.

[98] V. K. Y. Ho *et al.*, "Changing incidence and improved survival of gliomas," *Eur J Cancer*, vol. 50, no. 13, pp. 2309–2318, 2014, doi: 10.1016/j.ejca.2014.05.019.

[99] A. Woehrer, L. Bauchet, and J. S. Barnholtz-Sloan, "Glioblastoma survival: Has it improved? Evidence from population-based studies," *Current Opinion in Neurology*, vol. 27, no. 6. Lippincott Williams and Wilkins, pp. 666–674, 2014. doi: 10.1097/WCO.0000000000000144.

[100] M. J. van den Bent *et al.*, "Adjuvant procarbazine, lomustine, and vincristine chemotherapy in newly diagnosed anaplastic oligodendroglioma: Long-term follow-up of EORTC brain tumor group study 26951," *Journal of Clinical Oncology*, vol. 31, no. 3, pp. 344–350, Jan. 2013, doi: 10.1200/JCO.2012.43.2229.

[101] G. Cairncross *et al.*, "Phase III trial of chemoradiotherapy for anaplastic oligodendroglioma: Long-term results of RTOG 9402," *Journal of Clinical Oncology*, vol. 31, no. 3, pp. 337–343, Jan. 2013, doi: 10.1200/JCO.2012.43.2674.

[102] B. G. Baumert *et al.*, "Temozolomide chemotherapy versus radiotherapy in high-risk low-grade glioma (EORTC 22033-26033): a randomised, open-label, phase 3 intergroup study," *Lancet Oncol*, vol. 17, no. 11, pp. 1521–1532, Nov. 2016, doi: 10.1016/S1470-2045(16)30313-8.

[103] J. C. Buckner *et al.*, "Radiation plus Procarbazine, CCNU, and Vincristine in Low-Grade Glioma," *New England Journal of Medicine*, vol. 374, no. 14, pp. 1344–1355, Apr. 2016, doi: 10.1056/NEJMoa1500925.

[104] A. Omuro *et al.*, " Radiotherapy combined with nivolumab or temozolomide for newly diagnosed glioblastoma with unmethylated MGMT promoter: An international randomized phase III trial ," *Neuro Oncol*, Apr. 2022, doi: 10.1093/neuonc/noac099.

[105] D. A. Reardon *et al.*, "Effect of Nivolumab vs Bevacizumab in Patients with Recurrent Glioblastoma: The CheckMate 143 Phase 3 Randomized Clinical Trial,"

JAMA Oncol, vol. 6, no. 7, pp. 1003–1010, Jul. 2020, doi: 10.1001/jamaoncol.2020.1024.

[106] M. Lim *et al.*, " Phase III trial of chemoradiotherapy with temozolomide plus nivolumab or placebo for newly diagnosed glioblastoma with methylated MGMT promoter ," *Neuro Oncol*, May 2022, doi: 10.1093/neuonc/noac116.

[107] C. Dehais *et al.*, "Revolumab: A phase II trial of nivolumab in recurrent IDH-mutant high-grade gliomas.," *Journal of Clinical Oncology*, vol. 40, no. 16_suppl, pp. 2048–2048, Jun. 2022, doi: 10.1200/jco.2022.40.16_suppl.2048.

[108] "Nivolumab in Patients With IDH-Mutant Gliomas With and Without Hypermutator Phenotype - Full Text View - ClinicalTrials.gov." https://clinicaltrials.gov/ct2/show/NCT03718767 (accessed Aug. 31, 2022).

[109] F. Klemm *et al.*, "Interrogation of the Microenvironmental Landscape in Brain Tumors Reveals Disease-Specific Alterations of Immune Cells," *Cell*, vol. 181, no. 7, pp. 1643-1660.e17, Jun. 2020, doi: 10.1016/j.cell.2020.05.007.

[110] E. Friebel *et al.*, "Single-Cell Mapping of Human Brain Cancer Reveals Tumor-Specific Instruction of Tissue-Invading Leukocytes," *Cell*, vol. 181, no. 7, pp. 1626-1642.e20, Jun. 2020, doi: 10.1016/j.cell.2020.04.055.

[111] A. M. van der Leun, D. S. Thommen, and T. N. Schumacher, "CD8+ T cell states in human cancer: insights from single-cell analysis," *Nature Reviews Cancer*, vol. 20, no. 4. Nature Research, pp. 218–232, Apr. 01, 2020. doi: 10.1038/s41568-019-0235-4.

[112] S. Xu, L. Tang, X. Li, F. Fan, and Z. Liu, "Immunotherapy for glioma: Current management and future application," *Cancer Letters*, vol. 476. Elsevier Ireland Ltd, pp. 1–12, Apr. 28, 2020. doi: 10.1016/j.canlet.2020.02.002.

[113] M. Zarei *et al.*, "Clinical development of IDH1 inhibitors for cancer therapy," *Cancer Treatment Reviews*, vol. 103. W.B. Saunders Ltd, Feb. 01, 2022. doi: 10.1016/j.ctrv.2021.102334.

[114] R. G. W. Verhaak *et al.*, "Integrated Genomic Analysis Identifies Clinically Relevant Subtypes of Glioblastoma Characterized by Abnormalities in PDGFRA, IDH1, EGFR, and NF1," *Cancer Cell*, vol. 17, no. 1, pp. 98–110, Jan. 2010, doi: 10.1016/j.ccr.2009.12.020.

[115] A. Murat *et al.*, "Stem cell-related 'self-renewal' signature and high epidermal growth factor receptor expression associated with resistance to concomitant chemoradiotherapy in glioblastoma," *Journal of Clinical Oncology*, vol. 26, no. 18, pp. 3015–3024, 2008, doi: 10.1200/JCO.2007.15.7164.

[116] Q. Wang *et al.*, "Tumor Evolution of Glioma-Intrinsic Gene Expression Subtypes Associates with Immunological Changes in the Microenvironment," *Cancer Cell*, vol. 32, no. 1, pp. 42-56.e6, Jul. 2017, doi:

10.1016/J.CCELL.2017.06.003/ATTACHMENT/5A2EEA38-BDF2-430C-AE8A-6C31DF4E96A2/MMC9.ZIP.

[117] J. Wang *et al.*, "Clonal evolution of glioblastoma under therapy," *Nature Genetics 2016 48:7*, vol. 48, no. 7, pp. 768–776, Jun. 2016, doi: 10.1038/ng.3590.

[118] A. Kamoun *et al.*, "Integrated multi-omics analysis of oligodendroglial tumours identifies three subgroups of 1p/19q co-deleted gliomas," *Nature Communications 2016 7:1*, vol. 7, no. 1, pp. 1–11, Apr. 2016, doi: 10.1038/ncomms11263.

[119] M. Ceccarelli *et al.*, "Molecular Profiling Reveals Biologically Discrete Subsets and Pathways of Progression in Diffuse Glioma," *Cell*, vol. 164, no. 3, pp. 550–563, Jan. 2016, doi: 10.1016/J.CELL.2015.12.028/ATTACHMENT/E17DB294-EEA4-47B8-8710-8AC63E95EA33/MMC6.XLSX.

[120] I. Tirosh *et al.*, "Single-cell RNA-seq supports a developmental hierarchy in human oligodendroglioma," *Nature*, vol. 539, no. 7628, pp. 309–313, Nov. 2016, doi: 10.1038/nature20123.

[121] A. S. Venteicher *et al.*, "Decoupling genetics, lineages, and microenvironment in IDH-mutant gliomas by single-cell RNA-seq," *Science (1979)*, vol. 355, no. 6332, Mar. 2017, doi: 10.1126/science.aai8478.

[122] C. Ruiz-Moreno *et al.*, "Harmonized single-cell landscape, intercellular crosstalk and tumor architecture of glioblastoma," Cold Spring Harbor Laboratory, Aug. 2022. doi: 10.1101/2022.08.27.505439.

[123] C. P. Couturier *et al.*, "Single-cell RNA-seq reveals that glioblastoma recapitulates a normal neurodevelopmental hierarchy," *Nat Commun*, vol. 11, no. 1, p. 3406, Dec. 2020, doi: 10.1038/s41467-020-17186-5.

[124] X. P. Xie *et al.*, "Quiescent human glioblastoma cancer stem cells drive tumor initiation, expansion, and recurrence following chemotherapy," *Dev Cell*, vol. 57, no. 1, pp. 32-46.e8, Jan. 2022, doi: 10.1016/j.devcel.2021.12.007.

[125] R. C. Gimple, K. Yang, M. E. Halbert, S. Agnihotri, and J. N. Rich, "Brain cancer stem cells: resilience through adaptive plasticity and hierarchical heterogeneity," *Nat Rev Cancer*, pp. 1–18, Jun. 2022, doi: 10.1038/s41568-022-00486-x.

[126] M. Castellan *et al.*, "Single-cell analyses reveal YAP/TAZ as regulators of stemness and cell plasticity in glioblastoma," *Nature Cancer 2020 2:2*, vol. 2, no. 2, pp. 174–188, Dec. 2020, doi: 10.1038/s43018-020-00150-z.

[127] L. M. Richards *et al.*, "Gradient of Developmental and Injury Response transcriptional states defines functional vulnerabilities underpinning glioblastoma heterogeneity," *Nature Cancer 2021 2:2*, vol. 2, no. 2, pp. 157–173, Jan. 2021, doi: 10.1038/s43018-020-00154-9.

[128] L. Garofano *et al.*, "Pathway-based classification of glioblastoma uncovers a mitochondrial subtype with therapeutic vulnerabilities," *Nature Cancer 2020 2:2*, vol. 2, no. 2, pp. 141–156, Jan. 2021, doi: 10.1038/s43018-020-00159-4.

[129] R. A. Cairns and T. W. Mak, "Oncogenic isocitrate dehydrogenase mutations: Mechanisms, models, and clinical opportunities," *Cancer Discovery*, vol. 3, no. 7. Cancer Discov, pp. 730–741, Jul. 2013. doi: 10.1158/2159-8290.CD-13-0083.

[130] C. J. Pirozzi and H. Yan, "The implications of IDH mutations for cancer development and therapy," *Nature Reviews Clinical Oncology*, vol. 18, no. 10. Nature Research, pp. 645–661, Oct. 01, 2021. doi: 10.1038/s41571-021-00521-0.

[131] L. Dang *et al.*, "Cancer-associated IDH1 mutations produce 2-hydroxyglutarate," *Nature*, vol. 462, no. 7274, pp. 739–744, Dec. 2009, doi: 10.1038/nature08617.

[132] A. Linninger *et al.*, "Modeling the diffusion of D-2-hydroxyglutarate from IDH1 mutant gliomas in the central nervous system," *Neuro Oncol*, vol. 20, no. 9, pp. 1197–1206, Aug. 2018, doi: 10.1093/neuonc/noy051.

[133] J. A. Losman, P. Koivunen, and W. G. Kaelin, "2-Oxoglutarate-dependent dioxygenases in cancer," *Nature Reviews Cancer*, vol. 20, no. 12. Nature Research, pp. 710–726, Dec. 01, 2020. doi: 10.1038/s41568-020-00303-3.

[134] A. A. Chakraborty *et al.*, "Histone demethylase KDM6A directly senses oxygen to control chromatin and cell fate," *Science (1979)*, vol. 363, no. 6432, pp. 1217–1222, Mar. 2019, doi: 10.1126/science.aaw1026.

[135] M. Batie, J. Frost, M. Frost, J. W. Wilson, P. Schofield, and S. Rocha, "Hypoxia induces rapid changes to histone methylation and reprograms chromatin," *Science (1979)*, vol. 363, no. 6432, pp. 1222–1226, 2019, doi: 10.1126/science.aau5870.

[136] T. Laukka *et al.*, "Fumarate and succinate regulate expression of hypoxia-inducible genes via TET enzymes," *Journal of Biological Chemistry*, vol. 291, no. 8, pp. 4256–4265, Feb. 2016, doi: 10.1074/jbc.M115.688762.

[137] B. Thienpont *et al.*, "Tumour hypoxia causes DNA hypermethylation by reducing TET activity," *Nature*, vol. 537, no. 7618, pp. 63–68, Sep. 2016, doi: 10.1038/nature19081.

[138] J. Barman-Aksözen, C. Béguin, A. M. Dogar, X. Schneider-Yin, and E. I. Minder, "Iron availability modulates aberrant splicing of ferrochelatase through the iron- and 2-oxoglutarate dependent dioxygenase Jmjd6 and U2AF65," *Blood Cells Mol Dis*, vol. 51, no. 3, pp. 151–161, Oct. 2013, doi: 10.1016/j.bcmd.2013.05.008.

[139] F. Neri *et al.*, "TET1 is a tumour suppressor that inhibits colon cancer growth by derepressing inhibitors of the WNT pathway," *Oncogene*, vol. 34, no. 32, pp. 4168–4176, Aug. 2015, doi: 10.1038/onc.2014.356.

[140] K. Yamamoto *et al.*, "Loss of histone demethylase KDM6B enhances aggressiveness of pancreatic cancer through downregulation of C/EBPα," *Carcinogenesis*, vol. 35, no. 11, pp. 2404–2414, Nov. 2014, doi: 10.1093/carcin/bgu136.

[141] M. Agathocleous *et al.*, "Ascorbate regulates haematopoietic stem cell function and leukaemogenesis," *Nature*, vol. 549, no. 7673, pp. 476–481, Sep. 2017, doi: 10.1038/nature23876.

[142] L. Cimmino *et al.*, "Restoration of TET2 Function Blocks Aberrant Self-Renewal and Leukemia Progression," *Cell*, vol. 170, no. 6, pp. 1079-1095.e20, Sep. 2017, doi: 10.1016/j.cell.2017.07.032.

[143] N. Shenoy *et al.*, "Ascorbic acid–induced TET activation mitigates adverse hydroxymethylcytosine loss in renal cell carcinoma," *Journal of Clinical Investigation*, vol. 129, no. 4, pp. 1612–1625, Apr. 2019, doi: 10.1172/JCI98747.

[144] G. Ge *et al.*, "Restoration of 5-hydroxymethylcytosine by ascorbate blocks kidney tumour growth," *EMBO Rep*, vol. 19, no. 8, Aug. 2018, doi: 10.15252/embr.201745401.

[145] B. A. Olenchock *et al.*, "EGLN1 Inhibition and Rerouting of α-Ketoglutarate Suffice for Remote Ischemic Protection," *Cell*, vol. 164, no. 5, pp. 884–895, Feb. 2016, doi: 10.1016/j.cell.2016.02.006.

[146] J. P. Morris *et al.*, "α-Ketoglutarate links p53 to cell fate during tumour suppression," *Nature*, vol. 573, no. 7775, pp. 595–599, Sep. 2019, doi: 10.1038/s41586-019-1577-5.

[147] R. L. Bowman and R. L. Levine, "TET2 in Normal and Malignant Hematopoiesis," *Cold Spring Harbor perspectives in medicine*, vol. 7, no. 8. Cold Spring Harbor Laboratory Press, p. a026518, Aug. 01, 2017. doi: 10.1101/cshperspect.a026518.

[148] X. Wu and Y. Zhang, "TET-mediated active DNA demethylation: Mechanism, function and beyond," *Nature Reviews Genetics*, vol. 18, no. 9. Nature Publishing Group, pp. 517–534, Sep. 01, 2017. doi: 10.1038/nrg.2017.33.

[149] E. Mahfoudhi *et al.*, "TET2-mediated 5-hydroxymethylcytosine induces genetic instability and mutagenesis," *DNA Repair (Amst)*, vol. 43, pp. 78–88, Jul. 2016, doi: 10.1016/j.dnarep.2016.05.031.

[150] M. E. Figueroa *et al.*, "Leukemic IDH1 and IDH2 Mutations Result in a Hypermethylation Phenotype, Disrupt TET2 Function, and Impair Hematopoietic Differentiation," *Cancer Cell*, vol. 18, no. 6, pp. 553–567, Dec. 2010, doi: 10.1016/j.ccr.2010.11.015.

[151] F. Farshidfar *et al.*, "Integrative Genomic Analysis of Cholangiocarcinoma Identifies Distinct IDH-Mutant Molecular Profiles," *Cell Rep*, vol. 18, no. 11, pp. 2780–2794, Mar. 2017, doi: 10.1016/j.celrep.2017.02.033.

[152] H. Noushmehr *et al.*, "Identification of a CpG Island Methylator Phenotype that Defines a Distinct Subgroup of Glioma," *Cancer Cell*, vol. 17, no. 5, pp. 510–522, May 2010, doi: 10.1016/j.ccr.2010.03.017.

[153] W. Xu *et al.*, "Oncometabolite 2-hydroxyglutarate is a competitive inhibitor of α-ketoglutarate-dependent dioxygenases," *Cancer Cell*, vol. 19, no. 1, pp. 17–30, Jan. 2011, doi: 10.1016/j.ccr.2010.12.014.

[154] S. Turcan *et al.*, "IDH1 mutation is sufficient to establish the glioma hypermethylator phenotype," *Nature*, vol. 483, no. 7390, pp. 479–483, Mar. 2012, doi: 10.1038/nature10866.

[155] M. E. Figueroa *et al.*, "Leukemic IDH1 and IDH2 Mutations Result in a Hypermethylation Phenotype, Disrupt TET2 Function, and Impair Hematopoietic Differentiation," *Cancer Cell*, vol. 18, no. 6, pp. 553–567, Dec. 2010, doi: 10.1016/j.ccr.2010.11.015.

[156] R. J. Molenaar and J. W. Wilmink, "IDH1/2 Mutations in Cancer Stem Cells and Their Implications for Differentiation Therapy," *Journal of Histochemistry and Cytochemistry*, vol. 70, no. 1. SAGE Publications Ltd, pp. 83–97, Jan. 01, 2022. doi: 10.1369/00221554211062499.

[157] W. A. Flavahan *et al.*, "Insulator dysfunction and oncogene activation in IDH mutant gliomas," *Nature*, vol. 529, no. 7584, pp. 110–114, Jan. 2016, doi: 10.1038/nature16490.

[158] A. S. Modrek *et al.*, "Low-Grade Astrocytoma Mutations in IDH1, P53, and ATRX Cooperate to Block Differentiation of Human Neural Stem Cells via Repression of SOX2," *Cell Rep*, vol. 21, no. 5, pp. 1267–1280, Oct. 2017, doi: 10.1016/j.celrep.2017.10.009.

[159] S. Turcan *et al.*, "IDH1 mutation is sufficient to establish the glioma hypermethylator phenotype," *Nature*, vol. 483, no. 7390, pp. 479–483, Mar. 2012, doi: 10.1038/nature10866.

[160] J. A. Losman *et al.*, "(R)-2-hydroxyglutarate is sufficient to promote leukemogenesis and its effects are reversible," *Science (1979)*, vol. 340, no. 6127, pp. 1621–1625, Mar. 2013, doi: 10.1126/science.1231677.

[161] F. Wang *et al.*, "Leukemia stemness and co-occurring mutations drive resistance to IDH inhibitors in acute myeloid leukemia," *Nat Commun*, vol. 12, no. 1, pp. 1–13, Dec. 2021, doi: 10.1038/s41467-021-22874-x.

[162] Y. Machida *et al.*, "A potent blood–brain barrier-permeable mutant IDH1 inhibitor suppresses the growth of glioblastoma with IDH1 mutation in a patient-derived orthotopic xenograft model," *Mol Cancer Ther*, vol. 19, no. 2, pp. 375–383, Feb. 2020, doi: 10.1158/1535-7163.MCT-18-1349.

[163] S. Pusch *et al.*, "Pan-mutant IDH1 inhibitor BAY 1436032 for effective treatment of IDH1 mutant astrocytoma in vivo," *Acta Neuropathol*, vol. 133, no. 4, pp. 629–644, Apr. 2017, doi: 10.1007/s00401-017-1677-y.

[164] D. Rohle *et al.*, "An Inhibitor of Mutant IDH1 Delays Growth and Promotes Differentiation of Glioma Cells," *Science (1979)*, vol. 340, no. 6132, pp. 626–630, May 2013, doi: 10.1126/science.1236062.

[165] A. Spitzer *et al.*, "Mutant IDH Inhibitors Induce Lineage Differentiation in IDH-mutant Oligodendroglioma," *medRxiv*, p. 2021.11.16.21266364, Nov. 2021, doi: 10.1101/2021.11.16.21266364.

[166] S. K. Saha *et al.*, "Mutant IDH inhibits HNF-4α to block hepatocyte differentiation and promote biliary cancer," *Nature*, vol. 513, no. 7516, pp. 110–152, Sep. 2014, doi: 10.1038/nature13441.

[167] C. Lu *et al.*, "IDH mutation impairs histone demethylation and results in a block to cell differentiation," *Nature*, vol. 483, no. 7390, pp. 474–478, Mar. 2012, doi: 10.1038/nature10860.

[168] Y. Jin *et al.*, "Mutant idh1 dysregulates the differentiation of mesenchymal stem cells in association with gene-specific histone modifications to cartilage- and bone-related genes," *PLoS One*, vol. 10, no. 7, Jul. 2015, doi: 10.1371/journal.pone.0131998.

[169] R. Su *et al.*, "R-2HG Exhibits Anti-tumor Activity by Targeting FTO/m6A/MYC/CEBPA Signaling," *Cell*, vol. 172, no. 1–2, pp. 90-105.e23, Jan. 2018, doi: 10.1016/j.cell.2017.11.031.

[170] Y. Qing *et al.*, "R-2-hydroxyglutarate attenuates aerobic glycolysis in leukemia by targeting the FTO/m6A/PFKP/LDHB axis," *Mol Cell*, vol. 81, no. 5, pp. 922-939.e9, Mar. 2021, doi: 10.1016/j.molcel.2020.12.026.

[171] S. Ohba, K. Kuwahara, S. Yamada, M. Abe, and Y. Hirose, "Correlation between IDH, ATRX, and TERT promoter mutations in glioma," *Brain Tumor Pathology*, vol. 37, no. 2. Springer, pp. 33–40, Apr. 01, 2020. doi: 10.1007/s10014-020-00360-4.

[172] P. L. Sulkowski *et al.*, "2-Hydroxyglutarate produced by neomorphic IDH mutations suppresses homologous recombination and induces PARP inhibitor sensitivity," *Sci Transl Med*, vol. 9, no. 375, Feb. 2017, doi: 10.1126/scitranslmed.aal2463.

[173] P. L. Sulkowski *et al.*, "Oncometabolites suppress DNA repair by disrupting local chromatin signalling," *Nature*, vol. 582, no. 7813, pp. 586–591, Jun. 2020, doi: 10.1038/s41586-020-2363-0.

[174] S. Inoue *et al.*, "Mutant IDH1 Downregulates ATM and Alters DNA Repair and Sensitivity to DNA Damage Independent of TET2," *Cancer Cell*, vol. 30, no. 2, pp. 337–348, Aug. 2016, doi: 10.1016/j.ccell.2016.05.018.

[175] P. Wang *et al.*, "Oncometabolite D-2-Hydroxyglutarate Inhibits ALKBH DNA Repair Enzymes and Sensitizes IDH Mutant Cells to Alkylating Agents," *Cell Rep*, vol. 13, no. 11, pp. 2353–2361, Dec. 2015, doi: 10.1016/j.celrep.2015.11.029.

[176] S. Ohba, J. Mukherjee, W. L. See, and R. O. Pieper, "Mutant IDH1-driven cellular transformation increases RAD51-mediated homologous recombination and temozolomide resistance," *Cancer Res*, vol. 74, no. 17, pp. 4836–4844, Sep. 2014, doi: 10.1158/0008-5472.CAN-14-0924.

[177] F. J. Núñez *et al.*, "IDH1-R132H acts as a tumor suppressor in glioma via epigenetic up-regulation of the DNA damage response," *Sci Transl Med*, vol. 11, no. 479, Feb. 2019, doi: 10.1126/scitranslmed.aaq1427.

[178] S. Zhao *et al.*, "Glioma-Derived Mutations in *IDH1* Dominantly Inhibit IDH1 Catalytic Activity and Induce HIF-1α," *Science (1979)*, vol. 324, no. 5924, pp. 261–265, Apr. 2009, doi: 10.1126/science.1170944.

[179] A. M. Intlekofer *et al.*, "Hypoxia Induces Production of L-2-Hydroxyglutarate," *Cell Metab*, vol. 22, no. 2, pp. 304–311, Aug. 2015, doi: 10.1016/j.cmet.2015.06.023.

[180] P. Koivunen *et al.*, "Transformation by the (R)-enantiomer of 2-hydroxyglutarate linked to EGLN activation," *Nature*, vol. 483, no. 7390, pp. 484–488, Mar. 2012, doi: 10.1038/nature10898.

[181] S. P. Burr *et al.*, "Mitochondrial Protein Lipoylation and the 2-Oxoglutarate Dehydrogenase Complex Controls HIF1α Stability in Aerobic Conditions," *Cell Metab*, vol. 24, no. 5, pp. 740–752, Nov. 2016, doi: 10.1016/j.cmet.2016.09.015.

[182] C. Sun *et al.*, "Isocitrate dehydrogenase1 mutation reduces the pericyte coverage of microvessels in astrocytic tumours," *J Neurooncol*, vol. 143, no. 2, pp. 187–196, Jun. 2019, doi: 10.1007/s11060-019-03156-5.

[183] A. M. Intlekofer *et al.*, "Hypoxia Induces Production of L-2-Hydroxyglutarate," *Cell Metab*, vol. 22, no. 2, pp. 304–311, Aug. 2015, doi: 10.1016/j.cmet.2015.06.023.

[184] R. Chowdhury *et al.*, "The oncometabolite 2-hydroxyglutarate inhibits histone lysine demethylases," *EMBO Rep*, vol. 12, no. 5, pp. 463–469, May 2011, doi: 10.1038/embor.2011.43.

[185] P. Koivunen *et al.*, "Transformation by the (R)-enantiomer of 2-hydroxyglutarate linked to EGLN activation," *Nature*, vol. 483, no. 7390, pp. 484–488, Mar. 2012, doi: 10.1038/nature10898.

[186] J. Polívka *et al.*, "IDH1 mutation is associated with lower expression of VEGF but not microvessel formation in glioblastoma multiforme," *Oncotarget*, vol. 9, no. 23, pp. 16462–16476, Mar. 2018, doi: 10.18632/oncotarget.24536.

[187] S. C. Williams, M. A. Karajannis, L. Chiriboga, J. G. Golfinos, A. von Deimling, and D. Zagzag, "R132H-mutation of isocitrate dehydrogenase-1 is not sufficient for

HIF-1α upregulation in adult glioma," *Acta Neuropathol*, vol. 121, no. 2, pp. 279–281, Feb. 2011, doi: 10.1007/s00401-010-0790-y.

[188] B. Blouw *et al.*, "The hypoxic response of tumors is dependent on their microenvironment," *Cancer Cell*, vol. 4, no. 2, pp. 133–146, Aug. 2003, doi: 10.1016/S1535-6108(03)00194-6.

[189] H. Tarhonskaya *et al.*, "Non-enzymatic chemistry enables 2-hydroxyglutarate-mediated activation of 2-oxoglutarate oxygenases," *Nat Commun*, vol. 5, Mar. 2014, doi: 10.1038/ncomms4423.

[190] Y. Liu *et al.*, "IDH1 mutations inhibit multiple α-ketoglutarate-dependent dioxygenase Activities in astroglioma," *J Neurooncol*, vol. 109, no. 2, pp. 253–260, Sep. 2012, doi: 10.1007/s11060-012-0914-4.

[191] X. Wang *et al.*, "SLC1A1-mediated cellular and mitochondrial influx of R-2-hydroxyglutarate in vascular endothelial cells promotes tumor angiogenesis in IDH1-mutant solid tumors," *Cell Res*, vol. 32, no. 7, pp. 638–658, Jul. 2022, doi: 10.1038/s41422-022-00650-w.

[192] X. Fu *et al.*, "2-hydroxyglutarate inhibits ATP synthase and mTOR Signaling," *Cell Metab*, vol. 22, no. 3, pp. 508–515, Sep. 2015, doi: 10.1016/j.cmet.2015.06.009.

[193] M. R. Gilbert *et al.*, "Autophagy and oxidative stress in gliomas with IDH1 mutations," *Acta Neuropathol*, vol. 127, no. 2, pp. 221–233, Feb. 2014, doi: 10.1007/s00401-013-1194-6.

[194] J. Shi *et al.*, "Decreasing GSH and increasing ROS in chemosensitivity gliomas with IDH1 mutation," *Tumor Biology*, vol. 36, no. 2, pp. 655–662, Feb. 2015, doi: 10.1007/s13277-014-2644-z.

[195] K. Tateishi *et al.*, "Extreme Vulnerability of IDH1 Mutant Cancers to NAD+ Depletion," *Cancer Cell*, vol. 28, no. 6, pp. 773–784, Dec. 2015, doi: 10.1016/j.ccell.2015.11.006.

[196] K. Tateishi *et al.*, "The alkylating chemotherapeutic temozolomide induces metabolic stress in IDH1-mutant cancers and potentiates NAD+ depletion-mediated cytotoxicity," *Cancer Res*, vol. 77, no. 15, pp. 4102–4115, Aug. 2017, doi: 10.1158/0008-5472.CAN-16-2263.

[197] H. Nagashima *et al.*, "Poly(ADP-ribose) glycohydrolase inhibition sequesters NAD+ to potentiate the metabolic lethality of alkylating chemotherapy in IDH-mutant tumor cells," *Cancer Discov*, vol. 10, no. 11, pp. 1673–1689, Nov. 2020, doi: 10.1158/2159-8290.CD-20-0226.

[198] D. Yu *et al.*, "Triptolide suppresses IDH1-mutated malignancy via Nrf2-driven glutathione metabolism," *Proc Natl Acad Sci U S A*, vol. 117, no. 18, pp. 9964–9972, May 2020, doi: 10.1073/pnas.1913633117.

[199] X. Tang, X. Fu, Y. Liu, D. Yu, S. J. Cai, and C. Yang, "Blockade of glutathione metabolism in IDH1-mutated glioma," *Mol Cancer Ther*, vol. 19, no. 1, pp. 221–230, Jan. 2020, doi: 10.1158/1535-7163.MCT-19-0103.

[200] S. K. McBrayer *et al.*, "Transaminase Inhibition by 2-Hydroxyglutarate Impairs Glutamate Biosynthesis and Redox Homeostasis in Glioma," *Cell*, vol. 175, no. 1, pp. 101-116.e25, Sep. 2018, doi: 10.1016/j.cell.2018.08.038.

[201] M. Tönjes *et al.*, "BCAT1 promotes cell proliferation through amino acid catabolism in gliomas carrying wild-type IDH1," *Nat Med*, vol. 19, no. 7, pp. 901–908, Jul. 2013, doi: 10.1038/nm.3217.

[202] J. Biedermann *et al.*, "Mutant IDH1 differently affects redox state and metabolism in glial cells of normal and tumor origin," *Cancers (Basel)*, vol. 11, no. 12, Dec. 2019, doi: 10.3390/cancers11122028.

[203] S. M. Chan *et al.*, "Isocitrate dehydrogenase 1 and 2 mutations induce BCL-2 dependence in acute myeloid leukemia," *Nat Med*, vol. 21, no. 2, pp. 178–184, Jan. 2015, doi: 10.1038/nm.3788.

[204] F. Li *et al.*, "NADP+-IDH Mutations Promote Hypersuccinylation that Impairs Mitochondria Respiration and Induces Apoptosis Resistance," *Mol Cell*, vol. 60, no. 4, pp. 661–675, Nov. 2015, doi: 10.1016/j.molcel.2015.10.017.

[205] G. Karpel-Massler *et al.*, "Induction of synthetic lethality in IDH1-mutated gliomas through inhibition of Bcl-xL," *Nat Commun*, vol. 8, no. 1, Dec. 2017, doi: 10.1038/s41467-017-00984-9.

[206] C. S. Constantinescu, N. Farooqi, K. O'Brien, and B. Gran, "Experimental autoimmune encephalomyelitis (EAE) as a model for multiple sclerosis (MS)," *Br J Pharmacol*, vol. 164, no. 4, pp. 1079–1106, Oct. 2011, doi: 10.1111/j.1476-5381.2011.01302.x.

[207] H. Mestre *et al.*, "Cerebrospinal fluid influx drives acute ischemic tissue swelling," *Science (1979)*, vol. 367, no. 6483, Mar. 2020, doi: 10.1126/science.aaw7462.

[208] R. Tamura, K. Yoshida, and M. Toda, "Current understanding of lymphatic vessels in the central nervous system," *Neurosurgical Review*, vol. 43, no. 4. Springer, pp. 1055–1064, Aug. 01, 2020. doi: 10.1007/s10143-019-01133-0.

[209] F. E. Pulous *et al.*, "Cerebrospinal fluid outflow through skull channels instructs cranial hematopoiesis," *bioRxiv*, p. 2021.08.27.457954, Aug. 2021, doi: 10.1101/2021.08.27.457954.

[210] S. Watkins, S. Robel, I. F. Kimbrough, S. M. Robert, G. Ellis-Davies, and H. Sontheimer, "Disruption of astrocyte–vascular coupling and the blood–brain barrier by invading glioma cells," *Nat Commun*, vol. 5, no. 1, p. 4196, Sep. 2014, doi: 10.1038/ncomms5196.

[211] J. N. Sarkaria *et al.*, "Is the blood-brain barrier really disrupted in all glioblastomas? A critical assessment of existing clinical data," *Neuro Oncol*, vol. 20, no. 2, pp. 184–191, Jan. 2018, doi: 10.1093/neuonc/nox175.

[212] F. Ginhoux *et al.*, "Fate mapping analysis reveals that adult microglia derive from primitive macrophages," *Science (1979)*, vol. 330, no. 6005, pp. 841–845, Nov. 2010, doi: 10.1126/science.1194637.

[213] L. Geirsdottir *et al.*, "Cross-Species Single-Cell Analysis Reveals Divergence of the Primate Microglia Program," *Cell*, vol. 179, no. 7, pp. 1609-1622.e16, Dec. 2019, doi: 10.1016/j.cell.2019.11.010.

[214] P. Füger *et al.*, "Microglia turnover with aging and in an Alzheimer's model via long-term in vivo single-cell imaging," *Nat Neurosci*, vol. 20, no. 10, pp. 1371–1376, Oct. 2017, doi: 10.1038/nn.4631.

[215] T. L. Tay *et al.*, "A new fate mapping system reveals context-dependent random or clonal expansion of microglia," *Nat Neurosci*, vol. 20, no. 6, pp. 793–803, Jun. 2017, doi: 10.1038/nn.4547.

[216] M. Prinz, S. Jung, and J. Priller, "Microglia Biology: One Century of Evolving Concepts," *Cell*, vol. 179, no. 2. Cell Press, pp. 292–311, Oct. 03, 2019. doi: 10.1016/j.cell.2019.08.053.

[217] D. Mrdjen *et al.*, "High-Dimensional Single-Cell Mapping of Central Nervous System Immune Cells Reveals Distinct Myeloid Subsets in Health, Aging, and Disease," *Immunity*, vol. 48, no. 2, pp. 380-395.e6, Feb. 2018, doi: 10.1016/j.immuni.2018.01.011.

[218] A. Cugurra *et al.*, "Skull and vertebral bone marrow are myeloid cell reservoirs for the meninges and CNS parenchyma," *Science (1979)*, vol. 373, no. 6553, Jul. 2021, doi: 10.1126/science.abf7844.

[219] T. J. Alban *et al.*, "Global immune fingerprinting in glioblastoma patient peripheral blood reveals immune-suppression signatures associated with prognosis," *JCI Insight*, vol. 3, no. 21, Nov. 2018, doi: 10.1172/jci.insight.122264.

[220] S. Müller *et al.*, "Single-cell profiling of human gliomas reveals macrophage ontogeny as a basis for regional differences in macrophage activation in the tumor microenvironment," *Genome Biol*, vol. 18, no. 1, p. 234, Dec. 2017, doi: 10.1186/s13059-017-1362-4.

[221] R. L. Bowman *et al.*, "Macrophage Ontogeny Underlies Differences in Tumor-Specific Education in Brain Malignancies," *Cell Rep*, vol. 17, no. 9, pp. 2445–2459, Nov. 2016, doi: 10.1016/j.celrep.2016.10.052.

[222] Q. Li and B. A. Barres, "Microglia and macrophages in brain homeostasis and disease," *Nature Reviews Immunology*, vol. 18, no. 4. Nature Publishing Group, pp. 225–242, Apr. 01, 2018. doi: 10.1038/nri.2017.125.

[223] "Home :: Ivy Glioblastoma Atlas Project." http://glioblastoma.alleninstitute.org/ (accessed Jul. 26, 2022).

[224] S. Darmanis *et al.*, "Single-Cell RNA-Seq Analysis of Infiltrating Neoplastic Cells at the Migrating Front of Human Glioblastoma," *Cell Rep*, vol. 21, no. 5, pp. 1399–1410, Oct. 2017, doi: 10.1016/j.celrep.2017.10.030.

[225] Z. Chen, J. L. Ross, and D. Hambardzumyan, "Intravital 2-photon imaging reveals distinct morphology and infiltrative properties of glioblastoma-associated macrophages," *Proc Natl Acad Sci U S A*, vol. 116, no. 28, pp. 14254–14259, Jul. 2019, doi: 10.1073/pnas.1902366116.

[226] A. R. Pombo Antunes *et al.*, "Single-cell profiling of myeloid cells in glioblastoma across species and disease stage reveals macrophage competition and specialization," *Nat Neurosci*, vol. 24, no. 4, pp. 595–610, Apr. 2021, doi: 10.1038/s41593-020-00789-y.

[227] A. S. Venteicher *et al.*, "Decoupling genetics, lineages, and microenvironment in IDH-mutant gliomas by single-cell RNA-seq," *Science (1979)*, vol. 355, no. 6332, Mar. 2017, doi: 10.1126/science.aai8478.

[228] N. Abdelfattah *et al.*, "Single-cell analysis of human glioma and immune cells identifies S100A4 as an immunotherapy target," *Nat Commun*, vol. 13, no. 1, pp. 1–18, Dec. 2022, doi: 10.1038/s41467-022-28372-y.

[229] J. K. Sa *et al.*, "Transcriptional regulatory networks of tumor-associated macrophages that drive malignancy in mesenchymal glioblastoma," *Genome Biol*, vol. 21, no. 1, p. 216, Dec. 2020, doi: 10.1186/s13059-020-02140-x.

[230] A. X. Chen *et al.*, "Single-cell characterization of macrophages in glioblastoma reveals MARCO as a mesenchymal pro-tumor marker," *Genome Med*, vol. 13, no. 1, p. 88, Dec. 2021, doi: 10.1186/s13073-021-00906-x.

[231] S. Coy *et al.*, "Single Cell Spatial Analysis Reveals the Topology of Immunomodulatory Purinergic Signaling in Glioblastoma," *bioRxiv*, p. 2022.01.12.475925, Jan. 2022, doi: 10.1101/2022.01.12.475925.

[232] S. Goswami *et al.*, "Immune profiling of human tumors identifies CD73 as a combinatorial target in glioblastoma," *Nat Med*, vol. 26, no. 1, pp. 39–46, Jan. 2020, doi: 10.1038/s41591-019-0694-x.

[233] T. Hara *et al.*, "Interactions between cancer cells and immune cells drive transitions to mesenchymal-like states in glioblastoma," *Cancer Cell*, vol. 39, no. 6, pp. 779-792.e11, Jun. 2021, doi: 10.1016/j.ccell.2021.05.002.

[234] B. M. Andersen, C. Faust Akl, M. A. Wheeler, E. A. Chiocca, D. A. Reardon, and F. J. Quintana, "Glial and myeloid heterogeneity in the brain tumour microenvironment," *Nature Reviews Cancer*, vol. 21, no. 12. Nature Research, pp. 786–802, Dec. 01, 2021. doi: 10.1038/s41568-021-00397-3.

[235] S. D. MILLER, E. J. MCMAHON, B. SCHREINER, and S. L. BAILEY, "Antigen Presentation in the CNS by Myeloid Dendritic Cells Drives Progression of Relapsing Experimental Autoimmune Encephalomyelitis," *Ann N Y Acad Sci*, vol. 1103, no. 1, pp. 179–191, Mar. 2007, doi: 10.1196/annals.1394.023.

[236] J. Yan *et al.*, "Correction to: FGL2 promotes tumor progression in the CNS by suppressing CD103+ dendritic cell differentiation (Nature Communications, (2019), 10, 1, (448), 10.1038/s41467-018-08271-x)," *Nature Communications*, vol. 10, no. 1. Nature Publishing Group, pp. 1–1, Dec. 01, 2019. doi: 10.1038/s41467-019-08770-5.

[237] Y. Akasaki, G. Liu, N. H. C. Chung, M. Ehtesham, K. L. Black, and J. S. Yu, " Induction of a CD4 + T Regulatory Type 1 Response by Cyclooxygenase-2-Overexpressing Glioma ," *The Journal of Immunology*, vol. 173, no. 7, pp. 4352–4359, Oct. 2004, doi: 10.4049/jimmunol.173.7.4352.

[238] J. Wang, P. Liu, S. Xin, Z. Wang, and J. Li, "Nrf2 suppresses the function of dendritic cells to facilitate the immune escape of glioma cells," *Exp Cell Res*, vol. 360, no. 2, pp. 66–73, Nov. 2017, doi: 10.1016/j.yexcr.2017.07.031.

[239] A. de Leo, A. Ugolini, and F. Veglia, "Myeloid cells in glioblastoma microenvironment," *Cells*, vol. 10, no. 1. MDPI, pp. 1–20, Jan. 01, 2021. doi: 10.3390/cells10010018.

[240] T. Condamine *et al.*, "Lectin-type oxidized LDL receptor-1 distinguishes population of human polymorphonuclear myeloid-derived suppressor cells in cancer patients," *Sci Immunol*, vol. 1, no. 2, Aug. 2016, doi: 10.1126/sciimmunol.aaf8943.

[241] E. Chai, L. Zhang, and C. Li, "LOX-1+ PMN-MDSC enhances immune suppression which promotes glioblastoma multiforme progression," *Cancer Manag Res*, vol. 11, pp. 7307–7315, 2019, doi: 10.2147/CMAR.S210545.

[242] M. Massara *et al.*, "Neutrophils in gliomas," *Front Immunol*, vol. 8, no. OCT, p. 1349, Oct. 2017, doi: 10.3389/fimmu.2017.01349.

[243] A. Schernberg *et al.*, "Neutrophilia as a biomarker for overall survival in newly diagnosed high-grade glioma patients undergoing chemoradiation," *Clin Transl Radiat Oncol*, vol. 10, pp. 47–52, Mar. 2018, doi: 10.1016/j.ctro.2018.04.002.

[244] A. Rahbar *et al.*, "Enhanced neutrophil activity is associated with shorter time to tumor progression in glioblastoma patients," *Oncoimmunology*, vol. 5, no. 2, Feb. 2016, doi: 10.1080/2162402X.2015.1075693.

[245] J. Liang *et al.*, "Neutrophils promote the malignant glioma phenotype through S100A4," *Clinical Cancer Research*, vol. 20, no. 1, pp. 187–198, Jan. 2014, doi: 10.1158/1078-0432.CCR-13-1279.

[246] A. Manda-Handzlik and U. Demkow, "The Brain Entangled: The Contribution of Neutrophil Extracellular Traps to the Diseases of the Central Nervous System," *Cells*, vol. 8, no. 12, p. 1477, Nov. 2019, doi: 10.3390/cells8121477.

[247] T. R. Sippel *et al.*, "Neutrophil degranulation and immunosuppression in patients with GBM: Restoration of cellular immune function by targeting arginase I," *Clinical Cancer Research*, vol. 17, no. 22, pp. 6992–7002, Nov. 2011, doi: 10.1158/1078-0432.CCR-11-1107.

[248] P. P. Yee *et al.*, "Neutrophil-induced ferroptosis promotes tumor necrosis in glioblastoma progression," *Nat Commun*, vol. 11, no. 1, Dec. 2020, doi: 10.1038/s41467-020-19193-y.

[249] N. D. Mathewson *et al.*, "Inhibitory CD161 receptor identified in glioma-infiltrating T cells by single-cell analysis," *Cell*, vol. 184, no. 5, pp. 1281-1298.e26, Mar. 2021, doi: 10.1016/j.cell.2021.01.022.

[250] N. M. Amankulor *et al.*, "Mutant IDH1 regulates the tumor-associated immune system in gliomas," 2017, doi: 10.1101/gad.294991.116.

[251] M. S. Alghamri *et al.*, "G-CSF secreted by mutant IDH1 glioma stem cells abolishes myeloid cell immunosuppression and enhances the efficacy of immunotherapy," *Sci Adv*, vol. 7, no. 40, pp. 3243–3272, Oct. 2021, doi: 10.1126/sciadv.abh3243.

[252] X. Zhang *et al.*, "IDH mutant gliomas escape natural killer cell immune surveillance by downregulation of NKG2D ligand expression," *Neuro Oncol*, vol. 18, no. 10, pp. 1402–1412, 2016, doi: 10.1093/neuonc/now061.

[253] S. Luoto *et al.*, "TITLE: Computational characterization of suppressive immune microenvironments in glioblastoma", doi: 10.1158/0008-5472.CAN-17-3714.

[254] F. Ren *et al.*, "The R132H mutation in <scp>IDH</scp> 1 promotes the recruitment of <scp>NK</scp> cells through <scp>CX</scp> 3 <scp>CL</scp> 1/ <scp>CX</scp> 3 <scp>CR</scp> 1 chemotaxis and is correlated with a better prognosis in gliomas," *Immunol Cell Biol*, vol. 97, no. 5, pp. 457–469, May 2019, doi: 10.1111/imcb.12225.

[255] L. Mu *et al.*, "The IDH1 mutation-induced oncometabolite, 2-hydroxyglutarate, may affect DNA methylation and expression of PD-L1 in gliomas," *Front Mol Neurosci*, vol. 11, p. 82, Mar. 2018, doi: 10.3389/fnmol.2018.00082.

[256] L. Zhang, M. D. Sorensen, B. W. Kristensen, G. Reifenberger, T. M. Mcintyre, and F. Lin, "D-2-hydroxyglutarate is an intercellular mediator in IDH-mutant gliomas inhibiting complement and T cells," *Clin Cancer Res*, vol. 24, no. 21, pp. 5381–5391, 2018, doi: 10.1158/1078-0432.CCR-17-3855.

[257] M. Friedrich *et al.*, "Tryptophan metabolism drives dynamic immunosuppressive myeloid states in IDH-mutant gliomas," *Nat Cancer*, vol. 2, no. 7, pp. 723–740, Jul. 2021, doi: 10.1038/s43018-021-00201-z.

[258] C. jun Han *et al.*, "The oncometabolite 2-hydroxyglutarate inhibits microglial activation via the AMPK/mTOR/NF-κB pathway," *Acta Pharmacol Sin*, vol. 40, no. 10, pp. 1292–1302, Oct. 2019, doi: 10.1038/s41401-019-0225-9.

[259] I. Ugele *et al.*, "D-2-hydroxyglutarate and L-2-hydroxyglutarate inhibit IL-12 secretion by human monocyte-derived dendritic cells," *Int J Mol Sci*, vol. 20, no. 3, Feb. 2019, doi: 10.3390/ijms20030742.

[260] M. Friedrich *et al.*, "Dysfunctional dendritic cells limit antigen-specific T cell response in glioma," *Neuro Oncol*, May 2022, doi: 10.1093/neuonc/noac138.

[261] G. Kohanbash *et al.*, "Isocitrate dehydrogenase mutations suppress STAT1 and CD8+ T cell accumulation in gliomas," *Journal of Clinical Investigation*, vol. 127, no. 4, pp. 1425–1437, Apr. 2017, doi: 10.1172/JCI90644.

[262] L. G. Richardson *et al.*, "IDH-mutant gliomas harbor fewer regulatory T cells in humans and mice," *Oncoimmunology*, vol. 9, no. 1, Jan. 2020, doi: 10.1080/2162402X.2020.1806662.

[263] L. Bunse *et al.*, "Suppression of antitumor T cell immunity by the oncometabolite (R)-2-hydroxyglutarate," *Nat Med*, vol. 24, no. 8, pp. 1192–1203, Aug. 2018, doi: 10.1038/s41591-018-0095-6.

[264] M. Böttcher *et al.*, "D-2-hydroxyglutarate interferes with HIF-1α stability skewing T-cell metabolism towards oxidative phosphorylation and impairing Th17 polarization," *Oncoimmunology*, vol. 7, no. 7, Jul. 2018, doi: 10.1080/2162402X.2018.1445454.

[265] T. Xu *et al.*, "Metabolic control of TH17 and induced Treg cell balance by an epigenetic mechanism," *Nature*, vol. 548, no. 7666, pp. 228–233, Aug. 2017, doi: 10.1038/nature23475.

[266] L. Sun *et al.*, "Particulate matter of 2.5 μm or less in diameter disturbs the balance of TH17/regulatory T cells by targeting glutamate oxaloacetate transaminase 1 and hypoxia-inducible factor 1α in an asthma model," *Journal of Allergy and Clinical Immunology*, vol. 145, no. 1, pp. 402–414, Jan. 2020, doi: 10.1016/j.jaci.2019.10.008.

[267] D. Rohle *et al.*, "An inhibitor of mutant IDH1 delays growth and promotes differentiation of glioma cells," *Science (1979)*, vol. 340, no. 6132, pp. 626–630, May 2013, doi: 10.1126/science.1236062.

[268] P.-P. Zheng, M. van der Weiden, P. J. van der Spek, A. J. P. E. Vincent, and J. M. Kros, "Isocitrate dehydrogenase 1R132H mutation in microglia/macrophages in gliomas Indication of a significant role of microglia/macrophages in glial tumorigenesis," *Cancer Biol Ther*, vol. 13, no. 10, pp. 836–839, 2012, doi: 10.4161/cbt.20836.

[269] H. Binder *et al.*, "DNA methylation, transcriptome and genetic copy number signatures of diffuse cerebral WHO grade II/III gliomas resolve cancer heterogeneity and development," *Acta Neuropathol Commun*, vol. 7, no. 1, p. 59, Apr. 2019, doi: 10.1186/s40478-019-0704-8.

[270] J. Klughammer *et al.*, "The DNA methylation landscape of glioblastoma disease progression shows extensive heterogeneity in time and space," *Nat Med*, vol. 24, no. 10, pp. 1611–1624, Oct. 2018, doi: 10.1038/s41591-018-0156-x.

[271] H. Binder, M. Schmidt, L. Hopp, S. Davitavyan, A. Arakelyan, and H. Loeffler-Wirth, "Integrated Multi-Omics Maps of Lower-Grade Gliomas," *Cancers (Basel)*, vol. 14, no. 11, Jun. 2022, doi: 10.3390/cancers14112797.

[272] M. B. Stadler *et al.*, "DNA-binding factors shape the mouse methylome at distal regulatory regions," *Nature*, vol. 480, no. 7378, pp. 490–495, Dec. 2011, doi: 10.1038/nature10716.

[273] S. Pundhir *et al.*, "Enhancer and Transcription Factor Dynamics during Myeloid Differentiation Reveal an Early Differentiation Block in Cebpa null Progenitors," *Cell Rep*, vol. 23, no. 9, pp. 2744–2757, May 2018, doi: 10.1016/j.celrep.2018.05.012.

[274] R. L. Bowman *et al.*, "Macrophage Ontogeny Underlies Differences in Tumor-Specific Education in Brain Malignancies," *Cell Rep*, vol. 17, no. 9, pp. 2445–2459, Nov. 2016, doi: 10.1016/j.celrep.2016.10.052.

[275] D. Lau, A. M. Bobe, and A. A. Khan, "RNA Sequencing of the Tumor Microenvironment in Precision Cancer Immunotherapy," *Trends in Cancer*, vol. 5, no. 3. Cell Press, pp. 149–156, Mar. 01, 2019. doi: 10.1016/j.trecan.2019.02.006.

[276] T. Hara *et al.*, "Interactions between cancer cells and immune cells drive transitions to mesenchymal-like states in glioblastoma," *Cancer Cell*, vol. 39, no. 6, pp. 779-792.e11, Jun. 2021, doi: 10.1016/j.ccell.2021.05.002.

[277] E. Gangoso *et al.*, "Glioblastomas acquire myeloid-affiliated transcriptional programs via epigenetic immunoediting to elicit immune evasion," *Cell*, vol. 184, no. 9, pp. 2454-2470.e26, Apr. 2021, doi: 10.1016/j.cell.2021.03.023.

[278] F. P. Caruso *et al.*, "A map of tumor-host interactions in glioma at single-cell resolution," *Gigascience*, vol. 9, no. 10, pp. 1–14, 2020, doi: 10.1093/GIGASCIENCE/GIAA109.

[279] H. Zhu, X. Yu, S. Zhang, and K. Shu, "Targeting the Complement Pathway in Malignant Glioma Microenvironments," *Frontiers in Cell and Developmental Biology*, vol. 9. Frontiers Media S.A., Apr. 01, 2021. doi: 10.3389/fcell.2021.657472.

[280] R. Chaligne *et al.*, "Epigenetic encoding, heritability and plasticity of glioma transcriptional cell states," *Nat Genet*, vol. 53, no. 10, pp. 1469–1479, Oct. 2021, doi: 10.1038/s41588-021-00927-7.

[281] R. M. Rodriguez, B. Suarez-Alvarez, J. L. Lavín, M. J. Araú Zo-Bravo, A. M. Aransay, and C. Lopez-Larrea, "Signal Integration and Transcriptional Regulation of the Inflammatory Response Mediated by the GM-/M-CSF Signaling Axis in Human Monocytes," *CellReports*, vol. 29, pp. 860-872.e5, 2019, doi: 10.1016/j.celrep.2019.09.035.

[282] L. Cassetta *et al.*, "Human Tumor-Associated Macrophage and Monocyte Transcriptional Landscapes Reveal Cancer-Specific Reprogramming, Biomarkers, and Therapeutic Targets," *Cancer Cell*, vol. 35, no. 4, pp. 588-602.e10, Apr. 2019, doi: 10.1016/j.ccell.2019.02.009.

[283] Y. Lavin *et al.*, "Tissue-resident macrophage enhancer landscapes are shaped by the local microenvironment," *Cell*, vol. 159, no. 6, pp. 1312–1326, Dec. 2014, doi: 10.1016/j.cell.2014.11.018.

[284] C. F. de Souza *et al.*, "A Distinct DNA Methylation Shift in a Subset of Glioma CpG Island Methylator Phenotypes during Tumor Recurrence," *Cell Rep*, vol. 23, no. 2, pp. 637–651, Apr. 2018, doi: 10.1016/j.celrep.2018.03.107.

[285] R. Chanoch-Myers, A. Wider, M. L. Suva, and I. Tirosh, "Elucidating the diversity of malignant mesenchymal states in glioblastoma by integrative analysis," *Genome Med*, vol. 14, no. 1, p. 106, Sep. 2022, doi: 10.1186/s13073-022-01109-8.

[286] M. Friedrich *et al.*, "Tryptophan metabolism drives dynamic immunosuppressive myeloid states in IDH-mutant gliomas," *Nat Cancer*, vol. 2, no. 7, pp. 723–740, Jul. 2021, doi: 10.1038/s43018-021-00201-z.

[287] B. N. Devaiah and D. S. Singer, "CIITA and its dual roles in MHC gene transcription," *Front Immunol*, vol. 4, no. DEC, p. 476, 2013, doi: 10.3389/fimmu.2013.00476.

[288] R. S. Accolla, E. Ramia, A. Tedeschi, and G. Forlani, "CIITA-Driven MHC Class II Expressing Tumor Cells as Antigen Presenting Cell Performers: Toward the Construction of an Optimal Anti-tumor Vaccine," *Front Immunol*, vol. 10, p. 1806, Jul. 2019, doi: 10.3389/fimmu.2019.01806.

[289] P. Chuntova *et al.*, "Inhibition of D-2HG leads to upregulation of a proinflammatory gene signature in a novel HLA-A2/HLA-DR1 transgenic mouse model of IDH1R132H-expressing glioma," *J Immunother Cancer*, vol. 10, no. 5, p. 4644, May 2022, doi: 10.1136/jitc-2022-004644.

[290] G. C. Hon *et al.*, "5mC oxidation by Tet2 modulates enhancer activity and timing of transcriptome reprogramming during differentiation," *Mol Cell*, vol. 56, no. 2, pp. 286–297, Oct. 2014, doi: 10.1016/j.molcel.2014.08.026.

[291] A. Amorim *et al.*, "IFNγ and GM-CSF control complementary differentiation programs in the monocyte-to-phagocyte transition during neuroinflammation,"

Nat Immunol, vol. 23, no. 2, pp. 217–228, Feb. 2022, doi: 10.1038/s41590-021-01117-7.

[292] H. I. McFarland, S. R. Nahill, J. W. Maciaszek, and R. M. Welsh, "CD11b (Mac-1): a marker for CD8+ cytotoxic T cell activation and memory in virus infection.," *The Journal of Immunology*, vol. 149, no. 4, 1992.

[293] S. Fiorentini *et al.*, " CD11b Expression Identifies CD8 + CD28 + T Lymphocytes with Phenotype and Function of Both Naive/Memory and Effector Cells ," *The Journal of Immunology*, vol. 166, no. 2, pp. 900–907, Jan. 2001, doi: 10.4049/jimmunol.166.2.900.

[294] J. E. Christensen, S. Ø. Andreasen, J. P. Christensen, and A. R. Thomsen, "CD11b expression as a marker to distinguish between recently activated effector CD8+ T cells and memory cells," *Int Immunol*, vol. 13, no. 4, pp. 593–600, Apr. 2001, doi: 10.1093/intimm/13.4.593.

[295] A. P. Landry, M. Balas, S. Alli, J. Spears, and Z. Zador, "Distinct regional ontogeny and activation of tumor associated macrophages in human glioblastoma," *Sci Rep*, vol. 10, no. 1, p. 19542, Dec. 2020, doi: 10.1038/s41598-020-76657-3.

[296] V. Fedyuk *et al.*, "Multiplexed, single-molecule, epigenetic analysis of plasma-isolated nucleosomes for cancer diagnostics," *Nat Biotechnol*, pp. 1–10, Sep. 2022, doi: 10.1038/s41587-022-01447-3.

[297] N. Furth *et al.*, "H3-K27M-mutant nucleosomes interact with MLL1 to shape the glioma epigenetic landscape," *Cell Rep*, vol. 39, no. 7, May 2022, doi: 10.1016/j.celrep.2022.110836.

[298] K. F. Dekkers, A. E. Neele, J. W. Jukema, B. T. Heijmans, and M. P. J. de Winther, "Human monocyte-to-macrophage differentiation involves highly localized gain and loss of DNA methylation at transcription factor binding sites," *Epigenetics Chromatin*, vol. 12, no. 1, p. 34, Dec. 2019, doi: 10.1186/s13072-019-0279-4.

[299] M. Klug, S. Schmidhofer, C. Gebhard, R. Andreesen, and M. Rehli, "5-Hydroxymethylcytosine is an essential intermediate of active DNA demethylation processes in primary human monocytes," *Genome Biol*, vol. 14, no. 5, p. R46, May 2013, doi: 10.1186/gb-2013-14-5-r46.

[300] L. Zhang, M. D. Sorensen, B. W. Kristensen, G. Reifenberger, T. M. McIntyre, and F. Lin, "D-2-hydroxyglutarate is an intercellular mediator in IDH-mutant gliomas inhibiting complement and T cells," *Clinical Cancer Research*, vol. 24, no. 21, pp. 5381–5391, Nov. 2018, doi: 10.1158/1078-0432.CCR-17-3855.

[301] G. Notarangelo *et al.*, "Oncometabolite <scp>d</scp> -2HG alters T cell metabolism to impair CD8 $^{+}$ T cell function," *Science (1979)*, vol. 377, no. 6614, pp. 1519–1529, Sep. 2022, doi: 10.1126/science.abj5104.

[302] H. Babikir *et al.*, "ATRX regulates glial identity and the tumor microenvironment in IDH-mutant glioma," *Genome Biol*, vol. 22, no. 1, p. 311, Dec. 2021, doi: 10.1186/s13059-021-02535-4.

[303] F. Klemm *et al.*, "Compensatory CSF2-driven macrophage activation promotes adaptive resistance to CSF1R inhibition in breast-to-brain metastasis," *Nat Cancer*, vol. 2, no. 10, pp. 1086–1101, Oct. 2021, doi: 10.1038/s43018-021-00254-0.

[304] Y. Hao *et al.*, "Integrated analysis of multimodal single-cell data Graphical abstract," *Cell*, vol. 184, pp. 3573-3587.e29, 2021, doi: 10.1016/j.cell.2021.04.048.

[305] L. Borst *et al.*, "<scp>NKG2A</scp> is a late immune checkpoint on <scp>CD8</scp> T cells and marks repeated stimulation and cell division," *Int J Cancer*, vol. 150, no. 4, pp. 688–704, Feb. 2022, doi: 10.1002/ijc.33859.

[306] D. Tzachanis *et al.*, "Tob is a negative regulator of activation that is expressed in anergic and quiescent T cells," *Nat Immunol*, vol. 2, no. 12, pp. 1174–1182, Nov. 2001, doi: 10.1038/ni730.

[307] B. C. Sheu *et al.*, "Up-regulation of inhibitory natural killer receptors CD94/NKG2A with suppressed intracellular perforin expression of tumor-infiltrating CD8 + T lymphocytes in human cervical carcinoma," *Cancer Res*, vol. 65, no. 7, pp. 2921–2929, Apr. 2005, doi: 10.1158/0008-5472.CAN-04-2108.

[308] M. Gooden *et al.*, "HLA-E expression by gynecological cancers restrains tumor-infiltrating CD8 + T lymphocytes", doi: 10.1073/pnas.1100354108.

[309] B. Salomé *et al.*, "NKG2A and HLA-E define an alternative immune checkpoint axis in bladder cancer," *Cancer Cell*, vol. 40, no. 9, pp. 1027-1043.e9, Sep. 2022, doi: 10.1016/j.ccell.2022.08.005.

[310] K. C. Johnson, E. A. Houseman, J. E. King, K. M. von Herrmann, C. E. Fadul, and B. C. Christensen, "5-Hydroxymethylcytosine localizes to enhancer elements and is associated with survival in glioblastoma patients," *Nat Commun*, vol. 7, no. 1, p. 13177, Dec. 2016, doi: 10.1038/ncomms13177.

[311] T. van Hall *et al.*, "Monalizumab: inhibiting the novel immune checkpoint NKG2A," *J Immunother Cancer*, vol. 7, no. 1, p. 263, Dec. 2019, doi: 10.1186/s40425-019-0761-3.

[312] J. H. Cho *et al.*, "Calcineurin-dependent negative regulation of CD94/NKG2A expression on naive CD8+ T cells," *Blood*, vol. 118, no. 1, pp. 116–128, Jul. 2011, doi: 10.1182/blood-2010-11-317396.

[313] F. Salerno, R. A. W. van Lier, and M. C. Wolkers, "Better safe than sorry: TOB1 employs multiple parallel regulatory pathways to keep Th17 cells quiet," *Eur J Immunol*, vol. 44, no. 3, pp. 646–649, Mar. 2014, doi: 10.1002/eji.201444465.

[314] U. Schulze-Topphof *et al.*, "Tob1 plays a critical role in the activation of encephalitogenic t cells in cns autoimmunity," *Journal of Experimental Medicine*, vol. 210, no. 7, pp. 1301–1309, Jul. 2013, doi: 10.1084/jem.20121611.

[315] J.-C. Corvol *et al.*, "Abrogation of T cell quiescence characterizes patients at high risk for multiple sclerosis after the initial neurological event," *Proceedings of the National Academy of Sciences*, vol. 105, no. 33, pp. 11839–11844, Aug. 2008, doi: 10.1073/pnas.0805065105.

[316] K. Okochi, T. Suzuki, J. Inoue, S. Matsuda, and T. Yamamoto, "Interaction of anti-proliferative protein Tob with poly(A)-binding protein and inducible poly(A)-binding protein: implication of Tob in translational control," *Genes to Cells*, vol. 10, no. 2, pp. 151–163, Jan. 2005, doi: 10.1111/j.1365-2443.2005.00826.x.

[317] S. F. Hussain, D. Yang, D. Suki, K. Aldape, E. Grimm, and A. B. Heimberger, "The role of human glioma-infiltrating microglia/macrophages in mediating antitumor immune responses," *Neuro Oncol*, vol. 8, no. 3, pp. 261–279, Jul. 2006, doi: 10.1215/15228517-2006-008.

[318] L. Pedro and P. J. Rudewicz, "Analysis of Live Single Cells by Confocal Microscopy and High-Resolution Mass Spectrometry to Study Drug Uptake, Metabolism, and Drug-Induced Phospholipidosis," *Anal Chem*, vol. 92, no. 24, pp. 16005–16015, Dec. 2020, doi: 10.1021/acs.analchem.0c03534.

[319] S. Antona, I. Platzman, and J. P. Spatz, "Droplet-Based Cytotoxicity Assay: Implementation of Time-Efficient Screening of Antitumor Activity of Natural Killer Cells," *ACS Omega*, vol. 5, no. 38, pp. 24674–24683, Sep. 2020, doi: 10.1021/acsomega.0c03264.

[320] E. Lundberg and G. H. H. Borner, "Spatial proteomics: a powerful discovery tool for cell biology," *Nature Reviews Molecular Cell Biology*, vol. 20, no. 5. Nature Publishing Group, pp. 285–302, May 01, 2019. doi: 10.1038/s41580-018-0094-y.

[321] "Global DNA Hydroxymethylation Assay Kit (5hmc, Colorimetric) (ab233487) | Abcam." https://www.abcam.com/global-dna-hydroxymethylation-assay-kit-5hmc-colorimetric-ab233487.html (accessed Oct. 02, 2022).

[322] "Global DNA Methylation Assay Kit (5 Methyl Cytosine, Colorimetric) (ab233486)." https://www.abcam.com/global-dna-methylation-assay-kit-5-methyl-cytosine-colorimetric-ab233486.html (accessed Oct. 02, 2022).

[323] "hMeDIP kit." https://www.diagenode.com/en/documents/hmedip-kit-manual (accessed Oct. 02, 2022).

[324] N. bin Xie *et al.*, "Bisulfite-free and single-nucleotide resolution sequencing of DNA epigenetic modification of 5-hydroxymethylcytosine using engineered deaminase," *Chem Sci*, vol. 13, no. 23, pp. 7046–7056, May 2022, doi: 10.1039/d2sc01052f.

[325] T. D. Schmittgen and K. J. Livak, "Analyzing real-time PCR data by the comparative CT method," *Nat Protoc*, vol. 3, no. 6, pp. 1101–1108, May 2008, doi: 10.1038/nprot.2008.73.

[326] L. Bejarano, M. J. C. Jordão, and J. A. Joyce, "Therapeutic targeting of the tumor microenvironment," *Cancer Discovery*, vol. 11, no. 4. American Association for Cancer Research Inc., pp. 933–959, 2021. doi: 10.1158/2159-8290.CD-20-1808.

[327] "EANO Guidelines." https://www.eano.eu/publications/eano-guidelines/ (accessed Oct. 02, 2022).

[328] M. J. van den Bent *et al.*, "Interim results from the CATNON trial (EORTC study 26053-22054) of treatment with concurrent and adjuvant temozolomide for 1p/19q non-co-deleted anaplastic glioma: a phase 3, randomised, open-label intergroup study," *The Lancet*, vol. 390, no. 10103, pp. 1645–1653, Oct. 2017, doi: 10.1016/S0140-6736(17)31442-3.

V) ANNEXES

REVIEW

OPEN

New insights into the Immune TME of adult-type diffuse gliomas

Quentin Richard[a], *Alice Laurenge*[a], *Michel Mallat*[a], *Marc Sanson*[a,b,c] *and Luis Jaime Castro-Vega*[a]

Purpose of review
Adult-type diffuse gliomas are highly heterogeneous tumors. Bulk transcriptome analyses suggested that the composition of the tumor microenvironment (TME) corresponds to genetic and clinical features. In this review, we highlight novel findings on the intratumoral heterogeneity of IDH-wildtype and IDH-mutant gliomas characterized at single-cell resolution, and emphasize the mechanisms shaping the immune TME and therapeutic implications.

Recent findings
Emergent evidence indicates that in addition to genetic drivers, epigenetic mechanisms and microenvironmental factors influence the glioma subtypes. Interactions between glioma and immune cells contribute to immune evasion, particularly in aggressive tumors. Spatial and temporal heterogeneity of malignant and immune cell subpopulations is high in recurrent gliomas. IDH-wildtype and IDH-mutant tumors display distinctive changes in their myeloid and lymphoid compartments, and D-2HG produced by IDH-mutant cells impacts the immune TME.

Summary
The comprehensive dissection of the intratumoral ecosystem of human gliomas using single-cell and spatial transcriptomic approaches advances our understanding of the mechanisms underlying the immunosuppressed state of the TME, supports the prognostic value of tumor-associated macrophages and microglial cells, and sheds light on novel therapeutic options.

Keywords
adult-type diffuse gliomas, D-2-hydroxyglutarate, IDH mutation, immune tumor microenvironment, intratumoral heterogeneity, single-cell and spatial transcriptomics

INTRODUCTION

Adult-type diffuse gliomas are brain tumors with aggressive behavior characterized by cell migration into the brain parenchyma, thereby precluding curative surgical resection. Survival and quality of life of patients remain dismal with current standard of care consisting of surgery followed by adjuvant radiation and chemotherapy. In the current classification (WHO CNS5), isocitrate deshydrogenase (IDH1/2) mutations and 1p/19q codeletion along with histology define three major categories of adult diffuse gliomas: glioblastoma grade IV (IDH-wildtype); astrocytoma grade 2–4 (IDH-mutant without 1p/19q-codeletion); and oligodendroglioma grade 2–3 (IDH-mutant and 1p/19q-codeleted) [1] (Fig. 1). Of these, glioblastomas are the most aggressive tumors with patients having a median overall survival of 15 months. Patients with low-grade IDH-mutant gliomas have a more favourable prognosis, but these tumors invariably progress, recur as higher grades, and become resistant to therapy. It is increasingly recognized that the tumor microenvironment (TME) is a key factor of tumor progression and response to immunotherapies. Here we discuss the latest findings regarding the intratumoral heterogeneity of gliomas, with focus on the composition of the immune TME, highlight therapeutic implications, and provide research perspectives.

[a]Paris Brain Institute (ICM), Hôpital Pitié-Salpêtrière, Inserm U 1127, CNRS UMR 7225, Sorbonne Université, Genetics and Development of Brain Tumors Team, [b]Department of Neurology 2, Pitié-Salpêtrière Hospital and [c]Onconeurotek Tumor Bank, Paris, France

Correspondence to Luis Jaime Castro-Vega, MD, PhD, Genetics & Development of Brain Tumors, ICM - Paris Brain Institute, Hôpital Pitié, 47 Bd de l'Hôpital, 75013 Paris, France. Tel: +33 (0)1 57 27 40 99; e-mail: luis.castrovega@icm-institute.org

Curr Opin Neurol 2022, 33:000–000

DOI:10.1097/WCO.0000000000001112

KEY POINTS

- High intratumoral heterogeneity and environmental stimuli define aggressive and recurrent gliomas.
- Dynamic competition of resident and infiltrating macrophages occurs during glioma progression.
- Distinctive changes in the immune TME are linked to the IDH mutation status.
- Cell-extrinsic D-2HG impinges upon the function of immune cells.

INTRATUMORAL HETEROGENEITY OF IDH-WILDTYPE GLIOMAS

Bulk transcriptome profiling of The Cancer Genome Atlas (TCGA) glioma cohort suggested four tumor subtypes: proneural, neural, classical, and mesenchymal, characterized by defined genetic drivers [2]. Deconvolution analyses of the immune cell composition of these tumors, revealed that the mesenchymal subtype, which exhibits the worst prognosis, is enriched in neutrophils and tumor-associated macrophages (TAMs) [3]. This enrichment involves NF1 deficiency in malignant cells, which promotes chemoattraction of TAMs [3]. Longitudinal analyses showed that recurrent tumors increase the TAM population whereas temozolomide-related hypermutation correlates with enrichment of CD8+ T cells [3]. However,

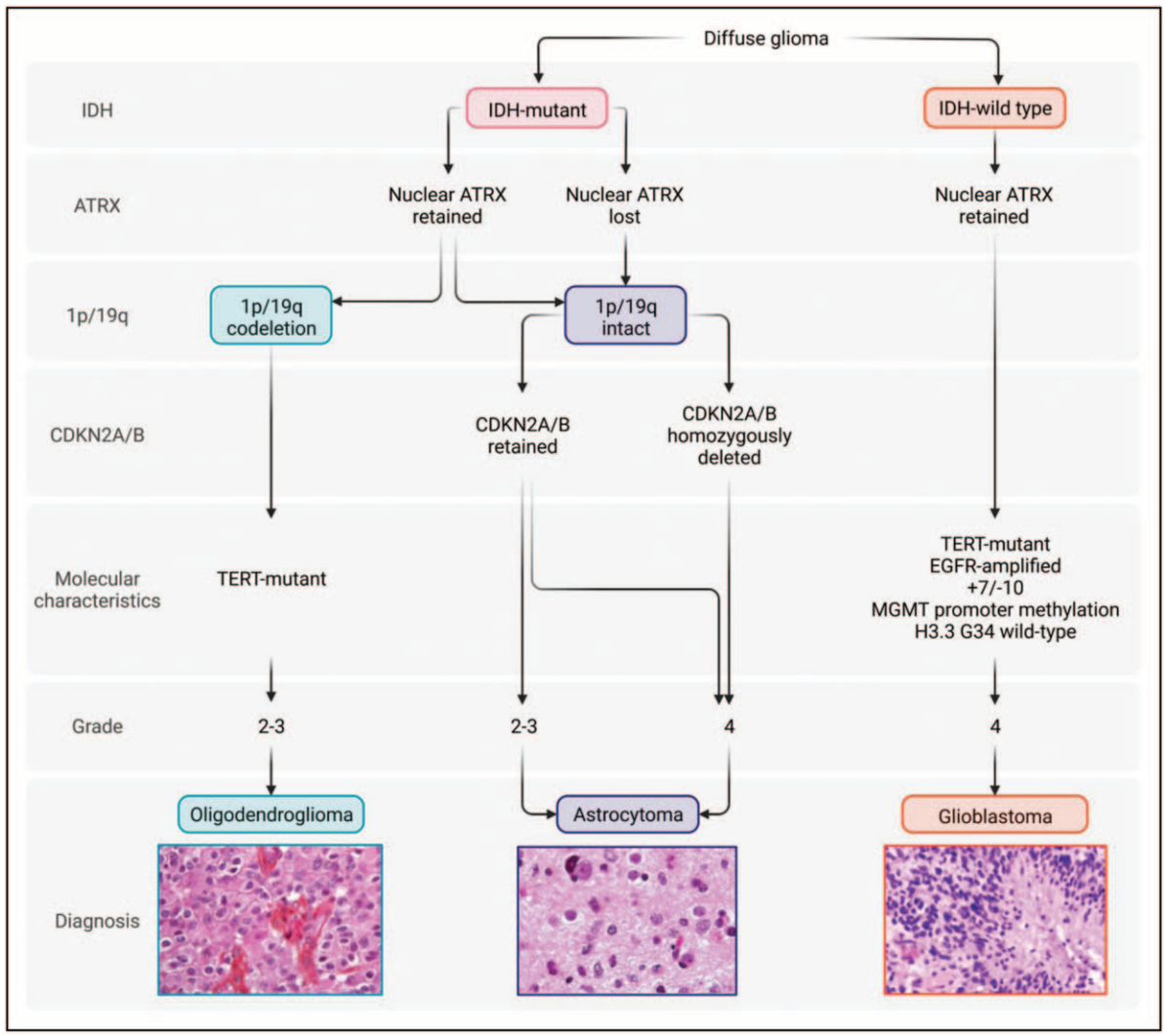

FIGURE 1. Adult-type diffuse glioma classification (WHO CNS5). The main genetic alterations of IDH-wildtype and IDH-mutant tumors and their corresponding histological appearance are indicated. IDH, isocitrate dehydrogenase.

these findings await confirmation, as it is possible that hypermutation might correlate with enrichment of CD8+ T cells in specific subpopulations (e.g. pediatric patients with CMMRD) rather than in temozolomide-related contexts. Previous bulk RNA-seq studies suggested that transition from proneural to mesenchymal subtype occurs with disease recurrence and resistance to treatment. However, it was not until the advent of powerful single-cell RNA sequencing (scRNA-seq) that a more accurate assessment of the intratumoral heterogeneity of gliomas, including malignant and immune cells, has been enabled.

It turned out that four cellular malignant states coexist in a given tumor: neural, progenitor-like (NPC-like) oligodendrocyte progenitor-like (OPC-like), astrocyte-like (AC-like), and mesenchymal-like (MES-like) [4] (Fig. 2a). These states, with the exception of MES-like are reminiscent of neurodevelopmental programs as they express astrocytic, oligodendroglial, and stem progenitor cell signatures to some extent. Importantly, it was shown that in addition to genetic drivers, the predominance of one state over the others defines the tumor subtype [4]. Evidence supporting dynamic interconversion between these states was provided in lineage-tracing experiments using a genetic mouse model and patient-derived xenografts, in which one single cell gives rise to the four archetypal subtypes [4].

This switching model argues for a dynamic plasticity of four different cell states, and contrasts with two other scRNA-seq studies supporting the cancer stem cell (CSC) hypothesis, in which a cellular hierarchy prevails [5,6▪,7▪]. Indeed, a signature of quiescent (nonproliferative) CSCs was identified, which differs from the transcriptional signatures of the four archetypal cellular states [6▪]. Importantly, chemotherapy exerts selection pressure on CSCs, and may account for therapy resistance to antimitotic drugs and temozolomide [6▪,7▪], thus emphasizing the need to target the right cells. Regardless of the cell of origin and the defined genetic drivers, the question remains about the factors that influence the plasticity and outcomes of glioblastoma cells.

Multiomics analyses of glioma cells at single-cell resolution revealed that intratumoral epigenetic diversity (but not genomic alterations alone) accounts for adaptive changes to environmental stimuli such as hypoxia and irradiation, leading to cell-state transitions [8▪,9▪▪]. Additional characterization of glioblastomas by spatially resolved transcriptomics showed that inflammation and hypoxia, as well as changes in metabolic activity and the neural environment contribute to the transcriptional heterogeneity that characterizes the four cellular archetypes [11▪]. In particular, expression of potassium channels and metabotropic glutamate receptors are important for the transition between

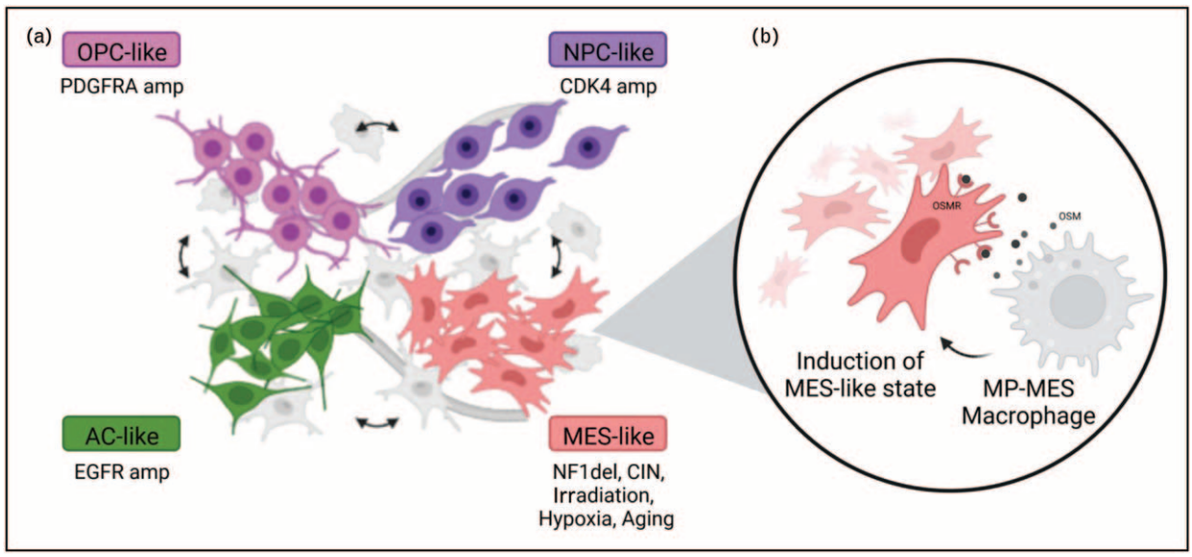

FIGURE 2. Intratumoral heterogeneity of glioma cells and immune-evasion mechanisms in the mesenchymal-like subtype. (a) The four cellular archetypes present in a given glioma, and their corresponding genetic drivers are indicated. Additional factors influencing the proportion of the MES-like state such as chromosome instability (CIN), hypoxia, irradiation, and a senescent environment are also indicated. (b) Induction of MES-like glioma cells by MES-like macrophages. MES, mesenchymal-like.

OPC-like and NPC-like tumors, whereas hypoxia leads to genomic instability in MES-like subtype [10▪▪]. Moreover, age-related changes in the neural environment promote enrichment in the MES-like subtype [10▪▪], a finding consistent with the fact that age is the main risk factor for glioblastoma development. Senescence in malignant cells also contributes to the development and heterogeneity of these tumors [11▪,12▪]. Of note, a transcriptional signature of senescence correlated with poor prognosis in human patients, whereas treatments with a senolytic agent improved the survival of mice bearing gliomas [11▪], and efficiently eliminated preirradiated tumors [12▪]. Therefore, targeting of senescent cells appears as a novel therapeutic option.

ROLES OF TAMs IN IMMUNE EVASION AND TUMOR PROGRESSION

In addition to the microenvironment and the genetic drivers, reciprocal crosstalks between malignant cells and TAMs contribute to the aggressive phenotype of MES-like tumors [13▪,14▪]. Serial transplantation experiments of CSCs from MES-like tumors showed that these cells are endowed with immune-evasive properties via demethylation of IRF8, CD73, and PD-L1 [13▪]. This epigenetic immunoediting process leads to the establishment of a myeloid-enriched TME deemed to play immunosuppressive roles. In coculture experiments, TAMs were found to stimulate transcriptional changes responsible for immune-evasiveness cells in CSCs, whereas in glioma-bearing mice, pharmacological elimination of TAMs resulted in increased survival and clearance of immune-evading tumors [13▪]. TAMs can directly induce the MES-like state of glioblastoma cells through a mechanism involving macrophage-secreted oncostatin M (OSM), a well known epithelial-to-mesenchymal transition inducer, which binds the cognate receptor (OSMR) expressed by malignant cells to activate STAT3 signaling [14▪]. Intriguingly, TAMs from MES-like tumors also display a mesenchymal-like phenotype probably induced by ligands produced by MES-like cancer cells that bind cognate receptors expressed by TAMs [14▪] (Fig. 2Bb).

TAM's phenotype and function are determined by ontogeny and environmental cues. Functional specificity or heterogeneity in TAMs has been addressed through scRNA-seq analyses of CD45+ or CD11b+ cells from GL261 tumors and human glioblastomas, which enabled an in-depth characterization of the myeloid compartment [15▪▪,16▪]. New subsets of dendritic cells, monocyte-derived macrophages (MDMs), and border-associated macrophages (BAMs) were uncovered for the first time. Analysis of newly diagnosed and recurrent tumors showed that the myeloid compartment is highly dynamic [15▪▪]. Elegant experiments of GL261 tumors growing in Cx3cr1CreER:R26-YFP mice (to fate-map microglia) and in Ccr2 knockout mice (MDMs recruitment is prevented) demonstrated that brain resident macrophages such as microglia, are outnumbered by MDMs upon recurrence [15▪▪]. Enrichment in pro-inflammatory and proliferative microglial cells has also been reported in high-grade glioblastomas in the contexts of the SETD2 mutation and EGFR overexpression [17,18]. The largest scRNA-seq study to date to characterize myeloid cells in human gliomas confirmed the MES-like phenotype of TAMs and hypoxia subtypes [19▪▪]. Signatures of TAMs were used to interrogate TCGA and scRNA-seq data, and indicated that immunosuppressive MDMs and inflammatory microglial cells correlate with worse and better prognosis, respectively [19▪▪]. This study highlighted the S100A4 protein in myeloid cells as a novel immunotherapy target [19▪▪].

IDENTIFICATION OF KEY LIGAND–RECEPTOR PAIRS

With regard to the composition of infiltrating T cells in IDH-wildtype gliomas, a combined scRNA-seq and T-cell receptor-sequencing analysis identified a subpopulation of CD8+ T cells expressing the inhibitory receptor CD161, which binds to CLEC2D expressed by malignant and myeloid cells to inhibit antitumoral activity [20▪]. Indeed, genetic inactivation of KLRB1 (the gene-encoding CD161) or blockade of CD161 resulted in enhanced killing activity by T cells *in vitro* and improved survival *in vivo* [20▪]. Thus, the authors suggest that targeting the CLEC2D–CD161 axis may synergize PD-1 blockade to enhance the antitumor function of distinct T-cell populations. Further analyses of spatially distinct regions revealed high regional heterogeneity of malignant and immune cells, and highlighted ligand–receptor interactions among glioma, myeloid cells, and T cells [19▪▪]. Similarly, a longitudinal study showed high heterogeneity of genomic alterations, neoantigens, and T-cell clones in recurrent tumors [21▪▪]. The spatiotemporal heterogeneity of the immune infiltrates emphasizes dynamic changes over time and the presence of tumor niches where the proximity (intercellular distances) is critical for immune cell activation/repression.

THE IMMUNE TME IN IDH-MUTANT GLIOMAS

The IDH enzyme catalyses the conversion of isocitrate to α-ketoglutarate (α-KG), whereas IDH1/2

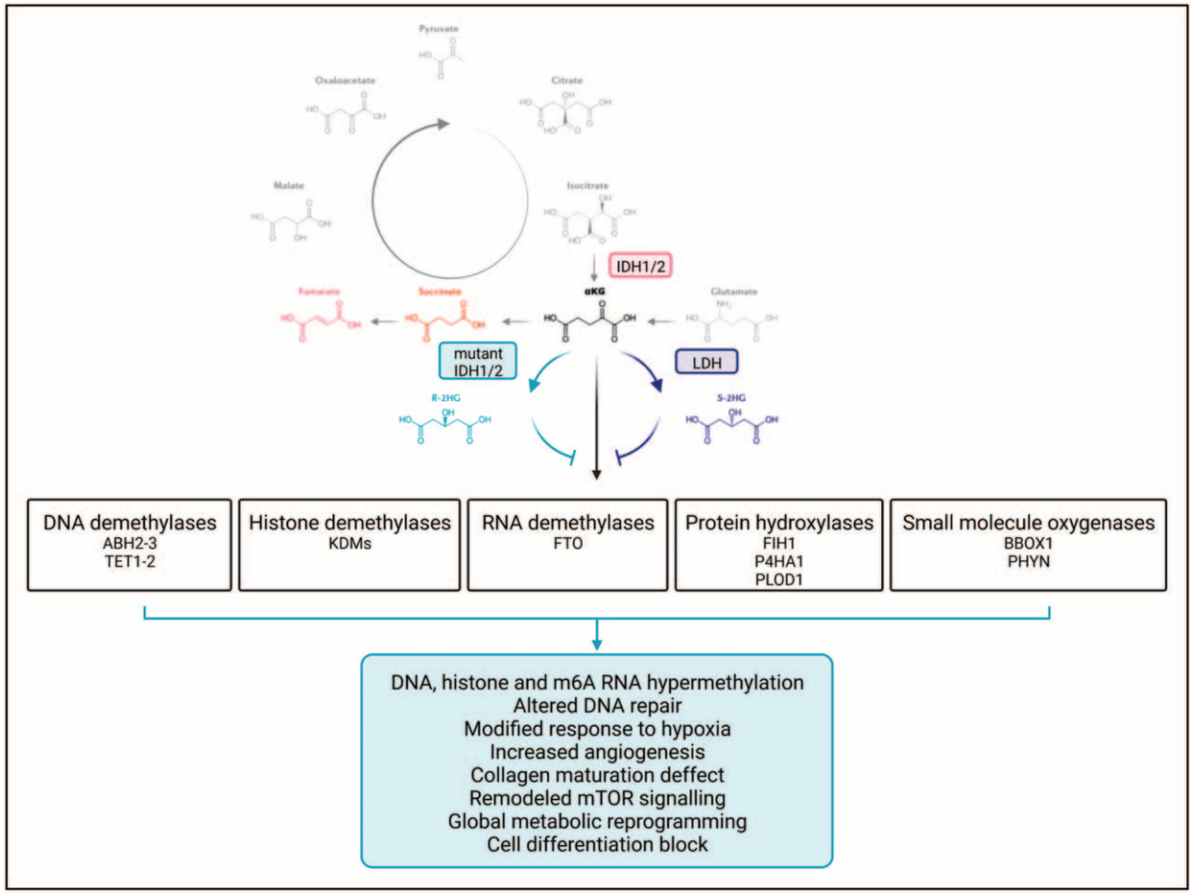

FIGURE 3. Effects of the IDH1/2 mutation. Enzymatic activity of IDH-wildtype produces α-ketoglutarate, whereas neomorphic IDH1/2 mutations produce D-2-hydroxyglutarate (D-2HG). Canonical examples of α-ketoglutarate-dependent enzymes and consequences of their inhibition by high levels of D-2HG are also indicated. IDH, isocitrate dehydrogenase.

mutations, which are frequent in diffuse gliomas, convert α-KG to D-2-hydroxyglutarate (D-2HG) [22] (Fig. 3a). It is believed that such accumulation drives cellular transformation by inhibiting α-KG-dependent dioxygenases [23], ultimately leading to widespread hypermethylation, blocking of cell differentiation and defective collagen maturation [24–28] (Fig. 3b). Moreover, IDH-mutant cells present dysregulation of the metabolic profile and redox state promoting glycolysis and enhancing the production of reactive oxygen species [29]. Strikingly, IDH-mutant, SDH-mutant, and FH-mutant tumors, which accumulate the oncometabolites D-2HG, succinate, and fumarate, respectively, do not only display epigenomic reprogramming but also exhibit a cold immune microenvironment [30].

Seminal studies using scRNA-seq of bulk tumors uncovered essential differences in the tumor architecture of IDH-wildtype and IDH-mutant gliomas [9▪▪,31,32]. On one hand, malignant cells from IDH-mutant tumors follow a hierarchical organization with cycling stem-like cells giving rise to noncycling astrocyte-like and oligodendrocyte-like lineages [9▪▪,31]. On the other hand, high-grade tumors undergo changes in the myeloid compartment with increased abundance of macrophages over microglia [32]. Initial analyses of the immune cell composition using TCGA bulk RNA-seq data, as well as experiments in syngeneic glioma models demonstrated a downregulation of immune-related signaling pathways and chemotaxis factors in IDH-mutant compared with IDH-wildtype gliomas [33,34]. Recent analyses of TCGA and immunohistochemical validations, confirmed a low expression of T-cell markers in IDH-mutant glioma, and revealed significant enrichment of CD4+ naive T cells and a reduction of memory T cells [35]. Low numbers of dendritic cells and immunosuppressive cells, including Tregs (Foxp3+) and TAMs (CD163+) were also shown, particularly in oligodendrogliomas [36]. Additional evaluation of the Chinese Glioma Genome Atlas (CGGA) cohort revealed higher infiltration of natural killer (NK) cells [37]. Moreover, IDH-mutant gliomas exhibit DNA

hypermethylation of the CD274 promoter leading to low expression of the immune ligand PD-L1 [36,38,39].

Two important studies using fluorescence-activated cell sorting followed by RNA-seq or CyTOF analyses of immune cells further confirmed that IDH-wildtype gliomas are more infiltrated by CD8+ and CD4+ T-cell subsets (including Tregs), as well as by MDMs, whereas IDH-mutant tumors display a high proportion of microglial cells and a high monocyte/MDM ratio. NK cells display immature and cytotoxic phenotypes in IDH-wildtype and IDH-mutant gliomas, respectively [40▪▪,41▪▪]. Establishing the differences in the abundance and functionality of the immune cell populations between these tumor types is crucial for the designing of efficient immunotherapeutic strategies.

Although, the IDH-mutated status was suggested to shape the TME, IDH-mutant astrocytomas and oligodendrogliomas differ in some genetic alterations, and exhibit different prognoses. In this regard, evaluation of TCGA and CGGA data indicated that immune infiltration is higher in astrocytomas than oligodendriogliomas [42]. Further analysis of bulk tumors using a combination of scRNA-seq and scATAC-seq approaches revealed a significant overexpression of chemotaxis factors CSF1 and FLT3LG in ATRX-mutated astrocytomas, and upregulation of CD163, a marker of immunosuppressive myeloid cells [43▪▪]. The causal role of the ATRX loss-of-function in shaping the myeloid compartment was confirmed in the SB28 mouse glioma model [43▪▪]. Thus, the effect of this genetic driver is reminiscent of the impact of NF1 deficiency in MES-like glioblastomas and raises the question whether genes affected by the codeletion 1p/19q that characterize IDH-mutant oligodendriogliomas (e.g. CSF1 encoded in 1p and TGFβ in 19q) account for TME changes.

Preclinical studies also explored how D-2HG acting in glioma cells could affect the TME [44,45]. Using a sleeping beauty transposon system to model IDH-mutant astrocytoma, it was shown that ATRX loss enhances DNA damage response via up-regulation of the ATM signaling pathway, which in turn was explained by D-2HG-induced hypermethylation of histone 3 (H3) [44]. The IDH mutation was also associated with hypermethylation of the activating mark H3K4me3 in the promoter region of the gene encoding granulocyte-colony stimulating factor (G-CSF) in CSCs [45]. Hence, CSC production of G-CSF was responsible for an expansion of immature granulocytic myeloid cells infiltrating the TME [45]. These results suggest that compared with IDH-wild type glioma, the overall low level of immune infiltrates in IDH-mutant gliomas involves altered expression of effectors acting on the recruitment or the differentiation of infiltrating immune cells via D-2HG-driven epigenetic alterations in malignant cells. Nevertheless, as this oncometabolite accumulates to millimolar levels in the TME [46,47], it may also affect the phenotypic and functional properties of immune cells.

CELL-EXTRINSIC ROLES OF D-2HG

Recent in-vitro studies provided evidence for the uptake of D-2HG by cells typically residing in the TME, via the sodium-dependent dicarboxylate transporter 3 (SLC13A3) [35] or the glutamate transporter SLC1A1 [48▪] (Fig. 4). Increased D-2HG levels were also found in T cells isolated from acute myeloid leukaemia (AML) patients harbouring IDH2 mutations [49], and in CD11b+ cells from an IDH-mutant mouse model [50▪▪]. Treatments with D-2HG used at nontoxic albeit high concentrations (>5 mmol/l) reduce IL-12 secretion and preclude LPS-induced glycolysis in dendritic cells [51], and prevent LPS-induced activation in murine microglia by affecting the AMPK/mTOR/NF-κB-signaling pathway [52]. In endothelial cells, D-2HG fuels mitochondrial respiration and angiogenesis [48▪].

With respect to cultured T cells, D-2HG promotes a metabolic switch from aerobic glycolysis towards oxidative phosphorylation in activated T cells and favors the growth or differentiation of Tregs [49]. In contrast, in-vivo studies using GL261 cells overexpressing IDH wildtype or IDH mutant showed decreased numbers of Tregs in IDH-mutant gliomas [53] and impaired T-cell activation by reducing proliferation and cytokine production [35]. Because the functional response of immune cells depends on environmental signals and cell–cell interactions, which may be prevented *in vitro*, there is a need to characterize the effects of D-2HG *in vivo*. In this regard, inhibition of the enzymatic function of the IDH mutation increased the CD4+ population and restored the antitumor activity of T cells [35]. Moreover, this therapeutic approach combined with PD-1 inhibition increased overall survival [35,54▪▪].

In addition, recent evidence demonstrated that D-2HG drives an immunosuppressive myeloid state by altering the tryptophan metabolism in MDMs via activation of AHR [55▪]. Pseudotime inference analyses using scRNA-seq data of flow cytometry-purified CD45+ cells from IDH-mutant and IDH-wildtype GL261 gliomas confirmed the high monocyte/MDM ratio previously observed in IDH-mutant human tumors [40▪▪] and further revealed a high monocyte/dendritic cell ratio [56▪]. The authors suggested an immature phenotype of monocyte-derived cells upon D-2HG exposure. However, in-vitro

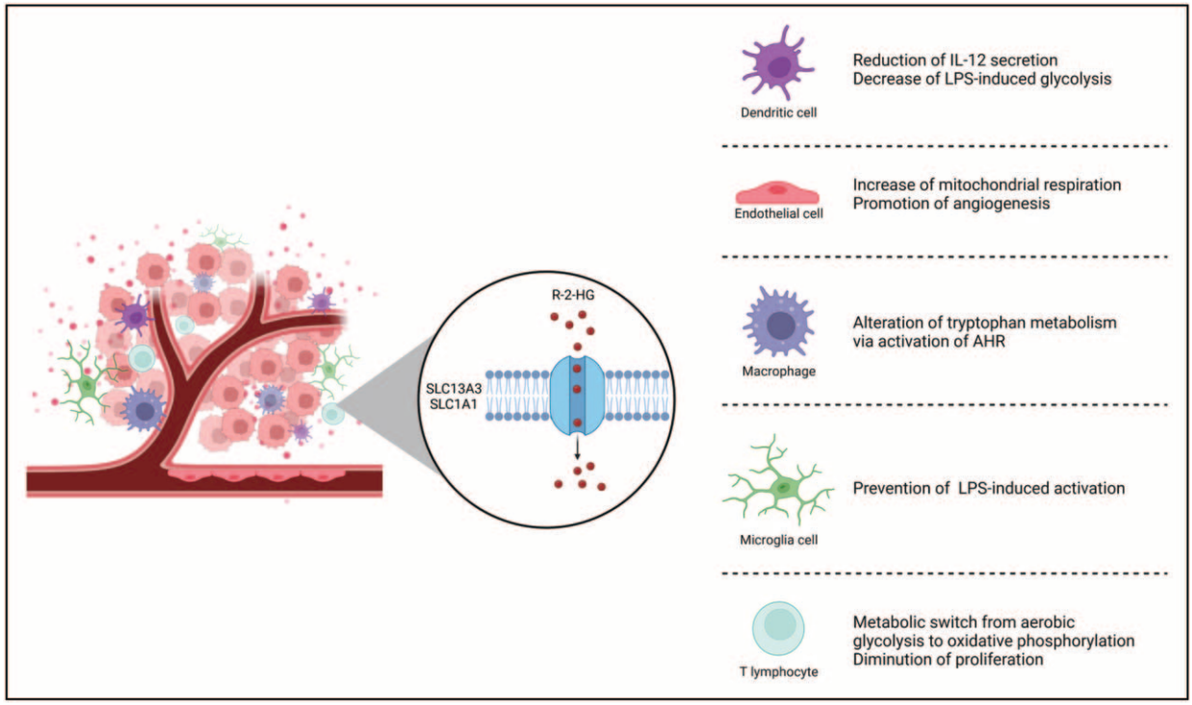

FIGURE 4. Cellular uptake of D-2-hydroxyglutarate. Cell types able to take up D-2HG according to in-vitro studies as well as two of the transporters so far reported are indicated. D-2HG, D-2-hydroxyglutarate.

experiments revealed conflicting results with a previous study showing that neither differentiation, nor antigen presentation of dendritic cells is affected by D-2HG [57]. This further emphasizes the challenges to characterize the effects of D-2HG on immune cell function *in vitro*.

Collectively, these data argue against a simple reduction of immune cell recruitment by chemotactic factors. More investigation is required to specify the roles of D-2HG as immunomodulator of the TME in IDH-mutant gliomas.

CONCLUSION

Although immunotherapy targeting the PD-L1/PD-1 axis has achieved advances in various cancers, phase III clinical trials failed to show efficacy in newly diagnosed and recurrent glioblastomas. The presence of dysfunctional T cells [58,59], as well as suppressive cells such as Tregs and TAMs in the TME may account for this lack of response. The comprehensive characterization of the immune TME at single-cell resolution and experimental evidence in mouse models point to prominent roles of TAMs and their interactions with malignant and T cells during tumor progression. Hence, focus on the myeloid compartment, and the immune checkpoints expressed by these cells is highly encouraged in order to uncover specific mechanisms leading to the immunosuppressive TME.

TAMs do not only offer a prognostic value but also are potential targets for therapies aimed at depleting/repolarizing these cells to a pro-inflammatory state thereby allowing effector T-cell infiltration and activation [60–63]. Nevertheless, targeting the myeloid population should be more specific as MDMs are more abundant in IDH wild-type gliomas and recurrent tumors (regardless of the IDH status) whereas microglial cells are the major population in IDH-mutant gliomas. Moreover, the pro-tumorigenic role of nonparenchymal macrophages, which are located in meninges, perivascular niches, and even within the cerebrospinal fluid, remains unexplored [64,65]. So far, a relatively small number of human gliomas have been profiled for scRNA-seq analysis of the TME. As more data will be generated, a more complete atlas of myeloid cells could help to identify novel subsets that correlate with clinical outcomes. Efforts are currently underway to better characterize TAM subtypes, ligand–receptor pairs, and immune checkpoints expressed by these cells [66]. It is becoming clear that glioblastoma progression requires not only genetic drivers but also microenvironment interactions [9▪▪,10▪▪,11▪,67▪]. While most of the work on immunoevading mechanisms and myeloid interactions has been done in MES-like gliomas [13▪,14▪,18,67▪], the immunomodulatory mechanisms operating in low-grade and IDH-mutant gliomas remain largely unknown.

Differences in the TME of astrocytomas and oligodendriogliomas suggested by bulk RNA-seq studies [36,42,68,69] may be linked to their distinct prognosis and need to be ascertained using scRNA-seq. IDH-mutant tumors are infiltrated by a low number of immune cells. Although results from clinical trials with IDH mutation inhibitors are promising [70], preclinical studies suggest that this approach may be more effective if combined with immunotherapies (checkpoint blockade or IDH1R132H vaccines) [35,54▪▪]. Although cell-extrinsic effects of D-2HG mediate some changes in the TME, the impact of this oncometabolite on the epigenome of immune cells remains unexplored. Hence, these are exciting times to discover additional roles of D-2HG in the TME of IDH-mutant gliomas.

Acknowledgements

We thank all members of the laboratory, as well as the guest speakers of the seminar series on the TME of gliomas held at the ICM – Paris Brain Institute for insightful discussions. We apologize to all colleagues whose contributions could not be cited because of space limitations. Figures were created with BioRender's web-based software, and pictures were kindly provided by Dr. Karima Mokhtari, Hôpital de la Pitié Salpêtrière, Paris, France.

Financial support and sponsorship

Work in the Genetics & Development of Bain Tumors Lab is supported by the grants Fondation Bristol Myers Squibb pour la Recherche en Immuno-Oncologie (BMS 2104009NA), French National Cancer Institute (INCa-PLBIO22-243), and Entreprises contre le Cancer Paris-Île-de-France (GEFLUC R20202DD). The group is supported by La Ligue Nationale contre le Cancer (Équipe Labellisée) and by the Site de Recherche Intégré sur le Cancer (SiRIC CURAMUS). A.L.-L. is supported by Fondation Recherche Médicale (FRM) scholarship, and Q.R. is supported by the French Ministry of Education and Research scholarship.

Conflicts of interest

There are no conflicts of interest.

REFERENCES AND RECOMMENDED READING

Papers of particular interest, published within the annual period of review, have been highlighted as:

- ▪ of special interest
- ▪▪ of outstanding interest

1. Louis DN, Perry A, Wesseling P, *et al.* The 2021 WHO Classification of Tumors of the Central Nervous System: a summary. Neuro Oncol 2021; 23:1231–1251.
2. Verhaak RGW, Hoadley KA, Purdom E, *et al.* Integrated genomic analysis identifies clinically relevant subtypes of glioblastoma characterized by abnormalities in PDGFRA, IDH1, EGFR, and NF1. Cancer Cell 2010; 17:98–110.
3. Wang Q, Hu B, Hu X, *et al.* Tumor evolution of glioma-intrinsic gene expression subtypes associates with immunological changes in the microenvironment. Cancer Cell 2018; 33:152.
4. Neftel C, Laffy J, Filbin MG, *et al.* An integrative model of cellular states, plasticity, and genetics for glioblastoma. Cell 2019; 178:835.e21–849.e21.
5. Gimple RC, Yang K, Halbert ME, *et al.* Brain cancer stem cells: resilience through adaptive plasticity and hierarchical heterogeneity. Nat Rev Cancer 2022; 22:497–514.
6. ▪ Xie XP, Laks DR, Sun D, *et al.* Quiescent human glioblastoma cancer stem cells drive tumor initiation, expansion, and recurrence following chemotherapy. Dev Cell 2022; 57:32.e8–46.e8.
This study identifies an expression signature of quiescent glioblastoma CSCs in mouse gliomas that is retrieved in humans independently of the glioma tumor subtypes, and accounts for tumor resistance to antimitotic drugs.
7. ▪ Couturier CP, Ayyadhury S, Le PU, *et al.* Single-cell RNA-seq reveals that glioblastoma recapitulates a normal neurodevelopmental hierarchy. Nat Commun 2020; 11:3406.
scRNA-seq comparative analysis using the neurodevelopmental hierarchy as a roadmap reveals cycling progenitor glioblastoma stem cells resistant to temozolomide.
8. ▪ Chaligne R, Gaiti F, Silverbush D, *et al.* Epigenetic encoding, heritability and plasticity of glioma transcriptional cell states. Nat Genet 2021; 53:1469–1479.
Multiomics single cell analysis, and in particular DNA methylation, confirms a hierarchal organization of IDH-mutant gliomas and further argues for plastic cellular states of IDH-wildtype tumors.
9. ▪▪ Johnson KC, Anderson KJ, Courtois ET, *et al.* Single-cell multimodal glioma analyses identify epigenetic regulators of cellular plasticity and environmental stress response. Nat Genet 2021; 53:1456–1468.
Multiomics single cell analysis identifies high epigenetic diversity in aggressive glioblastomas underlying adaptive changes to environmental stimuli.
10. ▪▪ Ravi VM, Will P, Kueckelhaus J, *et al.* Spatially resolved multiomics deciphers bidirectional tumor-host interdependence in glioblastoma. Cancer Cell 2022; 40:639.e13–655.e13.
Spatial transcriptomic analysis highlights the environmental factors that influence the archetypal cell state transitions in glioblastomas.
11. ▪ Salam R, Saliou A, Bielle F, *et al.* Cellular senescence in malignant cells promotes tumor progression in mouse and patient glioblastoma. bioRxiv 2022. doi: https://doi.org/10.1101/2022.05.18.492465.
This study identifies senescent glioblastoma cells whose expression signature correlates with poor prognosis in human patients. A preclinical proof-of-concept of a senolytic therapy is provided.
12. ▪ Fletcher-Sananikone E, Kanji S, Tomimatsu N, *et al.* Elimination of radiation-induced senescence in the brain tumor microenvironment attenuates glioblastoma recurrence. Cancer Res 2021; 81:5935–5947.
This study shows noncancer senescent cells, particularly astrocytes, are generated after irradiation and favor tumor progression. A preclinical proof-of-concept of a senolytic therapy is provided.
13. ▪ Gangoso E, Southgate B, Bradley L, *et al.* Glioblastomas acquire myeloid-affiliated transcriptional programs via epigenetic immunoediting to elicit immune evasion. Cell 2021; 184:2454.e26–2470.e26.
This study reveals epigenetic mechanisms in glioblastoma stem cells that underlie immune evasion and the establishment of a TME enriched on TAMs.
14. ▪ Hara T, Chanoch-Myers R, Mathewson ND, Myskiw C, *et al.* Interactions between cancer cells and immune cells drive transitions to mesenchymal-like states in glioblastoma. Cancer Cell 2021; 39:779.e11–792.e11.
TAMs induce the MES-like phenotype of glioma cells via OSM.
15. ▪▪ Pombo Antunes AR, Scheyltjens I, Lodi F, *et al.* Single-cell profiling of myeloid cells in glioblastoma across species and disease stage reveals macrophage competition and specialization. Nat Neurosci 2021; 24:595–610.
Characterization of the myeloid compartment of human and mouse glioblastomas at single-cell resolution and experimental evidence of a dynamic competition of resident and infiltrating macrophages during tumor progression.
16. ▪ Ochocka N, Segit P, Walentynowicz KA, *et al.* Single-cell RNA sequencing reveals functional heterogeneity of glioma-associated brain macrophages. Nat Commun 2021; 12:1151.
scRNA-seq analysis of TAMs heterogeneity in a mouse glioblastoma model.
17. Liu H, Sun Y, Zhang Q, *et al.* Pro-inflammatory and proliferative microglia drive progression of glioblastoma. Cell Rep 2021; 36:109718.
18. Yeo AT, Rawal S, Delcuze B, *et al.* Single-cell RNA sequencing reveals evolution of immune landscape during glioblastoma progression. Nat Immunol 2022; 23:971–984.
19. ▪▪ Abdelfattah N, Kumar P, Wang C, *et al.* Single-cell analysis of human glioma and immune cells identifies S100A4 as an immunotherapy target. Nat Commun 2022; 13:767.
scRNA-seq analysis of the myeloid compartment of a large series of human gliomas supports a prognostic value of subsets of TAMs and microglia cells.
20. ▪ Mathewson ND, Ashenberg O, Tirosh I, *et al.* Inhibitory CD161 receptor identified in glioma-infiltrating T cells by single-cell analysis. Cell 2021; 184:1281.e26–1298.e26.
scRNA-seq analysis of the lymphocytic infiltrate of gliomas identifies the inhibitory signal CLEC2D-CD161.

21. Schaettler MO, Richters MM, Wang AZ, *et al.* Characterization of the genomic ■■ and immunologic diversity of malignant brain tumors through multisector analysis. Cancer Discov 2022; 12:154–171.
Comprehensive multiregional analysis of immunologic diversity of gliomas reveals high spatial heterogeneity and ligand–receptor interactions, particularly with myeloid cells.

22. Dang L, White DW, Gross S, *et al.* Cancer-associated IDH1 mutations produce 2-hydroxyglutarate. Nature 2010; 465:966.

23. Xu W, Yang H, Liu Y, *et al.* Oncometabolite 2-hydroxyglutarate is a competitive inhibitor of α-ketoglutarate-dependent dioxygenases. Cancer Cell 2011; 19:17–30.

24. Noushmehr H, Weisenberger DJ, Diefes K, *et al.* Identification of a CpG island methylator phenotype that defines a distinct subgroup of glioma. Cancer Cell 2010; 17:510–522.

25. Turcan S, Rohle D, Goenka A, *et al.* IDH1 mutation is sufficient to establish the glioma hypermethylator phenotype. Nature 2012; 483:479–483.

26. Markolovic S, Wilkins SE, Schofield CJ. Protein hydroxylation catalyzed by 2-oxoglutarate-dependent oxygenases. J Biol Chem 2015; 290: 20712–20722.

27. Lu C, Ward PS, Kapoor GS, *et al.* IDH mutation impairs histone demethylation and results in a block to cell differentiation. Nature 2012; 483:474–478.

28. Sasaki M, Knobbe CB, Itsumi M, *et al.* D-2-hydroxyglutarate produced by mutant IDH1 perturbs collagen maturation and basement membrane function. Genes Dev 2012; 26:2038–2049.

29. Fack F, Tardito S, Hochart G, *et al.* Altered metabolic landscape in IDH-mutant gliomas affects phospholipid, energy, and oxidative stress pathways. EMBO Mol Med 2017; 9:1681–1695.

30. Thorsson V, Gibbs DL, Brown SD, *et al.* The immune landscape of cancer. Immunity 2018; 48:812.e14–830.e14.

31. Tirosh I, Venteicher AS, Hebert C, *et al.* Single-cell RNA-seq supports a developmental hierarchy in human oligodendroglioma. Nature 2016; 539:309–313.

32. Venteicher AS, Tirosh I, Hebert C, *et al.* Decoupling genetics, lineages, and microenvironment in IDH-mutant gliomas by single-cell RNA-seq. Science (New York, NY) 2017; 355:eaai8478.

33. Amankulor NM, Kim Y, Arora S, *et al.* Mutant IDH1 regulates the tumor-associated immune system in gliomas. Genes Dev 2017; 31:774–786.

34. Kohanbash G, Carrera DA, Shrivastav S, *et al.* Isocitrate dehydrogenase mutations suppress STAT1 and CD8+ T cell accumulation in gliomas. J Clin Invest 2017; 127:1425–1437.

35. Bunse L, Pusch S, Bunse T, *et al.* Suppression of antitumor T cell immunity by the oncometabolite (R)-2-hydroxyglutarate. Nat Med 2018; 24:1192–1203.

36. Mu L, Long Y, Yang C, *et al.* The IDH1 mutation-induced oncometabolite, 2-hydroxyglutarate, may affect DNA methylation and expression of PD-L1 in gliomas. Front Mol Neurosci 2018; 11:82.

37. Ren F, Zhao Q, Huang L, *et al.* The R132H mutation in IDH1 promotes the recruitment of NK cells through CX3CL1/CX3CR1 chemotaxis and is correlated with a better prognosis in gliomas. Immunol Cell Biol 2019; 97:457–469.

38. Berghoff AS, Kiesel B, Widhalm G, *et al.* Correlation of immune phenotype with IDH mutation in diffuse glioma. Neuro Oncol 2017; 19:1460–1468.

39. Röver LK, Gevensleben H, Dietrich J, *et al.* PD-1 (PDCD1) promoter methylation is a prognostic factor in patients with diffuse lower-grade gliomas harboring isocitrate dehydrogenase (IDH) mutations. EBioMedicine 2018; 28:97–104.

40. Klemm F, Maas RR, Bowman RL, *et al.* Interrogation of the microenvironmental ■■ landscape in brain tumors reveals disease-specific alterations of immune cells. Cell 2020; 181:1643.e17–1660.e17.
First comprehensive characterization of the immune landscape of human gliomas suggesting an influence of IDH mutation status.

41. Friebel E, Kapolou K, Unger S, *et al.* Single-cell mapping of human brain ■■ cancer reveals tumor-specific instruction of tissue-invading leukocytes. Cell 2020; 181:1626.e20–1642.e20.
First comprehensive characterization of the immune landscape of human gliomas suggesting an influence of IDH mutation status.

42. Zhao B, Xia Y, Yang F, *et al.* Molecular landscape of IDH-mutant astrocytoma and oligodendroglioma grade 2 indicate tumor purity as an underlying genomic factor. Mol Med 2022; 28:34.

43. Babikir H, Wang L, Shamardani K, *et al.* ATRX regulates glial identity and the ■■ tumor microenvironment in IDH-mutant glioma. Genome Biol 2021; 22:311.
scRNA-seq study showing differences in the TME between astrocytomas and oligondrogliomas, and a causal role of ATRX loss.

44. Núñez FJ, Mendez FM, Kadiyala P, *et al.* IDH1-R132H acts as a tumor suppressor in glioma via epigenetic up-regulation of the DNA damage response. Sci Transl Med 2019; 11:eaaq1427.

45. Alghamri MS, McClellan BL, Avvari RP, *et al.* G-CSF secreted by mutant IDH1 glioma stem cells abolishes myeloid cell immunosuppression and enhances the efficacy of immunotherapy. Sci Adv 2021; 7:eabh3243.

46. Linninger A, Hartung GA, Liu BP, *et al.* Modeling the diffusion of D-2-hydroxyglutarate from IDH1 mutant gliomas in the central nervous system. Neuro Oncol 2018; 20:1197–1206.

47. Pickard AJ, Sohn ASW, Bartenstein TF, *et al.* Intracerebral distribution of the oncometabolite d-2-hydroxyglutarate in mice bearing mutant isocitrate dehydrogenase brain tumors: implications for tumorigenesis. Front Oncol 2016; 6:211.

48. Wang X, Chen Z, Xu J, *et al.* SLC1A1-mediated cellular and mitochondrial ■ influx of R-2-hydroxyglutarate in vascular endothelial cells promotes tumor angiogenesis in IDH1-mutant solid tumors. Cell Res 2022; 32:638–658.
First evidence for the role of D-2HG on endothelial cells.

49. Böttcher M, Renner K, Berger R, *et al.* D-2-hydroxyglutarate interferes with HIF-1α stability skewing T-cell metabolism towards oxidative phosphorylation and impairing Th17 polarization. Oncoimmunology 2018; 7:e1445454.

50. Chuntova P, Yamamichi A, Chen T, *et al.* Inhibition of D-2HG leads to ■■ upregulation of a proinflammatory gene signature in a novel HLA-A2/HLA-DR1 transgenic mouse model of IDH1R132H-expressing glioma. J Immunother Cancer 2022; 10:e004644.
This study shows the effects of inhibiting the enzymatic function of the IDH mutation on immune cell compartments in a mouse glioma model.

51. Ugele I, Cárdenas-Conejo ZE, Hammon K, *et al.* D-2-hydroxyglutarate and L-2-hydroxyglutarate inhibit IL-12 secretion by human monocyte-derived dendritic cells. Int J Mol Sci 2019; 20:742.

52. Han C-J, Zheng J-Y, Sun L, *et al.* The oncometabolite 2-hydroxyglutarate inhibits microglial activation via the AMPK/mTOR/NF-κB pathway. Acta Pharmacol Sin 2019; 40:1292–1302.

53. Richardson LG, Nieman LT, Stemmer-Rachamimov AO, *et al.* IDH-mutant gliomas harbor fewer regulatory T cells in humans and mice. Oncoimmunology 2020; 9:1806662.

54. Kadiyala P, Carney Sv, Gauss JC, *et al.* Inhibition of 2-hydroxyglutarate elicits ■■ metabolic reprogramming and mutant IDH1 glioma immunity in mice. J Clin Invest 2021; 131:e139542.
This study demonstrates the efficacy of combined D-2HG inhibition/IR/TMZ with anti–PDL1 immune checkpoint blockade in a mouse astrocytoma model.

55. Friedrich M, Sankowski R, Bunse L, *et al.* Tryptophan metabolism drives ■ dynamic immunosuppressive myeloid states in IDH-mutant gliomas. Nat Cancer 2021; 2:723–740.
First evidence for the role of D-2HG on macrophages.

56. Friedrich M, Hahn M, Michel J, *et al.* Dysfunctional dendritic cells limit antigen-■ specific T cell response in glioma. Neuro Oncol 2022; noac138. doi: 10.1093/neuonc/noac138.
First evidence indicating that D-2HG affects dendritic cell differentiation and antigen presentation.

57. Zhang L, Sorensen MD, Kristensen BW, *et al.* D-2-hydroxyglutarate is an intercellular mediator in IDH-mutant gliomas inhibiting complement and T cells. Clin Cancer Res 2018; 24:5381–5391.

58. Woroniecka K, Chongsathidkiet P, Rhodin K, *et al.* T-cell exhaustion signatures vary with tumor type and are severe in glioblastoma. Clin Cancer Res 2018; 24:4175–4186.

59. Davidson TB, Lee A, Hsu M, *et al.* Expression of PD-1 by T cells in malignant glioma patients reflects exhaustion and activation. Clin Cancer Res 2019; 25:1913–1922.

60. Müller S, Kohanbash G, Liu SJ, *et al.* Single-cell profiling of human gliomas reveals macrophage ontogeny as a basis for regional differences in macrophage activation in the tumor microenvironment. Genome Biol 2017; 18:234.

61. Pyonteck SM, Akkari L, Schuhmacher AJ, *et al.* CSF-1R inhibition alters macrophage polarization and blocks glioma progression. Nat Med 2013; 19:1264–1272.

62. Goswami S, Anandhan S, Raychaudhuri D, Sharma P. Myeloid cell-targeted therapies for solid tumours. Nat Rev Immunol 2022. doi: 10.1038/s41577-022-00737-w.

63. Pittet MJ, Michielin O, Migliorini D. Clinical relevance of tumour-associated macrophages. Nat Rev Clin Oncol 2022; 19:402–421.

64. van Hove H, Martens L, Scheyltjens I, *et al.* A single-cell atlas of mouse brain macrophages reveals unique transcriptional identities shaped by ontogeny and tissue environment. Nat Neurosci 2019; 22:1021–1035.

65. Munro DAD, Movahedi K, Priller J. Macrophage compartmentalization in the brain and cerebrospinal fluid system. Sci Immunol 2022; 7:eabk0391.

66. Gupta P, Dang M, Bojja K, *et al.* Transcriptionally defined immune contexture in human gliomas at single-cell resoultion. Neuro-oncology 2020; 22(Suppl 2):ii112–ii1112.

67. Varn FS, Johnson KC, Martinek J, *et al.* Glioma progression is shaped by ■ genetic evolution and microenvironment interactions. Cell 2022; 185:2184.e16–2199.e16.
This study provides evidence for genetic alterations influencing glioma progression and emphasizes interactions with myeloid cells.

68. Zhang Y, Xie Y, He L, *et al.* 1p/19q co-deletion status is associated with distinct tumor-associated macrophage infiltration in IDH mutated lower-grade gliomas. Cell Oncol 2021; 44:193–204.

69. Lin W, Qiu X, Sun P, *et al.* Association of IDH mutation and 1p19q co-deletion with tumor immune microenvironment in lower-grade glioma. Mol Ther Oncolytics 2021; 21:288–302.

70. Mellinghoff IK, Ellingson BM, Touat M, *et al.* Ivosidenib in isocitrate dehydrogenase 1-mutated advanced glioma. J Clin Oncol 2020; 38:3398–3406.

université PARIS-SACLAY | ÉCOLE DOCTORALE Cancérologie : biologie - médecine - santé (CBMS)

Titre : Impact du R-2HG sur l'environement immunitaire des gliomes IDH1 mutés

Mots clés : Giomes, IDH, R-2HG, cellules CD11b+, Lymphocytes T, scRNA-Seq

Résumé : Les gliomes diffus de l'adulte sont les tumeurs cérébrales primaires les plus fréquentes qui, malgré des recherches fondamentales et cliniques approfondies, restent incurables. Une compréhension plus approfondie du microenvironnement tumoral (TME) hautement immunosuppressif des gliomes pourrait mettre en lumière de nouvelles stratégies thérapeutiques. L'objectif de ma thèse était d'étudier les compartiments immunitaires des tumeurs sauvages et mutantes pour le gène de l'isocitrate déshydrogénase (IDHwt et IDHm, respectivement).

Dans une première étude, nous avons réalisé un profilage transcriptomique/méthylomique en masse de cellules CD11b+ isolées de gliomes humains. Notre analyse intégrative indique que la méthylation du promoter de CIITA peut expliquer la downregulaion de ce gène et l'absence d'expression de molécule du CMH-I/II et donc l'absence de présentation des antigènes tumoraux aux lymphocytes T dans les gliomes IDHm.

Dans ce contexte, nous avons cherché à caractériser le compartiment des lymphocytes T par un séquencage ARN à l'échelle de la cellule unique. Nous avons constaté que les lymphocytes T des tumeurs IDHm sont caractérisés par un phénotype naïf, ainsi que par une forte expression de KLRC1 qui code la protéine NKG2A. Ce récepteur marque un programme d'activation des lymphocytes T indépendant du TCR et peut faire l'objet d'un blocage afin d'améliorer la cytotoxicité de ces cellules.

Dans l'ensemble, nos résultats indiquent des différences clés dans les compartiments myéloïdes et lymphoïdes des gliomes IDHwt et IDHm, tout en révélant des mécanismes de signalisation potentiels qui sous-tendent les phénotypes de ces populations immunitaires. La détermination de ces différences pourrait être pertinente pour la conception de thérapies immunitaires plus pertinentes pour les patients atteints de gliomes.

Title : Impact of R-2HG on the immune microenvironment of IDH1-mutant gliomas

Keywords : Giomas, IDH, R-2HG, CD11b+ cells, T cells, scRNA-Seq

Abstract : Adult-type diffuse gliomas are the most frequent primary brain tumors, which, despite extensive fundamental and clinical research, remain incurable. A deeper understanding of gliomas' highly immunosuppressive immune tumor microenvironment (TME) may shed light on novel therapeutic strategies. The goal of my PhD was to investigate immune cells compartments of isocitrate dehydrogenase wild-type (IDHwt) and mutant (IDHm) tumors.

In a first study, we performed a bulk transcriptome/methylome profiling of CD11b+ cells isolated from human gliomas. Our integrative analysis indicates that hypermethylation of CIITA promoter may explain the downregulation of MHC-I/II molecules in IDHm CD11b+ cells, and, therefore, the lack of antigen presentation to T cells.

In this context, we performed a single-cell RNA-seq profiling of the TME, focusing on the characterization of the T cell compartment. We found that T cells from IDHm tumors are characterized by a naïve phenotype, as well as the high expression of KLRC1, encoding NKG2A. This receptor marks the acquisition of a TCR-independant activation program and could be blocked toincrease the cytotoxicity of CD8 T cells.

Our findings point to critical differences in the myeloid and lymphoid compartments of IDHwt and IDHm gliomas while revealing potential signaling mechanisms underlying the phenotypes of these immune cell populations. Determining these differences could be relevant for the design of more precise targeted immune therapies for glioma patients.